Synthesis of phthalocyanines for dye sensitized solar cells and stabilised pigment systems.

Rugen-Hankey, Sarah

Synthesis of Phthalocyanines for Dye Sensitized Solar Cells and Stabilised Pigment Systems

Sarah Rugen-Hankey

EPSRC Engineering Doctorate Centre for Steel Technology
Swansea University
Department of Materials Engineering

ProQuest LLC.
789 East Eisenhower Parkway
P.O. Box 1346
Ann Arbor, MI 48106 – 1346

DECLARATION

This work has not previously been accepted in substance for any degree and is not being concurrently submitted in candidature for any degree.

Signed ....(candidate)

Date ....25th May 2010.....

STATEMENT 1

This thesis is the result of my own investigations, except where otherwise stated. Other sources are acknowledged by footnotes giving explicit references. A bibliography is appended.

Signed ....(candidate)

Date .....25th May 2010.....

STATEMENT 2

I hereby give consent for my thesis, if accepted, to be available for photocopying and for inter-library loan, after expiry of a bar on access approved by Swansea University

Signed ....(candidate)

Date .....25th May 2010.....

Acknowledgments

Firstly, I would like to thank my supervisor Dr. P.J. Holliman for his guidance, advice and patience throughout this four year research project. I am also grateful to Dr Ian Butler for his knowledge, support and guidance in the initial stages of this thesis.

I would also like to thank the industrial sponsors of my project Corus Colors for their contributions and continuing support, especially Mr Paul Jones and Dr Maarten Wijdekop.

I am extremely grateful to Steven Jones for his invaluable services and his expert advice on the XRPD and Andrew Davis for his continuing patience and advice in operating the SEM. The departmental technicians, Gwynfor Davies, Dennis Williams and Louise Simpson have also been invaluable in their knowledge and assistance through out this project. I would also like to extend my gratitude to those involved with X-ray crystallography at the University of Wales Cardiff and the mass spectrometry department at Swansea University and Dyesol UK Ltd. for the use of their IPCE measurement apparatus.

I also wish to extend my gratitude to my colleagues in the School of Chemistry at Bangor University and the School of Engineering in Swansea University for their support and friendships that have made the last four years of research a very enjoyable experience.

Finally, I would like to thank my family for their support, financially, emotionally and for their guidance over the past years and especially my husband Martin Rugen-Hankey for believing in me and always being there.

Abstract

This thesis reports the synthesis of novel phthalocyanine based photosensitizers for DSSC devices. Key precursors, halogenated phthalonitriles have been synthesised and characterised, which included a novel periodic acid method for forming 4,5-diiodophthalonitrile. Phthalonitrile derivatives with functionalities were synthesised from halogenated phthalonitriles *via* palladium cross coupling reactions. A novel fumaronitrile anchoring group was synthesised from commercially available methyl 4-(cyanomethyl)-benzoate along with the literature compound 4,5-bis(4-methoxycarbonylphenyl) phthalonitrile. Negishi coupling of 1,1'-dibromo- and ethynyl-ferrocene compounds to halogenated phthalonitriles are also described and characterised along with the synthesis of the solubilising group nonoxyphthalonitrile.

The effectiveness of the subphthalocyanine and statistical cyclotetramisation routes to phthalocyanine synthesis using the substituted phthalonitiles has been investigated in the preparation of substituted azaporphyrines and unsymmetrical phthalocyanines. The dyes contained different donor (*t*-butyl and nonoxy) and acceptor (carboxylic acid) functional groups, especially designed for sensitisation in DSSC devices. Ring expansion reaction of the subphthalocyanines was very dependent on the substituent and reaction conditions and, in many cases, was not a selective process. Statistical cyclotetramisation of mixed substituted phthalonitriles formed *pseudo* statistical mixtures where it proved hard to separate the individual compounds from each other.

Both the substituted azaporphyrines and unsymmetrical phthalocyanine dyes were used to sensitise naonparticular titiania and constructed into DSSC devices, in which IV and IPCE curves have been measured for each dye. DSSC photoactivity was observed for each unsymmetrical substituted dye.

This thesis also describes the synthesis and characterisation of magnesium-aluminium layered double hydroxide clays which, in turn, were used in the preparation of phthalocyanine-supported and phthalocyanine-intercalated layered double hydroxides. These substituted clays were then used for the preparation of stabilised pigment systems and were incorporated into model paint formulations based on a PVC matrix. Degradation studies were carried out using the CO_2 Flat Panel Reactor using UV irradiated panels coated with the paint formulations. The effect of clay particle

morphology, clay particle size, clay-pigment preparation method and pigment loading concentration were all investigated with results showing that > 5 % pigment loading was required to reduce PVC degradation rates. Reflectance measurements were also used to monitor degradation of the panels.

Contents

Acknowledgments iii
Abstract iv
Contents vi
Chapter 1 1
1: Introduction and Aims 2
1.1 Photovoltaic Devices 3
1.2 Dye-Sensitized Solar Cells (DSSC) 5
1.2.1 Semiconductor 6
1.2.2 Electrolyte 7
1.2.3 TCO Glass Substrate And The Counter Electrode 8
1.2.4 Sensitizers 8
1.2.5 The Principles Of DSSC Operation 12
1.2.6 Photovoltaic Performance 14
1.2.7 Developments In Sensitizers 16
1.3 Phthalocyanines 18
1.3.1 Structure 18
1.3.2 Derivitisation Of Phthalocyanines 20
1.3.3 Synthesis Of Phthalocyanines 22
1.3.4 Applications In DSSC devices 26
1.4 Commercialisation Of DSSC 32
Chapter 2 35
2.1 Introduction 36
2.2 Chlorinated Phthalonitriles 36
2.3 Iodinated Phthalonitrile 37
2.4 Redox Functional Groups 45
2.4.1 Synthesis Of Ferrocene Precursors 46
2.4.2 Synthesis Of Ferrocene Functionalized Phthalonitriles 48
2.5 Synthesis Of Anchoring Groups 55
2.6 Synthesis Of Alkoxy Solubilising Groups 59
2.7 Conclusions 60
Chapter 3 61
3.1 Cyclisation 62
3.1.1 Subphthalocyanine Synthesis 62
3.1.2 Isoindolinones 66
3.1.3 Synthesis Of Unsymmetrical Phthalocyanines 67
3.2 Conclusions 97
Chapter 4 99
4.1 Introduction 100
4.2 Working Electrode Preparation 100
4.2.1 Cell Construction 101
4.3 IV Curve Device Testing Data 103
4.4 Desorption 108
4.5 Electrolyte Testing 111
4.6 IPCE 112
4.7 Conclusions 116
Chapter 5 118
5.1 Introduction 119
5.1.1 Pre-Finished Steel 119
5.1.2 Degradation Of PVC 120

5.1.3 Layered Double Hydroxides (LDHs) 122
5.1.4 Layered Double Hydroxide Synthesis 124
5.1.5 Ion Exchange And Adsorption 125
5.2 Aims 126
5.3 Synthesis Of Synthetic Mg-Al LDH 126
5.4 Absorption Of Copper Phthalocyanine -4,4',4",4",'Tetrasulfonic Acid, Tetrasodium Salt (CuPc-Ts) On To LDH 129
5.5 Intercalation Of CuPc-Ts 130
5.6 Paint Formulation And Experimental Techniques 134
5.6.1 CO_2 Reactor 136
5.6.2 Calibration 137
5.6.3 BET Analysis 138
5.7 CO_2 Evolution Studies 139
5.8 Reflectance Measurements 147
5.9 Conclusions 152
Chapter 6 154
Chapter 7 161
7.1 Experimental 162
7.2 Instrumental Methods 162
Preparation of 4,5-Dichlorophthalic anhydride (1)[157] 164
Preparation of 4,5-Dichlorophthalimide (2)[157] 165
Preparation of 4,5-Dichlorophthalamide (3)[157] 166
Preparation of 4,5-Dichlorophthalonitrile (4)[157] 167
Preparation of 4-Iodophthalonitrile (5)[89] 168
Preparation of 4,5-Diiodophthalimide (6) 169
Preparation of Tetraiodophthalimide (7) 171
Preparation of Tertaiodophthalic anhydride (8) 172
Preparation of 4,5-Diiodophthalamide (9)[47] 173
Preparation of 4,5-Diiodopthalonitrile (10)[47] 174
Preparation of Ferrocene Aldehyde (11)[95] 175
Preparation of 2-Chloro-l-Ferrocenylethene (12)[95] 176
Preparation of Ethynylferrocene (13)[95] 177
Preparation of 1,1'-Dibromoferrocene (14)[158]. 178
Reaction between 1,1'-Dibromoferrocene (14) and 4,5-Dichlorophthalonitrile (4), Resulting in 4-Ferrocenyl-5-chlorophthalonitrile (15) and 4-(1-Bromoferrocene)-5-chlorophthalonitrile (16) 179
Reaction Between 1,1'-Dibromoferrocene (14) and 4—Iodo-phthalonitrile (5), Resulting in 4-Ferrocenyl-5-chlorophthalonitrile (17) and 4-(1-Bromoferrocene)-5-chlorophthalonitrile (18) 181
Preparation of Di-(4-methylbenzoate)-fumaronitrile (19) 183
Preparation of 4,5-Bis(4-methoxycarbonylphenyl)phthalonitrile (20)[64] 184
Preparation of 4-(4-Methoxycarbonylphenyl)phthalonitrile (21) 185
Preparation of 1,2-Dinonoxybenzene (22)[48] 186
Preparation of 1,2-Dibromo-4,5-dinonoxybenzene (23)[48] 187
Preparation of 4,5-Dinonoxyphthalonitrile (24)[48] 188
Preparation of Chloro[subphthalocyaninato]-boron (III)[61] (25) 189
Preparation of Chloro[tri *t*-butylsubphthalocyaninato]boron (III) (26)[61] 190
Preparation of Chloro[2,3,9,10,16,17-hexachlorosubphthalocyaninato]boron (III)[61] (27) 191
Preparation of Chloro[triiodosubphthalocyaninato]-boron (III)[61] (28) 192
Preparation of 1,3-Diiminoisoindoline [111] (29) 193
Preparation of *t*-Butyl-1,3-diiminoisoindoline (30)[111] 194

Preparation of Dichloro-1,3-diiminoisoindoline (31)[39,111] 195
Preparation of Diiodo-1,3-diiminoisoindoline (32)[111] 196
Preparation of Phthalocyanine (33)[118] 197
Preparation of 2,3,7,8,12,13,17,18- Octa(4-pentoxybenzoate)-5,10,15,20-tetrazaporphyrin zinc (34a) 198
Preparation of 2,3,7,8,12,13,17,18-Octa(benzoate)-5,10,15,20-tetrazaporphyrin zinc (34b) 199
Preparation of 2,3-(4-Pentoxybenzoate)-7^2,12^2,17^2-tri-*tert*-butyl-tribenzo-5,10,15,20-tetraazaporphyrin (35a) 200
Preparation of 2,3-(4-Pentoxybenzoate)-7^2,12^2,17^2-tri-*tert*-butyl-tribenzo-5,10,15,20-tetraazaporphyrin zinc (35b) 201
Preparation of 2,3-(4-Benzoate)-7^2,12^2,17^2-tri-*tert*-butyl-tribenzo-5,10,15,20-tetraazaporphyrin zinc (35c) 202
Preparation of 2,9,16–Tetra-*tert*-butyl-23,24-bis(4-pentoxycarboxyphenyl) phthalocyanine (36a) 203
Preparation of 2,9,16–Tetra-*tert*-butyl-23,24-bis(4-pentoxycarboxyphenyl) phthalocyanine Zinc (36b) 204
Preparation of 2,9,16-*tert*-Butyl-23,24-(4-carboxyphenyl)-phthalocyanine Zinc (36c) 205
Preparation of 2,3,9,10,16,17 – Nonoxy – 23,24- bis(4-pentoxycarboxyphenyl) phthalocyanine (37a) 206
Preparation of 2,3,9,10,16,17 – Nonoxy – 23,24- bis(4-pentoxycarboxyphenyl) phthalocyaninato zinc (37b) 207
Preparation of 2,3,9,10,16,17 – Tetra(*tert*-butyl) – 23,24- bis(4-carboxyphenyl) phthalocyanine Zinc (37c) 208
Preparation of 2,9,16,23-(Tetra-1-bromoferrocene)-3,10,17,24-chlorophthalocyaninezinc(II) (38) 209
Preparation of 2,9,16-(Tetra-1-bromoferrocene)-3,10,17-chloro-23,24- bis(4-methoxycarboxyphenyl) phthalocyaninezinc(II) (39) 210
Preparation of Chloro[2,9,16,(ferrocenylethynyl)subphthalocyanine] boron (III) (40) 211
Preparation of Chloro[2,9,16,(4-methoxycarboxyphenyl) subphthalocyanine] boron (III) (41) 212
Preparation of Butyl-(2-hydroxyethyl)-dimethylammonium Bromide[119] (42) 213
Preparation of Phthalocyanine zinc (43)[118] 214
Preparation of 2-*t*-Butyl-9,16,23-triiodo-phthalocyanine (44) 215
Layered Double Hydroxide Synthesis 216
Coprecipitation Method – (Small-LDH) 216
Urea Method – MgAl-HT (Large-LDH) 216
Adsorption of Copper Phthalocyanine 4,4',4'',4'''-Tetrasulfonic Acid Tetra Sodium Salt. (Small Pc-LDH, Large Pc-LDH) 217
Rehydration Method 218
Synthesis of MgAl-TA Layered Double Hydroxide 219
References 220

Chapter 1

Introduction

1. Introduction and Aims

With growing concern from the international community about climate change, pressure is mounting to produce renewable, green electricity without damaging the natural environment. The main focus is on cutting carbon dioxide emissions associated with the burning of fossil fuels. It is also predicted that world energy consumption will grow by 2 % each year for the next 25 years[1]. Thus, there is a need for renewable, non-polluting, energy recourses in order for our global infrastructure to continue working.

Every year enough energy reaches the earth's surface in the form of electromagnetic radiation from the sun to meet our annual global energy consumption 10,000 times over[2]. Photovoltaic (PV) devices are designed to generate direct current (DC) from semiconductors when they are illuminated with photons[3]. Photovoltaic solar cells are a desirable renewable energy source as they are free from noise and chemical pollution and can be made as portable devices, and therefore not dependent on the electrical grid. Photovoltaic systems based on *p/n* junction devices are already being installed on industrial structures and private residences. However, PV energy costs are not yet competitive due to the high manufacturing costs of these devices, with continued PV growth at present mainly based on government support[4].

Corus, Europe's second largest steel maker, manufactures, processes and distributes organically coated steel products to customers worldwide. However, with countries like China now able to produce low cost steel from integrated steelworks, this means that Corus cannot compete on price per tonnage of steel. For this reason Corus must add value to their products. One method of doing this is to develop a photovoltaic coating that can be applied to strip steel. Third generation photovoltaic, dye sensitised solar cells, are being developed as low cost PV devices, with a photosensitive dye used to sensitise a metal oxide semiconductor upon irradiation, producing electricity[3]. One possibility is that Corus can coat these devices onto strip steel and cover large industrial buildings with roofs covering areas of 10-20,000 m^2. This provides a large surface area for solar conversion as the UK receives between 900 – 1200 $kWh/m^2/yr$. If roofing material was coated with a photovoltaic material with an efficiency of 5 %, each 100 m^2 of PV coated roof would produce 4500 GWh of electricity[3]. This would provide clean, renewable, non-polluting energy on new structures and by utilizing large areas on existing buildings without the need for creating additional space for energy production.

The design and synthesis of phthalocyanine based photosensitive dyes for dye sensitised solar cells is therefore the main focus of this thesis. The first stage of this work aims to synthesise substituted phthalonitrile precursors for phthalocyanine synthesis, followed by an investigation into the cyclisation of these precursors to form the photosensitive dyes for sensitisation of titania for DSSC devices.

Phthalocyanines are also widely used as blue and green pigments in coatings that are used to coat strip steel. Continued development of these coatings has lead to some Corus coatings that are now guaranteed for up to 40 years; therefore studies to further increase life times of products forms the second part of this thesis. In detail, this will involve the synthesis and testing of phthalocyanine-layered double hydroxide pigments in order to study the stabilisation and colour effects of the new pigments to be coated on strip steel.

1.1 Photovoltaic devices

Photovoltaic devices consist of a semiconductor material that converts light energy into direct current (DC) electrical energy[3]. Semiconductors are materials that contain a valence and conduction band which are separated in energy by the band gap, typically measured in electron volts (eV). When energy in the form of a photon of light has energy greater than that of the band gap, an electron will be excited into the conduction band of the semiconductor. The electrons in the conduction band are then able to flow and conduct electricity through the material. If the photon has less energy than that of the band gap, the electrons will not be excited and the energy will either be reflected or absorbed as heat. Consequently PV devices may reach temperatures of 20 to 30 °C above the ambient temperature.

The precursors to the first modern PV devices, silicon *p/n* junction solar cells, were developed at Bell Laboratories by Chapin in 1954[3] even though the first functional photovoltaic device was developed in the nineteenth century in 1883 by Fritts[3]. The device was made by melting selenium on to a metal substrate with a gold leaf film as the top contact[3]. Since their first discovery, PV devices were first developed for energy production associated with space travel/exploration and are now regularly used in calculators, clocks, traffic signals and other small electrical devices.

Silicon solar cells, either monocrystalline (c-Si) or polycrystalline silicon (multi-Si), account for almost 90% of the total worldwide PV energy production. Silicon has a band gap of 1.1 eV, which is an excellent spectral match for the spectrum of sun light. Silicon *p/n* junction devices are made up of two components; namely a *p*-type semiconductor and an *n*-type semiconductor which when put together to form a *p/n* junction. The *n*-type layer is silicon doped with elements from group V, usually phosphorus, creating an anode. The *p*-type layer is doped with elements from group III, like boron, these are electron deficient relative to silicon and therefore create holes and become the electron receptor. When these layers are placed in contact with one another, electrons in the *n*-type layer will flow into the *p*-type layer and holes will diffuse from the *p*-type layer to the *n*-type region. The result is an electric field created in the region at the interface, the *p/n* junction. When irradiated by the sun, photons with energy greater than the bandgap of the semiconductor, will photoexcite the bound electrons in the *p*-type layer. This promotes an electron from the valence band into the conduction band of the semiconductor creating an electron pair hole. These electrons are then driven to the *n*-type layer by the electric field which induces electron flow. The electron will recombine with a 'hole' on the *p*-type layer doing work on the way[3]. These devices have reached efficiencies of 25 % for c-Si and 20 % for multi-Si under laboratory conditions. Commercial cells have efficiencies of 15 and 13 % respectively[3].

Cost is far the biggest problem with the 1st generation solar cells as silicon is an expensive commodity. The PV industry is supplied from microelectronics industry which employs two costly purification steps to obtain an extremely high purity grade of silicon[3]. Solar cells do not require such high purity, and so the PV industry has been supplied with off-cuts from the electronics industry but silicon is still an expensive feedstock. For this supply to continue, the microelectronics industry needs to expand at same rate as the PV industry, which is not the case[5]. Silicon also has an indirect band gap which means that a greater thickness of crystalline silicon, which is expensive to grow, is required to absorb the same amount of sunlight as other semiconductors. A larger volume of material means that a higher purity is required to minimise recombination losses that reduce efficiencies.

This has led to the development of 2nd generation solar cells, thin film solar cells, which make up the remainder of the commercialised PV market with amorphous silicon (a-Si), cadmium telluride (CdTe) and $Cu(InGa)Se_2$ the materials being used. These devices

have reached efficiencies of 7-8 % for the a-Si and CdTe and 9-10 % for the $Cu(InGa)Se_2$ modules. These devices apart from the a-Si, have the added problem of potential toxicity and environmental issues in both manufacturing and site of deployment.

1.2 Dye-sensitized Solar Cells (DSSC)

Third generation photovoltaics are being developed as a low cost alternative to their solid state counter parts and are based on organic thin film devices which are photoelectrochemical solar cells (PSC). Dye sensitized solar cells, first invented by Michael Grätzel and Brian O'Regan in 1991[6] and also known as Grätzel cells, are a type of PSC and consist of a photoelectrode, a redox electrolyte and a counter electrode. Several semiconductors, including single and polycrystalline forms of *n*- and *p*- silicon, gallium arsenide and cadmium sulphide have been used as the photoelectrodes. These materials, when combined with a redox electrolyte have reached efficiencies of approximately 10 % [3] but suffer from poor stability caused by photocorrosion of the electrode in the redox electrolyte.

Metal oxide semiconductors such as titanium dioxide (TiO_2), zinc oxide (ZnO) or tin oxide (SnO_2), have much better stability under irradiation in the redox electrolyte but have wide band gaps and therefore cannot absorb visible light. Sensitizers, such as organic dyes, are therefore used to absorb the visible light. These dyes are adsorbed onto the semiconductor surface and upon irradiation of solar energy, excitation of the dye and consequently injection of an electron into the conduction band of the semiconductor results in producing electricity which will be discussed in more detail later on in this chapter.

DSSCs consist of two transparent conducting, typically glass, electrodes. The working electrode is coated with a metal oxide, usually TiO_2. This is then sensitized for visible light by a dye which is adsorbed on to surface of the porous oxide. The counter electrode is coated with a catalytic amount of platinum which is then sandwiched together with the working electrode and the space between filled with typically an organic liquid electrolyte (Figure 1.1). The composition of the DSSC is discussed in this section.

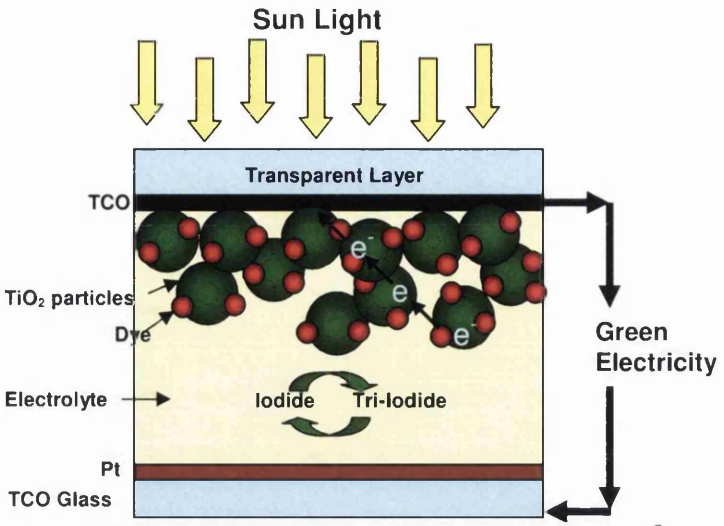

Figure 1.1, Schematic diagram of a DSSC, Redrawn [7]

1.2.1 Semiconductor

Wide band gap semiconductors are used in DSSCs, these include ZnO, Nb_2O_5, SnO_2 and TiO_2 (anatase)[8], with the later the preferred choice. Early studies of these devices involved the sensitisation of single and polycrystalline semiconductors. For example, ZnO was sensitised with organic dyes such as rose bengal, fluorescein and rhodamine resulting in low efficiencies[3] due to the relatively low surface area onto which the dye could adsorb and the narrow absorption range of the sensitizing dyes.

To increase surface area and hence dye loading, mesoporous semiconductors are now used with TiO_2 the preferred material of choice as it has good photochemical stability, a suitable band gap (3.2 eV), non-toxicity and is cheap to produce[9]. However, TiO_2 has three crystal structures; rutile, anatase and brookite. The rutile phase is the most thermodynamically stable form but the anatase phase is desired for applications in DSSCs. This is because the anatase phase has a wider band gap, which reduces the possibility of irreversible oxidiation of the electrolyte[10]. It also has a high dielectric constant which provides good electrostatic shielding of the electron injection from the excited state dye, preventing electron recombination before reduction of the dye by the redox mediator, usually iodine/iodide in the electrolyte. TiO_2 also has a high refractive index and is efficient at diffuse scattering of light inside the porous photoelectrode and so enhances light absorption.

The TiO_2 is deposited on to a substrate by either screen printing or doctor-blading as a mesoporous layer which is comprised of nanoparticles[3]. The morphology of the film is a

major variable in DSSC performance as the film should have a large enough surface area for dye adsorption while still producing good electronic conduction once the particles are sintered together[3]. The sensitising dye needs to be in contact with both the semiconductor and the electrolyte as the rate-determining step in DSSC is determined by the time taken for the diffusion of redox ions to reach the oxidised dye. It is therefore very important to control the level of porosity in the semiconductor layer in order to allow the electrolyte to penetrate the film. Porosity of 50-70 % is controlled by the addition of a polymer such as polyethylene glycol into the TiO_2 suspension before sintering[3]. The use of nanostructures such as nanotubes[11], wires[12] and rods[13] of TiO_2 are being investigated as their morphology provides a direct passageway for photoexcited electrons to reach the conducting substrate. The use of orientated anatase nanowires has produced efficiencies of 9.3 %[12].

1.2.2 Electrolyte

The electrolyte acts as the inner charge carrier between the counter electrode and the adsorbed dye on the working electrodes. It's role is to regenerate the dye back to its ground state. Currently, this is generally achieved by the tri-iodide/iodide redox couple contained in an organic solvent. There are three different types of electrolyte being explored; the liquid state, the quasi solid state and solid state electrolyte. The liquid electrolyte is the most commonly used electrolyte producing the best performances reported to date. These electolytes generally consist of a nonprotonic organic solvent (e.g., acetonitrile, propionitrile or methoxyacetonitrile), a mixture of iodides, (e.g.LiI, KI, NaI, imidazolium iodide derivatives and tetraalkylammonium iodide), and iodine. The mixture of iodides and iodine forms the redox couple (I^-/I_3^-) responsible for mediating the electrons between the photoelectrode and the counter electrode. Other redox couples such as Br_3^- / Br^- [14] and SeCN- / $SeCN_2$[15] have been investigated but the efficiencies do not match that of the tri-iodide / iodide.

A low viscosity organic solvent is desired as it affects the ionic conductivity of the electrolyte; fast ion diffusion producing a higher efficiency. The counter cations of the iodides also contribute to DSSCs function as they are believed to absorb on to the TiO_2 surface, shifting the conduction band of the TiO_2 electrode[16]. The cations also provide different ionic conductivity in the electrolyte. Other additives such as 4-*tert* butylpyridine (TBP) are added as it is known to suppress the dark current and improve

the photoelectric conversion efficiency[17]. TBP may also reduce the recombination of electrons in the conduction band of the semiconductor and the electron acceptor in the electrolyte through the coordination between the nitrogen atom and titanium ions in the semiconductor. This increases the fill factor and conversion efficiency dramatically[17].

The main problem with liquid electrolyte is the long term stability of the cell due to leakage which can be caused by insufficient sealing of the cells. If the cell is not sealed properly or the seal fails then the solvent in the liquid electrolyte will evaporate. To try and solve this issue, extensive research is going into the development of new electrolytes which remove the volatile solvent such as room temperature ionic liquids such as 1-hexyl-3-methylimidazolium iodide. These electrolytes are non-volatile, ideal for long term stability of PV devices as well as electrochemically stable, have high ion conductivity and they are non-flammable. However these electrolytes do not at the present deliver the performance of the liquid redox electrolytes.

1.2.3 TCO Glass Substrate and the Counter Electrode

Transparent conducting oxides (TCOs) are generally used for both the counter electrode and working electrode in DSSC devices. The TCO layer on the working electrode is used as the substrate for the deposition of the semiconductor and thus needs to have low sheet resistance for electrons to move freely around the circuit and high transparency for efficient solar cell performance. Indium-tin oxide is widely used as the TCO and has low sheet resistance but at elevated temperatures this resistance increases. Fluorine doped tin oxide is now more widely used as the TCO glass for this reason. For DSSC, the TCO layer on the counter electrode is coated with a catalytic layer of platinum or carbon, which catalyses the reduction of the tri-iodide back to iodide ions.

1.2.4 Sensitizers

Sensitizers developed for use in DSSC devises, have certain requirements for the system to function[18]. The dye must absorb light below a threshold wavelength of 920 nm with as broad a range as possible[19]. In addition, it must bind strongly to the semiconductor and therefore must possess anchoring groups such as carboxylate, sulfonate or phosphonate functional groups[19]. Upon irradiation the dye should inject electrons into the semiconductor with a quantum yield of unity[19]. The LUMO of dye must be sufficiently high in energy for charge injection into TiO_2 and the HOMO must be

sufficiently low in energy for regeneration of the oxidised dye by the electrolyte redox couple[18]. Electron transfer to TiO_2 must be rapid in comparison to the decay to the ground state of the dye[18]. Finally the sensitizer needs to be stable enough to ideally sustain $\geq 10^8$ turnover cycles corresponding to 20-25 years of exposure to irradiation[19].

There are two classifications of dyes being investigated for DSSC. These are inorganic and organic dyes. Inorganic dyes include metal complexes of polypyridyl, porphyrine[20], phthalocyanines[21] and inorganic quantum dots[22]. These usually have a higher thermal and chemical stability than organic dyes. Polypyridyl ruthenium complexes were the first high performance dyes to be utilized in DSSC devices and generally consist of 2,2'-bipyridyl-4,4'-dicarboxylic acid, in combination with a halide, cyanide, thiocyanate, acetyl acetonate, thiacarbamate or water substituent, all complexed to ruthenium[3]. These are the only dyes so far to achieve over 10 % efficiency under laboratory conditions. The N3 dye, [4,4'-dicarboxylic acid-2,2'-bipyridine dithiocyanato ruthenium(II)], reported in 1993[17] obtained an efficiency of 10 %. This has absorption maxima at 518 and 380 nm, with extinction coefficients of 1.3 and 1.33 x 10^4 M^{-1} cm^{-1}, respectively[19]. This was then superseded by a black ruthenium N749 dye, [tri(isothiocyanato)-2,2',2''-terpyridyl-4,4',4''-tricarboxylate) ruthenium(II)], in 1997. This dye extends a further 100 nm in to the IR than the N3 dye producing an efficiency of 10.4 %[23] (Figure 1.3). The combination of a self assembling guanidinium thiocyanate and the N3 dye further increased the efficiency of the device to 10.6 %[19] by increasing the cell open circuit voltage (V_{OC}). The tetrabutylammonium salt of the N3 dye, N719 after repeated purification and isolation at pH 4.3 has now reached efficiencies of 11.2 %[24]. The Z907 dye contains hydrophobic alkyl chains and is therefore more difficult to desorb from the surface of the TiO_2 when water is present produced efficiency of 9.0 %[25]. All four dyes, the N3, N719, N749 and Z907 ruthenium based dyes are all available commercially[26] for sensitizers of wide band gap semiconductors used in DSSC devices with the N719 dye the cheapest on the market at £555 for 1 g[26] while the N749 the most expensive at £1,800 per gram.

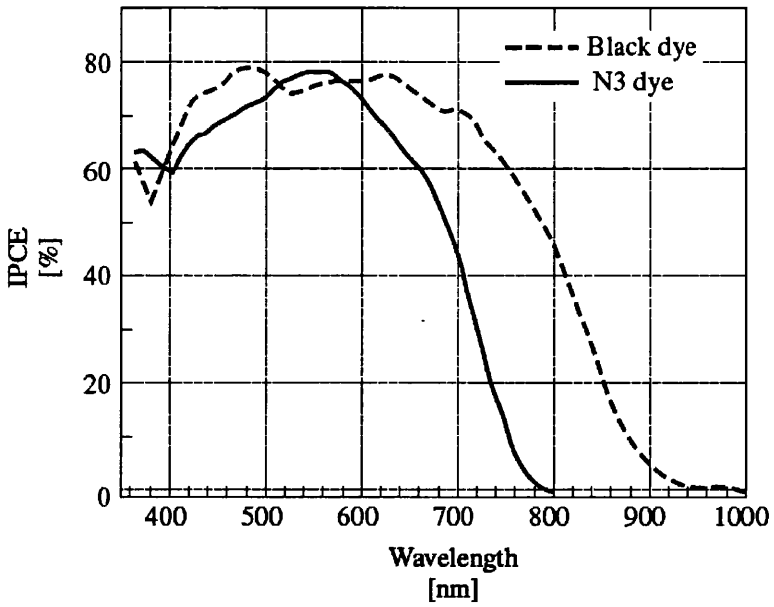

Figure 1.3. IPCE of the Black dye and N3[23].

Each ligand coordinated to the ruthenium metal is designed to manipulate the HOMO and LUMO level of the dye and to achieve effective electron injection into the conduction band of the semiconductor. The ruthenium complexes are reported to be anchored onto the TiO_2 surface by forming either an ester bond or a carboxylate bidentate coordination *via* the carboxylic acid groups. These groups provide good electronic interaction between the ligand and the conduction band of the TiO_2, resulting in effective electron injection. The dye then forms a monolayer, reaching near 100 %[3] coverage of the TiO_2, and anchors to the surface of the oxide. Absorption in the visible region of the solar spectrum is attributed to the metal-to-ligand charge-transfer transition. The energy levels of the HOMO and LUMO are reported to be mainly influenced by the d-orbitals of the Ru metal and the π^* orbital of the ligand, respectively[3]. The NCS ligand used in these ruthenium complexes shifts the HOMO level negatively[3]. This results in a red shift in the absorption properties of the complex and aids in the electron acceptance from the reduced redox electrolyte.

Further modifications of the polypyridyl ruthenium complexes are still being investigated to further improve the absorption range and stability. Extension of conjugation in the hydrophobic chains has lead to ruthenium dye C104 with 10.5 % efficiency[27]. While conjugation of a thiophene unit (C101) has given an efficiency of 11.3 %[28] (Figure 1.4). The phosphoric acid derivative of the Z907 dye has produced efficiencies of 8.0 %[29], lower than that of the carboxylate version, Z907. Phosphoric acid derivatives usually produce lower efficiencies as the acid is not in conjugation with

the polypyridyl plane and is therefore disadvantageous for electron injection but do not desorb easily from the surface of the semiconductor unlike the carboxylic acid derivatives[29].

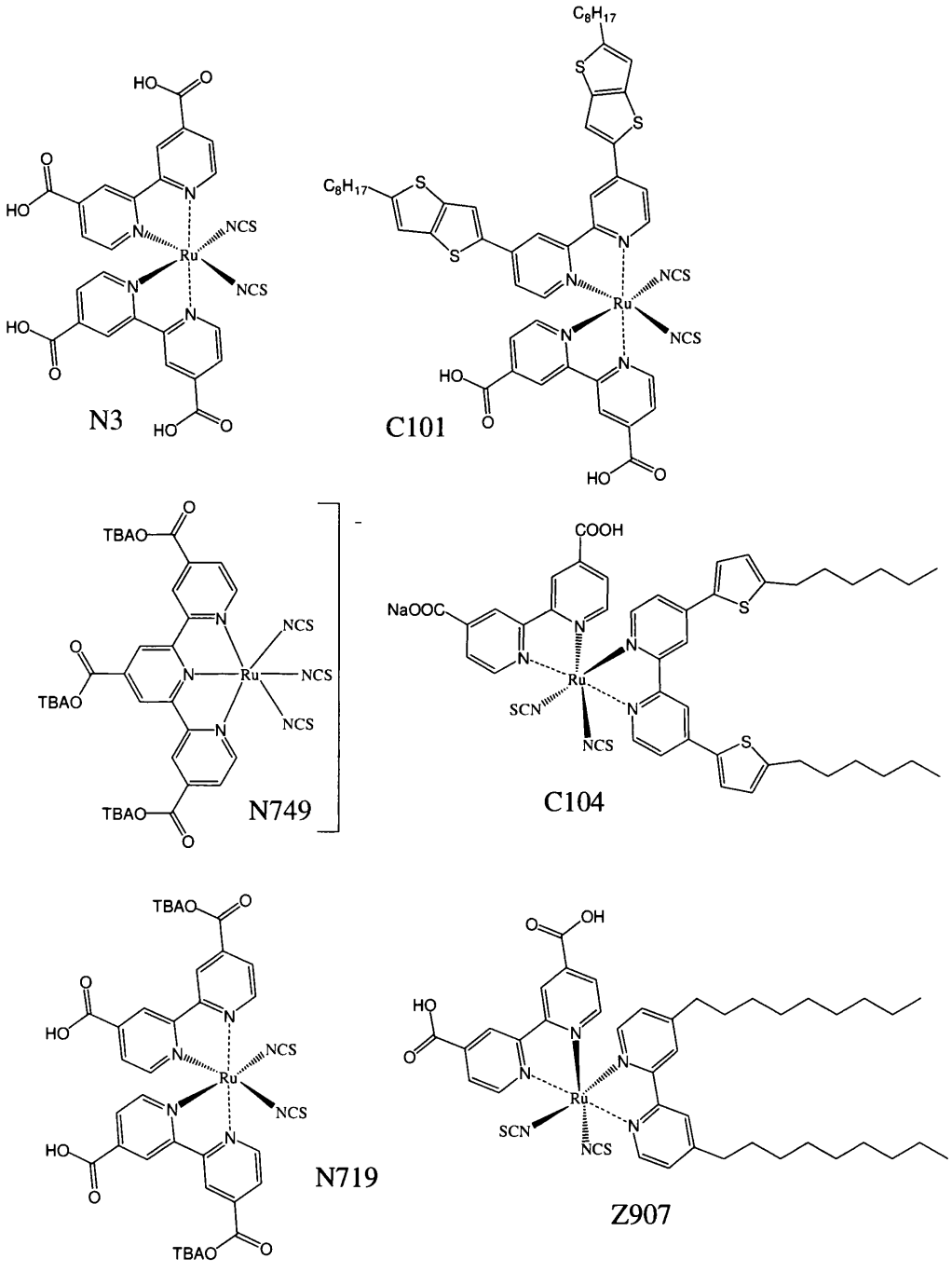

Figure 1.4, Structures of ruthenium dyes[23, 24, 27, 28].

1.2.5 The Principles of DSSC Operation

Dye-sensitized solar cells do not work by the same principle as conventional *p/n*-type devices but mimic photosynthesis by charge transfer between molecular orbitals[3]. The principles of DSSC operation will be outlined in the following section.

Firstly, the dye photosensitizers are excited upon solar irradiation from the ground state (S) to an excited state (S*). This arises from the metal to ligand charge transfer (MLCT) transition in the case of the ruthenium complexes (Eq 1). The excitation of the dye is followed by rapid injection of an electron into the conduction band of the semiconductor (Eq 2) which then oxidises the photosensitizer. The electron percolates through the semiconductor until it reaches the ITO layer and then passes around the external circuit in which it loses its energy by doing work. The electron then re-enters the cell *via* the counter electrode and is transferred to the liquid electrolyte where it reduces the tri-iodide species to iodide (Eq. 3). The oxidation of the iodide to the tri-iodide species (Eq. 4) then occurs regenerating the oxidised photosensitizer, completing the circuit (Eq. 5)[3].

$$S + h\nu \longrightarrow S^* \qquad \textit{Eq. 1}$$

$$S^* \longrightarrow S^+ + e^-(TiO_2) \qquad \textit{Eq. 2}$$

$$I_3^- + 2e^- \longrightarrow 3I^- \qquad \textit{Eq. 3}$$

$$3I^- - 2e^- \longrightarrow I_3^- \qquad \textit{Eq. 4}$$

$$S^+ + e^- \longrightarrow S \qquad \textit{Eq. 5}$$

The performance of the DSSC is determined by four main energy levels (Figure 1.5): the energy levels of the LUMO and HOMO of the photosensitizer, the Fermi level of the semiconductor and the redox potential of the I^-/I_3^- mediator. The photocurrent of the DSSC is determined by the difference in energy between the LUMO and HOMO of the photosensitizer. A small energy gap (E_g), the larger the photocurrent, due to a wider range of absorption in the visible region of the solar spectrum. For effective injection of electrons into the conduction band of the semiconductor the energy level of the LUMO of the dye must be sufficiently negative with respect to that of the conduction band of the TiO_2. Electronic coupling between the LUMO and the conduction band also contributes to effective electron injection[9].

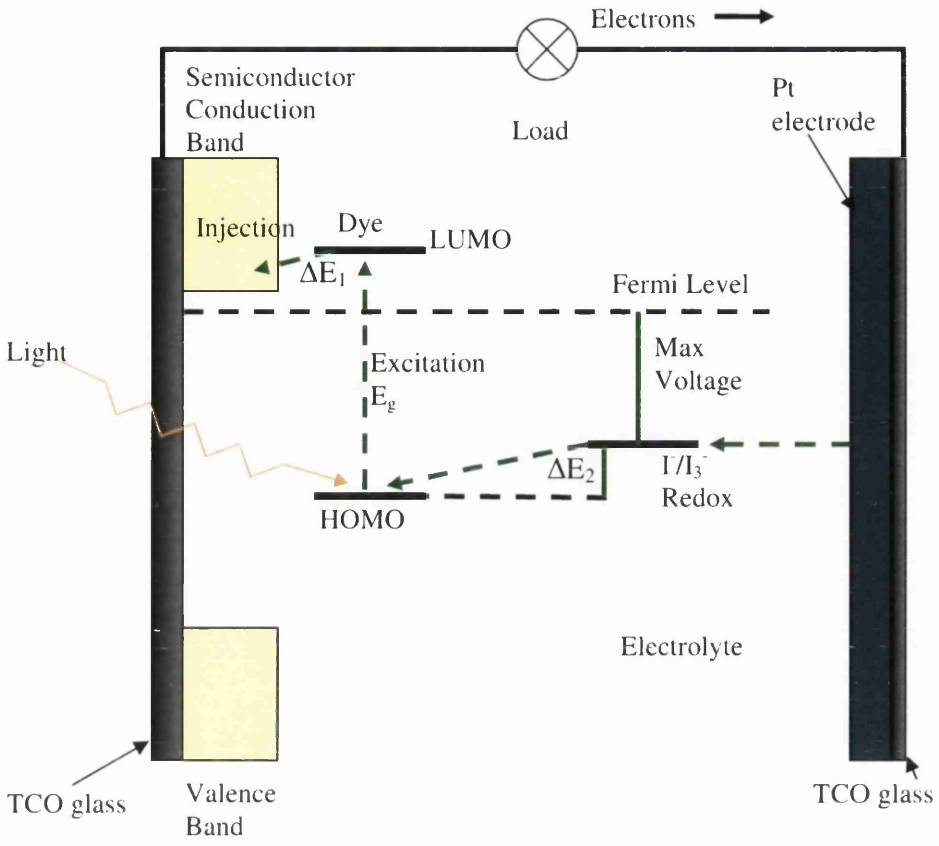

Figure 1.5, Schematic energy diagram of a DSSC, redrawn from[3]

Charge transport in DSSC devices is similar to that of photosynthesis, where chlorophyll is the photosensitizer and charge transport occurs in the membrane[3]. This differs from conventional *p/n*-type solar cells in several ways. Electrons are injected from the excited photosensitizer and therefore no holes are formed in the valence band of the semiconductor. This means there are no charge recombination processes associated with this part of the process. Instead, charge transport is through the semiconductor layer while photons are absorbed into the photosensitiser, therefore effective charge separation occurs at the interface. This is assisted by cations of Li^+ from the electrolyte and H^+ ions from the dye which are co-adsorbed onto the semiconductor surface. Dipoles are therefore formed with photosensitizer and the negatively charged iodide ions. This results in a potential drop across the interface which leads to reduced electron recombination[3].

1.2.6 Photovoltaic Performance

In order to evaluate cell efficiency for converting light into electricity, the following section will discuss the terminology used when discussing cell parameters and the standard test conditions used.

The power the solar cell produces may be calculated from the current (the number of free electrons flowing in the external circuit) multiplied by their potential.

$$P = IV$$

where P is power measured in Watts (W), I is current in Amps (A) and V is the voltage in volts (V).

Current *versus* voltage curves (I-V curves) are then used to evaluate cell performance (Figure 1.6). I-V curves have two extremes in load resistance with the maximum power output for the cell in between these two points. The extremes can be seen in the I-V curve in Figure 1.6. This shows where the maximum current, the short circuit current (J_{sc}), is produced when there is no resistance in the circuit and hence the voltage is zero. The maximum voltage, open circuit voltage (V_{oc}), is produced when there is a break in the circuit and hence there is no current. In between these two extremes is the maximum power of the cell (P_{max}). The voltage and the current at this P_{max} are denoted as V_{mp} and I_{mp}.

Cells are tested under standard conditions which assume that the cell is not shaded in any way. Standard sun light conditions are set at 1000 watts of solar energy per square meter (1000 W/m^2) or referred to as AM1.5 or one sun.

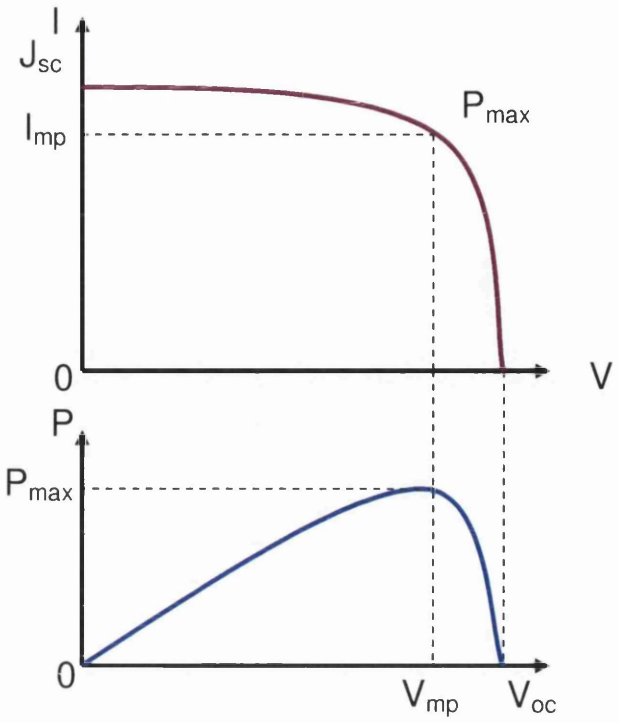

Figure 1.6. I-V curve and the Pmax – V curve of a photovoltaic device, redrawn from[3]

From the I-V curves, critical cell parameters can be calculated such as the overall cell efficiency (η) which, is the ratio of electrical power output (P_{out}) compared to solar input (P_{in})

$$\eta = \frac{P_{out}}{P_{in}}$$

Fill factor (FF) is another important measure of the quality of a solar cell. This is calculated by comparing the maximum power to the maximum theoretical power P_T (Figure 1.7)

$$FF = \frac{P_T}{P_{Max}} = \frac{J_{sc} \cdot V_{oc}}{I_{mp} \cdot V_{mp}}$$

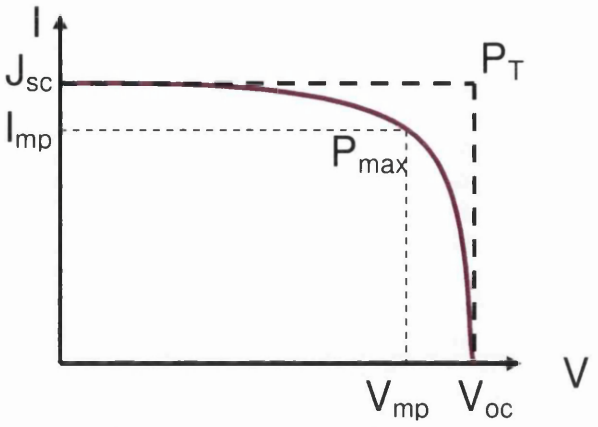

Figure 1.7. I-V curve of a photovoltaic device redrawn from[3]

IPCE is also used as a key parameter to assess the performance of a DSSC which is calculated by measuring device performance across the visible spectrum by using monochromatic radiation at a series of wavelengths and is the efficient quantum yield of the device. Thus, IPCE is the ratio of number of electrons flowing through the circuit compared to the number of photons incident on the cell. IPCE is the product of three factors, the light harvesting efficiency (LHE), the charge collection efficiency ϕ_{inj} and the charge injection yield ϕ_{el} and can be calculated as shown below.

$$IPCE = (LHE).\ \phi_{inj}.\ \phi_{el}.$$

1.2.7 Developments in Sensitizers

Ruthenium-based dyes are expensive to produce due to the price of ruthenium and the difficulties in purification. They are also lacking in absorbance in the red region of the visible spectrum; therefore alternatives are being investigated. Organic dyes are promising alternatives, with efficiencies becoming comparable to that of the ruthenium complexes[30]. One major advantage of organic dyes is that they can incorporate different light absorbing groups to extend the spectral range into the design of the molecule, with the general structure, donor - π conjugation bridge – acceptor[31]. For instance, dyes have been synthesized with [bis(9,9-dimethylfluoren-2-yl)amino]benzo[b]thiophene acting both as the electron donor, and as a bulky group that prevents dye aggregation and helps reduce charge recombination processes. The electron donor is connected to an acceptor, which in this case is the cyanoacrylic acid, by a thiophene molecule, designed to increase the molar extinction coefficient of the dye. These dyes have achieved

efficiency of 6.7 %[32] (Figure 1.8, A) and 7.4 % (Figure 1.8, B)[31]. Higher V_{oc} and I_{sc} have been achieved with a dye that incorporates a fused dithienothiophene unit with a difluorenylaminophenyl donor and a cyanoacrylic acid acceptor[33] (Figure 1.8, C) where an efficiency of 8.0 % has been observed. A coumarine based dye has reached efficiencies of 7.7 % [34] (Figure 1.8, D). Efficiencies of up to 9 % have been achieved with an indoline dye D149[30] due to a high J_{sc} value (Figure 1.8, E) while a polyene based dye has reached an efficiency of 6.8 %[35] (Figure 1.8, F). A large J_{sc} is observed for a cyanine dye[36] but the over all efficiency produced (7.6 %) was reduced due to a low V_{oc} and FF (Figure 1.8, G). A table of efficiencies and cell parameters of these dyes is shown in Table 1.1.

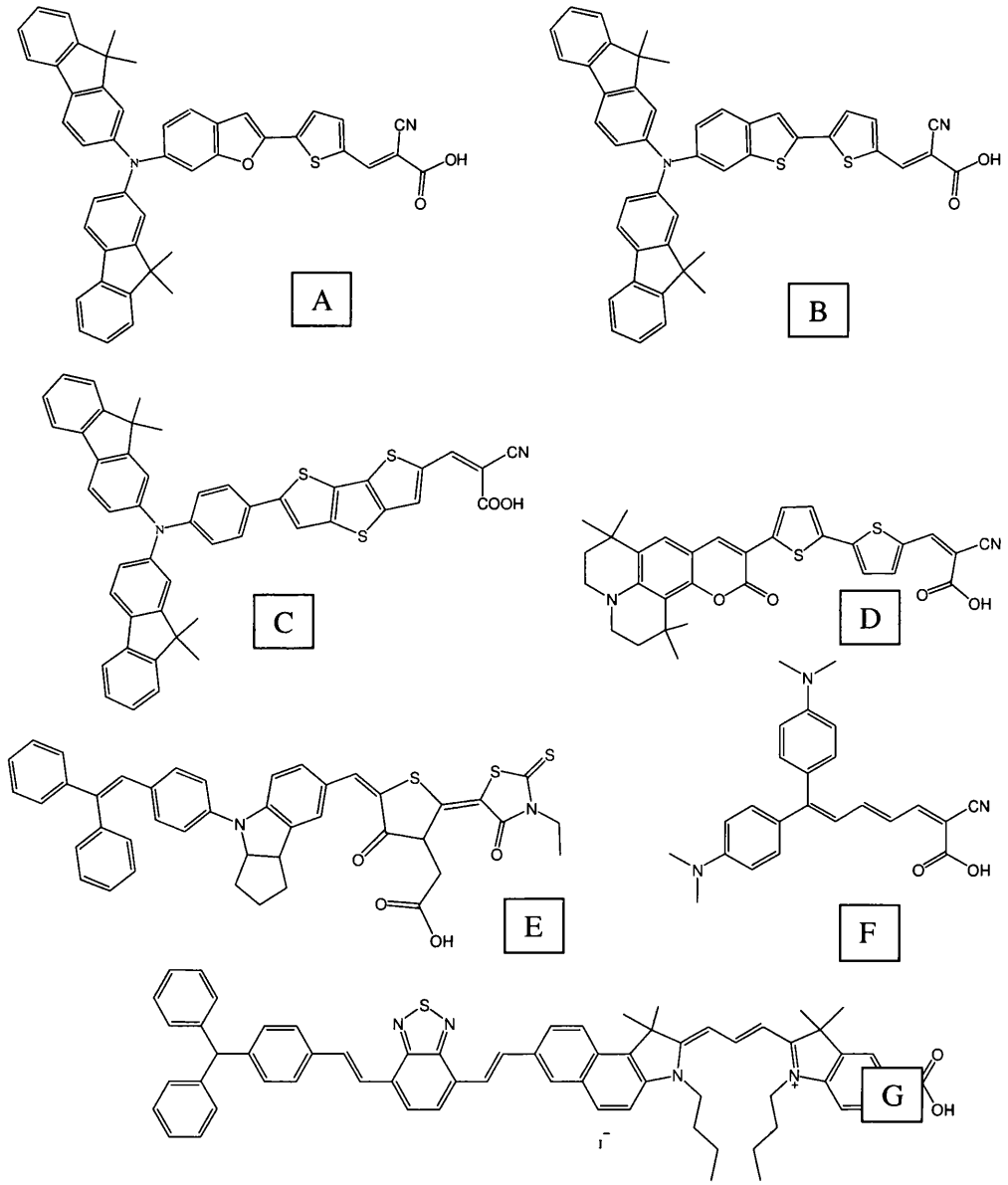

Figure 1.8, Structures of Organic Dyes for DSSC

Dye	Jsc (mA cm-^{2})	Voc (V)	FF	Area (cm^2)	H	Ref
A	14.39	0.70	0.66	0.18	6.7	[32]
B	15.33	0.74	0.66	0.18	7.4	[31]
C	14.33	0.73	0.76	0.159	8.0	[33]
D	14.3	0.73	0.74	0.25	7.7	[34]
E	19.96	0.65	0.69	-	9.0	[30]
F	12.9	0.71	0.74	0.245	6.8	[35]
G	22.10	0.54	0.48	0.15	7.6	[36]
N719	17.6	0.80	0.73	0.158	11.8	[24]

Table 1.1. Cell parameters of organic dyes as sensitzers in DSSC devices tested using liquid electrolytes under AM 1.5 irradiation

It is worth nothing that these efficiencies have been obtained under laboratory conditions using very small cell sizes which reduce resistance within the system, increasing efficiencies.

1.3 Phthalocyanines

Phthalocyanines are a promising alternative to the ruthenium complexes as they possess an intense absorbance in the far red/ near IR region of the solar spectrum. They have excellent chemical, light and thermal stability and possess the appropriate redox properties for sensitisation of wide band gap semiconductors. This section will therefore discuss the structure, synthesis of phthalocyanines and their applications in DSSC devices.

1.3.1 Structure

The most significant discovery at the beginning of the 20th century in terms of organic colourants was the discovery of phthalocyanines[37]. Since this time, phthalocyanine pigments and dyes have become established as a commercially successful group of green and blue pigments and blue dyes.

The original discovery of phthalocyanines was fortunate as it was found by chemists, in Scottish Dyes, Grangemouth, as a blue impurity when forming phthalimide from phthalic anhydride and ammonia[37]. The blue impurity was isolated and preliminary examination of this compound was carried out by M. Dunworth and H. Drescher of

Scottish Dyes Ltd[37]. The structural analysis, established the structure as iron phthalocyanine, with the iron originating from the vessel lining. The material was found to be crystalline and highly stable and was initially studied by Professor J.F. Thorpe F.R.S[37], and the Research Committee of the Dyestuffs Group of Imperial Industries, Ltd.

In 1934, a series of papers was published by Linsted[37] of Imperial College London describing this new class of organic compounds with unusual stability, brilliance in colour and with a structural resemblance to natural porphyrins. These papers include the discovery, preliminary investigations and a description of the preparative methods and properties of phthalocyanines. This was later followed by x-ray structural investigations by Robertson[38] in 1936.

The name phthalocyanine was derived from the term for naphtha and cyanine (rock oil and dark blue) and is a class of polycyclic pigments containing aromatic and/or heterocyclic ring systems[39]. The core phthalocyanine structure was found to be insoluble in most common organic media, dilute acids, alkalis and water and so is used commercially as both blue and green pigments in paints[39]. The insolubility of these compounds allows many impurities to be separated with ease. The absolute purification though is much more difficult due to insoluble mixtures which are very difficult to separate by common chromatographic methods.

The resonance structures of phthalocyanine (Figure 1.9) illustrate that all the pyrrole simultaneously contribute to the aromatic system accounting for the high stability.

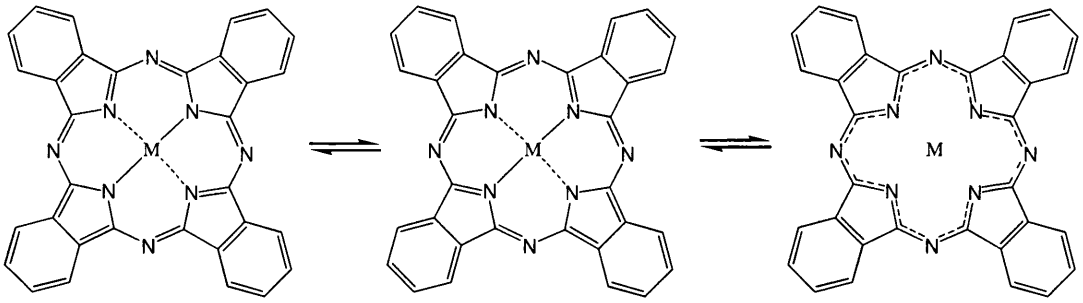

Figure 1.9, Resonance structures of copper phthalocyanine[39]

The core phthalocyanine system is structurally derived from the *a* – [18] - aniline molecule. This consists of a conjugative 18 π- electron hetero – macrocyclic system, which satisfies Huckle and Sondheimer's (4n + 2) electron rule. This therefore forms a

planar, completely conjugated aromatic system that exhibits surprising stability and generates intense bands in the absorption spectra with the most intense being the Q-band. This band lies in the visible region at wavelengths of 630 to 650 nm[40] and is the origin of the intense colour of the phthalocyanines. In addition to the Q-band, there is a strong absorption in the ultraviolet (UV) region between 320 and 370 nm, the B- band.

1.3.2 Derivitisation of Phthalocyanines

It has been reported that modification of the molecular structure allows for considerable control over the physical, optical and electronic properties of the phthalocyanines. Modification can be achieved both by the functionalisation of the aromatic macrocycle and also the incorporation of various metals into the central cavity of the macrocycle. Fine tuning of the physical properties of the phthalocyanine by added functionality is the main reason phthalocyanines are so versatile.

It should be noted that non-metalated phthalocyanines contain two isoindoline nitrogen's that are protonated while the other two are involved in the conjugated aromatic system. A split Q-band is therefore usually observed in non-metalated phthalocyanines as a result of their lower symmetry[41]. The central cavity of the aromatic ring can accommodate over seventy different metal and non metal ions, forming highly symmetrical, thermodynamically stable, fully delocalised dianions. Hence, metalated phthalocyanines show a single Q-band.

Incorporation of metal ions into the macrocycle can be used to manipulate the absorption spectra and hence can be advantageous when designing dyes for DSSC devices. A shift of *ca.* 100 nm in the Q-band can be observed between 620 and 720 nm as a function of metal size, coordination and oxidation state. Metals like magnesium(II), lithium (I) and zinc (II) show a bathochromic shift to λ_{max} around 670 nm while a deep red manganese phthalocyanine has been shown to give a Q-band of 808 to 828 nm[42]. Metals such as iron (II), cobalt(II) and ruthenium(II) that interact strongly with the macrocycle, shift the Q-band towards the blue region with λ_{max} of 630 to 650 nm.

The versatility of the macrocyclic core does not stop at the ability to accept different ions. As stated, substitution of the peripheral and nonperipheral protons with different functional groups also changes the phthalocyanines properties (Figure 1.10). The

addition of substituents can also be used to fine tune the adsorption Q-band and to increase solubility of the large complexes. The addition of substituents will affect the energy difference between the HOMO and the LUMO. If this energy difference is affected then a shift in light absorption is observed. A shift to a lower wavelength is known as a hypsochromic shift while a shift to a higher wavelength is known as a bathochromic shift.

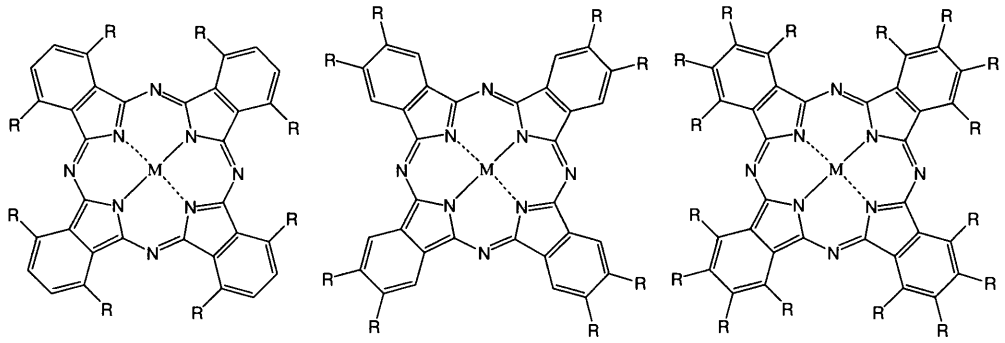

Figure 1.10, Nonperipheral (left), peripheral (centre) and hexadeca-substituted metallophthalocyanines[41]

It is reported that electron withdrawing substituents such as carboxyl and sulfonyl groups substituted in the peripheral positions cause a shift of the Q-band to the red region of the visible spectra, while electron donating groups such as amino, alkoxy or alkyl groups do not have much effect on the Q-band[43]. Non-peripheral substituents and octa-substitution of the phthalocyanines ring can cause stronger shifts in absorption spectra compared to the peripheral position. Phthalocyanines functionalised with eight alkoxy groups can lead to a maximum absoprtion in the visible spectrum at wavelengths exceeding 750 nm. By comparison, axial ligands coordinated to metalated phthalocyanines can influence the electronic structure of the macrocycle but only minor shifts in the Q-band are observed.

Extension of the π-system also has an influence on the absorption properties of the phthalocyanine. The extension of conjugation by the incorporation of an additional benzene ring into the isolindoline unit produces naphthalocyanines. This leads to red shifted Q-bands between 750-840[44] nm and increases by 20-30 nm per incorporated benzene ring with 2,3-anthracyanines producing a Q-band maxima between 830 and 935 nm[44]. However, these structures are very sensitive to light and often have to be prepared in darkness. The addition of a further isoindoline unit to phthalocyanine core ring structure produces super phthalocyanines, a macrocyclic core containing 5 isoindoline units, with further red shifted Q-band of 910-945 nm[45]. Strong shifts to the

red region of the spectra are achieved by oligomeric species of phthalocyanines with monomeric species absorbing at 664-701 nm, dimer species at 830-853 nm and trimer phthalocyanines absorbing around 944 nm[43].

1.3.3 Synthesis of Phthalocyanines

Disubstituted benzene derivatives such as phthalic acid, phthalonitrile, *o*-cyanobenzamide, phthalic anhydride, phthalimide, or diiminoisoindoline are used as phthalocyanine precursors with phthalonitrile (1,2-dicyanobenzene) used for the majority of laboratory synthesis (Figure 1.11) [46].

There are several synthetic routes to the formation of substituted phthalonitriles which can then undergo a cyclotetramerisation reaction to form the corresponding phthalocyanine derivative (Figure 1.11) [46]. Halogenated phthalonitriles can be used to form green phthalocyanine pigments when the peripheral and non-peripheral protons are substituted with chlorine atoms. Halogenated phthalonitriles are also important precursors to the synthesis of large numbers of substituted phthalocyanines with the limit being the extent of substituents that can be attached to the halogenated phthalonitrile. Iodinated, brominated and chlorinated phthalonitriles have been synthesised for further derivitisation by either post- or pre-cyclisation to form the substituted phthalocyanine. Brominated and mono iodinated phthalonitriles can be prepared from aminophthalonitriles while 4,5-diiodopthalonitriles have been synthesised by the iodination of phthalimide in fuming sulphuric acid[47]. Chlorinated phthalonitriles are prepared from the corresponding chlorinated anhydrides by conversion to the corresponding amide followed by a dehydration reaction to the nirtile. Halogenated phthalonitriles can also be synthesised by the cyanation of aromatic halides in the presence of copper cyanide producing yields of around 65 %[48,49].

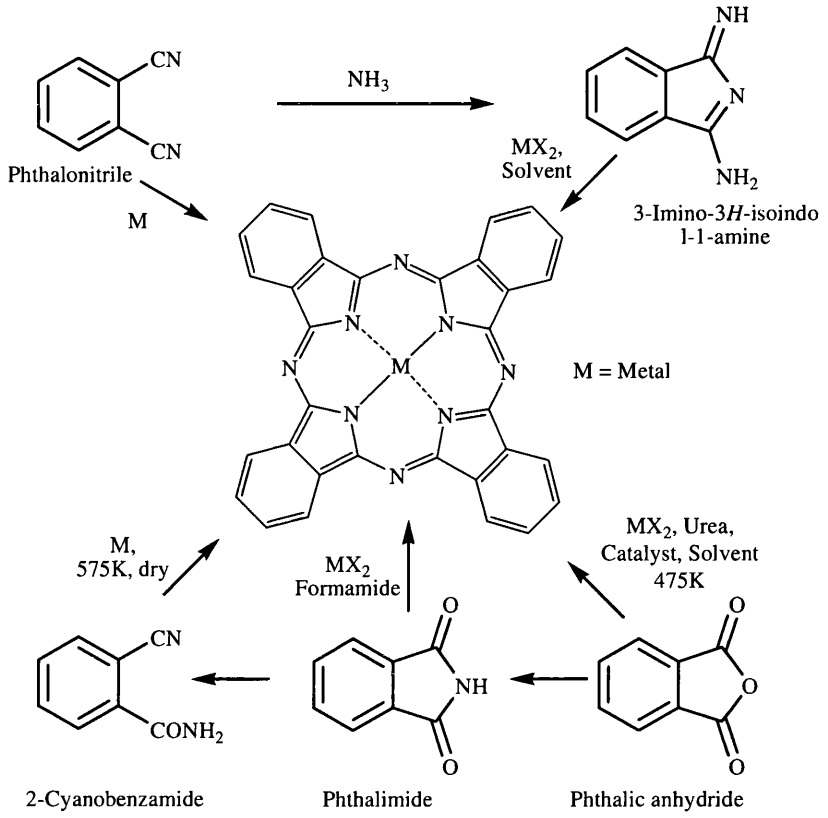

Figure 1.11, Synthetic routes to phthalocyanines.[46]

Substituted phthalocyanines can be prepared from halogenated phthalonitriles by various palladium cross coupling reactions between the desired functional groups and the halogenated phthalonitrile. For instance, halogenated phthalonitriles have been synthesised and used to prepare alkynylphthalonitriles, by palladium cross coupling of a terminal alkyne with a vinyl halide, and these, in turn, have been used to synthesis alkynylphthalocyanines[47,50,51]. The addition of alkynyl substituents can be used for the fine tuning of the adsorption band (Q band) as the addition of alkynyl groups results in a red shift of the Q band. Functionalised phthalonitriles have also been achieved by cross coupling reactions between halogenated phthalonitriles and derivitised boronic acids[52].

The Diels-Alder route[53] of preparing substituted phthalonitriles has also been investigated using 4,5-dicyanopyridazine which when subjected to a [4+2] cycloaddition between alkynes leads to the evolution of nitrogen. It has been reported that high reaction yields and the outstanding reactivity of the dicyanopyridizine towards the alkynes provides one pot synthesis of derivitised phthalonitriles that could only previously be obtained from long multistep syntheses.

The nucleophilic substitution of phthalonitriles and phthalocyanines is also possible with the nucleophilic substitution of poly-halogenated phthalocyanines with thiophenols in the presence of alkali in high boiling solvents[54].

Both metalated and non-metalated phthalocyanines can be formed by the cyclotetramisation of the substituted benzene derivatives described above. During the synthesis of metalated phthalocyanines the metal ion is believed to act as a template for the formation of the macrocycle and a kinetic organisational template effect is reported to take place. In this process the reactants wrap around the metal template, positioning the reactive sites in the correct orientation in close proximity to each other and the reaction continues spontaneously upon heating[55].

Non-metalated phthalocyanines can be synthesised from the cyclisation of diiminoisoindolines by the reaction of ammonia with phthalonitriles[41]. Diiminoisoindolines are then condensed under relatively mild conditions compared to the cyclisation of the phthalonitriles to form the corresponding free base phthalocyanine. Non-nucleophilic bases such as 1,8-diazabicyclo[5.4.0]undec-7-ene (DBU) can be used as an efficient reagent for cyclisation[41]. Free base phthalocyanines can be further prepared by reacting phthalonitriles with lithium in pentanol to form Lithium phthalocyanine. The metal can then readily be removed using a dilute aqueous acid[41].

The synthesis of octa- and tetra-substituted phthalocyanines is well documented but the synthesis of unsymmetrical phthalocyanines can be problematic[41]. Synthesis of unsymmetrical phthalocyanines can involve a mixed phthalonitrile cyclotetramerisation. This tends to lead to a mixture of products which cannot be readily separated using chromatographic methods because of their insolubility. However, it has been reported that target phthalocyanines can still be obtained in moderate yields by controlling the relative amounts of the phthalonitrile precursors[41]. Alternatively, the synthesis of substituted phthalocyanines with the introduction of substituents at particular positions can be achieved using a ring expansion reaction of sub-phthalocyanines[56].

Subphthalocyanines are composed of three isoindole units with a central boron atom (Figure 1.12). They have a 14 π-electron delocalized system with C_{3v} symmetry[57]. The

subphthalocyanine has a cone shaped structure and an axial halogen ligand (X in Figure 1.12) with the boron central atom in a tetrahedral orientation.

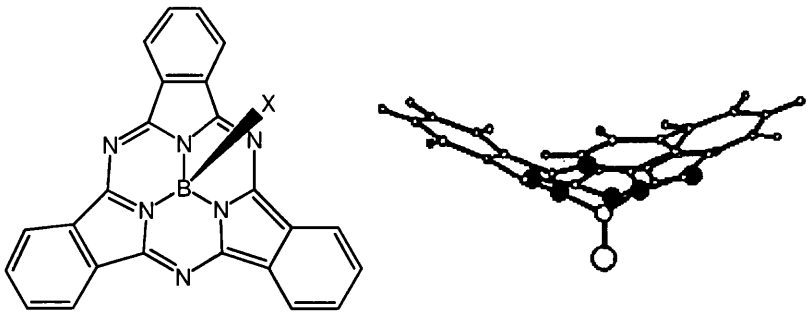

Figure 1.12, Structure (left) and crystal structure of a subphthalocyanine [58]

Subphthalocyanines were first synthesised by Ossko and Meller in 1972[59] by the reaction of phthalonitrile with boron tribromide or trichloride at 160 °C in 1-chloronaphthalene in a 20-40 % yield. They have attracted particular interest as intermediate materials for unsymmetrical phthalocyanine synthesis, in particular non-linear optics[60]. However, the synthetic use of subphthalocyanines has been hindered due to the difficulty in their purification due to reaction by-products which include polymerised phthalonitrile and mono and di-halogenated subphthalocyanines. Purification is also hindered by the subphthalocyanines solubility in trichloromethane, dichloromethane, acetone and dimethylformamide, but their insolubility in non-polar solvents such as hexane, which makes column chromatography difficult.

Higher yields of subphthalocyanines can be obtained by modified methods to that of Meller and Ossco. Treatment of the subphthalocyanine with sulfuric acid and re-precipitation in water can increase yields but is dependant on functional groups[61]. The use of phenylboron dichloride instead of a trihalogenated boron reagent has also been reported and this can prevent unwanted halogenation of the subphthalocyanine[61].

The synthesis of highly unsymmetrical subphthalocyanines has been achieved by the mixed condensation reaction with two different phthalonitriles in the presence of BCl_3 at 220 °C for 8 hours[62]. This gave a mixture of products and, by careful chromatography, the authors reported that the product was separated. Halogenated subphthalocyanines are achieved from the corresponding phthalonitriles and boron trichloride at 240 °C[63]. Torres *et al.* have reported that palladium cross coupling reactions on halogenated subphthalocyanines led to an unsymmetrical conjugated

phthalocyanine[63]. In addition ring expansion of subphthalocyanines can afford the desired unsymmetrical phthalocyanine[58] described in 1990 in a Japanese Patent. The subphthalocyanine is reacted with the appropriate 1,3-diiminoisoindoline derivative usually in a mixture of solvents (DMSO and 1-chloronaphthalene in a 1:2 ratio) then heated to 90 °C for 16 hours yielding the crude unsymmetrical subphthalocyanine. These workers reported that this method yielded higher yields than the equivalent statistical condensation method with products that were easily purified by column chromatography (Figure 1.13).

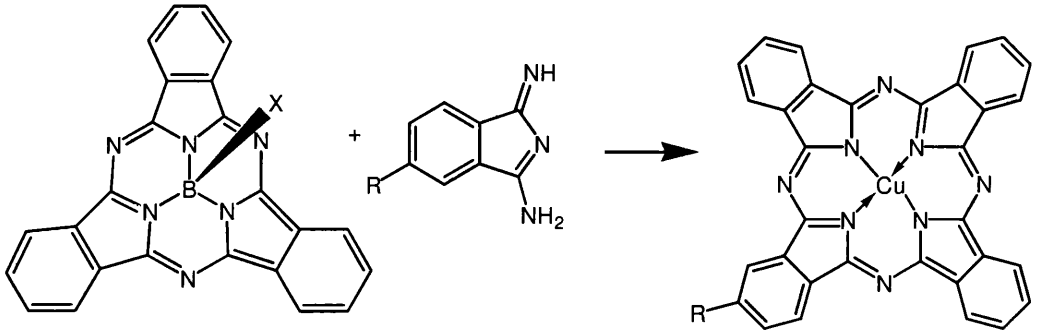

Figure 1.13. Synthetic pathway to unsymmetrical phthalocyanines.

1.3.4 Applications in DSSC devices

As stated previously, phthalocyanines are known for their intense absorption around 700 nm in the red/near-IR region. They have excellent photo, thermal and chemical stability which are desirable properties for long term stability and robustness[64]. The ability to fine tune the Q-band absorption and functionalise the phthalocyanine macrocyclic core to possess the desired functionality has made them attractive for a variety of applications such as cancer therapy[65], microelectronics[66] as well as photovoltaics[43]. Phthalocyanines have been successfully integrated into DSSC devices as well as solid state PV devices as they have relatively efficient charge carrier photogeneration because they can exibit both *n*- and *p*-type properties. Both copper and zinc phthalocyanines have been incorporated in to organic PV devices containing semiconducting polymers and/or acceptor carrier partners such as fullerenes[66-68].

Phthalocyanine sensitizers in DSSC devices have resulted in lower power efficiencies than those reported in polypyridyl complexes of the ruthenium based sensitizers with

power conversion efficiencies of 3.5 %[69] compared to 10-11 %[70]. Problems associated with dye aggregation on the metal oxide surface and lack of directionality in the excited state have until recently limited the phthalocyanines applications in DSSCs[71].

Nanocrystaline TiO_2 films have been sensitized by zinc, aluminium, ruthenium and titanium phthalocyanines[72-74] with the first symmetrical ruthenium phthalocyanine, substituted with methyl groups in the nonperipheral positions, synthesised in 1998[74]. The phthalocyanine was anchored to the semiconductor by axial pyridine 3,4-dicarboxylic acid ligands, which is essential for rapid injection of the electrons from the dye into the semiconductor. Apart from axial coordinated anchoring ligands, acid linkers have been directly attached to the macrocyclic core of the phthalocyanine. The main method of anchoring the dye is through anionic groups, generally carboxylic acids, but a variety of other anchors have been investigated[29,73,75]. Both carboxyl and sulfonic acid anchoring groups have been symmetrically substituted on the peripheral positions of zinc phthalocyanines with comparable efficiencies, 1.0 and 0.8 % respectively (Figure 1.14)[73]. The zinc phthalocyanine produced efficiencies of 1 % while substituting the central metal ion with aluminium reduced the device efficiency to 0.42 %[73]. This suggests that the metal ion also plays an important role in the sensitisation efficiency of the phthalocyanines.

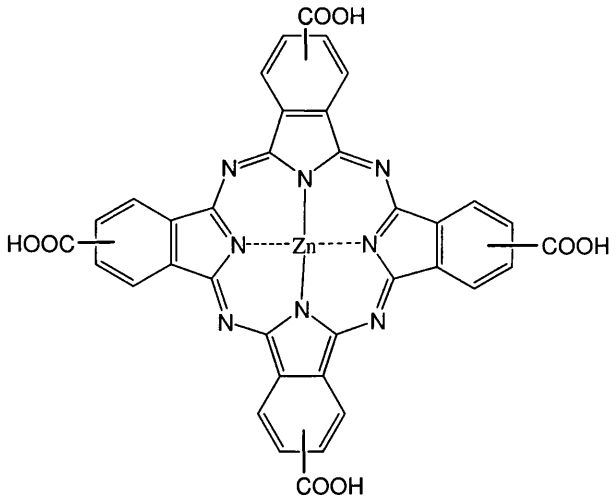

Figure 1.14, Structure of symmetrical carboxylated zinc phthalocyanine[73]

Other dye/oxide anchoring methods have been investigated without the use of traditional carboxylate linker groups. For instance, the semiconductor has been sensitised with phthalocyanines substituted with ester groups. Here the surface hydroxyl groups of the semiconductor were first deprotonated with a base. These sites then

reacted with the ester group forming surface bound dye *via* the dye carboxyls to form a new ester bond and hence anchoring the phthalocyanine to the semiconductor[75]. It was also found that the introduction of ether or alkyl linkers between the anchoring groups and the phthalocyanine macrocycle greatly reduces the incident photon-to-current conversion efficiency (IPCE) of the dye by 50 %[73].

It has been reported that phthalocyanines tend to aggregate on the surface of the semiconductor, which results in the deactivation of the dyes excited state and low sensitising efficiency[43]. Phthalocyanines can aggregate forming dimers, trimers and oligomers and that this can be responsible for the lack of solubility in many solvents. These aggregates also filter light, decreasing efficiency. In particular, the photochemical properties can be dramatically effected by the formation of aggregates in concentrated solutions[43]. Hence, the control over the formation of these aggregates is key to producing high efficiencies in phthalocyanine based systems. Sensitisation of TiO_2 films by phthalocyanines are therefore carried out at lower concentrations of 10^{-6}, 10^{-5} mol L^{-1} where the solution is dominated mostly by monomeric species.

Reduced aggregation and increased solubility and stability can be achieved by the addition of bulky substituents[76] such as alkyl or alkoxy groups substituted in the periphery and non-periphery positions as well as incorporation of axial ligands. This is because there are strong interactive forces between phthalocyanine molecules arising from $\pi - \pi$ interactions of the conjugated rings which leads to stacking of the molecules and hence low hydrophilicity and insolubility[77]. These substituents increase the distance between the planar macrocycle rings disrupting these forces. However, it has been reported that phthalocyanines substituted with long chain alkyl groups can lead to low photocurrent generation due to the energy loss through a non-radiative deactivation pathway[78]. Tyrosine substituents have also been used to reduce aggregation producing overall efficiencies of 0.54 %[79]. Tyrosine groups provide good solubility in solvents like ethanol which is the preferred solvent for sensitisation as the solvent is compatible with the semiconductor and favours adsorption of a non-aggregated monolayer[79]. *t*-Butyl groups have been proven to reduce aggregation between phthalocyanine units as reported by the synthesis of a titanium phthalocyanine[72] (Figure 1.15) which is anchored to the TiO_2 by an axial carboxylic acid with added solubility gained by substitution of bulky *t*-butyl on the peripheral position producing an efficiency of 0.2 %.

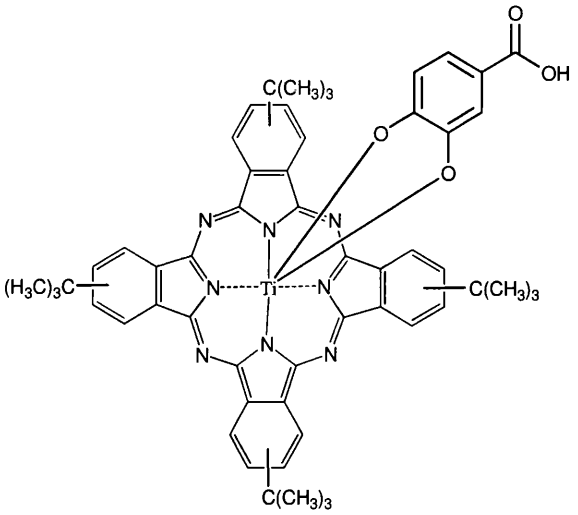

Figure 1.15, Structures of titanium[72] with coordinated axial ligands

To further increase efficiencies of phthalocyanines, unsymmetrical phthalocyanines have been synthesised to provide directionality of the electronic orbital in the excited state, with the aim of providing efficient electron transfer from the excited phthalocyanine dye to the TiO_2 conduction band. This electron injection occurs between LUMO of the phthalocyanine dye and the Ti 3d orbital[69]. The unsymmetrical nature of the phthalocyanine is reported to create a 'push-pull' system of electrons, with the solubilising groups acting as donors and the carboxylic acids the acceptor groups, which is believed to increase electron injection into the TiO_2[69]. The central atom is also reported to be key for effective photogeneration with the highest photoresponses found with zinc phthalocyanines.

Further work has been reported using zinc and ruthenium phthalocyanines substituted with alkoxy groups and anchored to the TiO_2 by carboxylate groups, separated from the chromophore by an ether linker[48]. The ruthenium phthalocyanine differed from the zinc counterpart by substitution with axial methylpyridine groups to reduce aggregation, producing an efficiency of 0.4 %. By comparison, the zinc derivative without the axial ligands produced an efficiency of 0.03 %[48] suggesting that the lower efficiency is a result of the increased aggregation. In addition zinc phthalocyanines with carboxylic acid anchoring groups separated from the macrocyclic core by phenyl groups instead of ether links, as well as the bulky *t*-butyl substituents have been reported (Figure 1.16)[64] with a power conversion efficiency of this compound is 0.57 %.

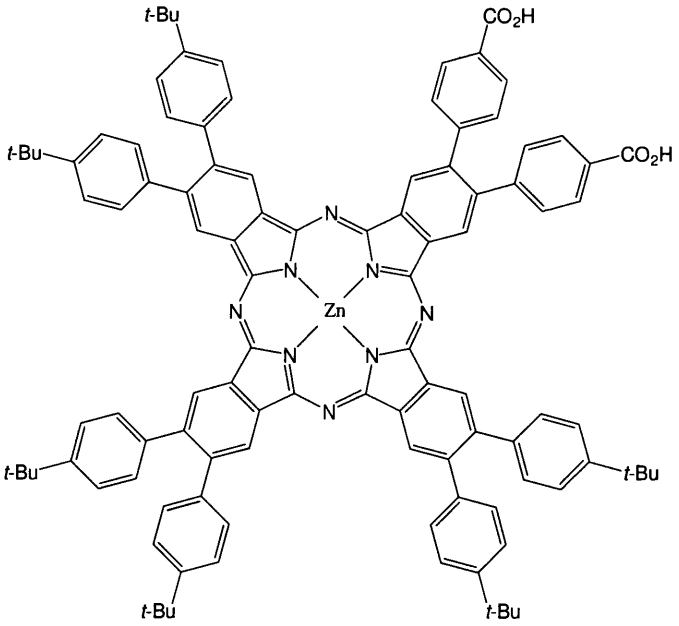

Figure 1.16. Zinc phthalocyanine (ZnPc) synthesised by S. Eu *et al.*[64].

The most successful phthalocyanine dyes for DSSC to date (Figure 1.17) are composed of pendant anchoring groups which have been reported to be essential for anchoring the dye to the surface of the TiO_2 and providing efficient electron injection[80]. The phthalocyanines have either three bulky alkyl groups or alkoxy groups which are donor groups, providing directionality in the charge transfer process, which then promotes charge injection. The bulky groups also help to prevent aggregation of the molecules which would otherwise filter light and decrease efficiency. Higher efficiencies of 3.05 %[48] were observed for the *t*-butly solubilising groups than the alkoxy groups on PCH003 (1.13 %)[80].

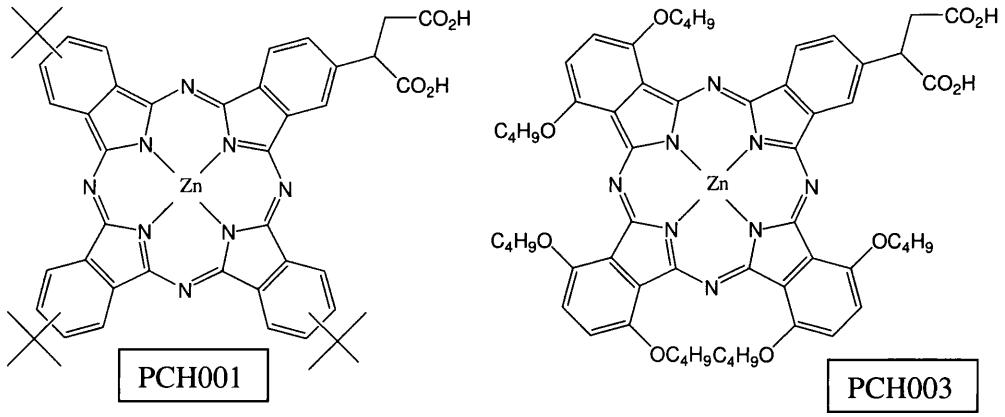

Figure 1.17. Substituted, unsymmetrical ZnPc; PCH001[80], PCH003[81].

Zinc phthalocyanine, PCH008 (Figure 1.18) has recently been reported, which has extended the molar extinction coefficient of the Q-band absorption by extending the π-conjugation and has achieved efficiencies of 2.35 %[82]. This has a reduced efficiency compared to PCH001 which must be linked to the extended conjugation on the anchoring group.

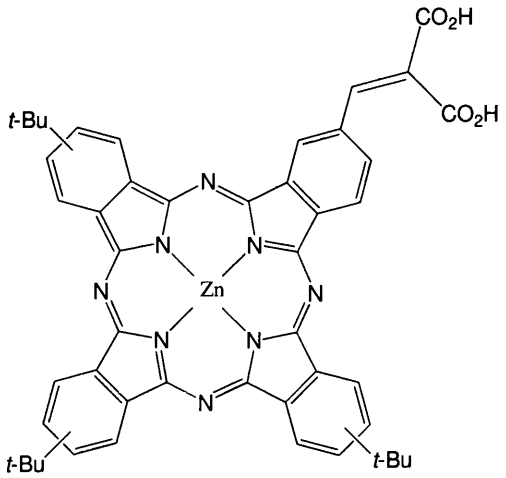

PCH008

Figure 1.18. Molecular structures of unsymmetrical phthalocyanine PCH008[82]

The zinc phthalocyanine dye, TT1 (Figure 1.19), has produced an efficiency of 3.5 %[83]. The phthalocyanine contains one carboxylic acid anchor instead of the pendant acids of PCH001, PCH003 and PCH008.

To further increase light harvesting, co-sensitisation of dyes that absorb different parts of the solar spectrum has been attempted but studies have shown that the resulting efficiency is usually somewhere in between that of the individual dyes. This is believed to be because of competition for space on the metal oxide surface leading to a lower coverage of each dye. However, a combination of three different organic dyes has been reported producing a higher efficiency of 6.5 %; more than that of the individual dyes, which in this case is believed to be due to synergistic effects of the dyes, where aggregation is not favourable and a more compact monolayer could have formed. An increased efficiency is also observed with the co-sensitisation of an organic dye JK2 with zinc phthalocyanine TT1 dye with a total power conversion efficiency of 7.74 %[83] (Figure 1.19).

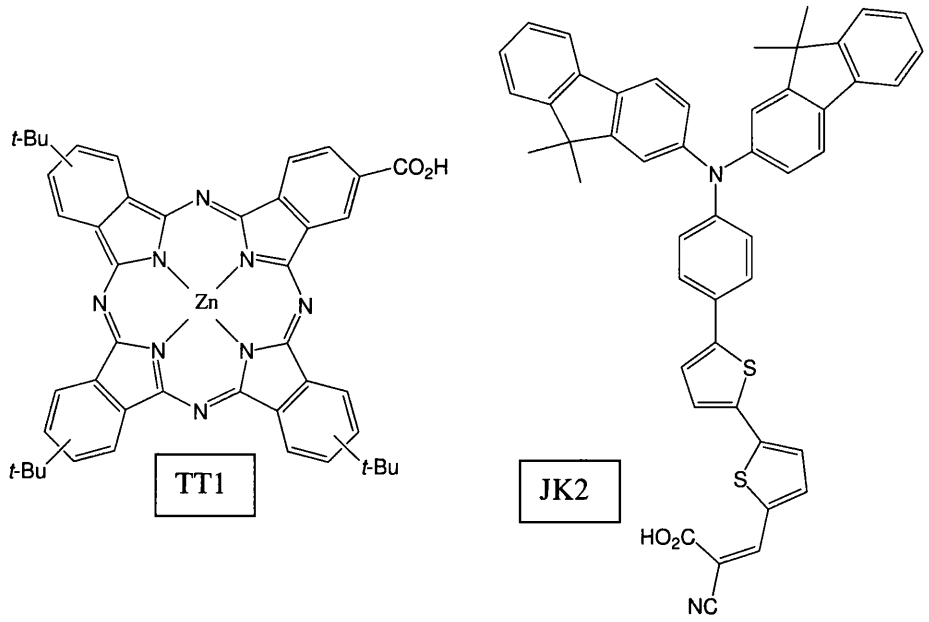

Figure 1.19. Structure of substituted, unsymmetrical ZnPc TT1 and the JK2 dye[83]

Co-sensitization has also been reported with chenodeoxycholic acid[84] (Figure 1.20) as the addition of this compound prevents aggregation between dyes molecules, which is believed to improve electron injection and the J_{sc} value. Phthalocyanine dye TT1 has also been co-sensitised with chenodeoxycholic acid with an increase in 0.6 % efficiency observed. As discussed earlier for co-adsorbed species, it has been reported that both molecules compete for the TiO_2 surface sites and hence reduce the amount of dye coverage on the semiconductor was observed.

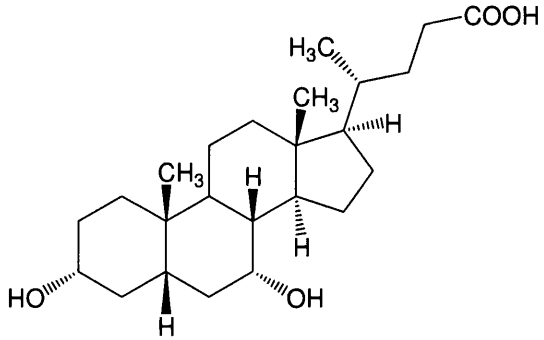

Figure 1.20, Structure of chenodeoxycholic acid

1.4 Commercialisation of DSSC

There are several factors affecting the production of DSSC devices for commercialisation. Firstly, the sheet resistance of the TCO substrate is relatively high and therefore limits the solar cell width to less than 1 cm, larger areas lead to loss of

efficiency and fill factor. Thus, modular systems consisting of several interconnected cells have been investigated[85]. This increases the photo-voltage but keeps the current low, which prevents the drop in efficiency. Incorporation of a conducting metallic grid to link the modules is problematic due to the liquid electrolyte, which contains iodine and iodide in an organic solvent, which in turn corrodes metal materials. This also means that good conductors like silver can not be used unless the cell is sealed carefully. For a continuous roll-to-roll commercial process, the glass substrates need to be replaced with transparent polymer substrates such as ITO-coated poly(ethylene terephthalate) (PET).

Continuous module fabrication of DSSCs has been proposed by Grätzel[85] and is shown in the schematic below (Figure 1.21). The TCO substrate is deposited on the substrate using chemical vapour deposition (CVD) which is then shaped into the cell areas by laser scribing. The nanoporous TiO_2 (anatase) semiconductor is then screen printed on top of the TCO. A porous insulating layer, TiO_2 in the rutile phase, is then printed and shaped on top of the semiconductor. The insulator prevents short circuiting by separating the counter electrode and the photoelectrode. The insulator can also act as a reflector that reflects light back into the photoelectrode increasing efficiency. The porous counter electrode is then applied over the top of the insulating layer. At this point, the layers are heat treated or sintered to remove any binders, additives and solvents. The dye is then adsorbed through the porous layers, onto the photoelectrode with the electrolyte then added to fill the holes of the porous later. The connectors are then deposited and the whole cell sealed. The advantages of this design are that only one TCO layer is required reducing production costs. The insulator can also act as a reflector. Due to the porous nature of the deposited layers, there is no free flowing layer of electrolyte and the counter electrodes have increased surface area, which increase catalytic activity, increasing efficiency for the electron exchange with the electrolyte. A series connection can be achieved by overlapping the counter electrodes with the back contacts of the adjacent photoelectrodes. Using this approach the printing of the semiconductors is a continuous process. An efficiency of 7 % has been achieved using a modular system consisting of 12 interconnected cells with a total cell area of 112 cm^2[2,86].

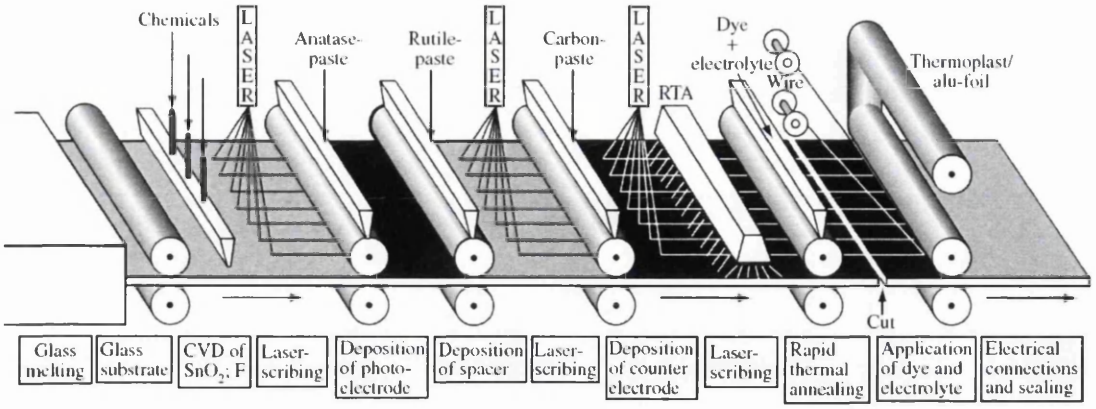

Figure 1.21. A continuous process for the fabrication of DSSC modules[10]

As discussed in Section 1.2.4, ruthenium based dyes are expensive to purchase and hence the quantities required for a role to role process would significantly increase the production costs for the photovoltaic device. This introduction has discussed the use of organic and inorganic alternative dyes for sensitisation of wide band gap semiconductors in particular phthalocyanines, which are believed to be cheaper to produce, absorb in the red region of the visible spectra and are stable, unlike the organic counterparts. This work will therefore focus on the design synthesis and testing of phthalocyanines for sensitisation in DSSC devices.

Chapter 2

Synthesis of Halogenated and Functionalised Phthalonitriles

2.1 Introduction

Phthalocyanine dyes require specific functionality in order to function efficiently as sensitizers in DSSC devices. Phthalonitriles are key precursors to phthalocyanines and they can be adapted to contain the desired DSSC functionality. This can be achieved through palladium cross coupling reactions with halogenated phthalonitriles, as discussed in Section 1.3.3. This chapter describes the synthesis of halogenated phthalonitriles followed by the design of tailor-made derivitised phthalonitriles for subsequent phthalocyanine synthesis.

2.2 Chlorinated Phthalonitriles

4,5-Dichlorophthalonitrile **(4)** was prepared according to a modified literature procedure shown in Figure 2.1[87], starting from the corresponding chlorinated acid firstly, by a dehydration reaction with acetic anhydride to form the anhydride **(1)**. The IR data showed the conversion to the anhydride **(1)** by the presence of the carbonyl functional groups at 1859 and 1781 cm^{-1}. Nitration of the anhydride was achieved by an adapted literature procedure[87], using urea as a low toxic source of nitrogen (as opposed to formamide), in a sealed autoclave system. It was found that 1.5 equivalents of urea were required to form the imide **(2)**. This conversion was monitored by IR spectroscopy with a shift in carbonyl groups to 1778 and 1711 cm^{-1} and the appearance of an NH stretch at 3225 cm^{-1}. Conversion to the amide **(3)** was then achieved by a base catalyzed nucleophilic addition using ammonium hydroxide, which was confirmed by mass spectrometry with an $M^{+}Na$ 254.9. The dehydration reaction of the primary carboxamido functionality into the nitrile is well documented[88] and can be achieved by many effective dehydrating agents. The dehydration of the amide, in this situation, was achieved by the treatment of the phthalamide in anhydrous dioxane and pyridine with trifluoroacetic anhydride. The off-white product was recrystalised from methanol and identified by IR. The absence of the carbonyl signals of the amide was observed along with the appearance of a signal at 2234 cm^{-1} confirming the presence of the nitrile **(4)** functional group.

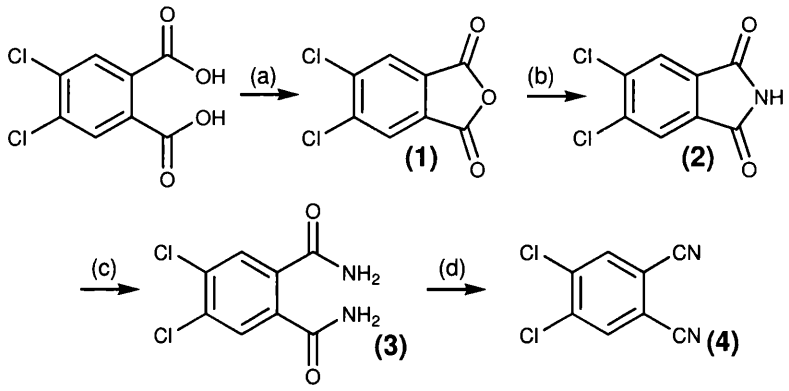

Figure 2.1, Synthetic scheme to the formation of 4,5-dichlorophthalonitrile (**4**)
Conditions: (a) Acetic anhydride, reflux, (b) urea, 200 °C, (c) NH_4OH, (d) anhydrous pyridine, phosphorus oxychloride, 0 °C

2.3 Iodinated Phthalonitrile

Mono-substituted phthalonitriles can be prepared from mono-iodinated phthalonitriles which, in turn, can be prepared from aminophthalonitriles according to the literature procedure[89]. 4-Aminophthalonitrile was reacted with sodium nitrate forming a diazonium salt, which was then reacted with a solution of potassium iodide forming 4-iodophthalonitrile (**5**) in high yield. Mass spectrometry confirmed the formation of the target molecule with an m/z of 254.94, ^1H and ^{13}C NMR also corresponded to literature[89].

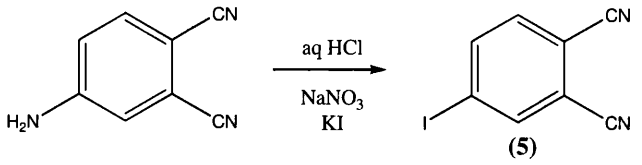

Figure 2.2, Synthetic pathway to 4-iodophthalonitrile (**5**)[89]

Previously, polyiodinated aromatics have been prepared from diazotization / iodination of iodinated anilines[90], which must be partially iodinated and also by the Jacobsens reaction, which involves the migration of iodines from iodinated aromatics to form mixtures of more or less iodinated products[91]. However, these methods have limited scope as they require uncommon starting materials and must already be partially iodinated. Diiodinated phthalonitriles for octa-substituted phthalocyanines have been previously prepared by direct aromatic iodination using molecular iodine[47]. This requires an oxidizing agent to be present, such as fuming sulfuric acid, to convert the iodine to a more powerful electrophile. The direct iodination of phthalimide has been

achieved by Leznoff *et al.*[47] with the aid of 30 % fuming sulfuric acid giving primarly the 4,5-diiodinated product **(6)** see Figure 2.3.

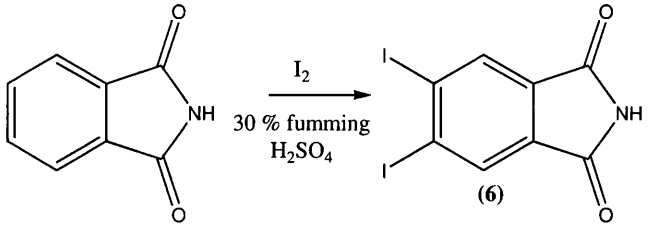

Figure 2.3, Synthetic pathway to 4,5-diiodophthalimide **(6)**[47]

4,5-Diiodophthalimide **(6)** was prepared using the conditions reported by Leznoff *et al.*[47]. Phthalimide was added to 30 % fuming sulphuric acid with iodine at 80 °C. The pale yellow solid was Soxhlet extracted for 48 h in acetone (1 L). After the addition of water to the acetone, the solvent was concentrated to a third of it's volume to give a yellow solid of the iodinated phthalimide which was characterised by ^{1}H NMR, ^{13}C NMR and low resolution EI mass spectrometry. A molecular ion of 398.9 was apparent in the low resolution EI^{+} mass spectrum, corresponding to the diiodinated phthalimide **(6)**. However a molecular ion (M^{+}) of 524.7 with relative intensity of 3 % was observed which is believed to be triiodophthalimide. This was not reported by Leznoff in the original synthesis[47]. After inspection of ^{1}H NMR, 4,5-diiodophthalimide **(6)** was identified by the resonance at 8.24 pm corresponding to the two aromatic protons and a broad singlet at 11.43 ppm due to the imide functional group.

Impurities were also detected in the ^{1}H NMR. After analysis of the starting material, the signals at 7.54, 7.57, 7.85, 8.13 and 8.33 ppm were ascribed to impurities in the starting material, phthalonitrile, while the resonance at 8.18 ppm were due to the iodination of the imide at the 3 and 4 position as reported in the literature[47]. A relatively low yield of 12 % was obtained, which differed from the 75 % yield reported in the literature[47].

Figure 2.4, Iodine sublimation during direct iodination of phthalimide

A possible reason for this significantly reduced yield can be attributed to the sublimation of iodine on the reaction vessel walls upon heating, preventing the deposited iodine from participating in the reaction (Figure 2.4). To compensate for this, the reaction was repeated but the addition of the iodine was added slowly over a period of four hours. This had no affect on improving the yield. To further increase the yield, excess iodine was added but again no improvement in yield was seen which could again be attributed to the sublimation of iodine on the reaction vessel.

Due to the low yielding nature of the electrophilic iodination of the imide, the same reagents were then placed in an in-house designed PTFE vessel within a Hastelloy™ stirring, sealed autoclave (see Figure 2.5). The reagents were then heated to 80 °C for 24 hours. The sealed system of the autoclave was used to prevent the sublimation of the iodine and encourage more of the iodine to react with the imide to increase yields. After removal of excess iodine, the solution was Soxhlet extracted using acetone for 48 hours and filtered. The solid obtained corresponded to 4,5-diiodophthalic acid formed as a by product by the hydrolysis of the iodinated phthalimide as reported by Leznoff [47]. This was confirmed by a mass spectrometry peak at 416.8 $[M-H]^-$. The solvent was concentrated to a third of its volume to give a bright yellow solid. Here an increased yield of 52 % (relative intensity of 100 %) was observed compared to the 12 % yield obtained from the open reaction conditions. A higher concentration of the triiodo species (relative intensity 11 %) was also identified under these reaction conditions, which was identified using mass spectrometry.

It has been reported that the use of the more powerful oxidizing agent can be used to achieve direct iodination[90] instead of fuming sulfuric acid. This would be advantageous

as fuming sulfuric acid is not only difficult to handle due to the inherent corrosive nature of the acid which resulted in the commissioning of specialized equipment (the autoclave) but is becoming more commercially limited.

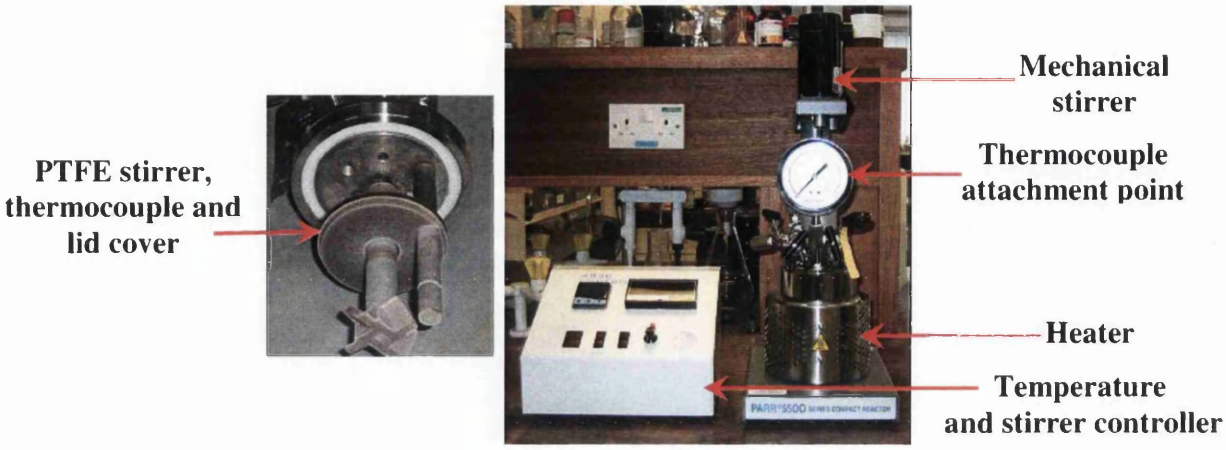

Figure 2.5. PTFE liner and automated stirring autoclave

On consulting the literature, it has been reported that periodination can be achieved by mercuration followed by iododemercuration with a triiodide anion, but this process takes two weeks to give yields of 40 % and significant impurities are reported as well as the inherent mercury toxicity[92]. Periodic acid has also been investigated to directly iodinate unactivated aromatic compounds such as benzene, nitrobenzene and chlorobenzene[90]. In this thesis, this method was also investigated to synthesize 4,5-diiodophthalimide **(6)** as large quantities of the imide were required for further synthesis of modified phthalocyanines.

The direct iodination of phthalimide was achieved in a solution of concentrated sulphuric acid, periodic acid and iodine. The iodinations were performed in a 3:1 mix of iodine to periodic acid ***(Eqn. 1)***.

$$H_5IO_6 + 3\,I_2 + 7\,H^+ \longrightarrow 7\,I^+ + 6\,H_2O \qquad (Eqn.\ 1)$$

In this reaction, the iodine is converted to I^+ which is a more powerful electrophile than I_2 alone. This reaction occurs as shown in Eqn. 1 and involves an inverse disproportionation reaction. The iodine in the periodic acid exists in a 7^+ oxidation state which combined with molecular iodine I^0 and acid to form the reactive species I^+. A two fold excess of I^+ was added to the reaction as it is reported to improve yields[90]. The

aromatic compounds were then added after the formation of the electrophile and heated to 80 °C for 24 hours. The ^{1}H NMR showed a mixture of unreacted imide and 3,4-diiodophthalimide as discussed earlier. This led to an 22 % crude yield of the imide **(6),** which is higher than that reported for the open system using 30 % fuming sulphuric acid. Sublimation of the iodine was also believed to be a contributing factor to the low yield here, therefore to try and compensate for this eight equivalents of I^+ were added to phthalimide.

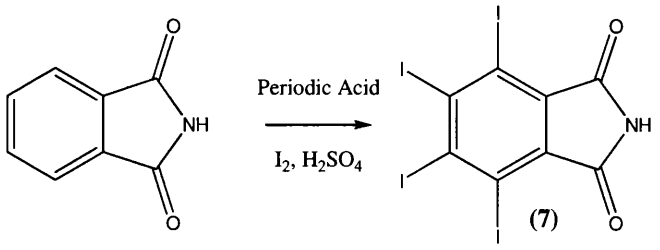

Figure. 2.6, Synthesis of tetraiodophthalimide (**7**)

In this attempt, a bright yellow solid was obtained in 75 % yield and was analyzed by a combination of ^{1}H NMR, ^{13}C NMR, EI^+ mass spectrometry, IR and CHN. It became apparent that iodination had occurred at all four positions of the aromatic ring, forming tetraiodophthalimide **(7).** The imide **(7)** does not contain any aromatic protons on the aromatic ring, which is consistent with the ^{1}H NMR. A resonance at 11.96 ppm is due to the imide proton, while four resonances are observed in the ^{13}C NMR due to the symmetry of the molecule. The C3 and C6 carbons are observed at 103.89 while the C4 and C5 carbons are observed at 134.88 ppm. The resonance at 135.51 (C2) is due to the quaternary carbon with the carbonyl signal observed at 165.16 (C1) ppm. High resolution EI^+ gave an M^+ of 650.6175 (calculated at 650.6181), which corresponds with the tetraiodinated imide **(7)**.

An autoclave synthesis of 4,5-diiodophthalimide **(6)** was attempted using the periodic acid method, 4 equivalents of I^+ and sulfuric acid were placed in the same PTFE lined autoclave as discussed earlier. The reaction was heated to 80 °C for 7 hours. Under these conditions, a mixture of iodinated imides along with 38 % of tetraiodophthalimide was synthesized. Pure tetraiodophthalimide **(7)** was obtained by sublimation of the crude compound at 200 °C. On consulting the literature, tetra-iodination of aromatic rings have previously been reported, with tetraiodophthalic anhydride synthesized using 60 % fuming sufuric acid with molecular iodine, at 65 °C. Tetraiodophthalic anhydride **(8)** was therefore attempted using the periodic acid method, using the open reaction

conditions employed for the tetraiodophthalimide (**7**) preparation. The reaction proceeded in good yield with no proton resonances in the ^{1}H NMR whilst four resonances were observed in the ^{13}C NMR. An HRMS EI^{+} was observed at 651.6022 (calculated 651.6021) confirming the presence of the tetraiodinated anhydride (**8**).

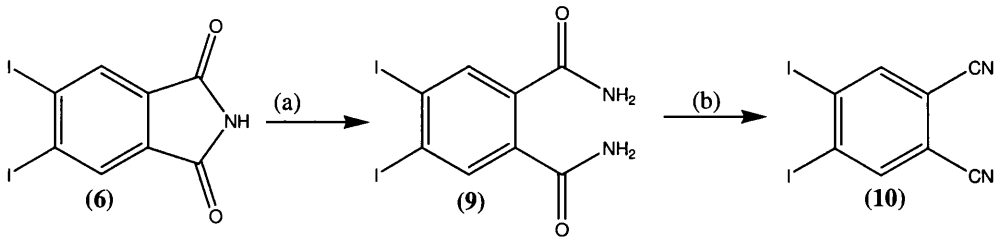

Figure 2.7, Synthesis of 4,5-diiodophthalonitrile (**10**), (a) NH_4OH, reflux, (b) dioxane, pyridine, trifluoroacetic anhydride, 0 °C

The formation of 4,5-diiodophthalonitrile (**10**) was then achieved *via* a similar synthetic scheme as the dichlorinated (**4**) species. Thus, the diiodophthalimide (**6**) was converted to the amide (**9**) without further purification, as pure diiodoamide (**6**) was formed after the base catalyzed nucleophilic addition using ammonium hydroxide (Figure 2.7).

The conversion of the tetraiodophthalimide (**7**) to the tetraiodinated amide was attempted in the anticipation of synthesizing tetraiodophthalonitrile. Palladium cross coupling reactions could then be attempted in the 3, 6 positions along with the 4, 5 positions. Cyclisation of the tetraiodophthalonitrile could also be attempted, producing novel phthalocyanines with possible applications as pigments. Conversion to the amide however was not achieved using the same reaction conditions as for the synthesis of the diiodophthalamide (**9**). After inspection of both ^{1}H and ^{13}C NMR as well as IR spectroscopy and mass spectrometry, it was clear that no change had occurred even after long reaction times. This could be due to the insolubility of the imide (**7**) observed in ammonium hydroxide solution. The conversion of tetraiodophthalimide (**7**) to the corresponding amide was also attempted using THF as the solvent. Here, the reaction proceeded in the presence of ammonium hydroxide along with a steady stream of $NH_{3(g)}$ but no conversion occurred as there was no evidence to indicate the target molecule in the IR or NMR spectroscopy, or the mass spectrometry. Instead, in the mass spectrometry, a molecular ion of M^{+} 651.6 was observed corresponding to the tetraiodophthalimide (**7**). This could be the result of the oxidation of the amide to the imide, followed by electrophilic substitution of iodine.

Due to the unsuccessful conversion of the tertaiodinated imide, direct iodination of the amide was attempted using the periodic acid method in both open and closed systems using the same reaction conditions as the tetraiodination of the imide. On analysis of the data, iodination had occurred, but the data showed conversion of the amide back to the imide (**7**). Mass spectrometry indicated that there was a mixture of unreacted amide and a mixture of di, tri and tetraiodinated phthalimide with an M^+ of 651.5. The direct iodination of phthalonitrile was therefore attempted using the same conditions as for iodination of the imide. Analysis was carried out using ^1H and ^{13}C NMR. The ^1H NMR showed resonances at 8.24 and 11.68 ppm. These signals correspond to aromatic protons and an N-H functional group. This indicated that conversion to the imide had occurred. There was no evidence of the presence of the nitrile functional group in the IR spectrum. Mass spectrometry again showed a molecular ion of 651.6 corresponding to the tetraiodinated imide (**7**). The peak at 253.7 could have been due to monoiodinated phthalonitrile but there was no other evidence to support this.

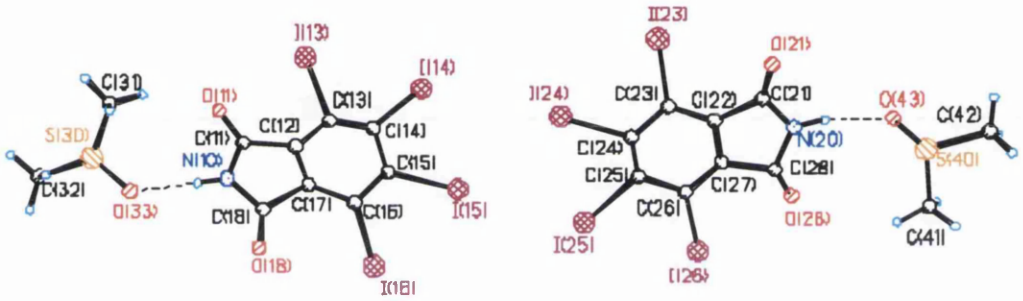

Figure 2.8. Crystal structure of tetraiodophtalimide (**7**)- The contents of the asymmetric unit (only one disorder component is shown for each DMSO molecule).

X-ray crystallography showed that the tetraiodophthalimide (**7**) was present (Figure 2.8). The crystals were grown in DMSO and showed the stacking of the imide surrounded by the DMSO molecules. These observations are supported by a previous report of the iodination of benzonitrile by D. Mattern[90]. In this prior work the cyano group was partially hydrolysed to the amide in the process. In the case of phthalonitrile, the cyano groups are in the 1,2-positions and so full hydrolysis has occurred to form the tetraiodinated phthalimide (**7**).

Figures 2.8 and 2.9 show the crystal structure and packing diagrams for the tetraiodophthalimide in the presence of DMSO solvation molecules. The data show that the flat benzene ring structure forms a stacking sequence of layers of the imide due to π-interactions, accounting for the insolubility and hence the problematic purification of

this compound. Figure 2.9 also shows the stacking sequence between the tetraiodophthalimide molecules and the DMSO interactions.

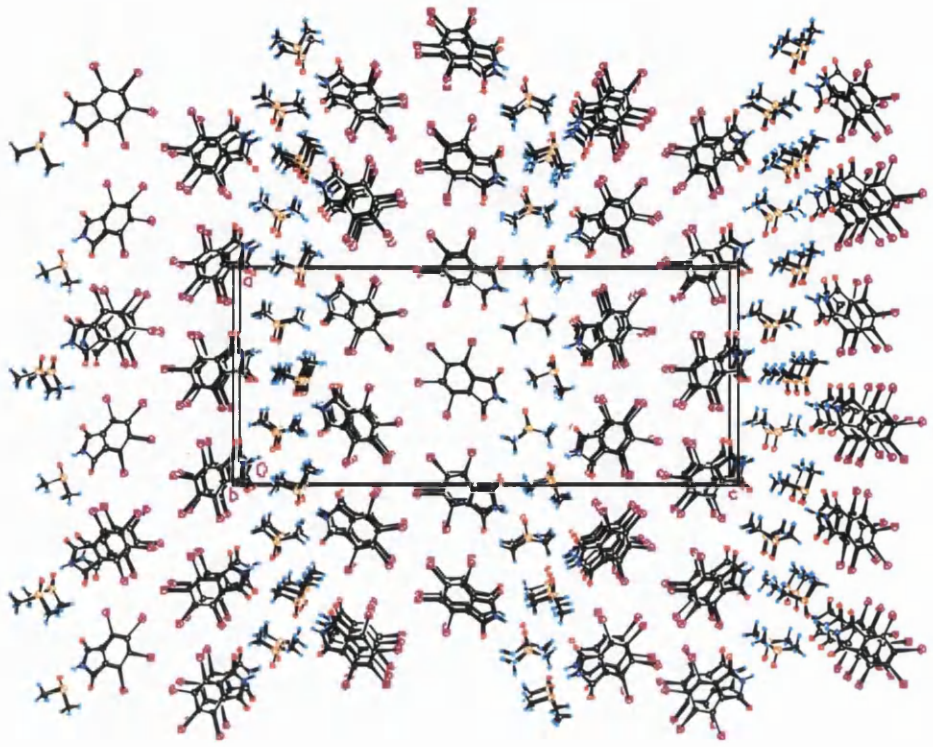

Figure 2.9. Crystal packing diagram for tetraiodophthalimide

Due to the unsuccessful synthesis of tetraiodophthalonitrile, direct cyclisation was attempted using tetraiodophthalic anhydride (**8**). Initially, the anhydride (**8**) was heated to 200 °C in chloronaphthalene with urea, sodium sulfate and zinc chloride but this resulted in decomposition products of the imide also producing yellow needles, which have not yet been identified. The bake process was then employed by reacting the anhydride (**8**) with urea and ammonium molybdate, but again only decomposition products were observed. Due to the unsuccessful cyclotetramisation of the anhydride (**8**), the attempted cyclotetramisation of the imide (**7**) was then attempted but again no target molecule was observed, neither that of any partial cyclisations. On consulting the literature, it was found that attempts to cyclise tetraiodophthalic anhydride had been unsuccessful with only partial cyclisation occurring producing a green residue. It was reported that the formation of iodinated phthalocyanines are not favorable because of their comparatively positive Gibbs free energy of formation compared to that of brominated phthalocyanines.

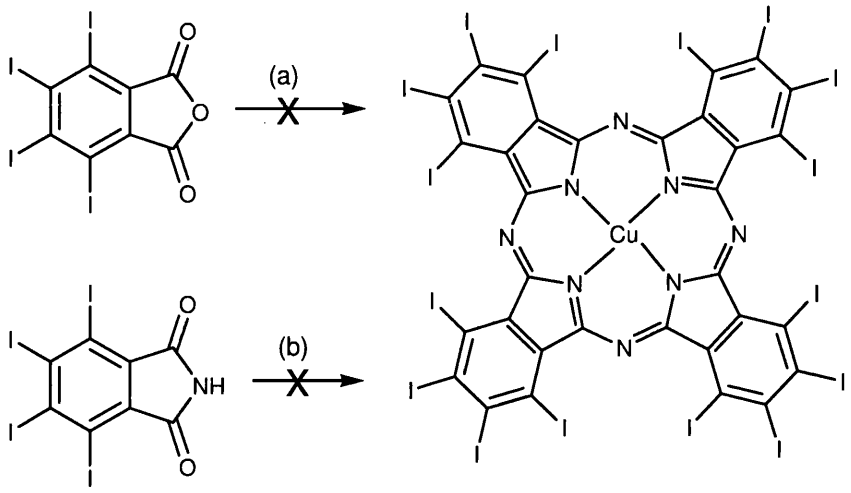

Figure 2.10, Attempted synthesis of iodinated phthalocyanine, (a,b) 200 °C, chloronaphthalene, urea, sodium sulfate and zinc chloride, (a,i) urea, ammonium molybdate, (b) 200 °C, chloronaphthalene, urea, sodium sulfate and zinc chloride

2.4 Redox Functional Groups

Ferrocene and its derivatives have been incorporated within the molecular structure of organic colourents or in combination with organic dyes (Figure 2.11) to stabilize systems against the very reactive singlet oxygen species that can form during degradation reactions[93]. Singlet oxygen is known to play an important role in the photodegradation of organic dyes and arises from the interaction of the triplet state of the dye and molecular oxygen. The introduction of effective singlet oxygen and triplet state quenchers such as ferrocene into dye systems has been reported to improve photostability of dyes without drastically affecting colour and intensity[93]. In this thesis, the functionalisation of phthalocyanines by binding of redox active moieties such as ferrocene, either directly attached to the nitrile or with an acetylene spacer, to the macrocycle core structure has been investigated.

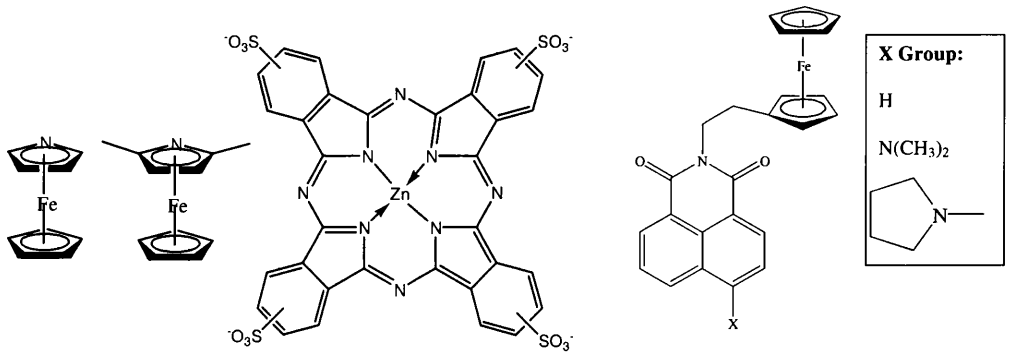

Figure 2.11. Ferrocene-naphthalimide dyes[93] and a sulfonated phthalocyanine stabilized by ferrocene derivatives[94].

2.4.1 Synthesis of Ferrocene Precursors

The formation of 1-ethynylferrocene **(13)** from ferrocene carboxaldehyde **(11)** was carried out in accordance with the literature procedure[95] (Figure 2.12).

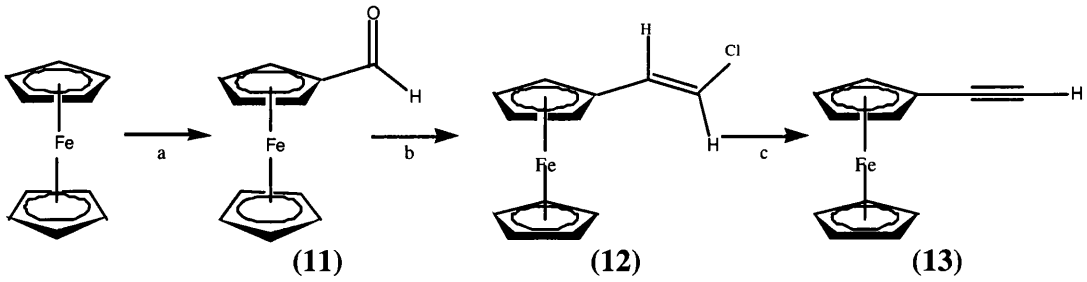

Figure 2.12, Preparation of 1-ethynylferrocene, (a) THF, n-BuLi, DMF, (b) THF, chloromethyltriphenylphosphonium chloride, t-BuOK and (c) t-BuOK, reflux.

In this synthetic procedure, ferrocene was monolithiated in dry THF with *n*-BuLi and then quenched with anhydrous DMF. Extraction included the addition of an acidified aqueous layer which allowed a higher yielding extraction from the organic crude reaction mixture. The red solid of the carboxaldehyde **(11)** was characterized and the data found in accordance with the literature. Analysis of the ^{1}H NMR confirmed the aldehyde was present with a signal at 9.93 ppm due to the proton on the aldehyde functional group. The two resonances at 4.56 and 4.78 ppm were due to the α- and β-resonances, respectively. The signal at 4.20 ppm with an integration of five is characteristic of the unsubstituted bottom cyclopentadiene ring of ferrocene.

The synthesis of 2-chloro-1-ferrocenylethene **(12)** was carried out by in accordance with a literature method[95] using a Wittig reaction between the chloromethyltriphenylphosphonium ylide and ferrocenecarboxaldehyde **(11)**. This produced both the E and Z isomer, which corresponded with the literature[95]. The Z and E isomers are easily distinguished in the proton and carbon spectra. ^{1}H NMR showed resonances at 6.07 and 6.39 ppm due to the *Z* isomer while the doublets at 6.20 and 6.57 ppm are due to the *E* isomer. The characteristic splitting of a monosubstituted ferrocene was also observed with a resonance corresponding to the unsubstituted cyclopentadiene ring at 4.11 ppm. The synthesis of 1-ethynylferrocene **(13)** was achieved by hydrochloric acid elimination from 2-chloro-1-ferrocenylethene **(12)** using potassium *t*-butoxide. Conformation of the synthesis of target compound **(13)** was obtained from ^{1}H NMR with a singlet at 2.74 ppm corresponding to the alkynyl functional group which

was confirmed with a molecular ion of 210.0132 found in the mass spectrum. A reduced yield was observed due to the formation of the bi-product 1,4-diferrocenyl-1,3-diyne (Figure 2.13) as reported in the literature[95], which was formed by a side reaction, between two terminal alkynes in the presence of base and air. The by-product was separated from the desired alkyne **(13)** by column chromatography, eluting in ethyl acetate and was identified by a molecular ion of 420.0289 in the mass spectrum.

Figure 2.13, 1,4-diferrocenyl-1,3-diyne[95]

1,1'-Dibromoferrocene **(14)**, is a precursor to many substituted ferrocenes and was synthesized in this thesis to prepare ferrocene functionalized phthalocyanines. 1,1'-Dibromoferrocene was therefore prepared on a relatively large scale using a modified literature procedure, yielding the product in 77 % yield, higher than the 60 % reported in the literature[96,97,98] (Figure 2.14).

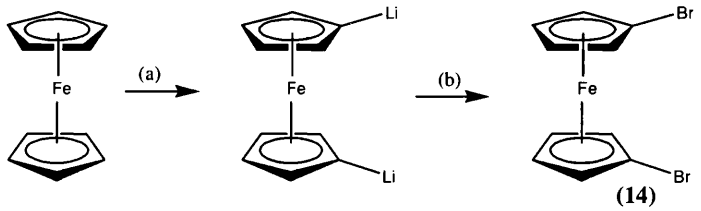

Figure 2.14, Synthesis of 1,1`-dibromoferrocene (14)[98], (a) n-BuLi, TMEDA, hexane, (b) -78 °C, 1,1,2,2-tetrabromoethane

In this synthetic procedure ferrocene was reacted with *n*-butyllithium in the presence of *N,N,N',N'*-tetramethylethane-1,2-diamine (TMEDA) in hexane. It is believed that TMEDA forms an insoluble complex with the dilithioferrocene shifting the equilibrium in favour of double deprotonation[99]. The reaction was then cooled and quenched with 1,1,2,2-tetrabromoethane. Excess 1,1,2,2-tetrabromoethane was removed under high vacuum. All data were found to be in accordance with the literature[98]. The ^{1}H NMR spectrum confirmed the presence of 1,1'-dibromoferrocene **(14)** with two resonances at 4.12 and 4.38 ppm. The signal at 4.38 ppm was due to the downfield α-protons, shifted by the deshielding influence of the bromine, while the upfield β protons were at 4.12 ppm.

2.4.2 Synthesis of Ferrocene Functionalized Phthalonitriles

In this thesis, the use of Negishi coupling has been explored to couple 1,1'-dibromoferrocene **(14)** to both mono **(5)** and di-halogenated phthalonitriles **(4)** previously synthesised, forming a direct link between these two functional groups, in a one pot synthesis. The aim was to take the functionalized phthalonitriles and cycilise them to form functionalized phthalocyanines. Direct attachment of ferrocene to a phthalonitrile has been achieved by Z. Jin *et al.*[100]. This involved a two step process with the formation and extraction of ferrocenium chloride before the addition of 4-diazoniumphthalonitrile bisulfate which was prepared from 4-aminophthalonitrile.

Here, a one-pot synthesis of functionalized phthalonitrile has been investigated using Negishi Coupling, which was first published in 1977[101] for the synthesis of unsymmetrical biaryls and diarylmethanes in high yields with high chemo- and regioselectivity. It was found that organozinc compounds readily react in an organometallic cross–coupling reaction catalysed by nickel or palladium catalysts. The Negishi coupling reaction has a broader scope than that of the synthesis of biaryls and diarylmethanes[102,103] and is now used in a wide variety of synthetic procedures. Heterocycles like halogenated furans and thiazoles have also been utilized[102] along with the coupling reaction being successfully used in the synthesis of complex molecules[103]. A proposed catalytic cycle of the palladium catalyst is illustrated in the Figure 2.15 although it should be noted that this has been the subject of some debate in the literature[104].

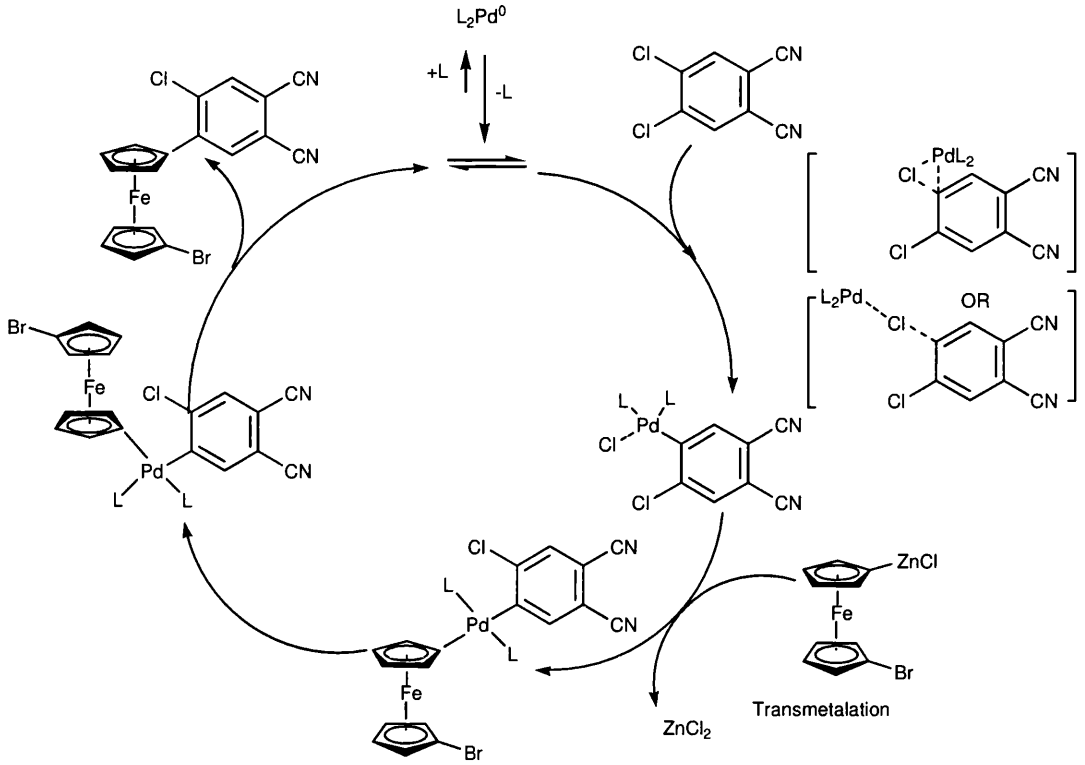

Figure 2.15, Negishi reaction pathway to 4-(1'-bromoferrocenyl)-5-chlorophthalonitrile **(16)** adapted from[104]

In the proposed cycle, the palladium catalyst starts in a zerovalent (M^0) state[104]. The addition of the organic halide compound firstly goes through an oxidative addition step to the palladium catalyst. This is then followed by trans-metalation with the organozinc compound. At this point in the cycle, both organic residues are linked to the palladium catalyst. Reductive elimination follows, forming the C-C bond and releasing the target molecule leaving the catalyst to follow the cycle again.

In this thesis, the coupling of dibromoferrocene and the halogenated phthalonitrile was achieved by the *in situ* formation of an organozinc compound (Figure 2.16). Two equivalents of 1,1'-dibromoferrocene **(14)** were lithiated with *n*-butyl lithium in anhydrous THF at -78 °C, under inert conditions. Zinc chloride was added forming the organozinc compound. This was then reacted with 4,5-dichlorophthalonitrile and the palladium catalyst.

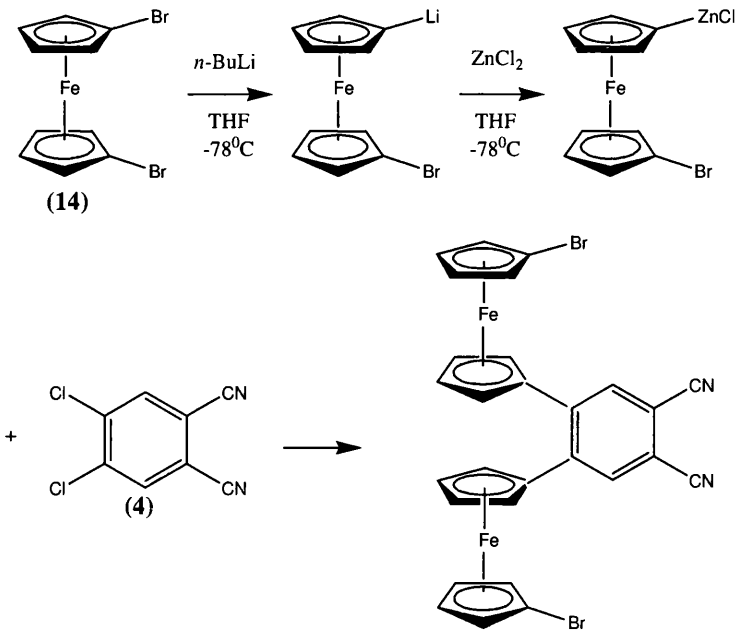

Figure 2.16, Attempted synthetic pathway to 4,5-(1-bromoferrocene)phthalonitrile

The desired compound 4,5-(1-bromoferrocene)phthalonitrile was not present on analysis of the ^{1}H NMR spectrum (Figure 2.17). Only three resonances associated with the cyclopentadiene rings were observed. The signal at 4.11 ppm with an integration of five was characteristic of an unsubstituted cyclopentadiene ring, which indicated that the bromine had been removed during the reaction. Signals at 4.49 and 4.80 ppm, both with intergrals of two, represented the β and α protons of the substituted cyclopentadiene ring attached to the phthalonitrile unit. The two resonances at 7.67 and 7.90 ppm represented the protons on the 3 and 6-position of the benzene ring on the phthalonitrile unit, indicating that coupling of two ferrocene units had not been successful and only one substitution had been achieved.

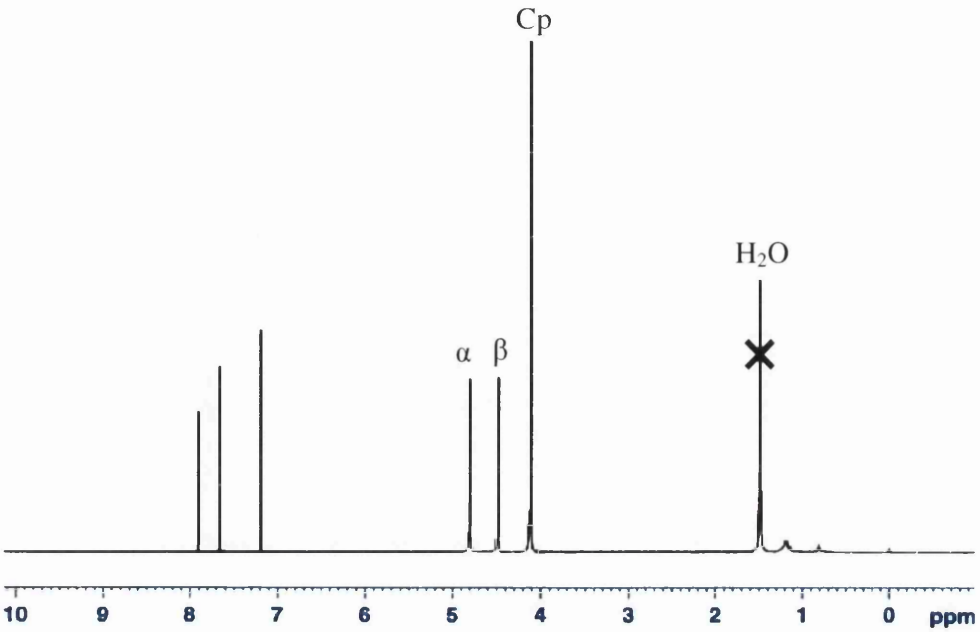

Figure 2.17. ^{1}H NMR spectra of 4-(ferrocenyl)-5-chlorophthalonitrile **(15)**

The loss of the bromine on the ferrocene was also confirmed by the ^{13}C NMR with the presence of three resonances associated with the ferrocene unit with signals at 70.22, 70.40 and 70.96 ppm which corresponded to the unsubstituted cyclopentadiene ring, the β and α protons respectively. The two resonances at 135.15 and 135.44 ppm, represented the carbons on the 3- and 6- positions of the phthalonitrile unit. The halogenated carbon gave a resonance at 136.68 ppm, whereas the carbon which joined the phthalonitrile and ferrocene units together produced a resonance at 145.81 ppm. High resolution mass spectrometry also confirmed the presence of the mono-substituted product **(15)** with an accurate mass of 345.9957 (calculated 345.9955, Cl^{35}). The structure was also confirmed using X-ray crystallography and is shown in Figure 2.18

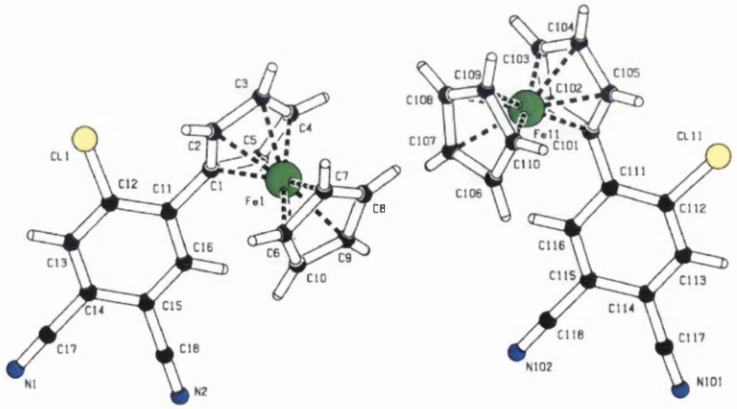

Figure 2.18. Crystal structure of 4-(ferrocenyl)-5-chlorophthalonitrile **(15)**

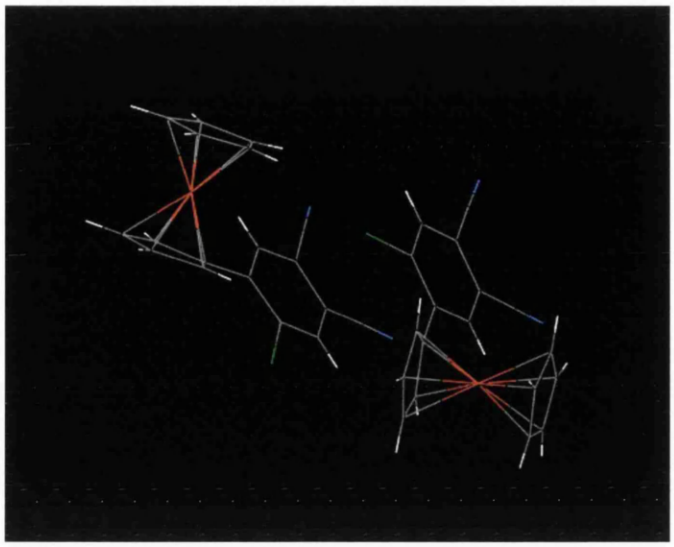

Figure 2.19, Crystal orientations of 4-(ferrocenyl)-5-chlorophthalonitrile **(15)** presented using Mercury software

The crystallography data (Figure 2.19) showed that the cyclopentadiene rings are eclipsed but the Cp rings are slightly tilted resulting in variations in the bond lengths between the central iron and cyclopentadienyl ring. The benzene rings of the phthalonitrile unit have formed a stacking sequence due to π-π interactions. The chlorine atoms are staggered, with the bulky ferrocene units pointing away from each other due to steric hinderance. The phthalonitrile unit is also rotated due to the steric repulsions of the large Cl atom and the Cp ring.

The reaction which produced **(15)** was then repeated and the reaction conditions monitored closely with the aim of synthesizing 4,5-(1-bromoferrocene)phthalonitrile. It was found that the addition of a small excess of butyl lithium to the reaction instead of an excess and also slow warming to room temperature after lithiation prevented the loss of bromine on the cyclopentadiene ring. However, the product of this reaction was found to be 4-(1'-bromoferrocene)-5-chlorophthalonitrile **(16)** (Figure 2.20) instead of the target compound by analysis of the ^{1}H and ^{13}C NMR, mass spectrometry and X-ray crystallography. For instance, there were four resonances at 4.14, 4.39, 4.61 and 4.91 ppm in the ^{1}H NMR, which showed the four proton environments attached to the ferrocene unit. The resonances at 4.14 and 4.39 are due to the β and α protons on the cyclopentadiene ring with the bromine substituent attached while signals at 4.61 and 4.91 are due to the β and α protons on the cyclopentadiene ring with the phthalonitrile substituent attached. This is consistent with a 1,1'-substituted ferrocene unit, which was also confirmed by the ^{13}C NMR, with six carbon environments associated with the

ferrocene unit. The resonance at 81.25 ppm corresponded to the carbon shifted downfield due to the electron withdrawing nature of the bromine.

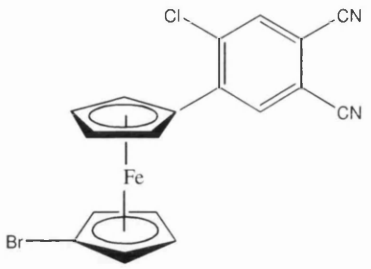

Figure 2.20, 4-(bromoferrocenyl)-5-chlorophthalonitrile **(16)**

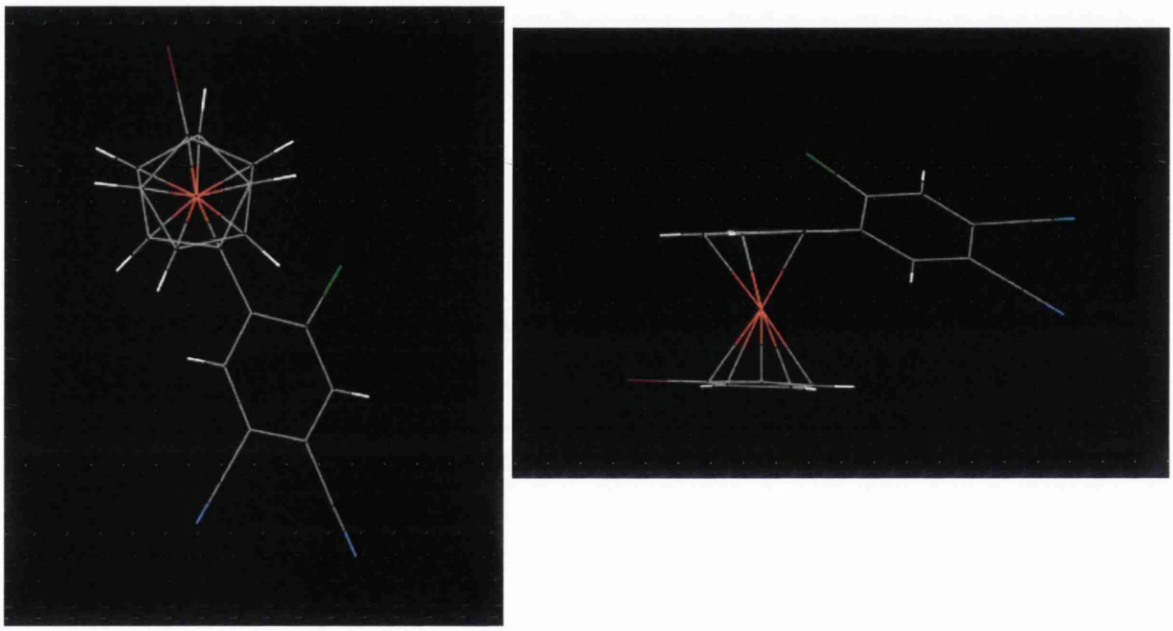

Figure. 2.21, Crystal orientations of 4-(bromoferocenyl)-5-chlorophthalonitrile **(16)**

The additional Br atom on the lower Cp ring has forced the Cp rings to be staggered in the solid state with the Br and the phthalonitrile unit 180 ° apart from each other. This is believed to be due to steric repulsions between the bulky ferrocene unit and the halogen.

Negishi coupling was also achieved using the iodinated phthalonitriles as described earlier in this chapter. In general in this work, it was found that these iodinated nitriles could be coupled with organic residues using shorter reaction times of 8 hours and lower reaction temperatures than that for the chlorinated phthalonitriles. It should be noted that, as stated previously, mono-substituted phthalonitriles can be used in the synthesis of unsymmetrical phthalocyanines. Thus, following the unsuccessful coupling of two ferrocene units to the dichlorophthalonitrile **(4)**, mono-substitution of 1,1'-

dibromoferrocene **(14)** using a mono iodinated phthalonitrile **(5)** was achieved (Figure 2.22). The organozinc compound was prepared in the same way as that discussed earlier for the chlorinated phthalonitrile coupling. Once the organozinc compound was prepared *in situ*, 4-iodophthalonitrile **(5)** was added in the presence of tetrakis(triphenylphosphine)palladium(0).

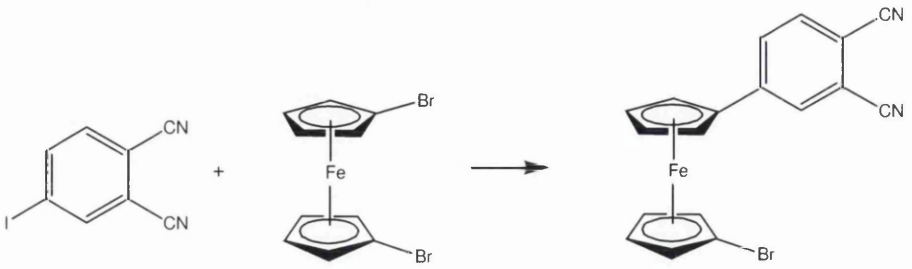

Figure. 2.22, Synthetic pathway to 4-(1-bromoferrocene)phthalonitrile **(17)**

Four resonances at 3.99, 4.19, 4.52 and 4.66 ppm, corresponding to the β and α protons on the bromine substituted cyclopentadiene ring and the β and α protons on the phthalonitrile substituted cyclopentadiene ring were observed in the ^{1}H NMR spectra. This is consistent with an 1,1'-substituted ferrocene. The carbon at the C4 position on the benzene ring has been shifted downfield in the ^{13}C NMR compared to the iodinated starting material **(5)**. The high resolution mass spectrometry data also confirmed **(17)** had been synthesized with an ion at $[M+NH_4]^+$ of 407.9797 (calculated 407.9793).

A by-product 4-(ferrocenyl)phthalonitrile **(18)** was also observed if excess butyl lithium was added to the reaction and if the reaction was allowed to warm up to rapidly. This product was isolated and analyzed by ^{1}H, ^{13}C NMR, mass spectrometry and X-ray crystallography. Three proton environments at 4.02, 4.49 and 4.68 ppm are shown in the ^{1}H NMR spectra, with the resonance at 4.02 ppm observed with an integration of five, consistent with an unsubstituted cyclopentadiene ring.

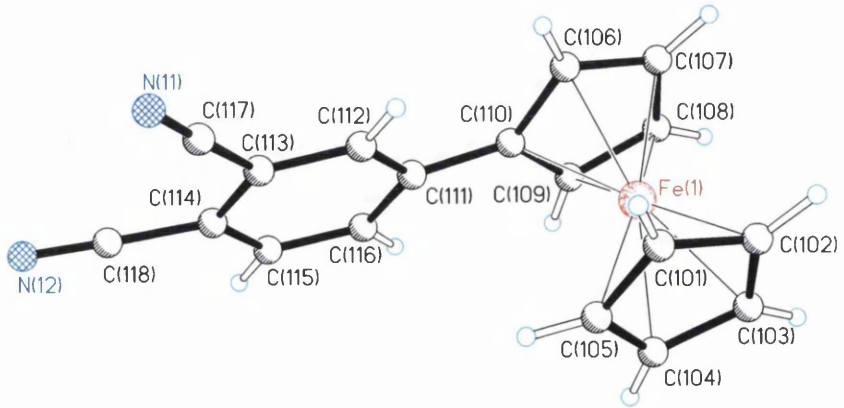

Figure. 2.23, Crystal structure of 4-ferrocenylphthalonitrile **(18)**

The carbon signals ascribed to the mono-substituted cyclopentadiene ring on the ferrocene appear at 70.21, 71.24 and 79.89 ppm in the ^{13}C NMR. The carbon signal associated with the unsubstituted cyclopentadiene ring appears at 67.14 ppm. A molecular ion of m/z 312.1 is observed in the mass spectrum indicating the loss of the bromine atom as observed in the crystal structure but there is also a m/z at 390.0 and 392.0, which produced a typical bromine splitting pattern with a relative intensity of 10 %. This is indicated that a small amount of the target molecule was synthesized but the majority of the product is as illustrated in Figure 2.23. This could be due to dilithiation, caused by excess butyl lithium, and quench, removing the bromine and replacing it with a proton upon work up.

2.5 Synthesis of anchoring groups

As discussed earlier, the synthesis of an anchoring group is essential to anchor the dye to the metal oxide semiconductor in a dye sensitized solar cell which can then lead to effective injection of an electron into the TiO_2. The first attempts to synthesise 4,5-bis(4-methoxycarbonylphenyl)phthalonitrile **(19)** by Negishi coupling of methyl iodobenzoate to the halogenated nitrile using Rieke zinc was unsuccessful. This would form an anchoring group with two acid groups, similar to that of the 2,2'-bipyridyl-4,4'-dicarboxylic acid ligand used in the ruthenium bases sensitizers. It is believed that two acid anchoring groups allow efficient electron injection into the semiconductor as if one acid group desorbs from the surface the other anchors the dye to the TiO_2 surface. Rieke zinc was used to prepare the aryl organozinc intermediate, which it was hoped would couple to the halogenated nitriles. The Rieke zinc was prepared in accordance with the literature[105] by the reduction of anhydrous zinc chloride with lithium metal in THF. The suspension was then sonicated until a black suspension of zinc particles appeared. On addition of methyl iodobenzoate the black suspension disappeared suggesting that the zinc nanoparticles had formed the desired organo-zinc compound. Dichlorophthalonitrile **(4)** was then added to the solution at – 78 °C, followed by reflux. Unfortunately, the reaction failed to yield the desired product which was confirmed by the lack of diagnostic peaks in the aromatic region of the ^{1}H NMR.

Due to the unsuccessful synthesis of **(19)** and after consulting the literature[106], it was found that 3,4-diaryl substituted fumaronitriles possess the correct functional groups to

be able to incorporate into a phthalocyanine like macrocycle and it would be possible that that these molecules could be derivitised to possess two acid anchoring groups similar to that of the target compound (**19**). Unfortunately, this resulted in the loss of the phenyl group, which eventually would result in the reduction of conjugation in any resulting macrocycle. 3,4-Diaryl substituted fumaronitriles have been studied in the literature, as these compounds are precursors to 3,4-diaryl substituted maleimides, which have applications in red OLEDs[106].

In this thesis, diphenyl substituted fumaronitrile was prepared from phenyl substituted acetonitriles by oxidative coupling in I_2 containing an alcoholic alkoxide. The reaction then proceeded by the reaction scheme shown below (Figure 2.24) where deprotonation of the benzylic carbon on the acetonitrile group occurred, followed by halogenation at this site. The iodinated intermediate was then further deprotonated followed by nucleophilic substitution with a subsequent elimination step producing sodium iodide and methanol.

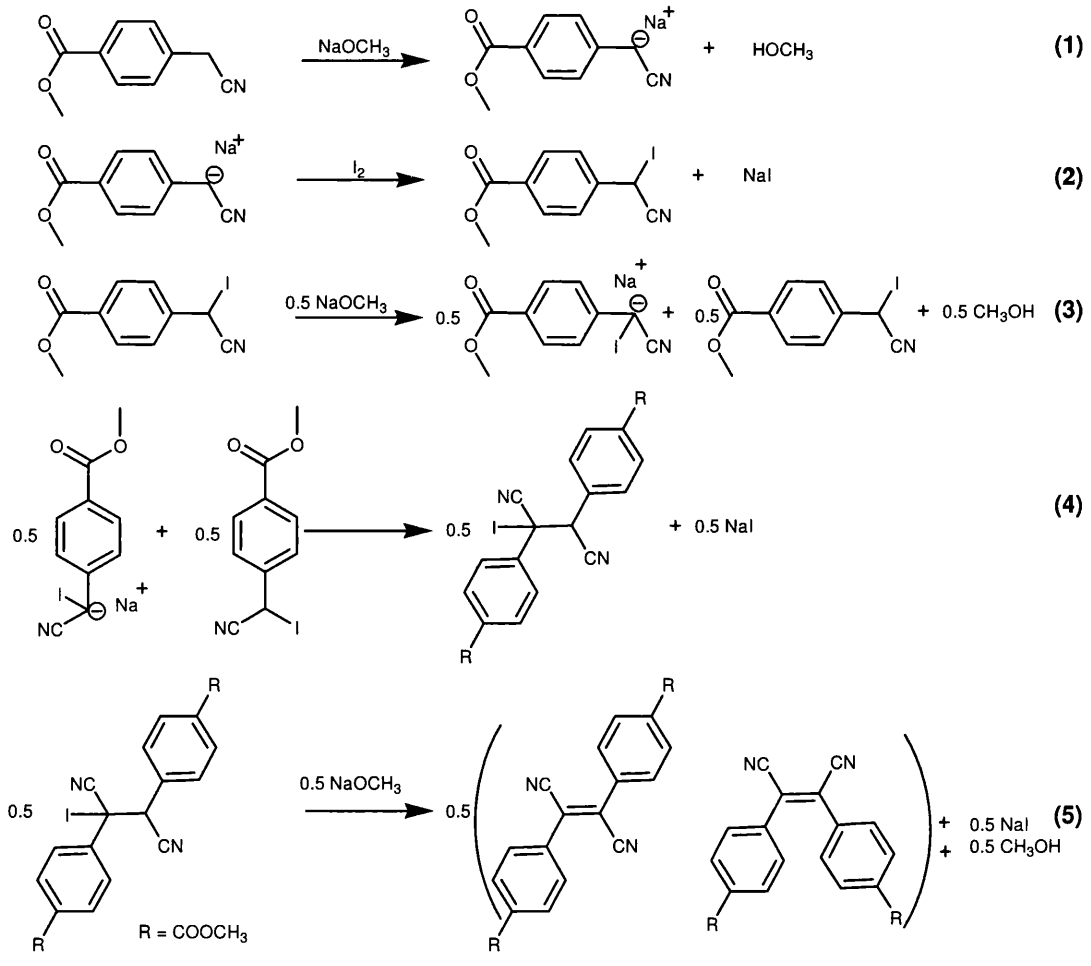

Figure 2.24, Reaction pathway to di-(4-methylbenzoate)-fumaronitrile (**21**) adapted from[106]

On inspection of the ^{1}H NMR, the absence of a signal corresponding to a CH_2 group indicated that the oxidative coupling had taken place with the ester protecting group still present, with the signal at 3.99 ppm observed. The aromatic protons of the phenyl group were observed at 7.92 and 8.21 ppm. The protecting group in the ^{13}C NMR was observed at 52.69 ppm, while the nitrile functional group was observed at 115.95 ppm. IR spectroscopy confirmed the presence of the nitrile group with a signal at 2222 cm^{-1} and the carbonyl functional group of the protected acid observed at 1727 cm^{-1}. This was confirmed by the HRMS with a peak at 347.1029 $[M + H]^+$ (calculated = 347.1026).

At this point in the work, it was found that S. Eu *et al.*[64] has just reported the preparation of the 4,5-bis(4-methoxycarbonylphenyl)phthalonitrile anchoring group by utilizing the Suzuki-Miyaura cross coupling of the boronic acid derivative 4-(methoxycarbonylphenyl)-boronic acid to 4,5-dichlorophthalonitrile[64]. The coupling proceeded *via* an oxidative addition of palladium to the organohalide. It was reported that 4,5-dichlorophthalonitrile was used to form the organo-palladium species. A base, potassium hydroxide, was used to remove the halogen from the catalyst along with a transmetalation reaction with the boronic acid derivative to form the organopalladium compound. These authors[64] then reported that reductive elimination occurred to produce the desired product (**20**).

An electron rich, high steric hinderance phosphine (S-Phos) was added to the reaction to make the palladium catalyst coordinatively unsaturated. This ligand has been reported to have been used to prepare extremely hindered biaryls in excellent yields[107].

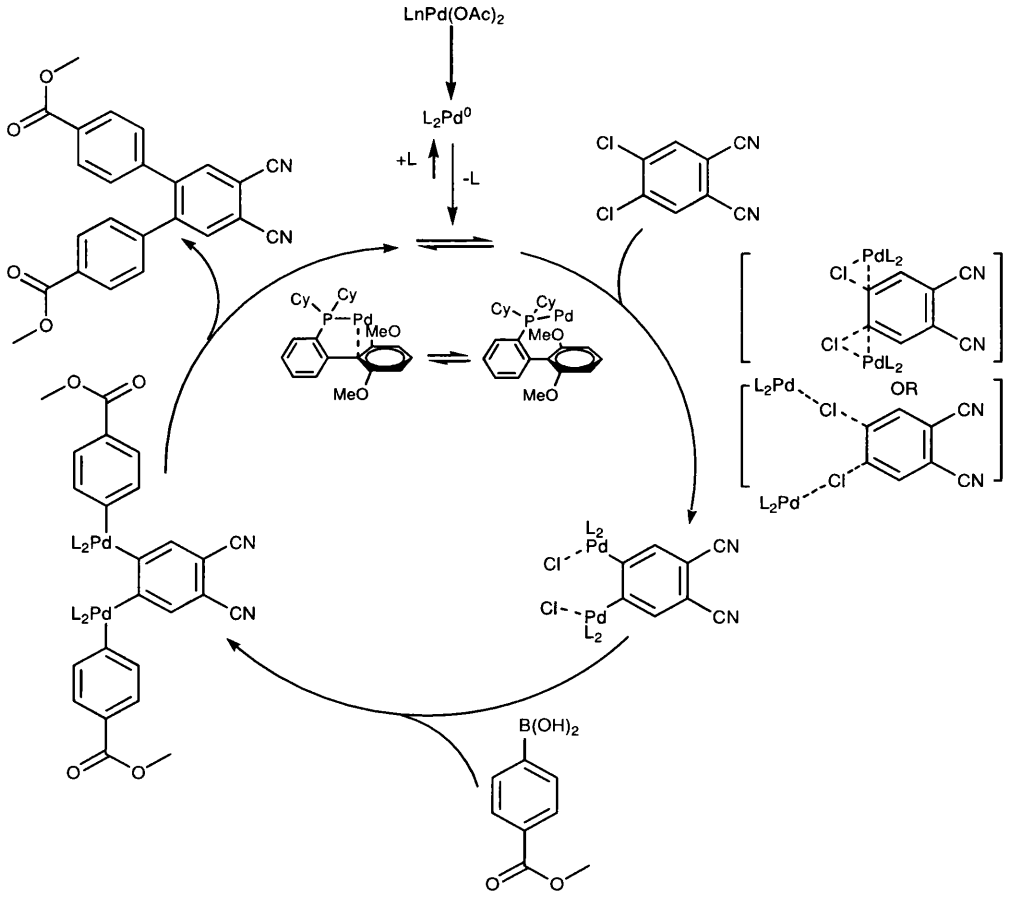

Figure 2.25, Suzuki coupling reaction mechanism to synthesis **(20)**, adapted from[107]

In this thesis, the preparation of 4,5-bis(4-methoxycarbonylphenyl)phthalonitrile **(20)** was accomplished by a Suzuki-Miyaura cross-coupling reaction between 4,5-diiodophthalonitrile **(10)** instead of dichlorophthalonitrile as reported in the literature. Analysis of the ^{1}H NMR spectrum confirmed the structure of **(20)**. The resonance at 7.91 ppm corresponded to the C3 and C6 protons, which indicated that both halogens had been substituted with the substituted phenyls. The protecting ether group was also present at 3.94 ppm, which agreed with the literature. This was also confirmed by high resolution mass spectrometry with a molecular ion at 414.1451 (Calculated 414.1453).

The preparation of an anchoring group that contains one anchoring group, 4-(4-methoxycarbonylphenyl)phthalonitrile (**21**) was synthesised using 4-iodophthalonitrile (**5**) the same conditions as described above for the synthesis of anchoring group (**20**). A signal at 3.90 ppm confirmed the presence of the methyl protecting group in the ^{1}H NMR spectrum which was also observed in the ^{13}C NMR spectrum with a signal at 52.48 ppm. The nitrile functional groups were observed at 115.24 and 116.76 ppm while the aromatic protons on the benzene ring with the anchoring groups attached are

observed at 127.29 and 131.31 ppm and the carbonyl group is represented at 166.26 ppm. The formation of anchoring group (**21**) was also confirmed by a HRMS at 280.1079 (calculated = 280.1081).

2.6 Synthesis of Alkoxy Solubilising Groups

Alkyl and alkoxy substituents can be used to impart solubility on phthalocyanines by preventing the stacking of the planar macrocycles[41,71] and therefore have had successful applications in liquid crystals displays[40]. Alkyl and alkoxy phthalonitriles can be formed by the reaction of either hydroxyl or chlorinated benzene rings[48,108]. The synthesis of 4,5-dinoxyphthalonitrile (**24**) was achieved by literature methods[48].

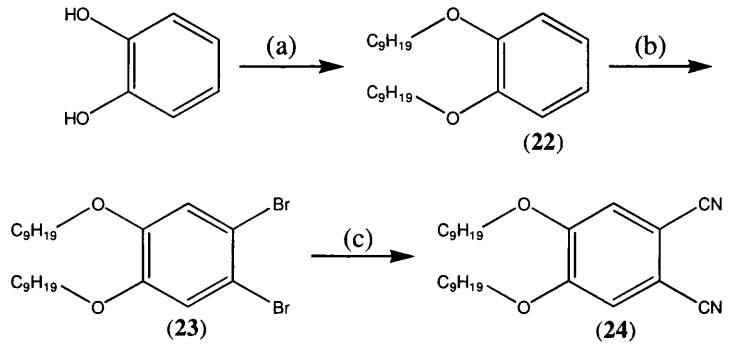

Figure 2.26. Synthesis of 4,5-dinonoxyphthalonitrile (**24**), (a) 1-bromononane, NaOH, tetrabutylammonium bromide, (b) bromine, 0°C,CH_2Cl_2, (c) CuCN, DMF, reflux

In this procedure, catechol was added to a solution of 1-bromononane with sodium hydroxide solution and tetrabutylammonium bromide forming 1,2-dinonoxybenzene (**22**). This was confirmed by ^{1}H NMR and mass spectrometry, 380.3523 (Calculated = 380.3528). The nitrile was obtained by first reacting 1,2-dinonoxybenzene with bromine to give 1,2-dibromo-4,5-nonoxybenzene (**23**). A shift in the aromatic region of the ^{1}H NMR from 6.91 to 7.06 ppm corresponded to the addition of the bromine onto the aromatic ring, which is in line with the literature[48]. The brominated product was then converted to the nitrile by the Rosenmund-von-Braun reaction with CuCN[48]. The oxidative addition of the aryl halide to the copper cyanide forms a Cu(III) species, which then readily undergoes reductive elimination to form the corresponding aryl nitrile[48]. The presence of the nitrile group was confirmed by IR with an absorbance at 2229 cm^{-1}. Again there was a downfield shift in the ^{1}H NMR spectra from 7.06 to 7.12 ppm caused by the deshielding of the proton by the nitrile functional group. The HRMS

also confirmed the presence of (**24**) by a molecular ion at 430.3426 (calculated = 430.3433).

2.7 Conclusions

The preparation of the building blocks, for the synthesis of unsymmetrical phthalocyanines has been discussed in this chapter with halogenated phthalonitriles of (**4**) and (**5**) produced in good quantities. 4,5-Diiodophthalonitrile (**10**) can be synthesized from its imide precursor using periodic acid, a cheaper and solid reagent that is easier to handle than 30 % fuming sulphuric acid and iodine and so is better suited for synthesizing large quantities of this starting material. Negishi coupling of 1,1'-dibromoferrocene (**14**) to both iodo (**5**) and dichlorophthalonitriles (**4**) has also been investigated, with the coupling of two ferrocene units to the phthalonitrile proving unsuccessful. However, it was found that, with adequate control of reaction conditions such as temperature and time, the formation of 4-(bromoferrocenyl)-5-chlorophthlonitrile (**16**) and 4-(1-bromoferrocenyl)-phthalonitrile (**17**) can be achieved in good yields. The various methods of synthesizing anchoring groups have been described with the synthesis of the novel anchoring group (**19**) and the synthesis of (**20**). The final functionalized phthalonitrile was the solubilising unit (**24**), synthesized to help prevent aggregation and solubility of the phthalocyanine units. The cyclisation of these compounds to synthesis unsymmetrical phthalocyanines is discussed in Chapter 3.

Chapter 3

Synthesis of Unsymmetrical Phthalocyanines

3.1 Cyclisation

The synthesis of novel unsymmetrical phthalocyanines can be carried out by either a mixed phthalonitrile cyclotetramisation, or by a subphthalocyanine expansion. Cyclotetramisation tends to lead to a *pseudo* statistical mixture of products which cannot be readily separated, while subphthalocyanine expansion can lead to the introduction of substituted phthalonitriles into the ring system, forming a substituted phthalocyanine without the formation of the *pseudo* statistical by-products. However, it has been reported[109] that this can depend on the nature of the substituent as discussed in Section 1.3.3. This chapter describes the investigation into the synthesis of unsymmetrical phthalocyanine dyes, comparing both approaches, from the tailor-made derivitised phthalonitriles, which were specifically designed to reduce aggregation with dye in solution and on the metal oxide surface and improve directionality in the excited state, as discussed in Chapter 2.

3.1.1 Subphthalocyanine Synthesis

Subphthalocyanines were prepared by a modified literature procedure first reported by Ossko and Meller in 1972[59]. In this approach, phthalonitrile was recrystalized and dried over phosphorus pentoxide for 48 hours prior to use. Without this drying procedure, it was found that no product was obtained. The phthalonitrile was reacted with a solution of boron trichloride in DCM in 1-chloronaphthalene at 150 °C under inert conditions (Figure 3.1). The low boiling dichloromethane was instantly distilled from the reaction resulting in the bronze solid (**25**).

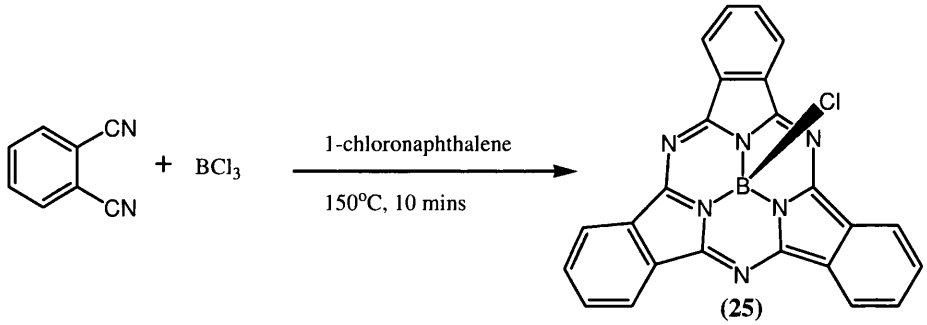

Figure 3.1, Structure of a subphthalocyanine (**25**)

Figure 3.2 shows a comparison of the UV-visible spectra of the synthesised subphthalocyanine (**25**) and zinc phthalocyanine (**43**, discussed later), with the data in

accordance with the literature[41,61]. The subphthalocyanine (**25**) UV-visible spectrum consists of two bands; the Soret band around 308 nm and the Q band at 564 nm due to the π-π* transitions. There is a shoulder at 520 nm which has been reported to be due to vibronic transitions[61]. The Q-band of the zinc phthalocyanine is shifted around 120 nm to the red region of the spectrum relative to the subphthalocyanine (**25**) due to the increased conjugation resulting from the addition of the isoindoline unit. The zinc phthalocyanine also consists of two intense bands, the Soret band and the Q band at 340 and 670 nm respectively due to the π-π* transitions in the conjugated macrocycle. The peak at around 600 nm is due to vibrational overtones of the Q band[41].

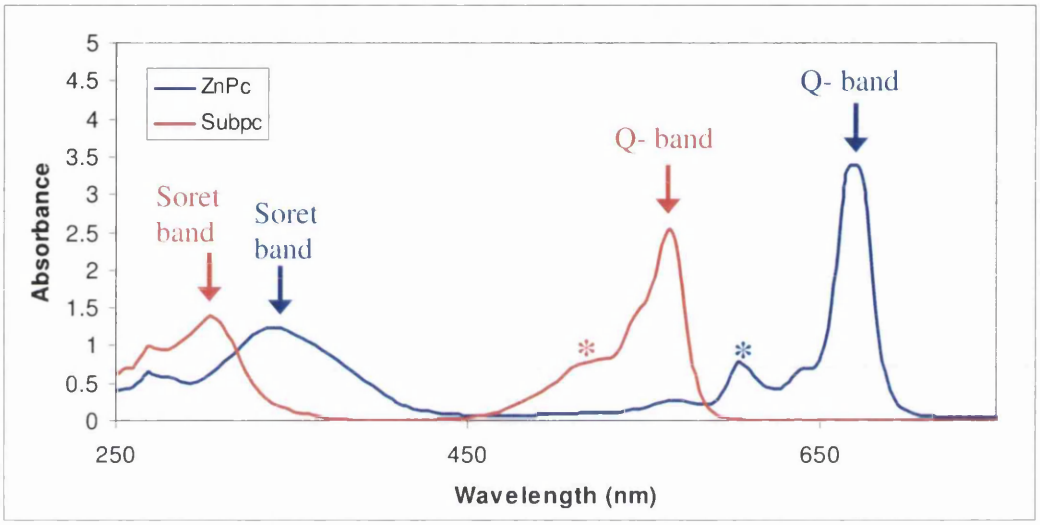

Figure 3.2 UV-visible spectral plot of subphthalocyanine (**25**) and zinc phthalocyanine, * = vibrational overtones of the Q-band[41]

Analysis of the ^{1}H NMR spectrum confirmed the structure of (**25**) with an A_2B_2 splitting pattern exhibited at 7.92 and 8.92 ppm [57]. An M^+ of 430 corresponded to the target molecule but contamination with both the mono and dichloro substituted subphthalocyanines with molecular ions at 464 and 500 was observed. These undesired halogenated derivatives are caused by the halogen-containing boron trichloride as reported in the literature[57]. Re-precipitation in concentrated H_2SO_4 has been reported[57] to remove these by-products but, when attempted, it was found that the halogenated contaminants were still present but in reduced amounts. To fully prevent halogen contamination, triphenyl boron can be used but the presence of an organic base, 1,8-diazabicyclo[5.4.0]undec-7-ene (DBU) in naphthalene is required[61]. However, this approach was not attempted in this thesis.

After successful synthesis of subphthalocyanine (**25**), the synthesis of chloro[2,9,16-tri-*t*-butylsubphthalocyanine]boron(III) (*t*-SubPc) (**26**) was attempted according to literature procedure[61]. The aim here was that the *t*-butyl groups would add additional solubility to the resulting phthalocyanine after ring expansion and enable easier purification and to include directionality of electron injection for DSSC devices by inducing a 'push-pull system as described for the Grätzel phthalocyanine dye as discussed in Section 1.3.4. In this approach, *t*-butylphthalonitrile was dried over phosphorus pentoxide before use and then reacted with boron trichloride as discussed earlier. The reaction was heated to 250 °C but, on analysis of the proton NMR, it was apparent that the *t*-SubPc had not been formed. Elevated temperatures of 270 °C were attempted but again this yielded no *t*-SubPc (**26**). At this point, boron trichoride in xylene was reacted with the *t*-butylphthalonitrile. Xylene, a higher boiling solvent than the dichloromethane, was chosen in order to be able to heat the reaction mixture up rapidly to higher temperatures before the lower boiling solvent was distilled off. The reaction was heated to 260 °C for 3 hours. After filtration, a dark purple solid was obtained and purification was attempted by Soxhlet extraction in diethyl ether. On inspection of the ^{1}H NMR, it was apparent that large quantities of impurities were still present in the sample. The residue was then subjected to column chromatography but this had no affect on purification. Mass spectrometry revealed that the M^{+} ion 599 of the target compound (**26**) was present as a weak signal along with significant impurities.

Due to the unsuccessful synthesis of workable quantities of the *t*-SubPc (**26**), chloro[2,3,9,10,16,17-hexachlorosubphthalocyaninato]boron (III) (**27**) and chloro[triiodosubphthalocyaninato]-boron (III) (**28**) derivatives were synthesised. This was done so that after synthesis of the subphthalocyanine post derivitisation could be achieved by palladium cross coupling reactions. The synthesis was carried out using the same procedure as with the subphthalocyanine (**26**) but with elevated reaction temperatures of 240 °C[61].

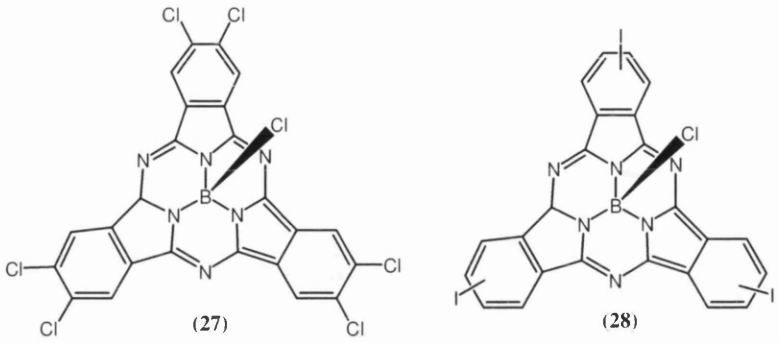

Figure 3.3, Chloro[2,3,9,10,16,17-hexachlorosubphthalocyaninato]boron (III) (**27**) and chloro[triiodosubphthalocyaninato]-boron (III) (**28**)

Conformation that subphthalocyanines (**27**), (**28**) had been prepared was through high resolution mass spectrometry with molecular ions at 632.8602 (calculated = 632.8598) for chloro[2,3,9,10,16,17 hexachlorosubphthalocyanine] boron(III) (**27**) and M^+ 807.7805 (calculated = 807.7799) for chloro[2,9,16-triiodosubphthalocyanine]boron(III) (**28**). A hyposochromic shift of *ca.* 8 nm was observed for the halogenated subphthalocyanines in the UV-visible spectrum (Figure 3.4) compared to that of the unsubstituted subphthalocyanine due to the electron withdrawing nature of the chloro and iodo substituents.

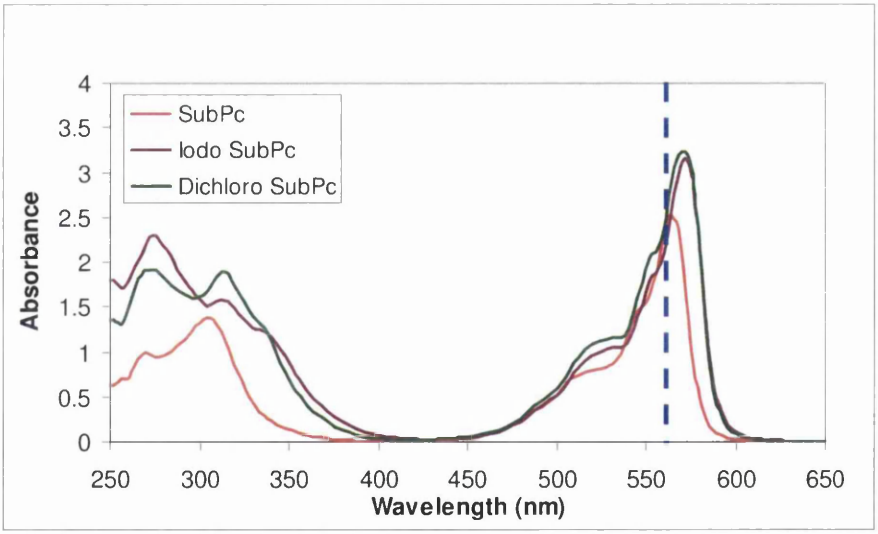

Figure 3.4, UV-visible spectrum of dichloro (**27**), monoiodo (**28**) subphthalocyanine in THF 9.05 x 10^{-6} M

On consulting the literature[110], it was found that a *t*-butyl subtriazaporphyrine has been reported by cyclising di(4-tert-butylphenyl)fumarornitrile with boron trichloride to form *t*-butyl subtriazaporphyrine. It was therefore decided to synthesise

chloro[2,3,9,10,16,17-(4-methoxybenzoate)-subtriazaporphyrine (Figure 3.5) from di-(4-methylbenzoate)-fumaronitrile **(19)** to incorporate acid anchoring groups into the subphthalocyanine structure by reacting with boron trichloride at elevated temperatures of 259 °C. The aim was to expand the resulting subtriazaporphyrine, forming an unsymmetrical azaporphyrine derivative, with the desired functionality to anchor to a metal oxide for applications in DSSC devices. Synthesis was attempted using these conditions but the target molecule was not obtained and starting material was seen in the ^{1}H NMR. This could be due to lack of solubility of the fumaronitrile or the strong electron withdrawing nature of the protected acid functional group making cyclisation energetically unfavourable.

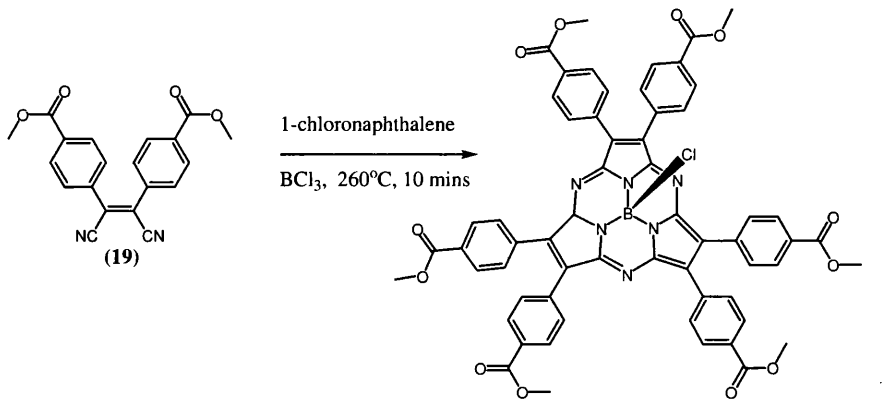

Figure 3.5, Attempted synthesis of subtriazaporphyrine

On consulting the literature again, it was found that subphthalocyanines with alkyl chains require more elevated temperatures to form along with the addition of a superbase phosphazene[1-*t*-buytl-4,4,4-tris(dimethylamino)-2,2-bis [trisdimethylamino]phosphoranylidenamino]-2λ^5,4 λ^5-catenadi(phosphazene)](P4-*t*-Bu) as a catalyst[61] but due to time restrictions this was beyond the scope of this project[61].

3.1.2 Isoindolinones

A ring expansion reaction of the subphthalocyanine with 1,3-diiminoisoindoline and derivatives is required to form the desired unsymmetrical phthalocyanine as discussed in Section 1.3.3. Hence, the synthesis of a series of isoindolinones was investigated in this thesis.

1,3-Diiminoisoindolines and their derivatives were prepared in preparation for ring expansion condensation reactions with subphthalocyanines. Synthesis of 1,3-

diiminoisoindoline (**29**), 5-*t*-butyl-1,3-diiminoisoindoline (**30**), 4,5-dichloro-1,3-diiminoisoindoline (**31**) and 4,5-diiodo-1,3-diiminoisoindoline (**32**) was achieved in accordance with literature procedures[111]. In each case, a steady stream of ammonia gas was passed through a solution of methanol containing the desired phthalonitrile starting material in the presence of sodium methoxide, first at room temperature and then at reflux. The progress of the reactions was recorded by IR by monitoring the disappearance of the CN functional groups at 2230 cm^{-1}.

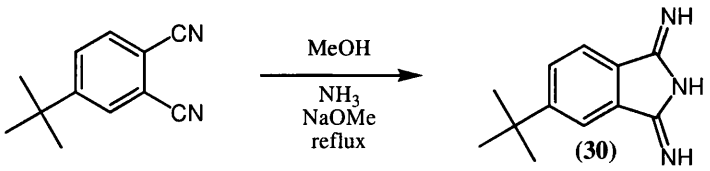

Figure.3.6, Synthesis of 5-*t*-butyl-1,3-diiminoisoindoline (**30**)

The isoindoline derivative, di-(4-methylbenzoate)-2,5-diimino-pyrrole, of di-(4-methylbenzoate)-fumaronitrile (**19**) was attempted for the incorporation of acid anchoring groups into the phthalocyanine structure upon subphthalocyanine expansion. Ammonia gas was bubbled through the solution containing the acid derivative at reflux temperature, but on analysis of the data, it was found that the di-(4-methylbenzoate)-2,5-dimino-pyrrole did not form. Longer reaction times were attempted but again the target molecule was not present. On analysis of the ^1H NMR spectrum, only starting material was present which was confirmed by the presence of the CN functional group in the IR spectrum. Reaction with the fumaronitrile with either the ammonia to form an isoindoline derivative or the boron trichloride to form a subtriazaporphyrine proved unsuccessful. This could indicate that either the reaction condition for these preparations were not correct or that formation of these products is unfavourable with the protected acid functional group and the absence of the benzene ring.

3.1.3 Synthesis of Unsymmetrical Phthalocyanines

The ring expansion of subphthalocyanine (**25**) with 1,3-diiminoisoindoline (**29**) was synthesised to test the reaction conditions required to form the unmetallated phthalocyanine (**33**). On consulting the literature, it was found that the formation of the desired phthalocyanine is very dependent on the solvent that is used[65]. Solvent mixtures of DMSO and chloronapthalene, varying in ratio depending upon the solubility of the reactants are most widely used in ring expansion reactions. Hence, these conditions were attempted when reacting subphthalocyanine (**25**) with isolindoline (**29**) (Figure

3.7). Upon heating, trace amounts of blue material could be seen around the edges of the reaction vessel but on work up no target material was detected. On changing the solvent to dimethylaminoethanol (DMAE) and heating for 24 hours at 140 °C, a blue precipitate was formed. This yielded the non-metalated phthalocyanine (**33**) in 43 % yield, which was confirmed with a molecular ion observed at 514.1645 (calculated 514.1649) in the mass spectrum as reported in the literature[112].

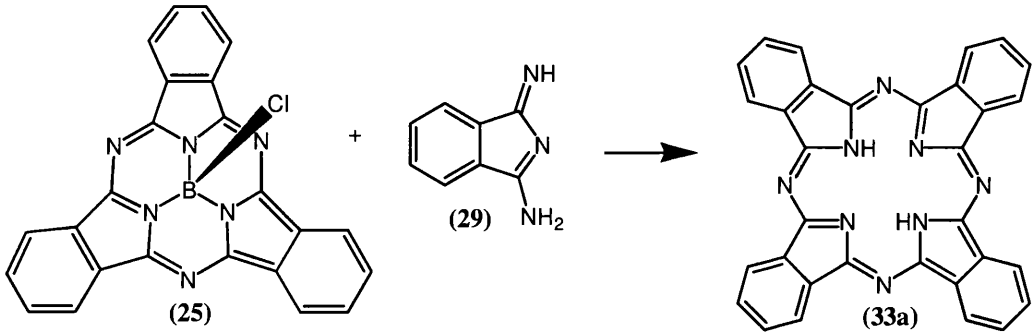

Figure 3.7 Synthetic pathway to non-metalated phthalocyanine (**33a**).

Due to unsuccessful conversion of di-(4-methylbenzoate)-fumaronitrile (**19**) to the di-(4-methylbenzoate)-2,5-dimino-pyrrole, the ring expansion of the subphthalocyanine (**25**) was attempted with the use of the parent compound (**19**). The use of nitriles in ring expansion reactions are not widely reported but Matlaba *et al.*[113] synthesised unsymmetrically substituted zinc phthalocyanines using this method. The ring expansion was attempted in DMSO and chloronapthalene due to the greater solubility of the reactants in this solvent. Upon heating, a blue/green solution formed. On removal of the solvent, the residue was dissolved in toluene and a blue precipitate was observed, which was separated by centrifuge. It was found that the blue precipitate was that of the unsubstituted zinc phthalocyanine with a molecular ion of 576 observed in the mass spectrum. The UV-visible spectrum showed the characteristic Soret and Q band of a metalated zinc phthalocyanine with absorbances at 344 and 664 nm relating to the Soret and Q band respectively in accordance with the literature[114]. Analysis of the blue/green solution using mass spectrometry identified a mixture consisting of molecular ions of 576 and 1154 which were identified as zinc phthalocyanine and a possible dimer of the phthalocyanine respectively. This suggested that the subphthalocyanine had been broken apart during the ring expansion into dimers.

In order to form the zinc phthalocyanine, an initial ring opening reaction of the subphthalocyanine must have occurred, as suggested by Sastre *et al.*[109], forming an open four unit compound (Figure 3.8). In order to form the zinc phthalocyanine, this open unit must have cleaved leaving a fragment consisting of two joined isoindoline units, which could then undergo self condensation with the aid of the metal to form the zinc phthalocyanine. There was no evidence of self condensation of the fumaronitrile (**19**) forming the symmetrical product. The cyclisation may not have occurred as it was unfavourable to form the desired compound due to the loss in conjugation compared to the symmetrical highly conjugated zinc phthalocyanine.

Originally, it was thought that the ring opening expansion of subphthalocyanines selectively formed the desired phthalocyanine without the formation of by-products[61]. However, it is also reported that the ring opening expansion of subphthalocyanines is dependant on the nature of the substituents and the conditions such as temperature and solvent as reported by Sastre *et al.*[109]. The formation of the unsubstituted zinc phthalocyanine also provides evidence for the idea that the ring opening reaction is a multistep process and hence, not as selective as first though as reported in the literature[109].

Due to the unsuccessful attempts to synthesise the unsymmetrical 2,3-(4-methoxybenzoate)-tetrabenzo-5,10,15,20-tetraazaporphyrin zinc (Figure 3.8), it was decided to test di-(4-methylbenzoate)-fumaronitrile (**19**) alone to see if cyclotetramisation was possible and then to test this symmetrical molecule for any photovoltaic activity. Cyclization was achieved in the presence of DBU and zinc acetate in pentanol at 130 °C. The expected product, 2,3,7,8,12,13,17,18- octa(4-methoxybenzoate)-5,10,15,20-tetraazaporphyrin zinc was not obtained but a molecular mass of 1897 was observed. The peak corresponded to 2,3,7,8,12,13,17,18- octa(4-pentoxybenzoate)-5,10,15,20-tetraazaporphyrin zinc (**34a**). It is believed that an exchange reaction between the acetate and pentanoate groups present in the solvent occurred during cyclotetramisation. A similar effect has been observed and reported recently[64].

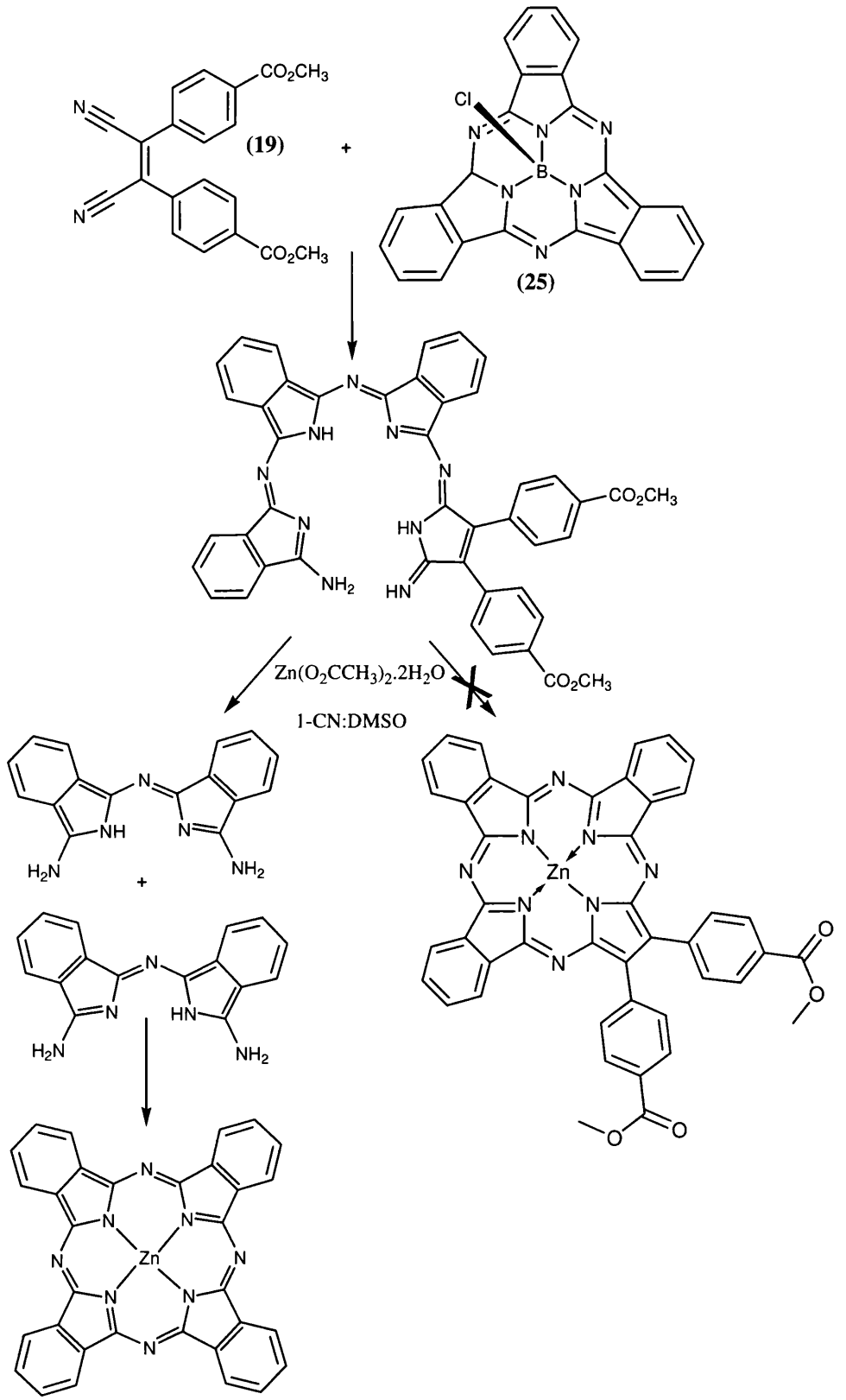

Figure 3.8. Scheme showing the attempted synthesis of 2,3-(4-methoxybenzoate)-tribenzo-5,10,15,20-tetraazaporphyrin zinc

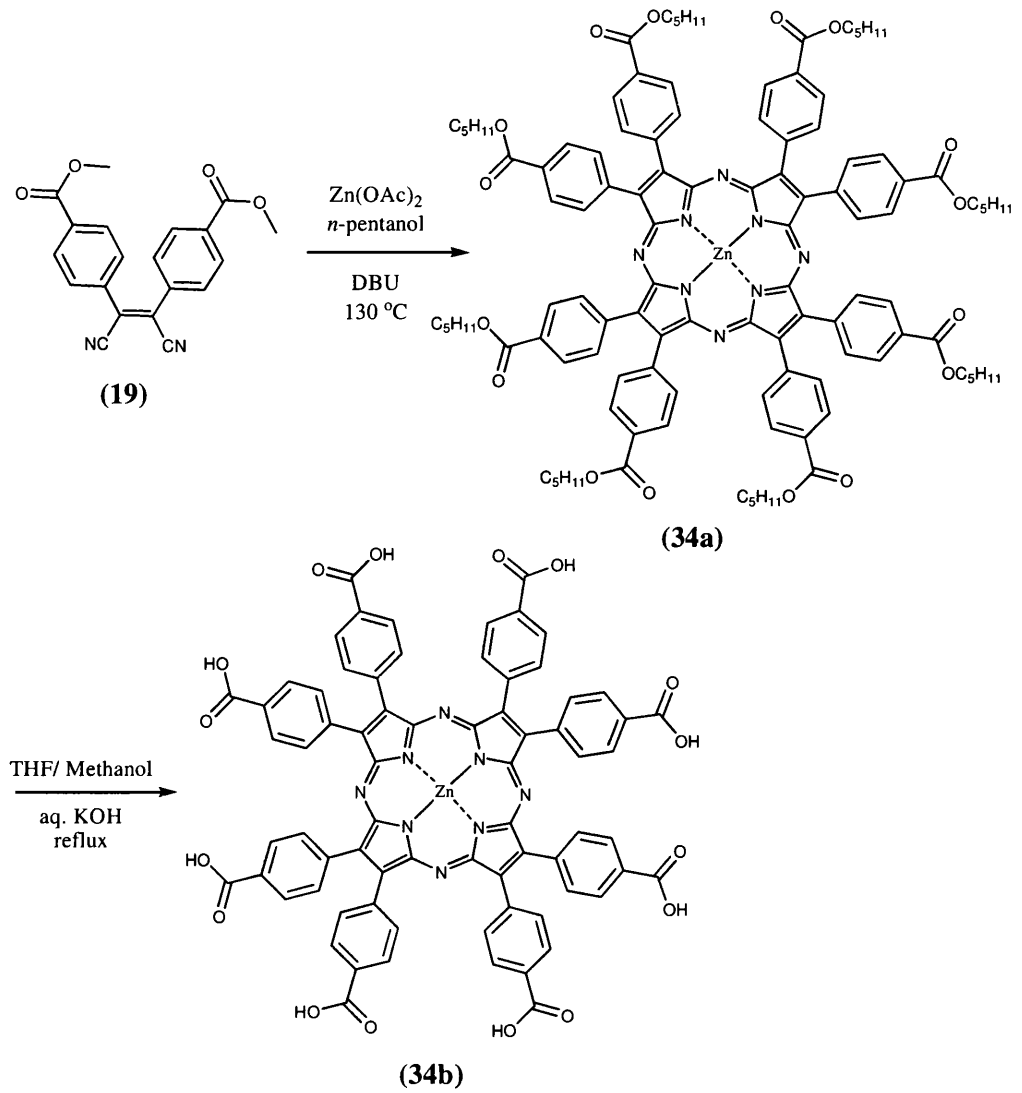

Figure 3.9, Synthesis of 3,7,8,12,13,17,18- octa(4-benzoate)-5,10,15,20-tetraazaporphyrin zinc (**34b**)

The ^{1}H NMR (Figure 3.10) of **(34a)** confirmed the presence of the pentanoate groups with a triplet observed at 0.91 ppm for the methyl group, the presence of signals at 1.44 and 1.81 ppm representing the alkyl chain. The triplet at 4.33 ppm is shifted down field due to its close proximity to the oxygen of the pentanoate in comparison to the singlet which would have been observed if exchange had not occurred. The benzene groups are represented by the mutiplet at 8.05 ppm.

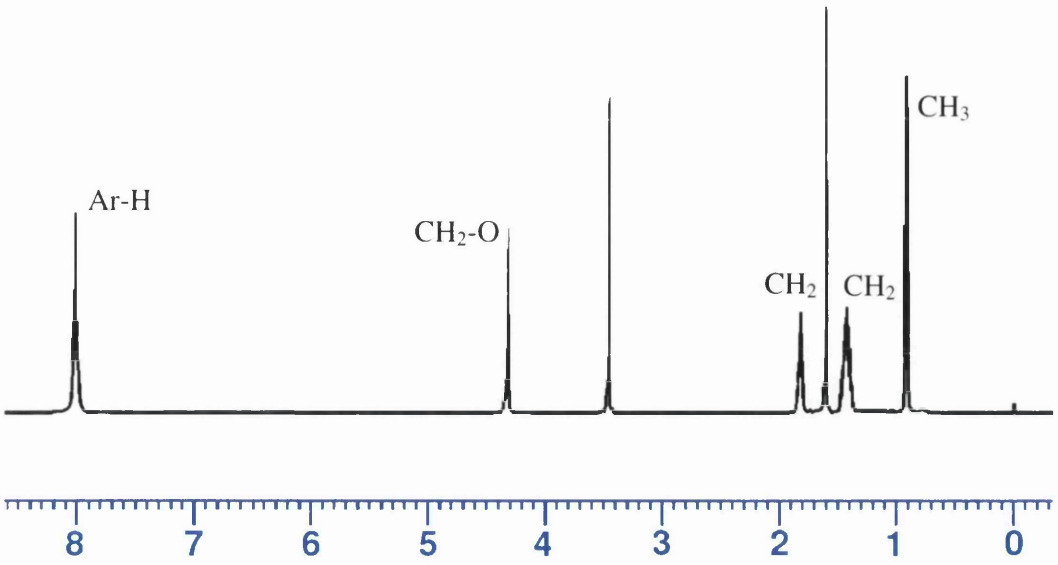

Figure 3.10. ^{1}H NMR of 3,7,8,12,13,17,18- octa(4pentoxybenzoate)-5,10,15,20-tetraazaporphyrin zinc (**34a**) (solvent THF)

As the target compound could be formed from this derivative by hydrolysis, (**34a**) was employed for the next stage without further purification. In our approach, base catalysed hydrolysis of the pentanoate groups was achieved in a methanol/THF mix containing aqueous potassium hydroxide. Mass spectrometry identified a molecular ion of 1337 for 2,3,7,8,12,13,17,18-octa(benzoate)-5,10,15,20-tetrazaporphyrin zinc (**34b**). UV-visible spectra of the ester (**34a**) and hydrolyzed azaporphyrine (**34b**) are shown in Figure 3.11. The peak positions of the Soret and Q band of the protected azaporphyrine (**34a**) are 380 and 640 nm, respectively. A hypsochromic shift is observed for the Q band by *ca.* 30 nm and a bathochromic shift is observed for the Soret band compared to that of a zinc phthalocyanine. This is due to the reduced conjugation with in the macrocycle compared to a phthalocyanine core structure. The deprotected azaporphyrin (**34b**) has broader peaks that (**34a**) which may reflect increased aggregation of the macrocycles within the solution. This reaction proved that cyclotetramisation was possible with the fumaronitrile **(19)** and due to the unsuccessful synthesis of the *t*-SubPc (**26**) in workable quanities it was therefore decided to form unsymmetrical azaporphyrines using the statistical mixed cyclotetramisation approach.

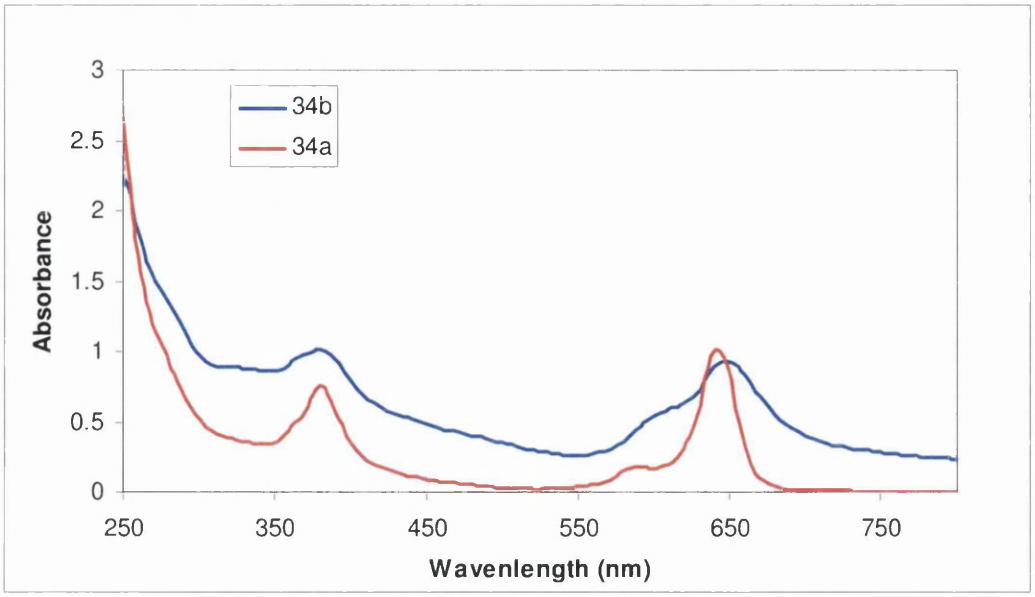

Figure 3.11, UV-visible of 2,3,7,8,12,13,17,18-octa(4-pentoxybenzoate)-5,10,15,20-tetrazaporphyrin zinc (**34a**) and 2,3,7,8,12,13,17,18-octa(benzoate)-5,10,15,20-tetrazaporphyrin zinc (**34b**) in THF, 9.05 x 10^{-6} M, ε = 1.02 x 10^{5} at 648 nm

As discussed in Section 1.3.3, the statistical method produces a *pseudo* statistical mixture of products, as a varing ratio of products has been formed in this thesis depending on the solubility and reactivity of the substituted phthalonitriles. Figure 3.12 shows the statistical mixture of products that can occur with cyclotetramisation with two different substituted phthalonitriles which are difficult to separate. The ratio of the desired target molecule can be increased by manipulation of the reaction conditions and ratio of reactants added[109]. In this work *t*-butylphthalonitrile was reacted in a statistical condensation with di-(4-methylbenzoate)-fumaronitrile (**20**) with a ratio of 3:1 in pentanol in the presence of DBU. A combination of one anchoring group to three *t*-butylphthalonitrile was chosen to induce enhanced electron injection into the TiO_2 photoelectrode of a DSC by inducing a 'push-pull' system similar in principle to that described for the Grätzel phthalocyanine dyes as discussed in Section 1.3.4 by creating an unsymmetrical phthalocyanine.

Mass spectrometry showed that the expected molecular ion was not present but instead 2,3-(4-pentoxybenzoate)-7^2,12^2,17^2-tri-*tert*-butyl-tribenzo-5,10,15,20-tetraazaporphyrin (**35a**) was observed. Exchange with pentanoate groups had occurred as discussed earlier which gave a molecular ion of 1012. A *pseudo* statistical mixture of products was also observed which was expected as the reaction was not selective (Figure 3.12).

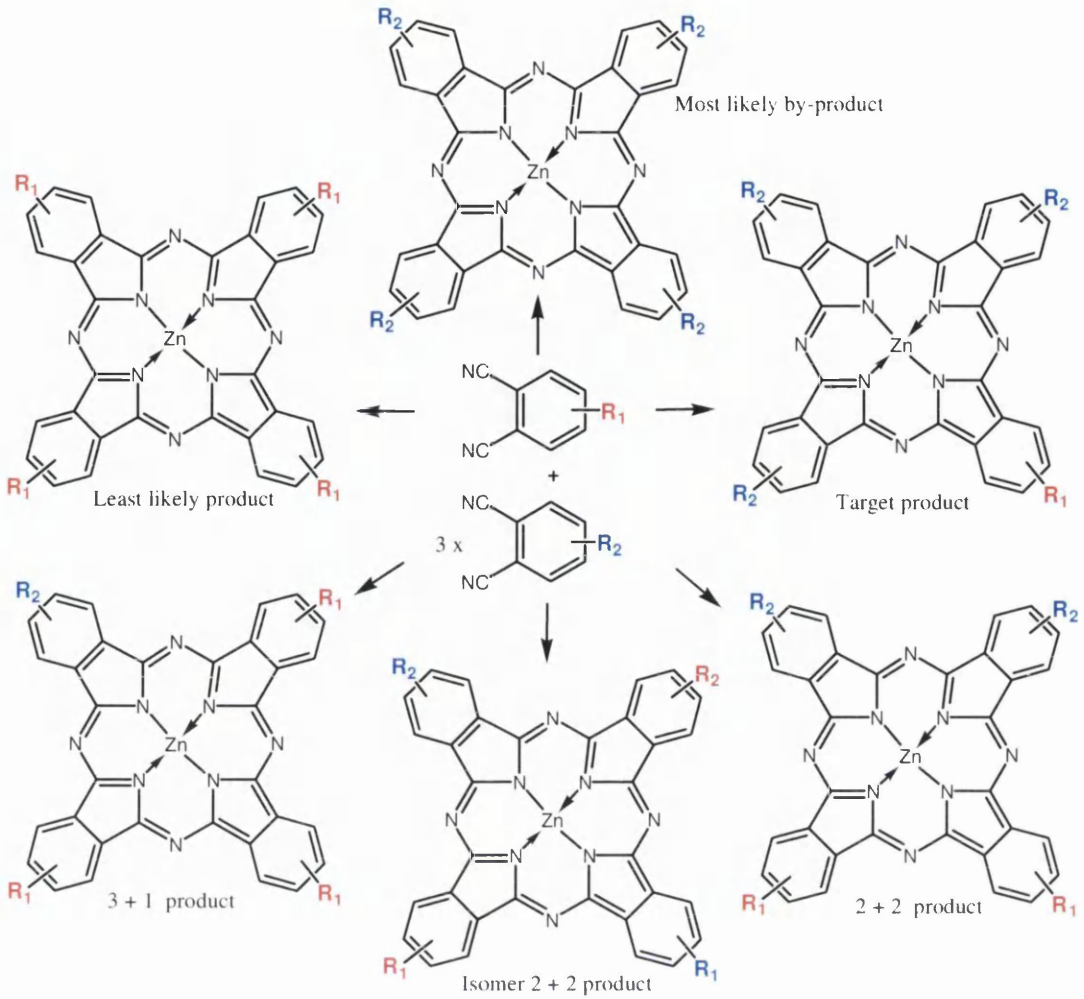

Figure 3.12. *Pseudo* statistical mixture of products formed by reacting two different phthalonitriles

Purification was attempted using column chromatography but the mass spectral data still showed a *pseudo* statistical mixture of products with the most likely symmetrical product, 2,9,16-tetra-*tert*-butyl phthalocyanine (**35ai**) present with a 100 % molecular ion of 738 in the mass spectrum. The product formed with the cyclisation with two acid anchoring groups, 2,3,7,8-(4-pentoxybenzoate)-12^2,17^2-di-*tert*-butyl-tribenzo-5,10-15,20-tetraazoporphyrin (**35aii**) with a molecular ion of 1286 (relative intensity 3 %) was also observed. It is worth noting that not all of the statistical by-products were present and hence the purification process had separated out the other statistical by-products or the reaction conditions and the ratio of reactants had made the formation of the other statistical by-products less favourable. It was also apparent that the exchange with the pentanoate groups has occurred on all the methoxy substituents but as discussed earlier, the ester groups will be hydrolysed to form the desired deprotected macrocycle.

To afford the zinc derivative (**35b**), zinc(II) was inserted into the core of the macrocycle using anhydrous zinc acetate. The resulting compounds displayed molecular ions of 800, 1075, and 1350 with a ratio of 100:8:3 in the mass spectrum, which corresponded to the symmetrical by-product 2,9,16-tetra-*tert*-butyl phthalocyanine zinc (**35bi**), the desired product 2,3-(4-penyoxybenzoate)-7^2,12^2,17^2-tri-*tert*-butyl-tribenzo-5,10,15,20-tetraazaporphyrin zinc (**35b**) and the *pseudo* statistical mixture of the esters 2,3,7,8-(4-pentoxybenzoate)-12^2,17^2-di-*tert*-butyl-tribenzo-5,10-15,20-tetraazoporphyrin zinc (**35bii**) respectively. It is worth noting that the relative intensity of the desired target molecule (**35b**) has dropped by half while the symmetrical product (**35bi**) and the statistical product (**35bii**) remained the same. The purification of the dyes by column chromatography had therefore removed a significant amount of the desired product as well as some of the impurities.

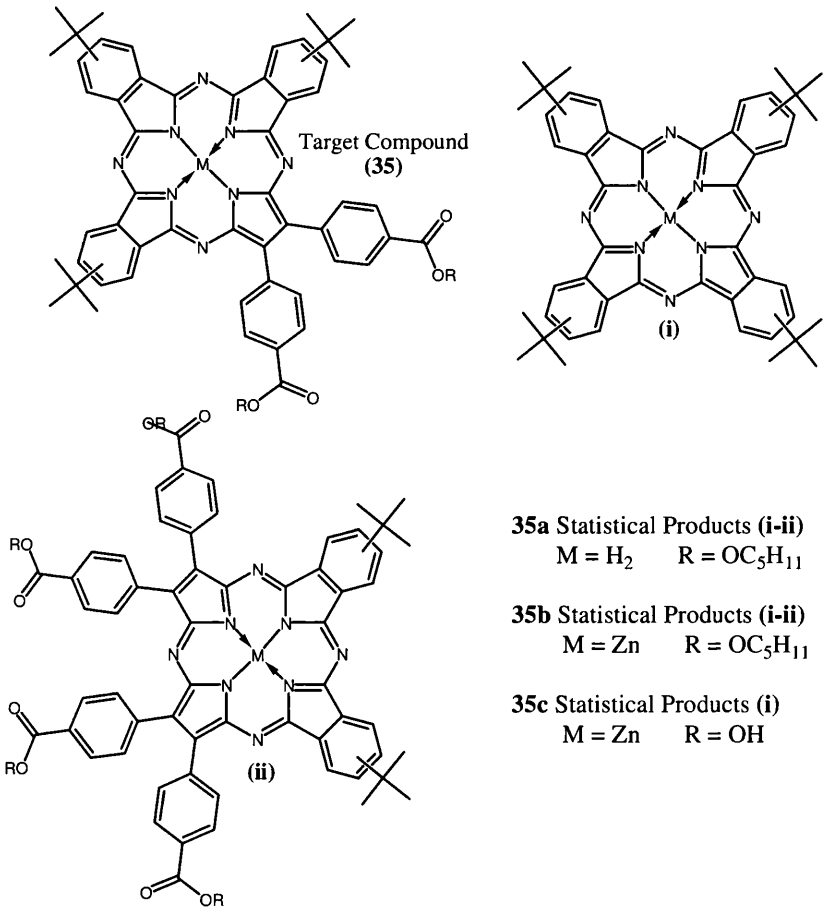

Figure 3.13. *Pseudo* statistical products formed from the reaction between t-butyl phthalonitrile and di-(4-methylbenzoate)-fumaronitrile (**20**) in a 1:3 ratio.

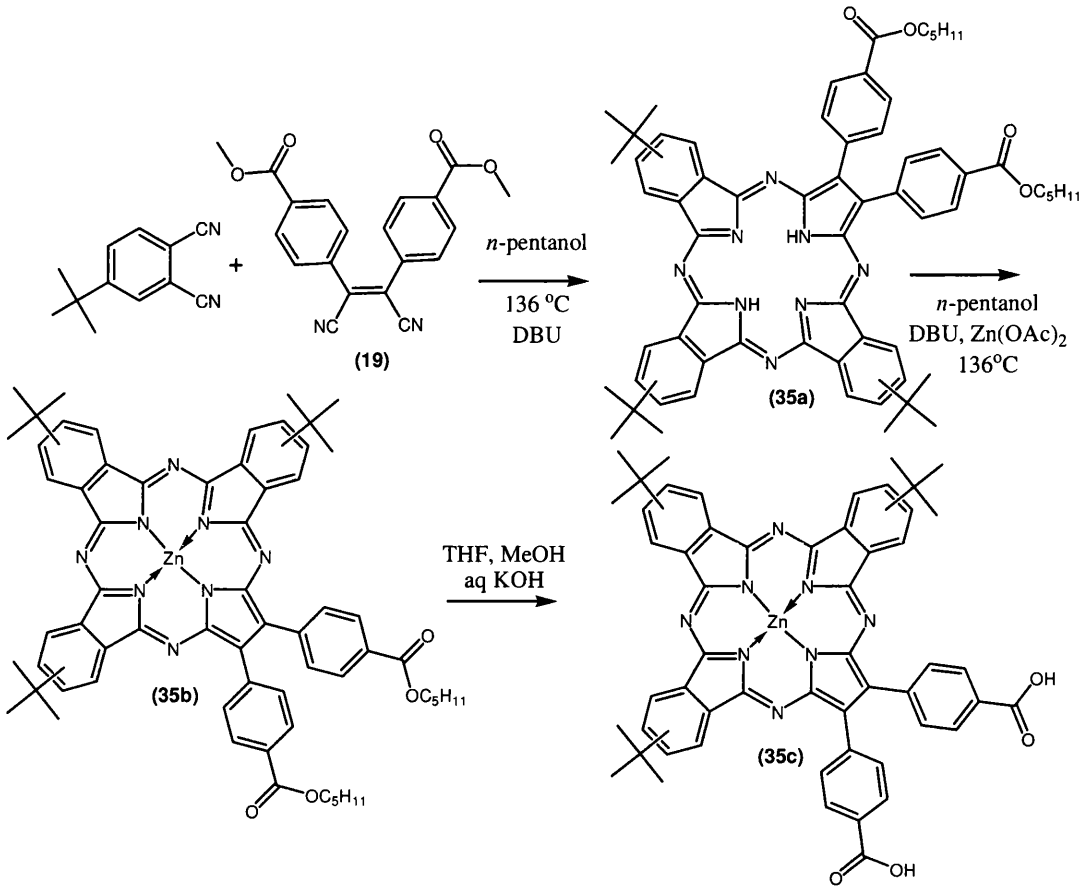

Figure 3.14, Synthetic scheme to 2,3-benzoate-72,122,172-tri-tert-butyl-tribenzo-5,10,15,20-tetraazoporphyrin zinc (**35c**)

The base catalysed hydrolysis of the ester groups was carried out as described for azaporphyrin (**34b**) in THF/methanol containing KOH. In an attempt to purify the *pseudo* statistical mixture, azaporphyrin (**35c**) was then dissolved in dichloromethane and heated to reflux. Molecular ions of 800 and 969.2620 (calculated 969.2627) with relative intensities of 25 : 100 were observed in the mass spectrum, which corresponded to the symmetrical by-product 2,9,16-tetra-*tert*-butyl phthalocyanine zinc (**35ci**) and the desired compound 2,3-(4-benzoate)-7^2,12^2,17^2-tri-*tert*-butyl-tribenzo-5,10,15,20-tetraazaporphyrin zinc (**35c,** Figure 3.14).

It is worth noting that after careful column chromatography, the purification of (**35c**) was more effective as there are no longer any molecular ions which related to the *pseudo* statistical mixture of products associated with the acid groups and a greatly

reduced amount of the symmetrical bi-product (**35ci**) with relative intensities of 100 (**35c**) to 25 % (**35ci**) respectively (Figure 3.15).

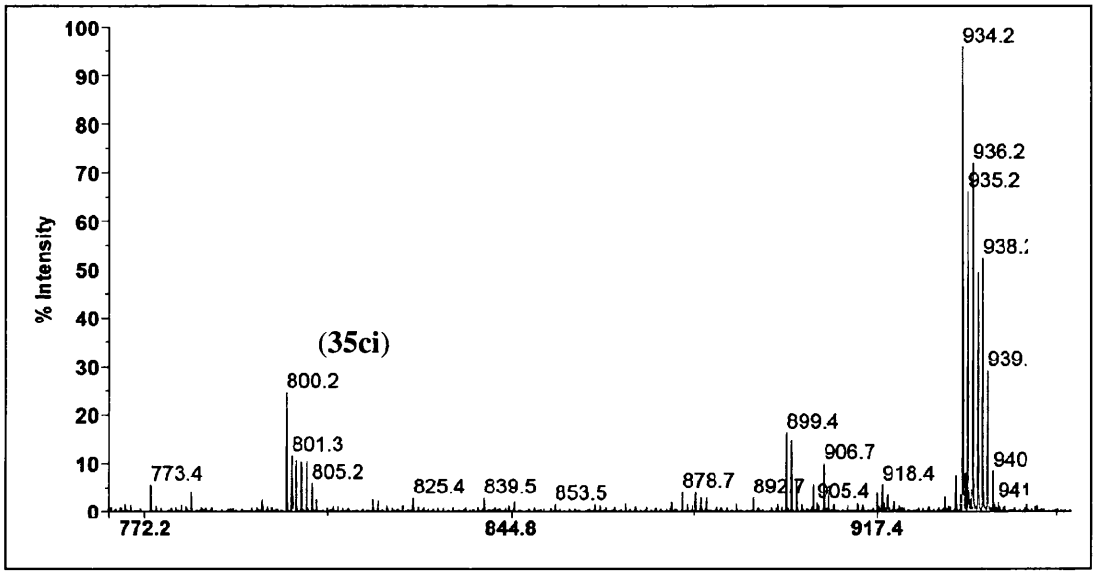

Figure 3.15, Mass spectrum of 2,3-(4-benzoate)-7^2,12^2,17^2-tri-*tert*-butyl-tribenzo-5,10,15,20-tetraazaporphyrin zinc (**35c**)

The ^{1}H NMR spectrum showed that there were two peaks relating to the solubilising *t*-butyl groups which were present at 1.18 and 1.27 ppm along with the absence of the peaks corresponding to the pentanoate groups. The OH and carbonyl stretches of the carboxylic acids are observed at 3439 and 1716 cm^{-1} in the IR spectrum which is consistent with literature reports relating to these acid anchoring groups[64]

The UV-visible spectra of the products from the synthesis of tetraazaporphyrins (**35a**),(**35b**), and (**35c**) is shown in Figure 3.16. The Q-band for (**35a**) has been split due to the reduced symmetry of the molecule, which has occurred from the protonated nitrogens in the core of the macrocycle and the loss of the phenyl group. Once metalated (**35b**), an intense band is observed at 672 nm; this could potentially be due to the tetra-*tert*-butyl phthalocyanine zinc impurity. The tetraazaporphyrin (**35c**) shows that this intense band is no longer present which again could be due to the reduced *t*-butyl impurity.

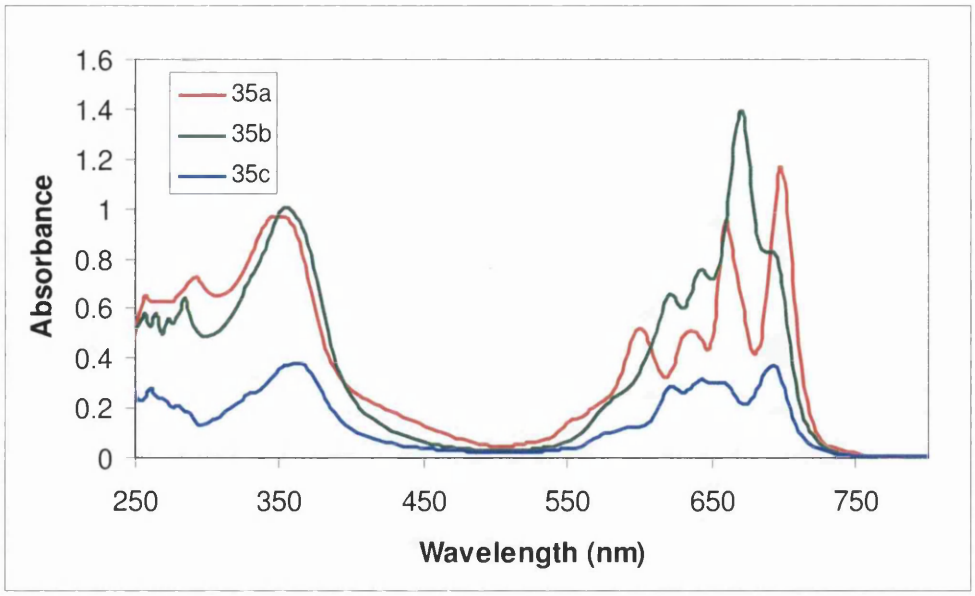

Figure 3.16. UV-visible spectra of tetraazaporphyrin (**35a**), (**35b**), (**35c**) in THF, 9.06 x 10^{-6} M

At this stage in this work, the compound 4,5-bis(4-methoxycarbonylphenyl)phthalonitrile (**20**) was reported in the literature by S. Eu *et al.*[64], as discussed in Chapter 2, and hence this was synthesised for comparison with the fumaronitrile (**19**) anchoring group. Following this, the synthesis of 2,9,16-tri-*tert*-butyl-23,24- bis-4-carboxyphenyl-phthalocyanines zinc (**36c**) was prepared in the same manner as for 2,3-(4-benzoate)-7^2,12^2,17^2-tri-*tert*-butyl-tribenzo-5,10,15,20-tetraazaporphyrin zinc (**35c**).

Cyclisation was achieved using a statistical mixture of starting materials in a 3:1 ratio between the solubilising groups, *t*-butyl phthalonitrile, and the anchoring group (**20**) in pentanol in the presence of DBU (Figure 3.17). Exchange with the pentoxy groups from the solvent was observed for all the statistical products as observed previously and was confirmed in the mass spectrum. The pentoxy derivative of the desired compound, 2,9,16 – tri-*tert*-butyl-23,24-bis-4-pentoxycarboxyphenyl-phthalocyanine (**36a**), was observed with a molecular ion of 1062 (relative intensity 60). The *pseudo* statistical products were also present with molecular ions of 738, 1387 and 1711 with relative intensities of 100:24:8 which corresponded to the symmetrical 2,9,16,23-tetra-*tert*-butyl phthalocyanine (**36ai**), 2,9-di-*tert*-butyl-16,17,23,24-bis-4-pentoxycarboxyphenyl-phthalocyanine (**36aii**) and 2-*tert*-butyl-9,10,16,17,23,24-bis-4-pentoxycarboxyphenyl-phthalocyanine (**36aiii**) respectively (Figure 3.17, 3.18). Thus, the majority of the product is the tetra-*tert*-butyl phthalocyanine with a 100 % molecular ion detected in the

mass spectrum. As no pure product was formed, the ^{1}H NMR also showed a mixture of products.

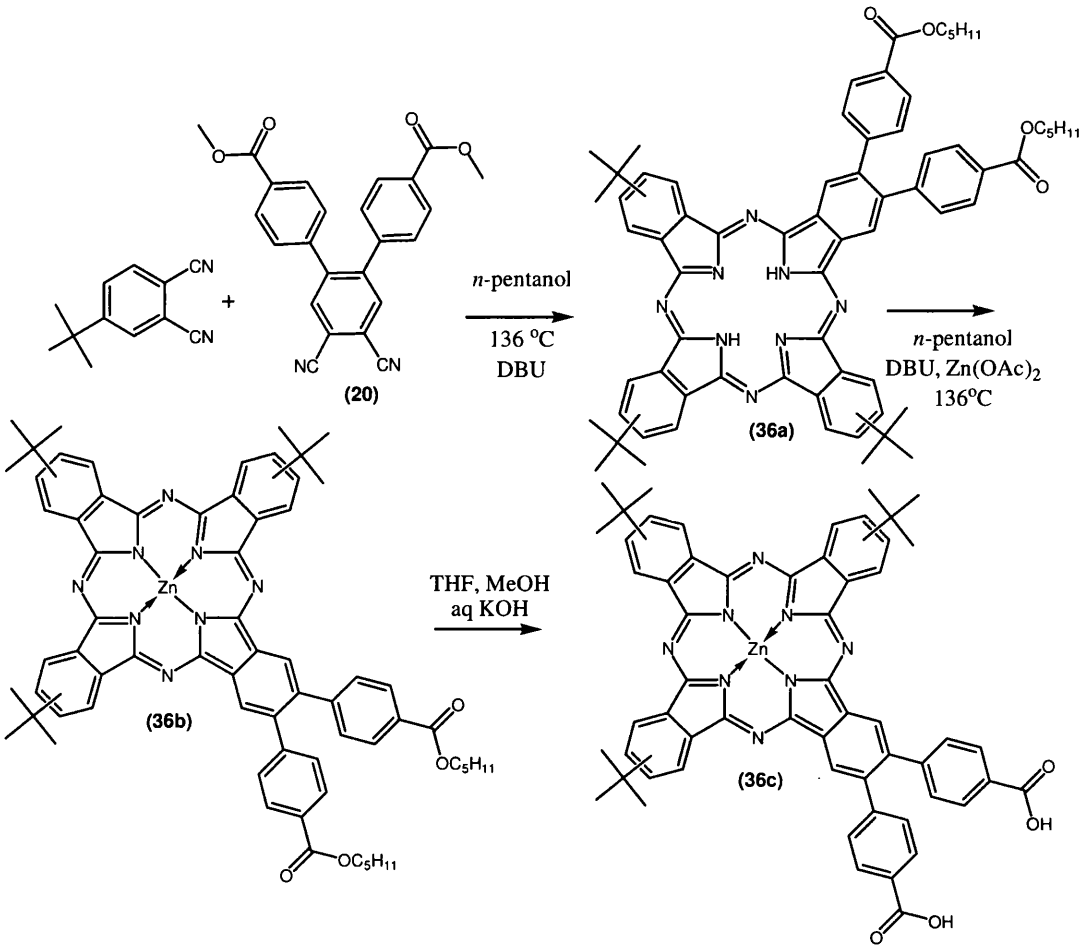

Figure 3.17, Synthesis of 2,9,16-*tert*-butyl-23,24-(4-carboxyphenyl)-phthalocyanines zinc (**36c**)

Zinc was then incorporated in to the core of the macrocycle without further purification with the aim of reducing the amount of by-products by each sub-sequential step. Once metalated, phthalocyanine (**36a**) was subjected to column chromatography with the aim of further removing excess by-products. Characterisation of the metalation was achieved by mass spectrometry with a molecular ion observed at 1125 of the 2,9,16-tri-tert-butyl-23,24-(4-pentoxycarboxphenyl)-phthalocyanine zinc (**36b**) with a relative intensity of a 100 %. The symmetrical tetra-*t*-butyl phthalocyanine zinc (**36bi**), 2,9,di-*t*-butyl-16,17,23,24-(4-pentoxycarboxphenyl)-phthalocyanine zinc (**36bii**), and the 2-*t*-butyl-9,10,16,17,23,24-(4-pentoxycarboxyphenyl)-phthalocyanine zinc (**36biii**) by-products were also present with molecular ions observed at 800, 1448 and 1773 with relative intensities of 37, 54 and 23 respectively. Column chromatography reduced the

amount of the symmetrical product (**36bi**) with the majority of the product, the target compound (**36b**).

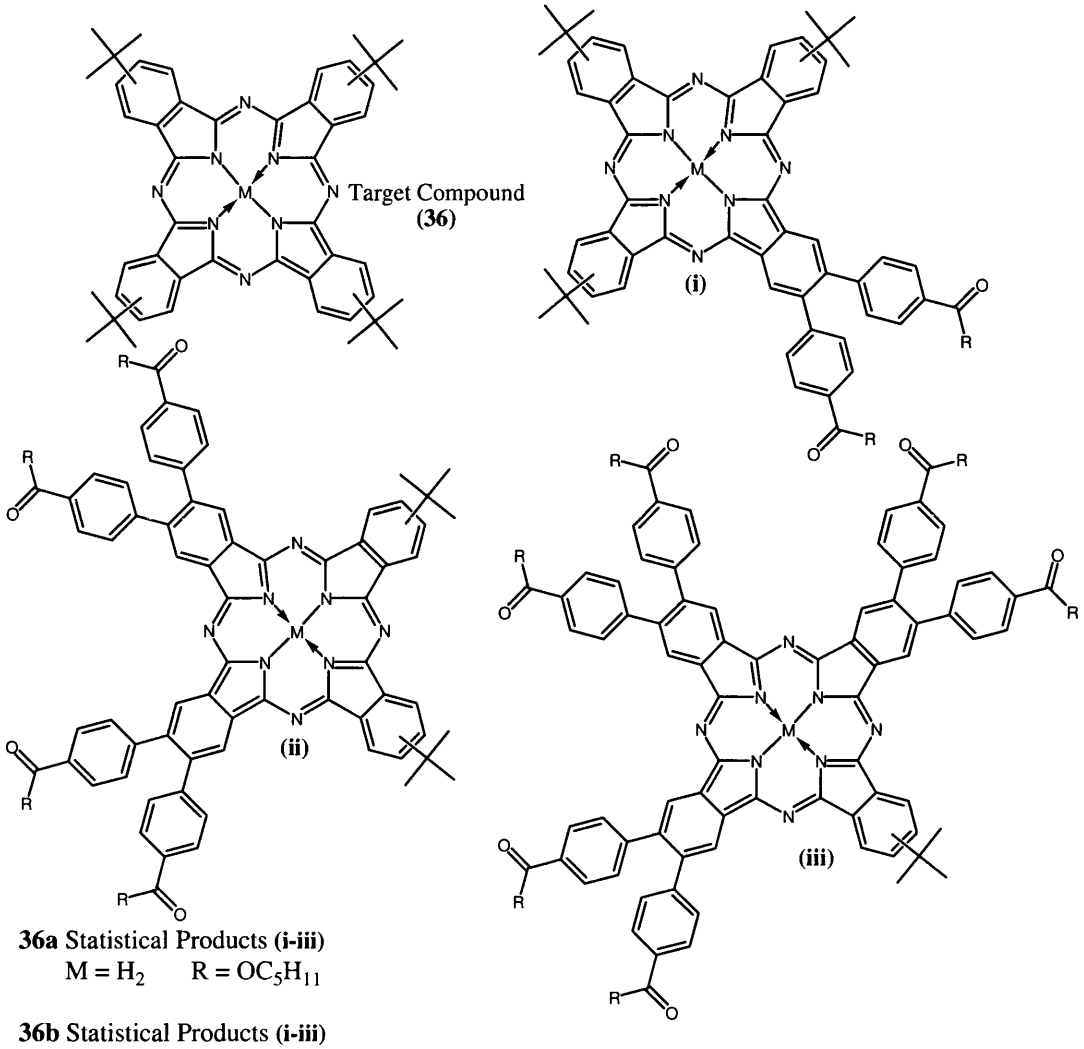

Figure 3.18, Schematic showing the potential *pseudo* statistical products formed during the synthesis of 2,9,16-*tert*-butyl-23,24-(4-carboxyphenyl)-phthalocyanines zinc (**36c**)

Basic hydrolysis of the phthalocyanine (**36b**) was achieved in the same manner as discussed for (**35b**). On analysis of the mass spectrum, it was clear that the tetra-*tert*-butyl phthalocyanine zinc (**36ci**) product still remained with a molecular ion of 800 along with the statistical product (Figure 3.19). The *pseudo* statistical products are therefore more difficult to remove than for azaporphyrin (**35c**) and it is clear that improved methods of purification are required to deliver pure target compound as the literature reports[64,71] that purification of unsymmetrical phthalocyanines can be

achieved by column chromatography. However, it is the reaction conditions that are most commonly varied to promote the formation of the desired statistical product rather than achieving pure products from column chromatography.

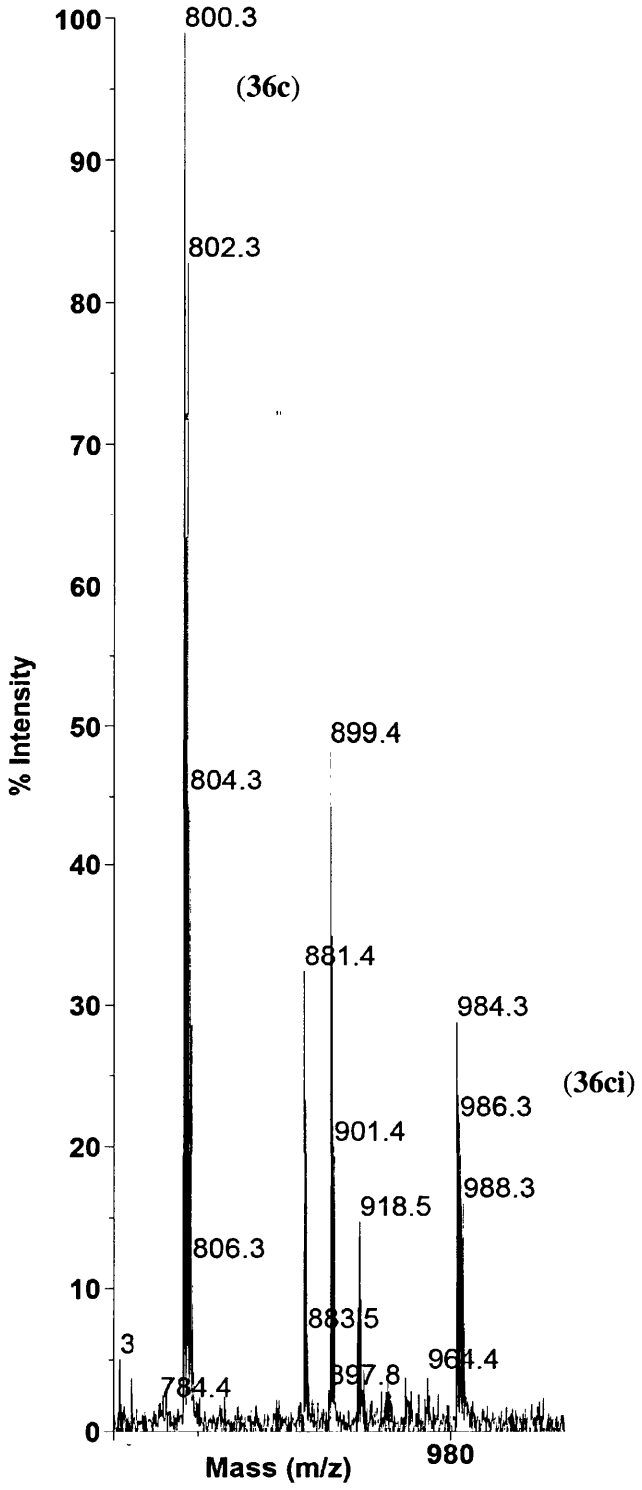

Figure 3.19, Mass spectrum of the products formed during the synthesis of 2,9,16-*tert*-butyl-23,24-(4-carboxyphenyl)-phthalocyanines zinc **(36c)** showing a mixture of product and by-products

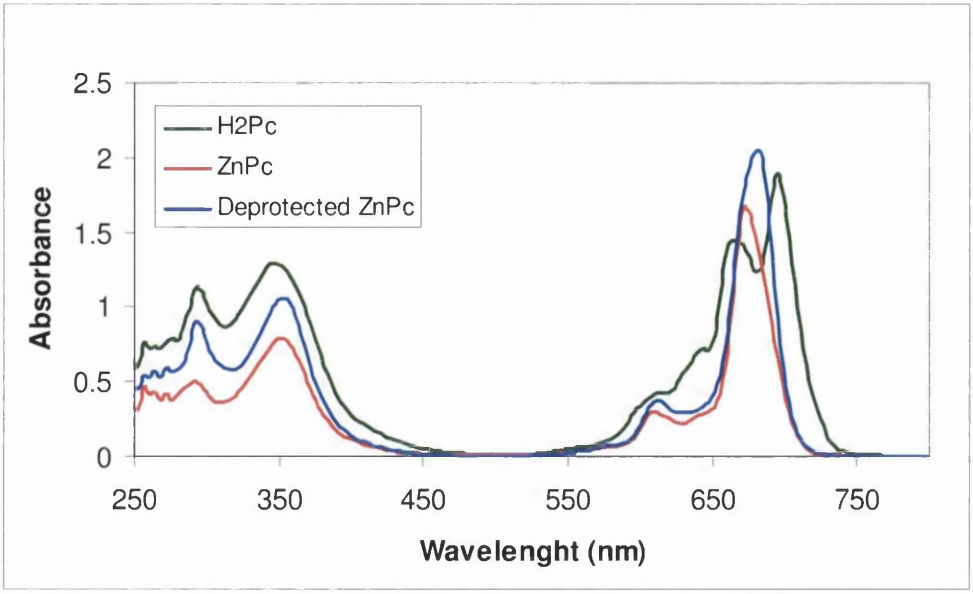

Figure 3.20, UV-visible spectrum of phthalocyanines (**36a**), (**36b**) and (**36c**) in THF, 9.05 x 10^{-6} M

The UV-visible spectra of the phthalocyanines (**36a**), (**36b**) and (**36c**) are shown in Figure 3.20. The Q-band is spilt in the free base phthalocyanine (**36a**) represented in red but is not fully defined which could be due to the statistical impurities present. On metalation, one intense Q-band is observed, which is retained upon deprotection. The ^{1}H NMR reflects this *pseudo* statistical mix as the aromatic peaks are not resolved and multiplets are observed. The signals which correspond to the pentanoate groups in the protected group are no longer present, indicating that hydrolysis has occurred to remove these groups. This is also confirmed in the IR spectrum of the deprotected compound **(36c)** with a signal at 3443 and 1715 cm^{-1} which correspond to the O-H stretch and carbonyl stretch respectively which, corresponds to the literature values[64].

Following this, the incorporation of alkoxy solubilising groups on the phthalocyanine core structure was attempted for comparison with phthalocyanine **(36c)**. The aim here was to prevent aggregation of phthalocyanine dye molecules in solution and within devices to try to increase cell performances. The incorporation of the alkoxy phthalonitrile (**24**) (synthesis discussed in Chapter 2, Section 2.6) with the anchoring group (**20**) under the same conditions as discussed for phthalocyanine (**36a**) was therefore achieved (Figure 3.21).

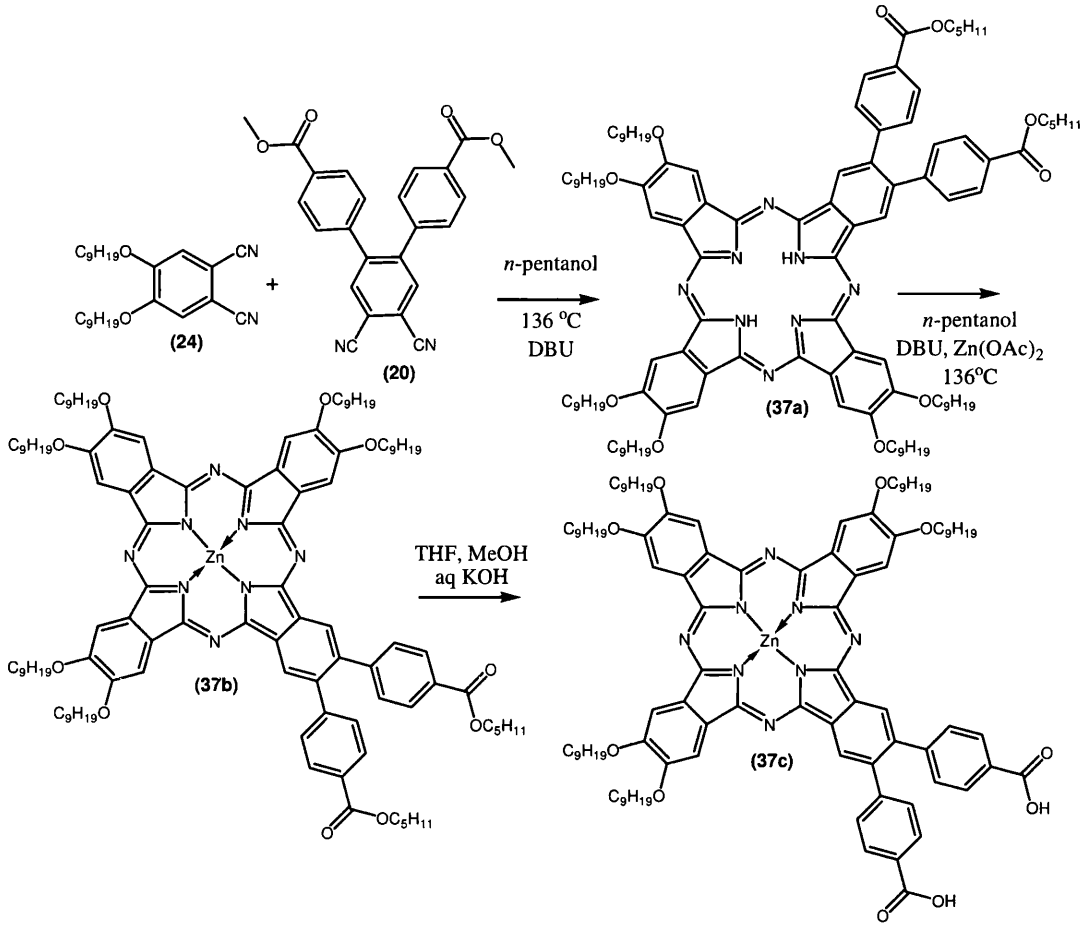

Figure 3.21, Synthesis of phthalocyanine (2,3,9,10,16,17-nonoxy-23,24-(4-carboxyphenyl)-phthalocyanine zinc (**37c**)

The synthetic procedure was carried out using a statistical mixture of starting materials as described previously. The potential products are shown in Figure 3.22. The pentoxy derivative of the desired compound 2,3,9,10,16,17-nonoxy-23,24-(4-pentoxycarboxyphenyl)-phthalocyanine (**37a**) was observed in the mass spectrum with a molecular ion of 1748 (Figure 3.23).

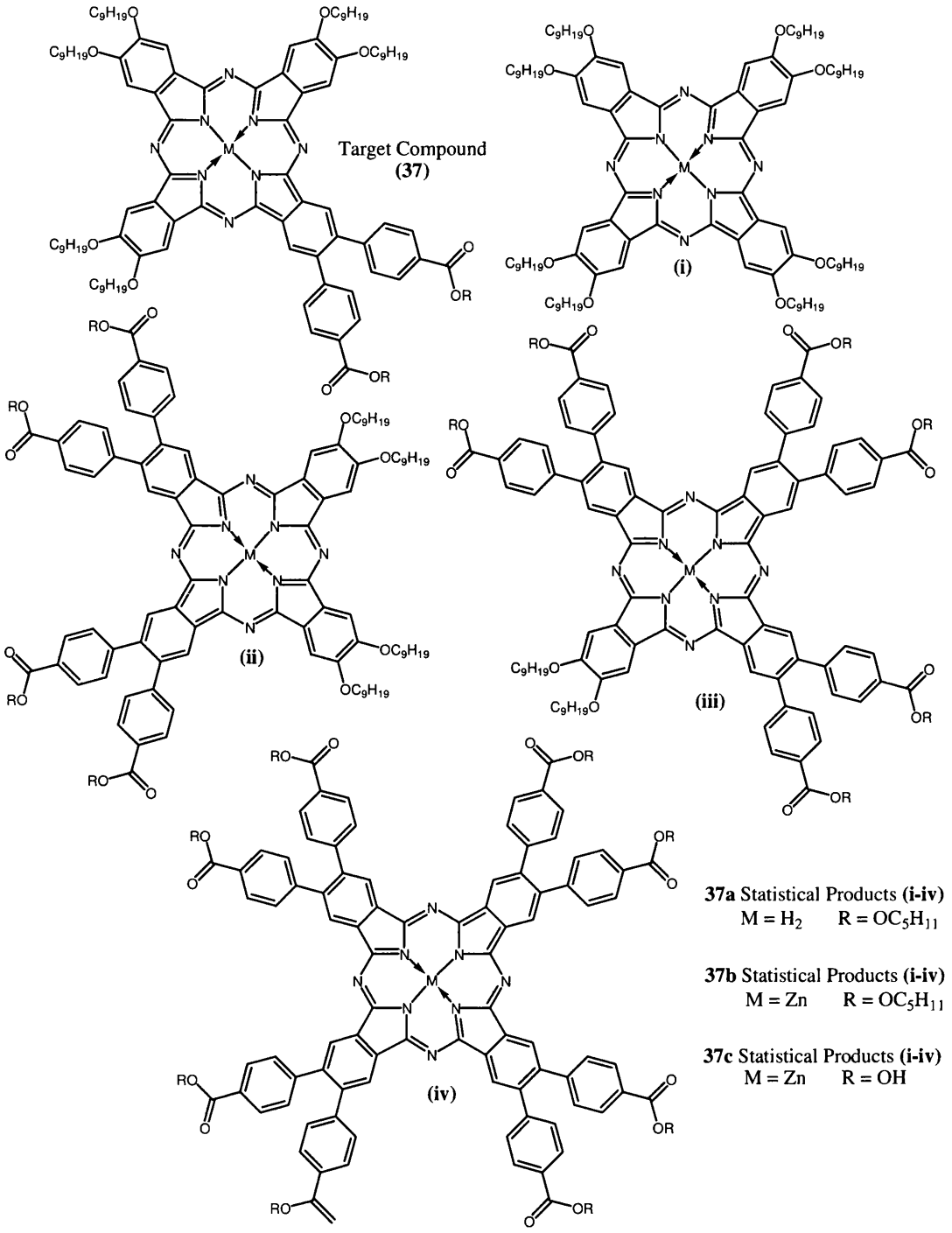

Figure 3.22, *Pseudo* statistical products formed during the synthesis of 2,3,9,10,16,17-nonoxy-23,24-(4-carboxyphenyl)-phthalocyanine zinc (**37c**)

A *pseudo* statistical mixture of products were formed under these conditions with molecular ions of 1652, 1842, 1938 and 2035, which correspond to the symmetrical tetra-nonoxy-phthalocyanine (**37ai**) (Figure 3.23), phthalocyanines substituted with two (**37aii**), three (**37aiii**) and the symmetrical tetra - 2,3,9,10,16,17,23,24-(4-pentoxycarboxyphenyl)-phthalocyanine (**37aiv**). The mass spectral data (Figure 3.23)

based on the intensity of the molecular ions suggest a ratio of 9:6:3:1 of products (**37ai**). (**37a**), (**37aii**), (**37aiii**) and (**37aiv**).

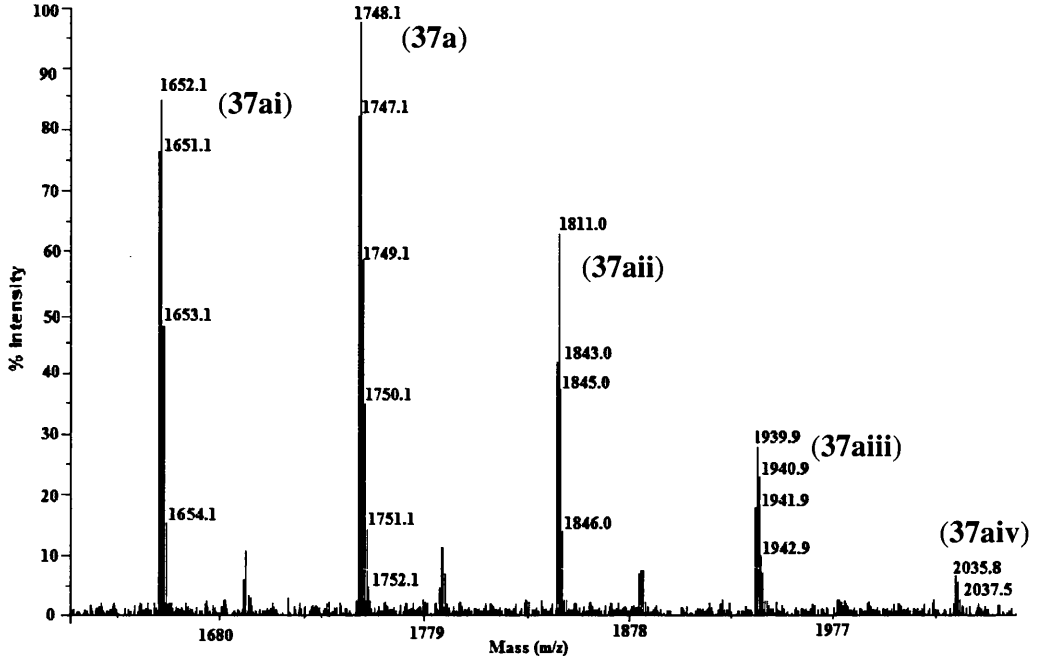

Figure 3.23, Mass spectrum of the *pseudo* statistical mix of products from the preparation of **37a**

Metalation was then achieved using the same conditions as discussed previously. The mass spectrum showed that the unmetallated symmetrical alkoxy phthalocyanine (**37ai**) was still present along with the metalated version (**37bi**) with molecular ions of 1652 and 1714, respectively. Hence, only partial metallation of the symmetrical product had occurred. This could be due to the reduced solubility observed with the alkoxy solubilising groups in this solvent. The 2,3,9,10,16,17-nonoxy-23,24-(4-pentoxycarboxyphenyl)-phthalocyanine zinc (**37b**) was observed at 1809 in the mass spectrum with a relative intensity of 100 %. Again a *pseudo* statistical mix of phthalocyanines (**37bii** and **37biii**) was observed with molecular ions of 1905 and 2001. It is worth noting that from the relative intensities in the mass spectrum the amount of the by-products (**37bii** and **37biii**) have been reduced in the purification procedure with the symmetrical 2,3,9,10,16,17,23,24-(4-pentoxycarboxyphenyl)-phthalocyanine (**37biv**) no longer present.

Basic hydrolysis of the ester groups was attempted using the same conditions as described previously but it was found that the phthalocyanine mixture was not soluble enough in a mixture of methanol/THF and aqueous KOH for the hydrolysis to be achieved. On consulting the literature, it was found that hydrolysis of esters can be achieved in pyridine with aqueous KOH[48]. This was attempted and proved successful

and yielded the desired product 2,3,9,10,16,17-nonoxy-23,24-(4-carboxyphenyl)-phthalocyanine zinc (**37c**) but with a relative intensity of 62 %. The symmetrical alkoxy phthalocyanine (**37ci**) along with the nonmetalated derivative (**37ai**) were still found to be present along with the 2,3,9,10-nonoxy-16,17,23,24-(4-carboxyphenyl)-phthalocyanine zinc (**37cii**) with relative intensities of 100, 14 and 18 respectively. The statistical bi-product (**37ciii**) was removed during the purification procedure but so was a large quantity of the desired product (**37c**).

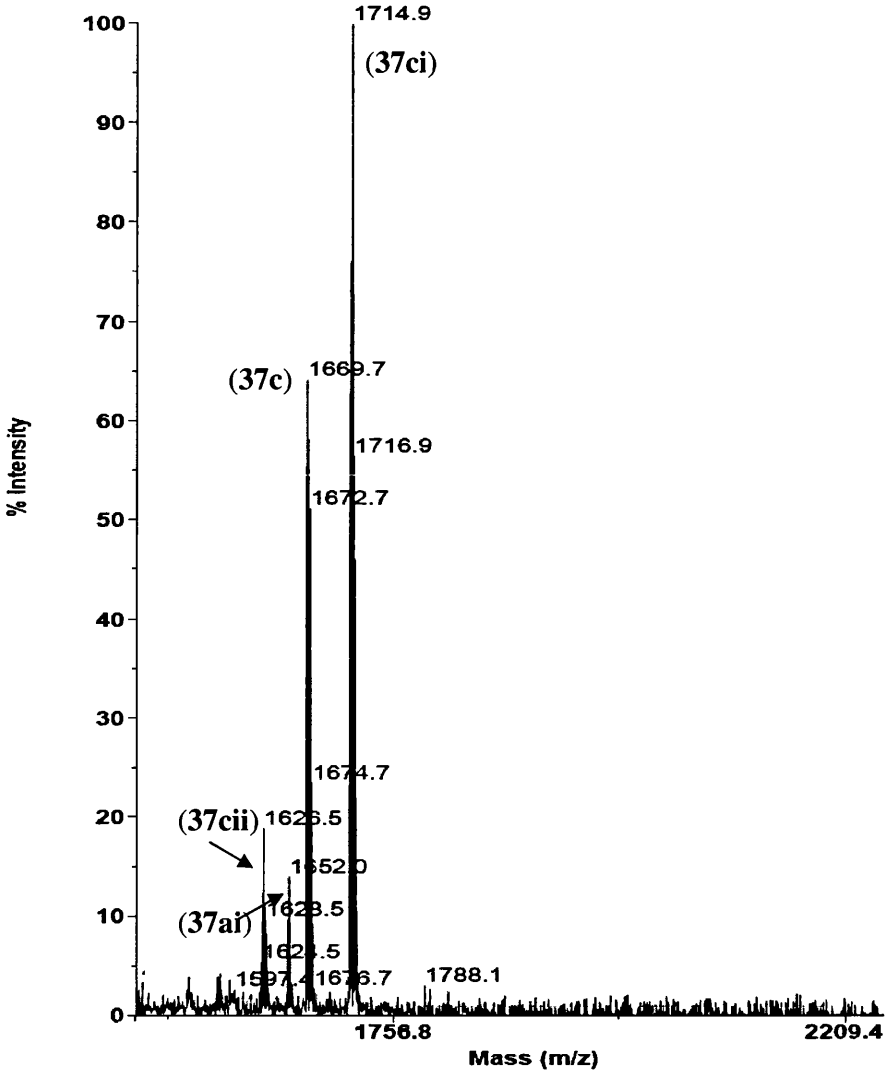

Figure 3.24, Mass spectrum of 2,3,9,10,16,17-nonoxy-23,24-(4-carboxyphenyl)-phthalocyanine zinc (**37c**)

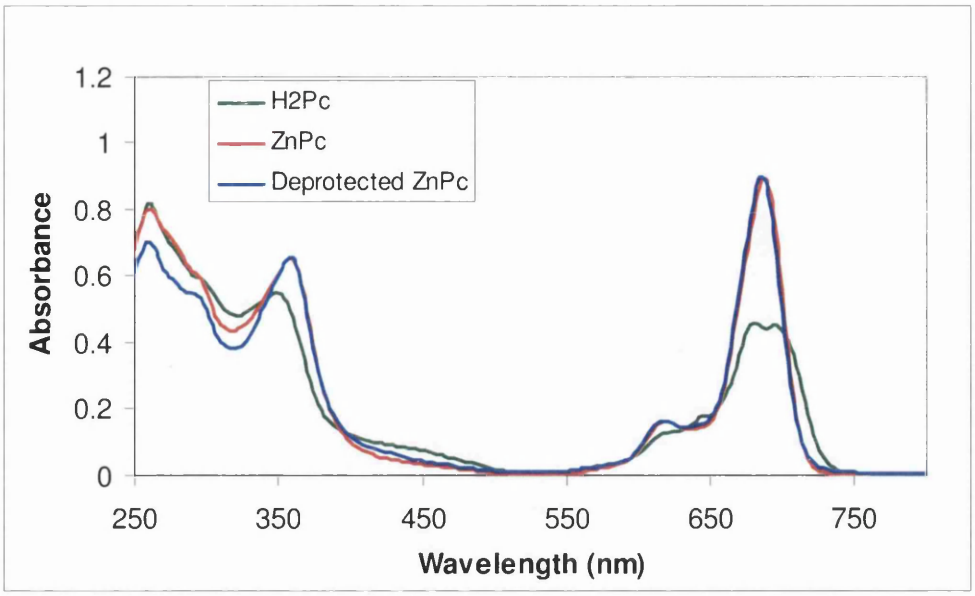

Figure 3.25. UV-visible of phthalocyanines (**37a**), (**37b**) and (**37c**) in THF, 9.05 x 10^{-6} M

The UV-visible spectrum of the phthalocyanines **37a-37c** shows the Soret band at 348 nm for (**37a**) and 360 nm for (**37b**) and (**37c**). The Q band related to the non-metalated phthalocyanine 680 and 696 nm, (Figure 3.25), H_2Pc, **37a** was not as split as the other corresponding non-metallated macrocycles, compounds **(35a)** and **(36a)**. This could be due to a higher amount of impurities detected in the mass spectrum. The metallated phthalocyanine (**37b**) and the acid derivative (**37c**) contain one intense Q-band at 684 nm due to the increased symmetry[41]. The IR confirms the presence of the carboxylic acid with signals at 3420 and 1719 cm^{-1} due to the OH and carbonyl stretches which corresponds to literature values[64]. The peaks in the ^1H NMR spectrum are not fully resolved and hence multiplets have been reported which is due to the *pseudo* statistical mixture of products present resulting in similarly positioned signals overlapping in the spectra. The signals at 0.93, 1.46, 1.89 and 4.33 ppm correspond to the nonoxy solubilising groups. Again, there are broad signals in the aromatic region that corresponded to the aromatic protons. There are two doublets at 7.43 and 8.01 which could represent the aromatic protons on the carboxyphenyl groups.

The addition of ferrocene units to the phthalocyanine core has also been investigated within this thesis, with the original aim of acting as a redox site to interact with the DSSC electrolyte couple for added stability against single oxygen attack and also increased dye solubility. Literature reports that ferrocene units have been attached to porphyrins and phthalocyanines for investigations into the electronic coupling between

the ferrocene units[115]. It has been reported that m*eso*-tetraferrocenylporphyrin (Figure 3.26), which forms a mixed valence species with the Fe ^{III} and Fe ^{II} bis(cyclopentadienyl units), does lead to an interaction between the ferrocene[115] units. However, it has also been reported that 2,9,16,23-tetraferrocenylphthalocyanine (Figure 3.26) does not exhibit such interactions[100] due to the large steric separation between the units. Instead these workers reported that the ferrocene units are all oxidized at the same potential and the units are essentially behaving independently. UV-visible absorption studies showed that there is a red shift of this compound in the Q band compared to unsubstituted phthalocyanine due to the interaction of the ferrocene with the phthalocyanine π-system in the excited state.

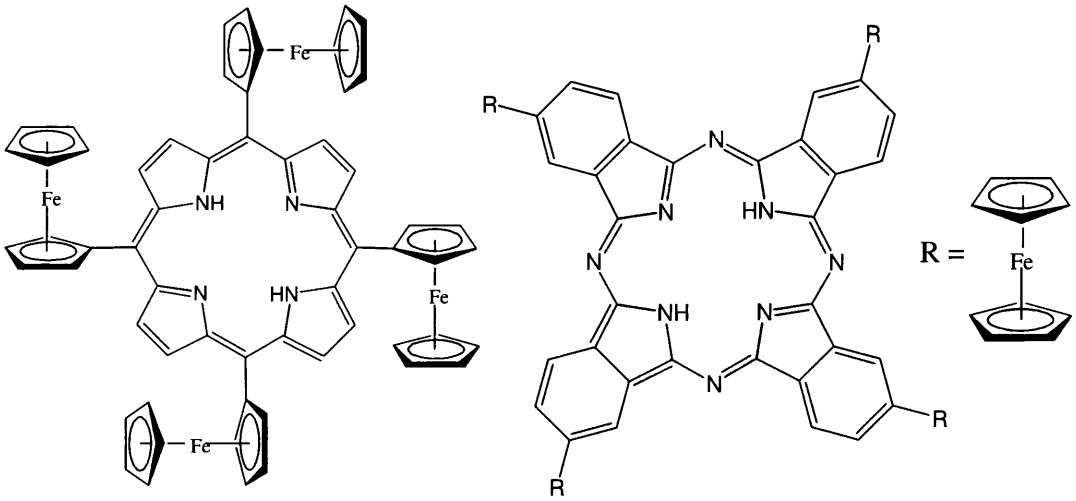

Figure 3.26. Molecular structure of *meso*-tetraferrocenylporphyrin[14] and 2 9,16,23-tetraferrocenylpthalocyanine[100,115].

In this thesis, cyclotetramisation of 4-(1-bromoferrocene)-5-chlorophthalonitrile **(16)** was achieved in pentanol in the presence of DBU and zinc acetate. The solubility of the ferrocene substituted phthalocyanine was greatly reduced compared to the alkoxy and *t*-butyl derivatives and hence purification became a problem as column chromatography could not be fully utilized. The target compound 2,9,16,23-(tetra-1-bromoferrocene)-3,10,17,24-chlorophthalocyaninezinc(II) **(38)** was obtained in low yield due to problems with solubility. Two products were obtained; one with the ferrocene containing a bromine substituent on the lower cyclopentadiene ring and the other without the halogen, as determined by mass spectrometry. Molecular ions of 1687 and 1767 were observed respectively. The ^{1}H NMR reflected this with six signals at 4.20, 4.29, 4.33, 4.47, 4.58 and 4.65 which corresponded to the two differently substituted ferrocenes. The UV-visible spectral data are shown below (Figure 3.27). The data show a

bathochromic shift in absorbance in the Q band to 708 nm compared to that of the alkoxy and *t*-butyl derivatives.

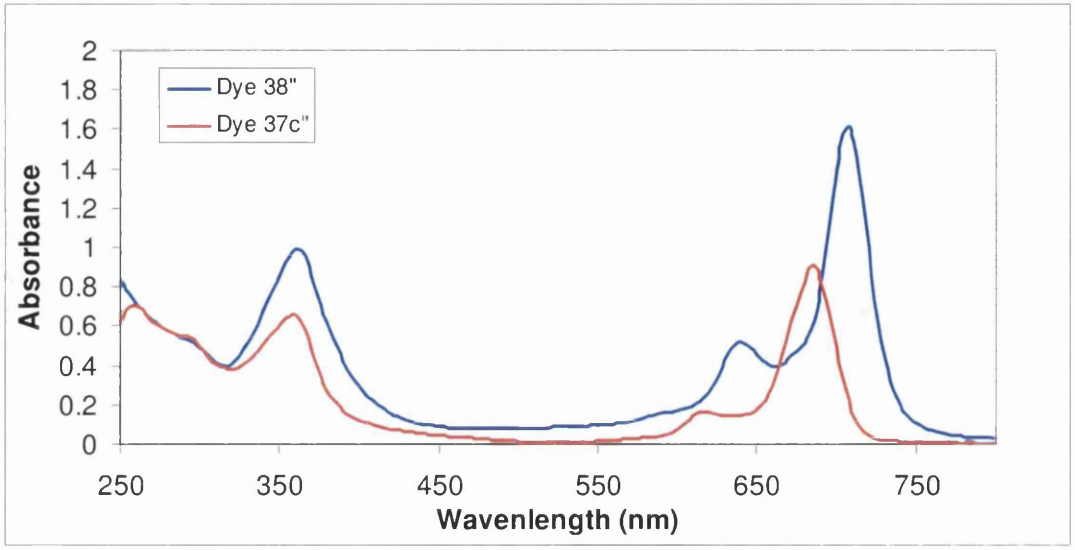

Figure 3.27, UV-visible spectra of 2,9,16,23-(tetra-1-bromoferrocene)-3,10,17,24-chlorophthalocyaninezinc(II) (**38**) in THF, 9.05 x 10-6 M

In order to incorporate ferrocene units into a macrocycle for a DSC dye, ferrocene phthalonitrile **(16)** was cyclised in a statistical condensation with 4,5-bis(4-methoxycarbonylphenyl)phthalonitrile **(20)** in a ratio of 3:1 in *n*-pentanol with zinc acetate in the presence of DBU. Initial data showed that the cyclisation was successful with a molecular ion of 1850 observed in the mass spectrum. There were no signs of the other statistical products in the mass spectrum but further purification was hindered due to the reduced solubility observed for this product. On base catalysed hydrolysis in THF/methanol in the presence of aqueous KOH, decomposition of the compound was observed with an unidentified molecular ion of 1384 observed in the mass spectrum.

Due to the unsuccessful hydrolysis of (**38**), ferrocene acetylene **(13)** was coupled to chloro[triiodosubphthalocyaninato]-boron (III) **(28)** using a Sonogashira coupling with the aim of forming an unsymmetrical phthalocyanine functionalised with ferrocene units. Sonogashira coupling was first reported in 1975 by Kenkichi Sonogashira[116] and Nobue Hagihara for the preparation of internal acetylenes. The coupling reaction involves the reaction of a terminal alkyne with an aryl halide under mild conditions allowing a larger number of functional groups to be tolerated. This has included the coupling of ethnylferrocene to phthalocyanine core structures (Figure 3.28)[50] with the Q

band again shifted to the red region of the spectrum compared to that of an unsubstituted zinc phthalocyanine.

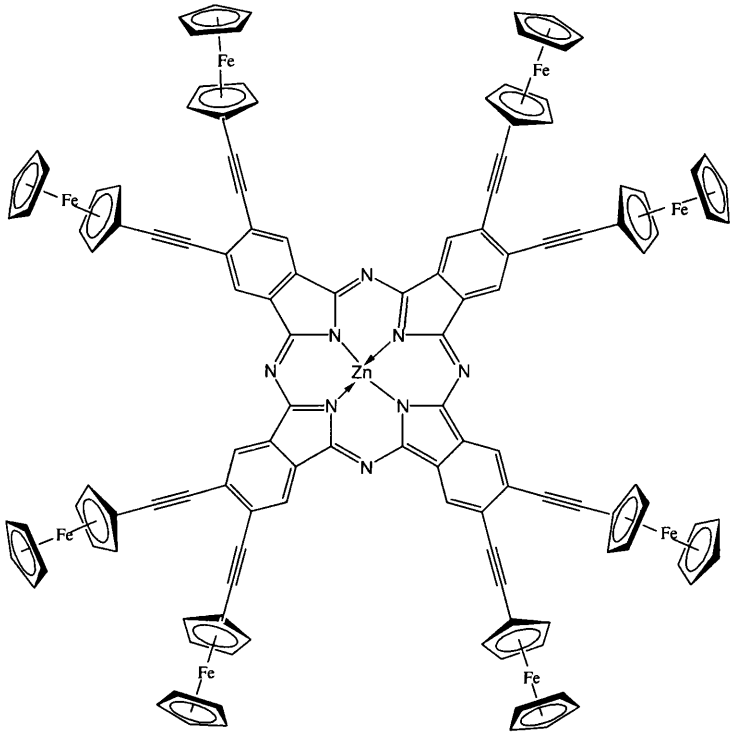

Figure 3.28. 2,3,9,10,16,17,23,24-octakis(ferrocenylethynyl)phthalocyaninezinc(II)[50]

The mechanism (Figure 3.29)[117] of Sonogashira coupling has been much discussed in the literature. However, it is currently generally accepted that the reaction proceeds through oxidative addition of an aryl halide to a palladium (0) catalyst (step 1) forming a palladium (II) complex (step 2). It is suggested that the deprotonation of the acetylene is achieved by the interaction of copper halide (step 4) and the reaction with base (step 5), as the amines are not basic enough to deprotonate the acetylene alone. In the absence of copper iodide, the reaction does not proceed. An organo-copper compound is formed (step 4 – 6) which then reacts with the oxidative addition product from step 2 and undergoes transmetalation with the copper acetylide (step 3). This regenerates the copper halide and it is believed that both the organic residues are now linked to the Pd (II) catalyst. Both the organic ligands are then *trans* orientated and convert to *cis* in a *trans-cis* isomerisation, which is followed by the reductive elimination regenerating the Pd(0) catalyst. Glaser coupling of two acetylenes is a side reaction of this mechanism.

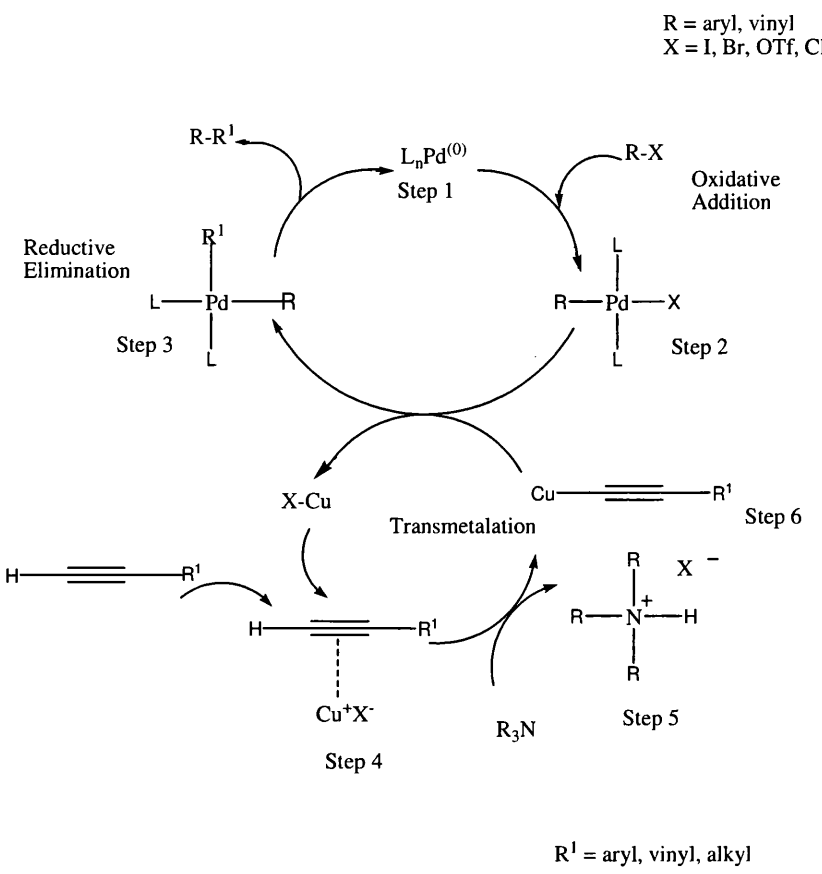

Figure 3.29, General mechanism for Sonogashira coupling, redrawn from[117].

Due to the unsuccessful synthesis of (**39**), ferrocene acetylene (**13**) was coupled to chloro[triiodosubphthalocyaninato]-boron (III) (**28**) using Sonogashira coupling in the presence of copper iodide, a palladium catalyst, $(PPh_3)_4Pd$, in diethylamine and heated to reflux for 6 hours. The aim of this was to introduce the ferrocene functional group into the phthalocyanine macrocycle and study the effects. After careful column chromatography, chloro[2,9,16,(ferrocenylethynyl)subphthalocyanine] boron (III) (**40**) eluted in a mixture of petroleum spirit and ethyl acetate (1:1 mix by volume).

The purple solid of chloro[2,9,16,(ferrocenylethynyl)subphthalocyanine] boron (III) (**40**) (Figure 3.30) was characterised by ^{1}NMR with signals at 4.28, 4.33 and 4.63 corresponding to the mono-substituted ferrocene unit with the signal at 4.33 representing the unsubstituted cyclopentadiene ring. The aromatic protons on the subphthalocyanine were observed at 8.01 and 8.80 ppm. The mass spectrum also confirmed the presence of the ferrocene subphthalocyanine with a molecular ion at 1054. There was a bathochromic shift in the UV-visible absorption spectrum of *ca.* 36 nm compared to the unsubstituted subphthalocyanine (**25**)

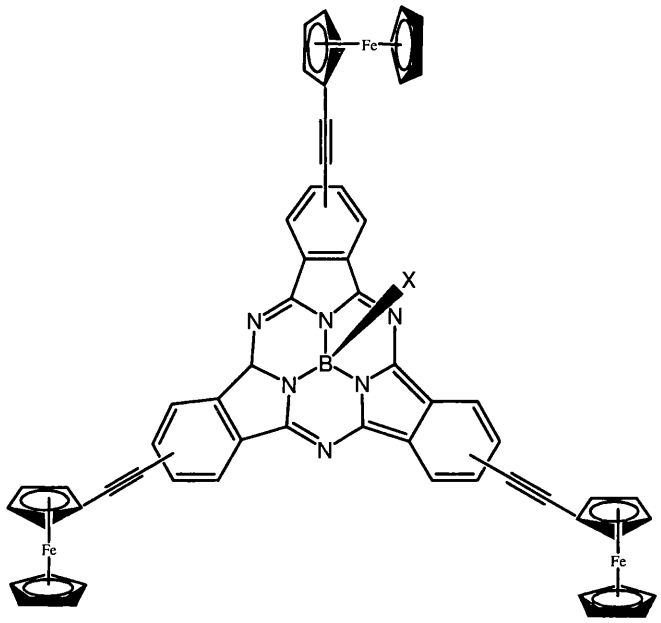

Figure 3.30, Structure of Chloro[2,9,16,(ferrocenylethynyl)subphthalocyanine] boron (III) **(40)**

Due to the mixture of products allied to the difficulty in purification observed during the statistical condensations, coupling of 4-(methoxycarbonylphenyl)-boronic acid was attempted and achieved on the iodinated sites of chloro[triiodosubphthalocyanine] boron **(28)** (Figure 3.31) with aim of incorporating acid anchoring groups onto the subphthalocyanine. The idea was that this molecule could then undergo a ring expansion reaction with *t*-butyl isoindolinone **(30)**, forming an unsymmetrical phthalocyanine with a higher degree of purity than that observed in the statistical condensations. Suzuki-Miyaura cross coupling with the boronic acid derivative and chloro[triiodosubphthalocyanine] boron **(28)** was achieved using the same conditions as reported for the formation of 4,5-bis(4-methoxycarbonylphenyl)phthalonitrile (**20**) to produce **(41)**. After careful column chromatography in ethyl acetate and petroleum spirit, the target molecule was separated. The mass spectrum confirmed the presence of the substituted subphthalocyanine, chloro[2,9,16,(4-methoxycarboxyphenyl) subphthalocyanine] boron (III) **(41)** with a molecular ion observed at 833.2065 (calculated = 833.2089). A peak at 3.92 ppm in the ^{1}H NMR spectrum corresponded to the methyl group of the ester. The UV-visible spectral data showed (Figure 3.32) a bathochromic of *ca.* 14 nm was observed compared to subphthalocyanine **(26)** due to the extended conjugation.

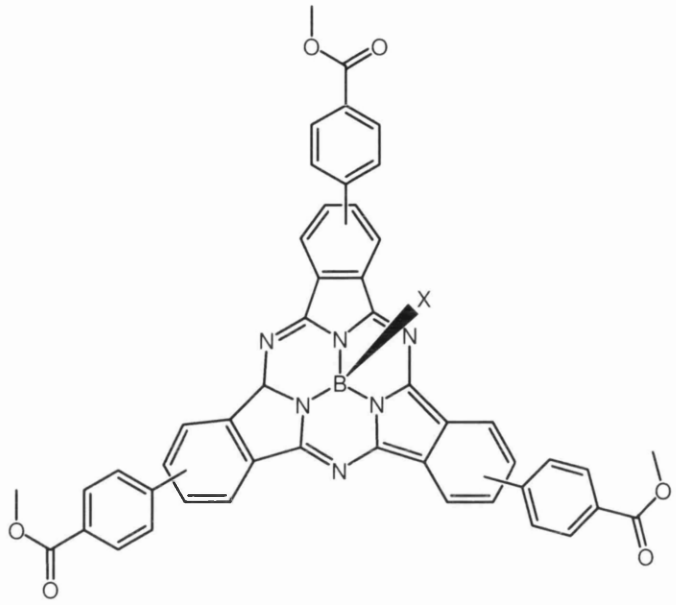

Figure 3.31. Structure of chloro[tri(4-methoxycaboxyphenyl)subphthalocyanine] boron **(41)**

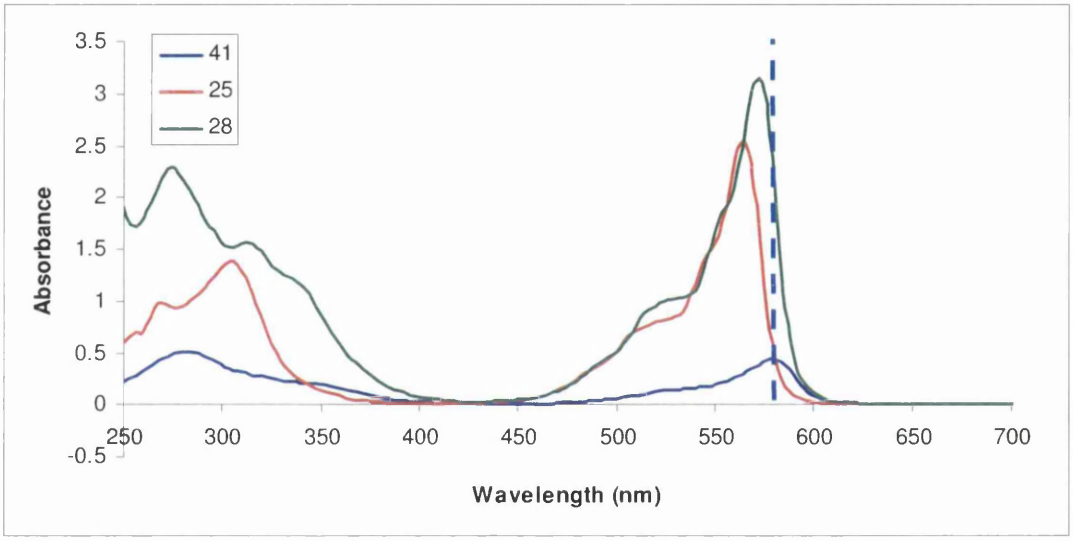

Figure 3.32. UV-visible spectra of chloro[2,9,16,(4-methoxycarboxyphenyl) subphthalocyanine] boron (III) **(41)**, Cloro[subphthalocyaninato[-boron (III) (**25**) and Chloro[triiodosubphthalocyaninato]-boron (III) (**28**) 9.05 x 10^{-6} M, CH_2Cl_2

Ring expansion of **(41)** was then attempted by reaction with 4-*t*-butyl-1,3-isoindoline **(30)** in dimethylaminoethanol. The reaction mixture turned from a vivid purple solution to a green solution but on work up, it was apparent that the expansion had not been achieved successfully and instead that degradation of chloro[tri(4-methoxycaboxyphenyl)subphthalocyanine] boron **(41)** had occurred. It was therefore decided that derivitisation would be attempted after ring expansion of the halogenated subphthalocyanines.

Ring expansion reactions between subphthalocyanines and isoindolines were therefore investigated to synthesise unsymmetrical phthalocyanines. On consulting the literature, it was found that ionic liquids have been investigated as potential environmentally friendly solvents for a variety of organic reactions including Diels-Alder reactions, aldol condensations, Heck reactions and for subphthalocyanine expansions[118]. Tetrabutylammonium bromide, 1,1,3,3-*N,N,N'N'*-tetramethylguanidinium trifluoroacetate and butyl(2-hydroxyethyl)dimethylammonium bromide have recently been used in the synthesis of metal free and metallated phthalocyanines[114]. Industrially these solvents could be advantageous due to their low vapour pressure, thermal stability, high ionic conductivity and the fact that they can be recycled easily by an initial extraction of the reaction mixture with water to separate the ionic liquid, followed by subquential drying[112]. In this thesis, the ionic liquid butyl(2-hydroxyethyl)dimethylammonium bromide **(42)** was prepared according to literature procedure[119]. Thus, dimethylethanolamine was reacted with butyl bromide. It was then found that recrystallisation from a THF:petroleum spirit mix in a 3:1 ratio allowed the ionic liquid to crystallise out of solution. On addition of petrol as suggested in the literature[119], the product did precipitate out of solution but did so readily on addition of THF. On consulting the literature, it was found that the data obtained had some discrepancies with the literature data[119]. The mass spectrum of the ionic liquid gave a high resolution molecular ion of 146.1541 (Calculated 146.1539). This corresponded to the organic ion without the bromine counter ion while the literature data stated a molecular ion of 137. The ^{1}H NMR showed resonances 1.04, 1.45, 1.80 and 3.50 ppm which corresponded to the butyl chain. The methyl groups were observed with a single resonance at 3.19 ppm.

Subphthalocyanines have been expanded in the literature using the butyl(2-hydroxyethyl)dimethylammonium bromide **(42)** ionic liquid to form metallated, unsymmetrical phthalocyanines[118]. Solubilising groups attached to the periphery positions such as methyl groups and *t*-butyl groups were present along with NO groups. In this thesis, subphthalocyanine (**25**) was expanded with phthalonitrile using the ionic liquid to compare to the isoindolinone synthesis described earlier. The ionic liquid **(42)**, phthalonitrile and zinc acetate were heated to 140 °C for 5 hours. The resulting blue solid was then diluted with water and filtered. The solid was then washed with water to remove any ionic liquid which could then be re-used in further reactions. The solid was then placed in a Soxhlet extractor in dichloromethane to remove any unreacted

subphthalocyanine **(25).** The resulting solid was dried and all data correlated with the literature for zinc phthalocyanine **(43)** with a molecular ion at 577 and a characteristic UV-visible spectrum with a Q band at 680 nm and a Soret band at 352 nm. It should be noted that this reported synthetic procedure of producing unsymmetrical phthalocyanines from subphthalocyanines does not require the use of the isoindolinone derivatives as the DBU and ionic liquid produced a derivative of this nature during the reaction mechanism[118]. The isoindoline unit then attacks the subphthalocyanine leading to ring opening of the subphthalocyanine leading to an open four unit system The suggested reported mechanism is shown in Figure 3.33[118]. This is very advantageous as one step of the reaction pathway has been eliminated and the use of ammonia gas is therefore not required.

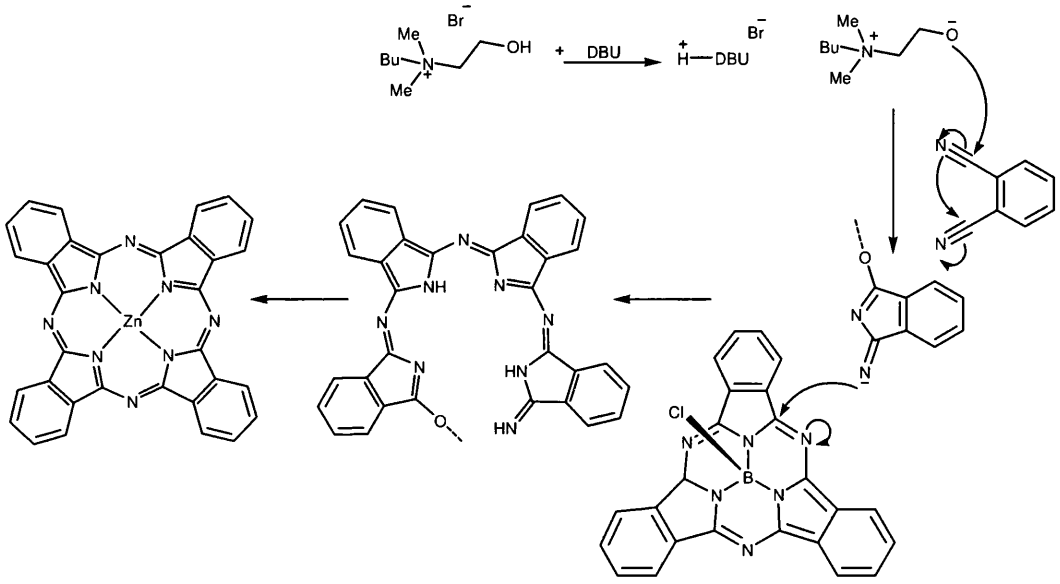

Figure 3.33, Mechanism for ionic liquid synthesis, redrawn from [118].

Thus, in this thesis similar conditions to those reported by Chaulan and Kumari[114] have been applied to the ring opening expansion of chloro[triiodosubphthalocyaninato]-boron (III) **(28)** and *t*-butylphthalonitrile. Once again the reaction mixture was washed with water to remove the ionic liquid. The blue residue was then dissolved in ethyl acetate and put through a plug of alumina to remove any unwanted solid impurities. On analysis of the mass spectrum, it was clear that the majority of the product was the 2,9,16,23-*t*-butyl-phthalocyanine but there was another peak at 1604, which is believed to be the dimer of the 2,9,16,23-*t*-butyl-phthalocyanine. However, there is no evidence of the desired product **(44)** or of the symmetrical iodinated product which could be due to solubility issues with the iodophthalonitrile **(5)**.

Due to the unsuccessful synthesis of (**44**) using the ionic liquid method, the reaction was then carried out using the isolindoline method[65]. Chloro[triiodosubphthalocyaninato]-boron (III) (**28**) was reacted with the *t*-butly-1,3-isoindoline (**30**) in a 1:5 ratio (Figure 3.34). The reaction was heated for 8 hours at 80 °C. The precipitate was filtered and washed to remove impurities.

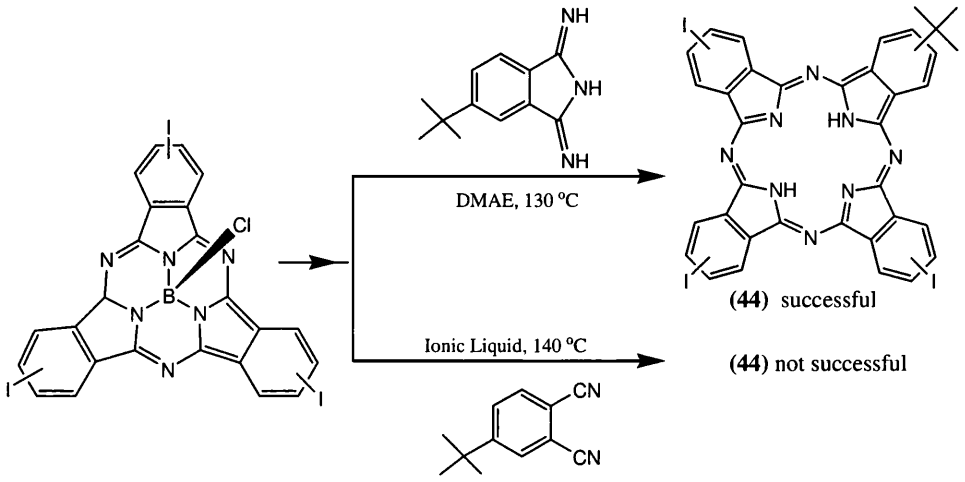

Figure 3.34, Synthetic pathway to 2-*t*-butyl-9,16,23-triiodo-phthalocyanine (**44**)

On analysis of the mass spectrum, it was clear to see that the desired metal free phthalocyanine of 2-*t*-butyl-9,16,23-triiodo-phthalocyanine (**44**) was obtained with a molecular ion of 947.9176 (calculated 947.9177). There was no symmetrical iodinated product leading to the conclusion that dimers were not made and self condensation did not occur. Thus, a pure product had been produced which would eliminate the problems of purification associated with the statistical method. This therefore leads to the idea that the subphthalocyanine expansion depends on the nature of the substituent. The UV-Visible spectrum of (**44**) is shown in Figure 3.35. The Q-band is split due to the lack of symmetry in the macrocycle.

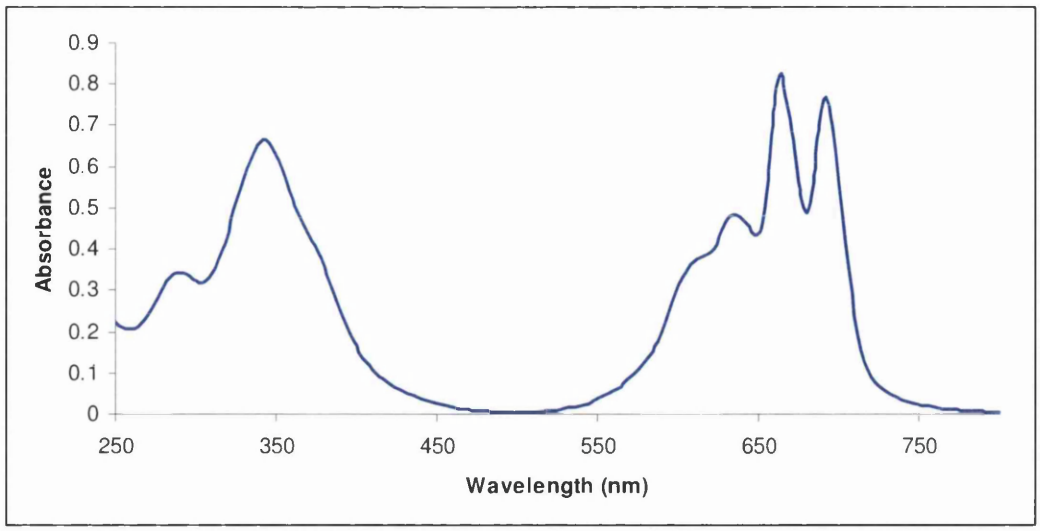

Figure 3.35, UV-visible spectrum of 2-*t*-butyl-9,16,23-triiodo-phthalocyanine (**44**), 9.05 x 10-6 M, THF

This was an important result because it should open up the potential to couple acid linkers groups to yield desired unsymmetrical products and without the impurities obtained from the statistical method. However, there was insufficient time remaining to try to investigate this result further.

3.2 Conclusions

The data in this chapter show that the synthesis of subphthalocyanines appears to be dependent on the nature of the substituent on the starting material. Thus, the formation of subphthalocyanines that contained electron withdrawing groups such as iodinated and chlorinated subphthalocyanines (**27** and **28**) were easier to obtain than the subphthalocyanines that contained solubilising *t*-butyl, electron donating group. This could be due to the reduced reactivity of the phthalonitrile group due to the substituent.

The data also show that using the statistical cyclisation procedure to synthesise unsymmetrical phthalocyanines produced *pseudo* statistical mixtures of products that were problematic to separate. Interestingly, the azaporphyrins produced were easier to purify than the phthalocyanines which was believed to be due to a change in core structure of the azaporphyrines leading to differences in solubility between the by-products leading to better separation by column chromatography. It was also observed that solubilising groups have a large effect on the synthesis of the phthalocyanine. For instance, ferrocene groups reduced solubility while the *t*-butyl and alkoxy groups increased solubility of the macrocycle. Phthalocyanines that contained alkoxy groups

contained the most impurities as separation could not be achieved using column chromatography which was believed to be due to their similar affinities to the alumina and eluting solvents.

Our data also showed that post derivistisation of halogenated subphthalocyanines can be achieved by palladium cross coupling reactions. However, expansion of these into phthalocyanines did not prove successful which was believed to be due to the degradation of the subphthalocyanine. It is postulated that pure dyes can be achieved by the post derivitasion of the synthesised ring expanded iodosubphthalocyanine with *t*-butyl-1,3-iosindoline, 2-tert-butyl-9,16,23-triiodophthalocyanine (**44**), as no statistical products were observed. Therefore the expansion of subphthalocyanines has been proved to be a selective method of producing the desired unsymmetrical phthalocyanines, but is very dependent on the nature of the reactants, solvent and can be a multistep process.

Chapter 4

Testing of Dye Sensitized Solar Cell Devices

4.1 Introduction

The UV-visible spectroscopic data in Chapter 3 show that the dyes **(34b)**, **(35c)**, **(36c)** and **(37c)** all absorb radiation in the red region (650-720 nm) of the visible spectrum when in solution. These compounds have therefore been tested for their dye sensitisation properties in DSSC devices prepared using nanoparticulate titania and FTO coated glass substrates. This chapter describes the method of preparation of the DSSC devices along with a discussion of the IV curves observed for each dye and the corresponding IPCE data.

4.2 Working Electrode Preparation

Commercial, screen printed working electrodes were used in these studies to ensure consistency of DSSC device preparation. The working electrodes were purchased from Dyesol Ltd and consist of FTO coated glass (3.2 mm thick). Onto this glass substrate, the TiO_2 working electrode was screen printed with an effective area of 8 x 11 mm. Previous measurements using a profilometer have shown such screen printed working electrodes to have film thicknesses of *ca.* 12 μm for transparent electrodes and 18 μm for opaque electrodes. The working electrode films were calcined at 450 °C for thirty minutes to remove any surface impurities and improve connections between the TiO_2 particles prior to dyeing.

The electrodes were then immersed in the ethanol dye solutions, 0.3 mM for N719 and 0.05 mM for the dyes **(34b)**, **(35c)**, **(36c)** and **(37c)**, and left in the dye solution for 16 hours, after which time the dye had penetrated the entire TiO_2 electrode (Figure 4.1). Excess dye was removed from the surface of the electrode by washing with ethanol.

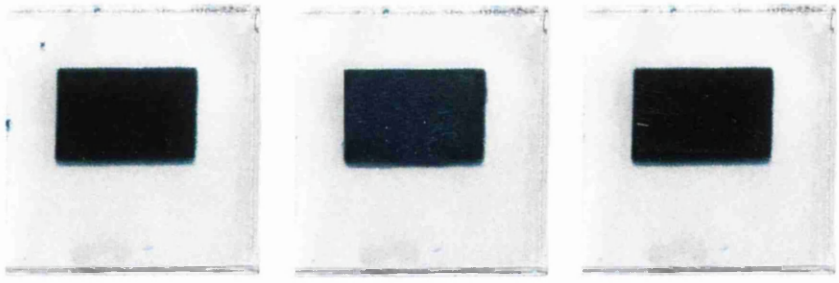

Figure 4.1, Photographs of dyes **(34b)**, **(35c)**, **(36c)** and **(37c)** adsorbed on to the transparent TiO_2 films

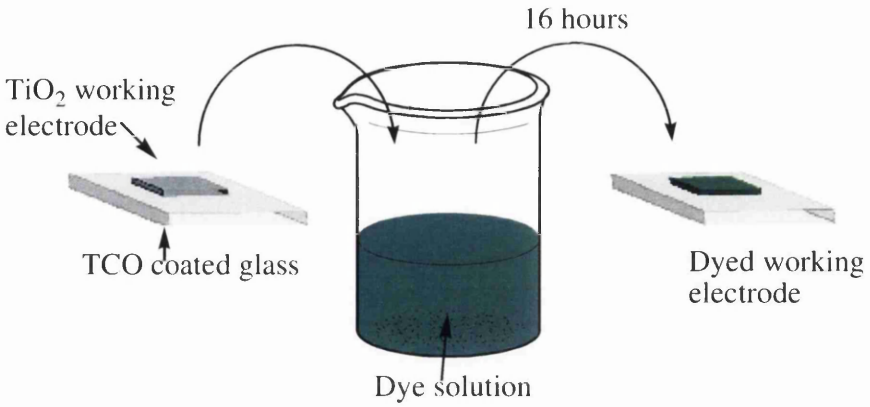

Figure 4.2, Dyeing of the working electrode

The dye sensitised working electrode was then shaped to 8 x 10 mm using a plastic template. The counter electrodes used were also purchased from Dyesol and consisted of a piece of FTO coated glass (15 $\Omega\ \square^{-1}$) with a catalytic amount of platinum deposited on the conducting side. A hole was drilled through this counter electrode using a 0.8 mm drill bit. The FTO surface was then washed with ethanol to remove any debris and the platinum catalyst activated by heating to 400 °C for 30 minutes to remove any surface impurities or oxides. The platinum was then stored under vacuum at room temperature to prevent oxidation before use.

4.2.1 Cell construction

Cells were constructed as soon as possible after the preparation of the working and counter electrodes. The working electrode was attached to the counter electrode by placing a pre-cut gasket of 25 μm thickness Surlyn® (Dupont) around the TiO_2 working electrode. The electrodes were then sealed together by placing the electrodes on a surface heated to *ca.* 100 °C while applying manual pressure.

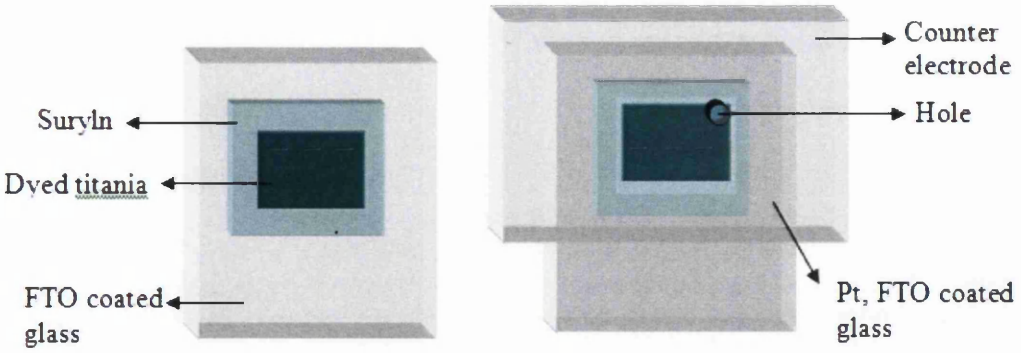

Figure 4.3, Schematic of DSSC device construction (T-shaped devices)

The electrolyte, also purchased from Dyesol, was vacuum injected into the space between the working and counter electrode created by the Surlyn. The hole in the counter electrode was then sealed with a glass cover slip using a glass microscope slide and Surlyn. Finally to provide electrical contact, silver paint was placed on the conducting side of the working and counter electrodes as shown below in Figure 4.4.

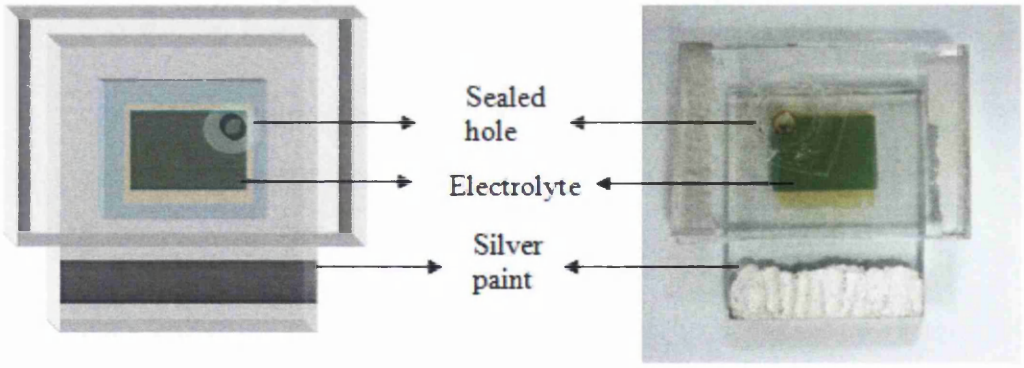

Figure 4.4, Completed DSSC device construction (left) schematic of the device design) and (right) photograph of a completed device

It is important to note that a set of five cells were prepared for each dye and variable tested in this chapter. The efficiencies and parameters are reported in this chapter with the variability of the device efficiencies are indicated in the tables of data. If a cell did not produce a working device or did not follow the same trend as the other devices, that cell was discarded and not included in the data sets.

4.3 IV curve device testing data

Following DSSC device construction, IV curves were used to test the activity of the dyes synthesised in Chapter 3 when used as the sensitiser in the DSSC devices. In this data, the current-voltage (IV) curves are shown in blue and the power-voltage curves are shown in red for opaque (solid lines) and transparent (broken lines) working electrodes and are measured at 1 sun. The data are shown in Figures 4.5-4.9 as follows:- sensitised by N719 dye (Figure 4.5) azaporphyrin **(34b)** (Figure 4.6), azaporphyrin **(35c)** (Figure 4.7), phthalocyanine **(36c)** (Figure 4.8) and phthalocyanine **(37c)** (Figure 4.9).

The IV curves for the opaque and transparent working electrodes sensitised by the N719 dye is shown below (Figure 4.5). From this data, the cell parameters to assess the performance of the cell are determined and summarised in Table 4.1. The V_{oc} of both the transparent and opaque films remains constant while the I_{sc} decreases from 15.31 to 12.90 mA cm^{-2} with the transparent electrode. This is due to less dye adsorbing onto the transparent electrode and therefore less electrons being injected into the TiO_2. A low fill factor is observed with these cells which is related to the series resistance of the devices which presumably is related to the fabrication of the device.

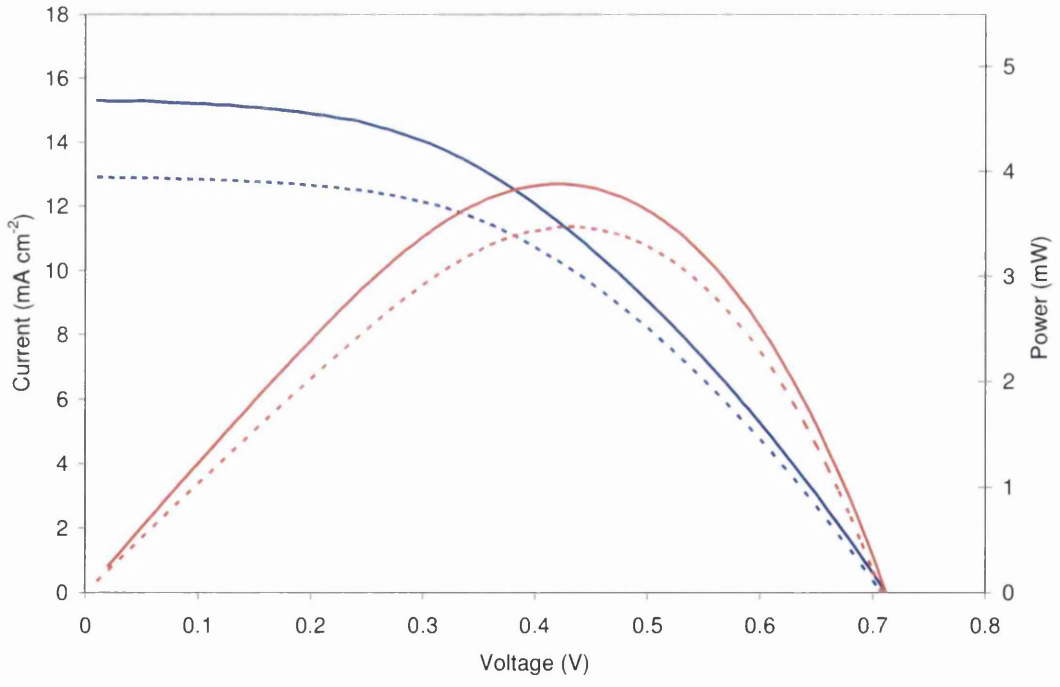

Figure 4.5, IV and PV curve of a DSSC sensitised with N719, (IV) curves are shown in blue and the power-voltage curves are shown in red for opaque (solid lines) and transparent (broken lines) working electrodes and are measured at 1 sun

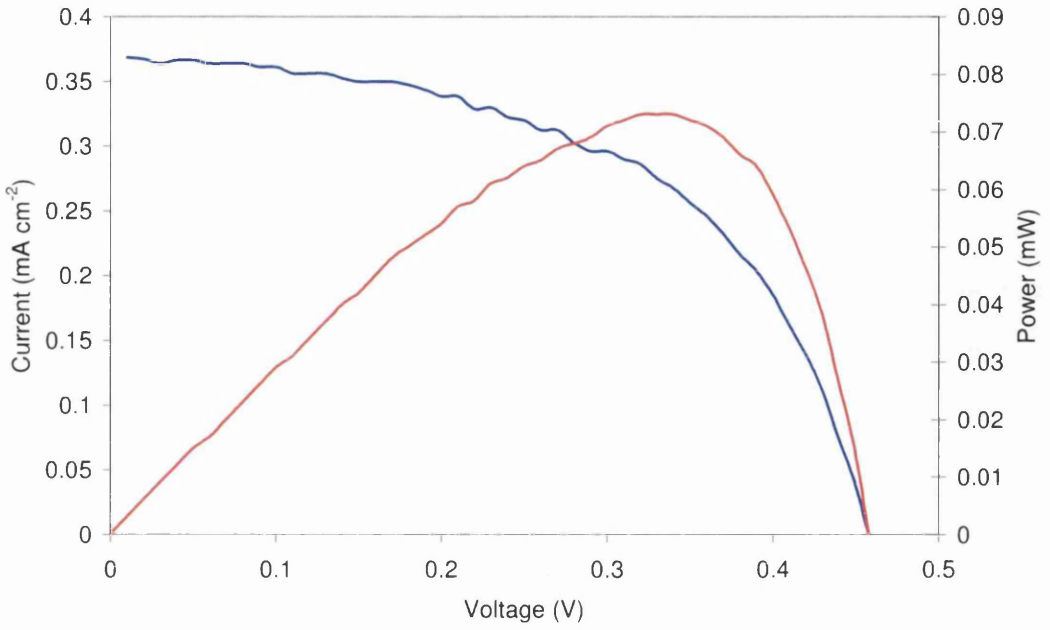

Figure 4.6. IV and PV curve of a DSSC sensitised with **34b,** (IV) curves are shown in blue and the power-voltage curves are shown in red for opaque (solid lines) and transparent (broken lines) working electrodes and are measured at 1 sun

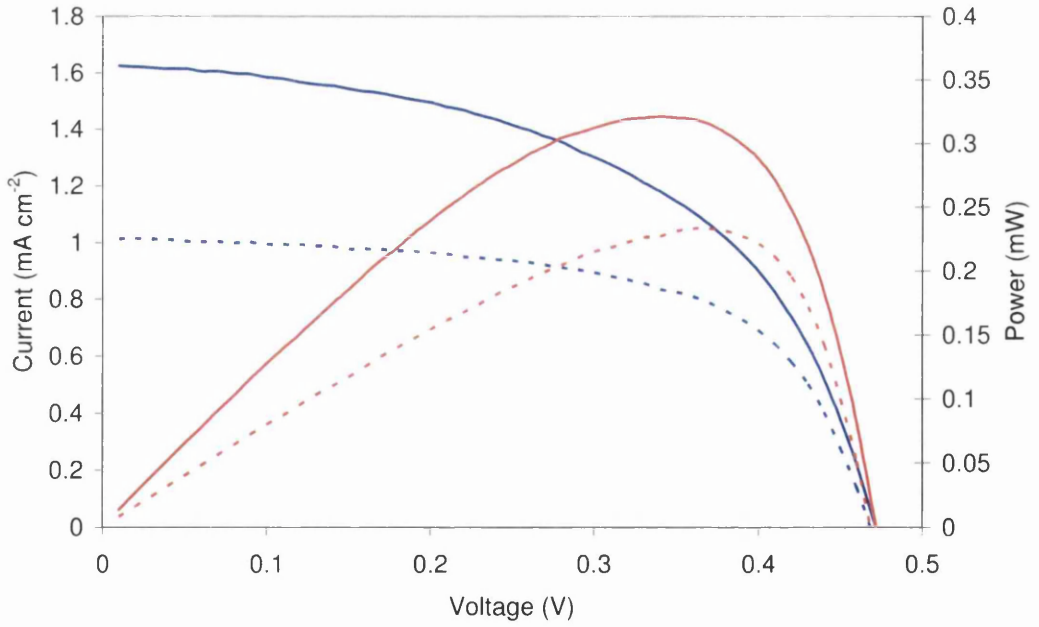

Figure 4.7. IV and PV curve of a DSSC sensitised with **35c,** IV curves are shown in blue and the power-voltage curves are shown in red for opaque (solid lines) and transparent (broken lines) working electrodes and are measured at 1 sun

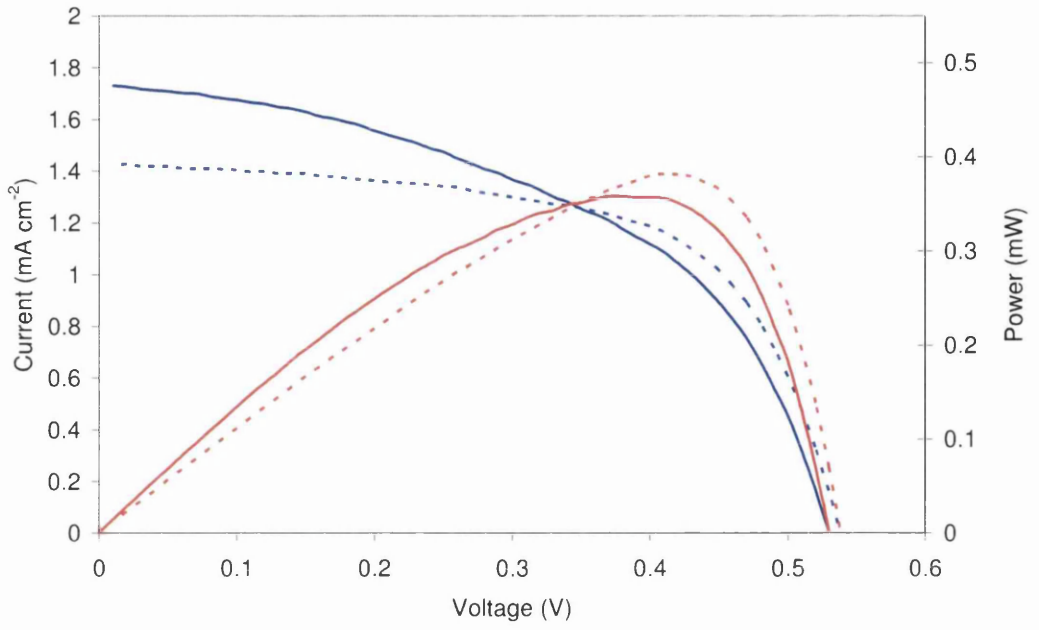

Figure 4.8. IV and PV curve of a DSSC sensitised with **36c,** IV curves are shown in blue and the power-voltage curves are shown in red for opaque (solid lines) and transparent (broken lines) working electrodes and are measured at 1 sun

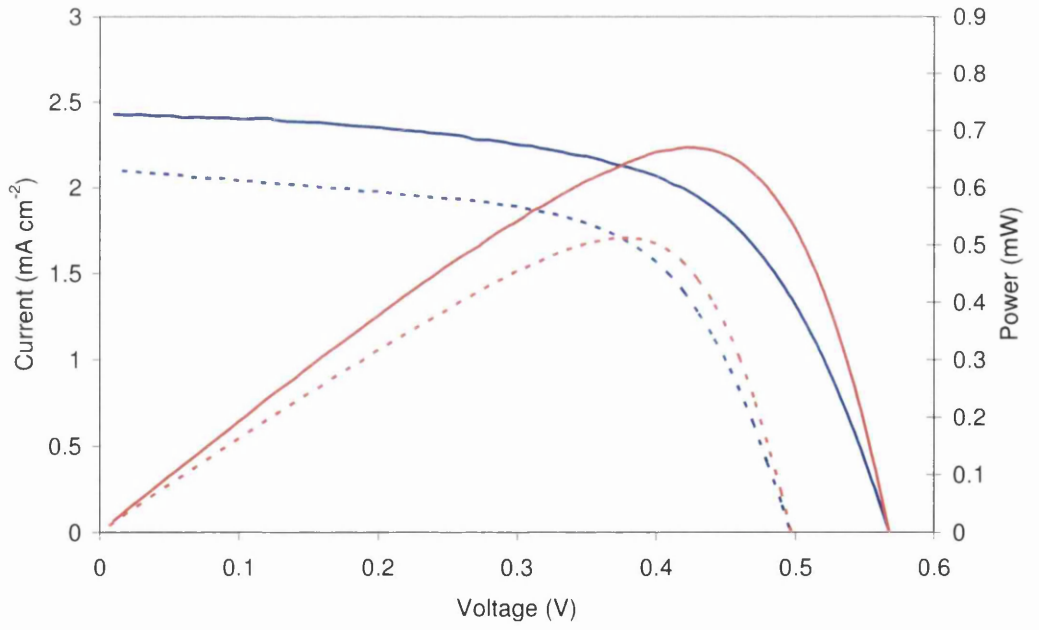

Figure 4.9. IV and PV curve of a DSSC sensitised with **37c,** IV curves are shown in blue and the power-voltage curves are shown in red for opaque (solid lines) and transparent (broken lines) working electrodes and are measured at 1 sun

	Opaque Working Electrode				
	N719	**34b**	**35c**	**36c**	**37c**
V_{oc} (V)	0.71	0.57	0.45	0.56	0.58
Isc (mA cm^{-2})	15.31	0.37	1.63	1.73	2.42
Ff	0.47	0.72	0.53	0.62	0.62
Ŋ	4.89±0.2	0.12±0.01	0.42±0.1	0.5±0.1	0.76±0.1

	Transparent Working Elecrode			
	N719	**35c**	**36c**	**37c**
V_{oc} (V)	0.71	0.46	0.54	0.51
Isc (mA cm^{-2})	12.90	1.01	1.42	2.10
Ff	0.46	0.61	0.62	0.62
Ŋ	4.4±0.2	0.27±0.1	0.48±0.1	0.62±0.01

Table 4.1, Cell parameters for dyes N719, **34b**, **35c**, **36c** and **37c** , measured at 1 sun

The cell parameters of these devices are summarised in Table 4.1. The azaporphyrin **(34b)** was adsorbed onto an opaque film and tested for photovoltaic activity. The overall cell efficiency produced was 0.1 % despite the V_{oc} being 0.57 V and a good fill factor of 0.72. However, the low efficiency can be ascribed to the very low Isc . This can be linked to the symmetrical nature of the azaporphyrin and the lack of conjugation compared to a phthalocyanine. This is believed to result in poor electron injection from the dye into the titania working electrode. Hence, this dye was not tested further.

Unsymmetrical azaporphyrine **(35c)** was synthesised to contain solubilising *t*-butyl groups, designed with the secondary aim of providing directionality of electron injection and also to prevent aggregation between the dye macrocycles as discussed in Section 1.3.4, compared to the symmetrical analogue **(34b).** This azaporphyrine dye produced a higher efficiency of 0.4 %. However, in this case a low V_{oc} was observed with this dye, which could be due to a number of factors. Firstly, it could indicate that the HOMO and LUMO energy levels of the dye do not match well to the titania conduction band which could be caused by the lack of conjugation caused by the fumaronitrile anchoring group **(19)**. It could also indicate cell short circuits or enhanced

recombination rates. Device short cuts can probably be ruled out as similar V_{oc} is observed for both transparent and opaque cells.

Phthalocyanine (**36c**) was synthesised to further increase the conjugation forming a phthalocyanine core structure to see if this would affect DSSC performance. This did occur with increased V_{oc} and I_{sc} observed, an overall improvement of efficiency was measured to 0.5 %. It should be noted that earlier mass spectral data showed that this dye contained a higher degree of by-product impurities and hence it is likely that DSSC devices prepared from this dye could produce higher efficiencies if a purer dye sample had been obtained.

Phthalocyanine dye (**37c**) differed from phthalocyanine dye (**36c**) by substitution of the solubilising *t*-butyl groups with the alkoxy solubilising groups. A slight increase in V_{oc} was observed compared to the *t*-butyl derivative (**36c**) but poor I_{sc} was still observed. This could be due to the higher degree of statistical impurities in the system compared to the other dyes synthesised as discussed in Chapter 3. The opaque films produced higher efficiencies than that of the transparent films, with the higher I_{sc} accounting for this. It should be noted that the commercial opaque films are known to be thicker than the transparent films and hence more dye should have been adsorbed onto the titania photoelectrodes for the opaque films. Hence, more electrons should have been injected into the semiconductor resulting in higher efficiencies.

Cell Parameters	0 Hours			
	35c	**36c**	**37c**	**N719**
V_{oc} (V)	0.47	0.56	0.57	0.68
I_{sc} (mA cm^{-2})	0.78	1.83	2.43	15.76
Ff	0.61	0.62	0.61	0.45
ŋ	0.2±0.01	0.6±0.07	0.8±0.04	4.0±0.1

Cell Parameters	48 hours			
	N719	**35c**	**36c**	**37c**
V_{oc} (V)	0.72	0.47	0.56	0.57
I_{sc} (mA cm^{-2})	15.29	0.89	1.43	2.21
Ff	0.49	0.61	0.62	0.62
ŋ	4.9±0.2	0.3±0.01	0.5±0.03	0.8±0.1

Table 4.2, Cell parameter observed at the time of construction 0 hours and after 48 hours

DSSC devices were then constructed for opaque cells to study the effects of aging on device efficiency for 48 hours after device construction (Table 4.2). The overall efficiencies of some of the cells had increased over this time. In particular, the N719 cells showed an increase in the open circuit voltage and a slight decrease in I_{sc} This aging effect in N719 sensitized DSSC is a well known phenomenon. The effect could be due to the final equilibrium between the dye and the electrolyte which would not be fully in equilibrium immediately after device construction. There might also be a slight excess of dye on the surface of the TiO_2 which is poorly attached to the film during the first measurements which desorbs from and readsorbs to the surface over time. Tertiary butyl pyridine (TBP) is known to increase V_{oc} by suppressing the dark current[3], which arises from the reduction of the triiodide by conduction band electrons. The I_{sc} has slightly decreased during time but an overall increase in efficiency is observed from 4.0 to 4.9 %. In comparison to this, the phthalocyanine dyes do not shown significant increases in efficiency over time. The V_{oc} of the cells do not change but the I_{sc} does vary slightly over time. This could be due to the by product impurities in the system which might or might not possess photovoltaic activity but which occupy space on the titania surface. It could also suggest some surface rearrangement of the dye on the surface but the data suggest that, if this is taking place, the effect is less significant than for N719. This could suggest that once bound to the surface the phthalocyanine dyes are much less likely to desorb (whether they are the desired photoactive dyes or not). There is some evidence to support this from the desorption experiments described in the following section.

4.4 Desorption

Dye desorption was also attempted with 1 M NaOH from opaque films to correlate the amount of dye absorbed with efficiencies. However, it was found that full desorption was not observed with dye left on the TiO_2 films as shown in Figures 4.10 and 4.11.

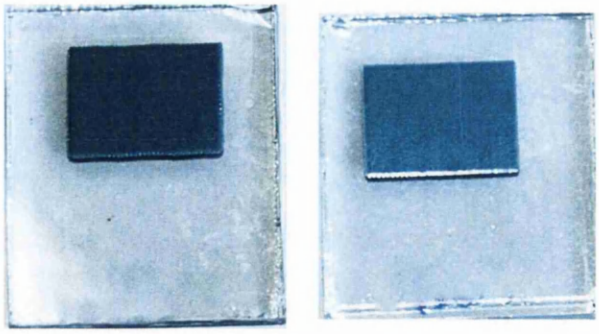

Figure 4.10, Images of opaque films sensitised with **(36c)** before and after desorption in 1M NaOH

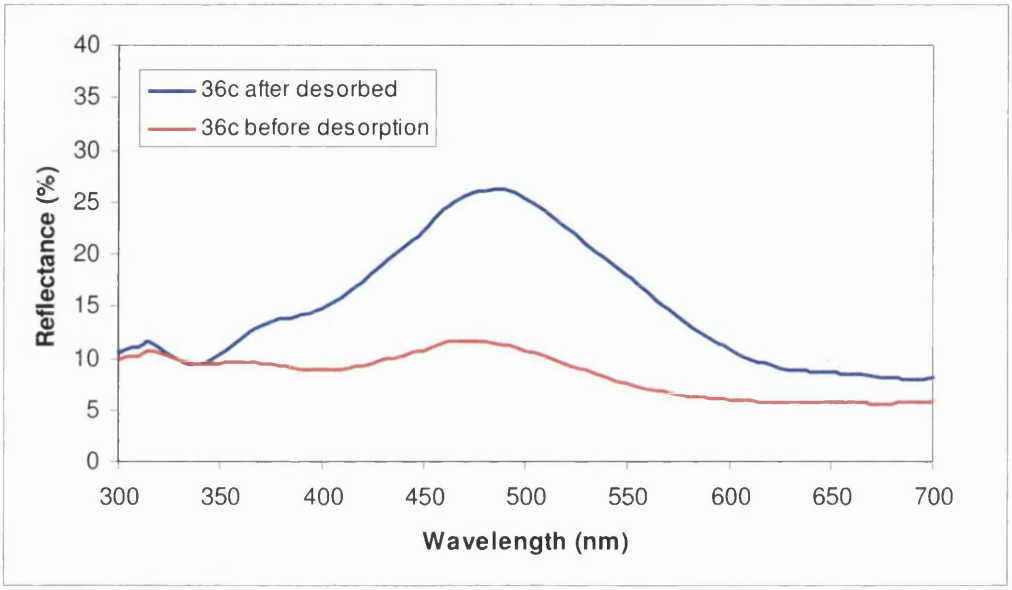

Figure 4.11, Reflectance spectra of phthalocyanine dye **(36c)** before and after desorption in NaOH from opaque films

Reflectance data shown in Figure 4.11 shows that full desorption of the dye (**36c**) did not occur. The residual phthalocyanine material which is believed to be still adsorbed onto the surface could be the statistical by-product impurities observed in the mass spectrum of this compound (see Chapter 3). If time had permitted, further work would have been carried out to further purify the dye. However, to investigate this issue further, the phthalocyanine dye (**36c**) was first absorbed onto TiO_2 powder and then desorbed using NaOH (aq) with the aim of leaving the impurities on the surface of the TiO_2, and then using the resulting solution to sensitise the TiO_2 on the working electrode. However this did not prove successful as the after sensitisation of the TiO_2 and subsequent desorption, residual dye was still adsorbed on the TiO_2 working electrode. It is therefore believed that impurities were still present in the solution or that

the phthalocyanine dyes do not desorb easily. Due to time restraints this was not investigated further.

To try and further improve the overall cell efficiencies, chenodeoxycholic acid (CDCA) was added to a solution of phthalocyanine dye (**36c**), and left to absorb onto opaque working electrodes. This was done to explore whether an increase in efficiency would be observed partly because CDCA is known to help reduce dye aggregation during dye adsorption[84] and also because time constraints did not permit a full investigation into separation methods of the statistical by-products of the dyes. It is worth noting that this could be beneficial in commercial processes as expensive purification processes could be avoided reducing the cost of the dye. As stated above, it has been reported in the literature that CDCA reduces aggregation of phthalocyanine dye molecules for DSSC applications, increasing efficiencies[84]. These workers have reported that the acid adsorbs competitively to the semiconductor surface to help improve dye uptake. Here, a concentration of 2.25 M of CDCA was added to a 0.05 mM solution of phthalocyanine dye (**36c**) as this had produced the highest efficiencies in the literature reports[84].

Cell Parameters	36c	36c + CDCA
V_{oc} (V)	0.53	0.50
Isc (mA cm^{-2})	2.11	1.90
Ff	0.58	0.57
Ŋ	0.6±0.08	0.5±0.05

Table 4.3, Cell parameters observed for opaque films sensitised with phthalocyanine dye (**36c**) and dye (**36c**) with CDCA

A small decrease in efficiency is observed on addition of the CDCA but this was not beyond the expected errors associated with the experiment. Further analysis showed that slight decreases in I_{SC}, V_{oc} and fill factor has lead to the decrease in efficiency. This could be due to the competitive absorption between the acid and the phthalocyanine dye which is perhaps slightly limiting dye uptake. As observed in desorption experiments, by-product impurities could also be absorbed onto the surface of the TiO_2 and with competitive adsorption more of the photoactive dye could be prevented from absorbing and hence reducing efficiencies. It could also be postulated that the *t*-butyl groups could be preventing aggregation of the phthalocyanine molecule and coabsorption could

therefore have a negative impact and decrease efficiencies rather that reducing aggregation and hence improving cell performances. These data further emphasise the need to re-test this dye after dye purification has been successfully achieved.

4.5 Electrolyte Testing

It is well known that the electrolyte has a large impact on dye performance in DSSC cells[120,3]. In particular, TBP has a significant effect on the ruthenium based dyes[120,17]. Therefore, with the same aim of increasing DSSC efficiency of the dyes synthesised in this thesis, electrolyte tests were briefly examined using phthalocyanine dye (**36c**).

Cell Parameters	Concentration of TBP added to electrolyte		
	0.0 M	**0.1 M**	**0.28 M**
V_{oc} (V)	0.51	0.56	0.57
I_{sc} (mA cm^{-2})	4.13	1.76	2.51
Ff	0.56	0.55	0.63
D	1.2±0.04	0.5±0.01	0.9±0.1

Table 4.4, The table above shows the DSSC device, sensitised with (**36c**) dye, performance against electrolyte compositions containing 0.0, 0.1 and 0.28 M *t*-butylpyridine

It has also been reported that TBP can also affect the overall efficiency of the cell as it is know to increase V_{oc} by increasing electron percolation[3]. To see if TBP concentration had any effect on dye performance, an electrolyte of composition: 3-propyl-1-methyl-imidazolium iodide (0.6 M), iodine (0.04 M), lithium iodide (0.025 M), guanidinium thiocyanate (0.05M) and acetonitrile was made. Concentrations of 0.1 and 0.28 M of TBP were then added to the electrolyte solution. DSSC devices were constructed using commercial opaque titiania working electrodes and then sensitised with phthalocyanine dye (**36c**) using the three different electrolyte solutions. The cell parameters of these tests are shown in Table 4.4. It was found that, when comparing the the electrolyte formulation described above with devices prepared using the Dyesol electrolyte which has been optimised for ruthehium dyes, the overall efficiency of the devices broadly doubled with the I_{sc} mainly accounting for this. Looking at the data in Table 4.4 alone, with increase in TBP in the electrolyte from 0.1 M to 0.28 M, a slight increase in V_{oc}

was observed as shown in the literature[120] but the I_{sc} decreased, reducing the overall efficiency of the cell.

Cell Parameters	Concentration of TPB exposed to the sensitised working electrode				
	0.0 M	**0.1 M**	**0.3 M**	**0.6 M**	**Neat**
V_{oc} (V)	0.51	0.55	0.57	0.6	0.58
Isc (mA cm^{-2})	4.13	2.28	2.90	1.74	2.36
Ff	0.56	0.56	0.58	0.47	0.56
ŋ	1.2±0.03	0.7±0.06	1.0±0.08	0.5±0.08	0.8±0.04

Table 4.5, DSSC cell parameters observed with sensitised opaque films with **36c** exposed to TBP before cell construction

The dyed working electrode was also exposed to solutions of 0.1, 0.3, 0.6 M and neat TBP solutions before being assembled into cells with the electrolyte solution. The data (Table 4.5) show that, with increasing TBP concentration, the V_{oc} increased due to the suppression of the dark current as discussed earlier. It was found that the best cell performance achieved by exposing the cells to TBP before cell construction was using a 0.3 M TPB solution but the overall cell efficiencies did not improve compared to the electrolyte solution that contained no TBP added.

4.6 IPCE

IPCE data were measured for the **N719**, **35c**, **36c** and **37c** dyes to study the incident photon-to-current conversion efficiency between 200 and 800 nm. The data are shown below in Figures 4.12 to 4.16 and will be discussed in this section.

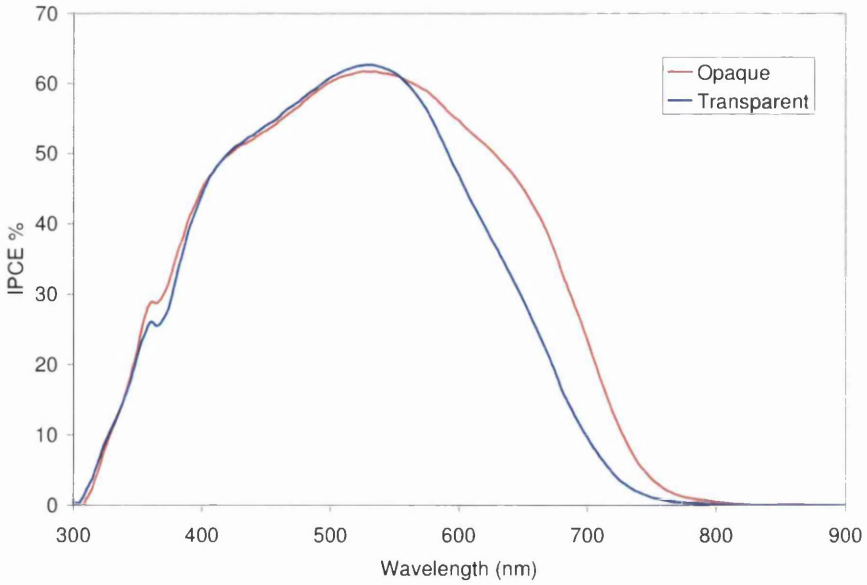

Figure 4.12. IPCE of DSSC devises sensitised with N719 dye onto opaque and transparent TiO_2 working electrodes

The IPCE data for the N719 dye are shown above (Figure 4.12) for transparent and opaque TiO_2 films. High IPCE values are observed in the wavelength range between 480 to 650 nm for the N719 dye. However, there is poor conversion of photons into electricity in the red region (*ca.* 650 nm) of the visible spectrum, which is ascribed to low light absorption in this region which is typical for the N719 dye[3]. In addition, it can be seen that the opaque film has a slightly broader absorption than the transparent film with the IPCE response reaching out to slightly *ca.* 700 nm whilst the transparent film cuts off at below 700 nm. Both films give rise to similar IPCE of 60 % observed at a *ca.* 535 nm.

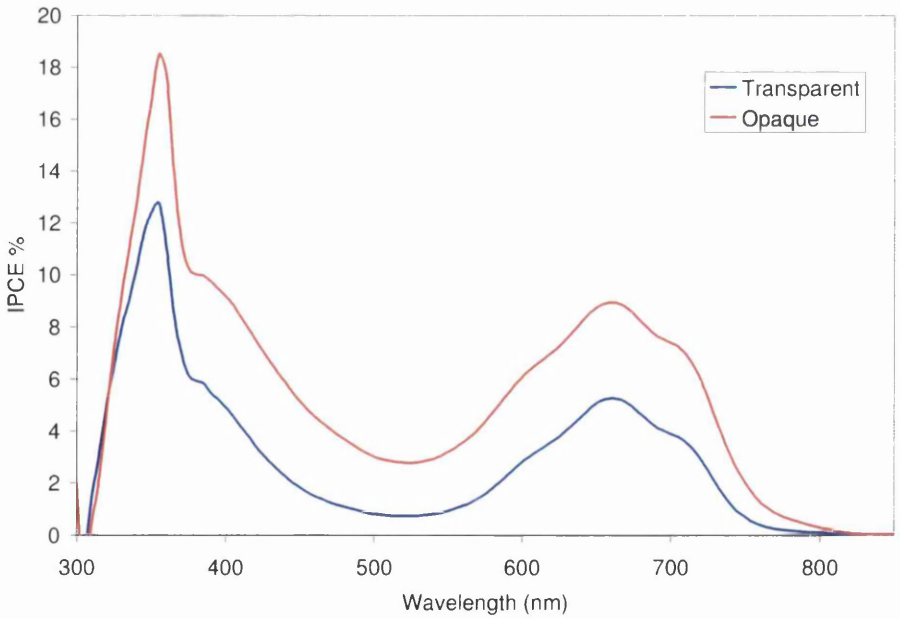

Figure 4.13. IPCE of a DSSC device sensitised with azaporphyrin dye **35c**

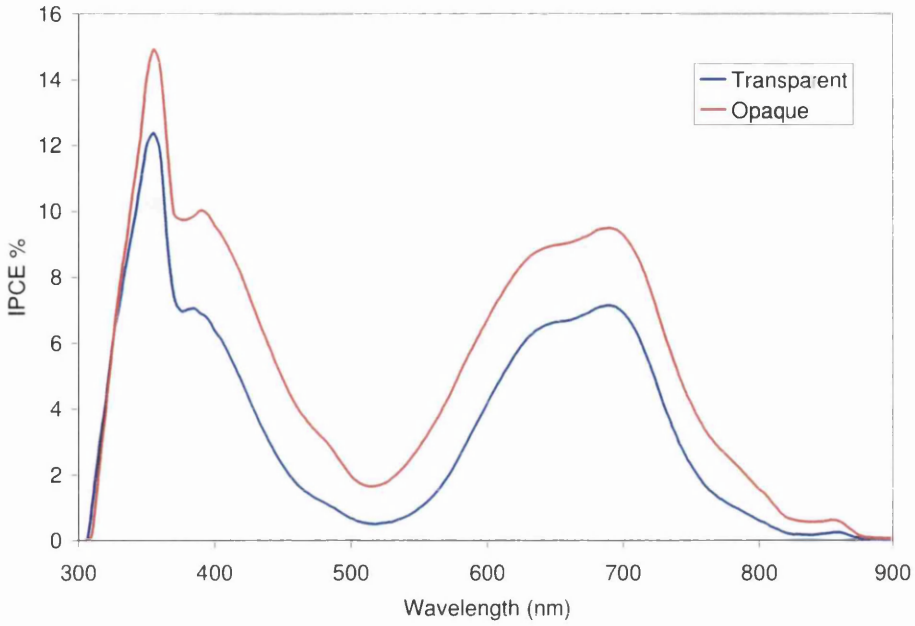

Figure 4.14, IPCE of a DSSC device sensitised with phthalocyanine dye **36c**

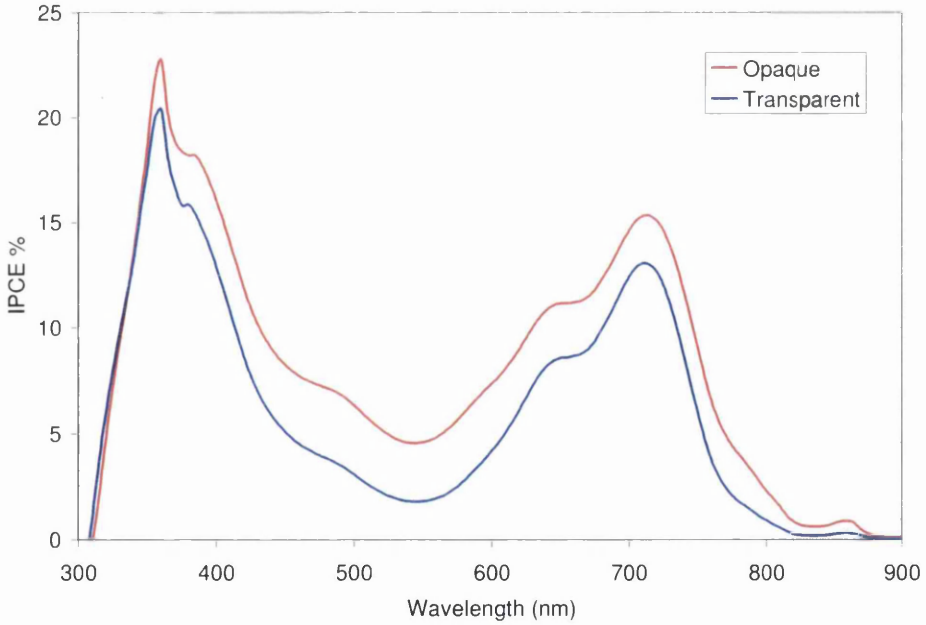

Figure 4.15, IPCE of a DSSC device sensitised with phthalocyanine dye **37c**

Figures 4.13 to 4.15 show the IPCE data for the various dyes synthesised within this thesis. Overall, it can be observed that opaque films have higher IPCE values than transparent films, which correlates with IV curves and efficiencies discussed above, using both the transparent and opaque electrodes. This could be due to a combination of electrode thickness and the particle size of the TiO_2 particles which make up the films.

The opaque films contain larger titania particles which should result in lower metal oxide surface area for dye absorption and also in the scattering of light (hence the films are opaque), The opaques films are approximately 50 % thicker than the transparent films and so overall the opaque films should adsorb more dye than transparent films leading to increased photon capture and hence electron injection.

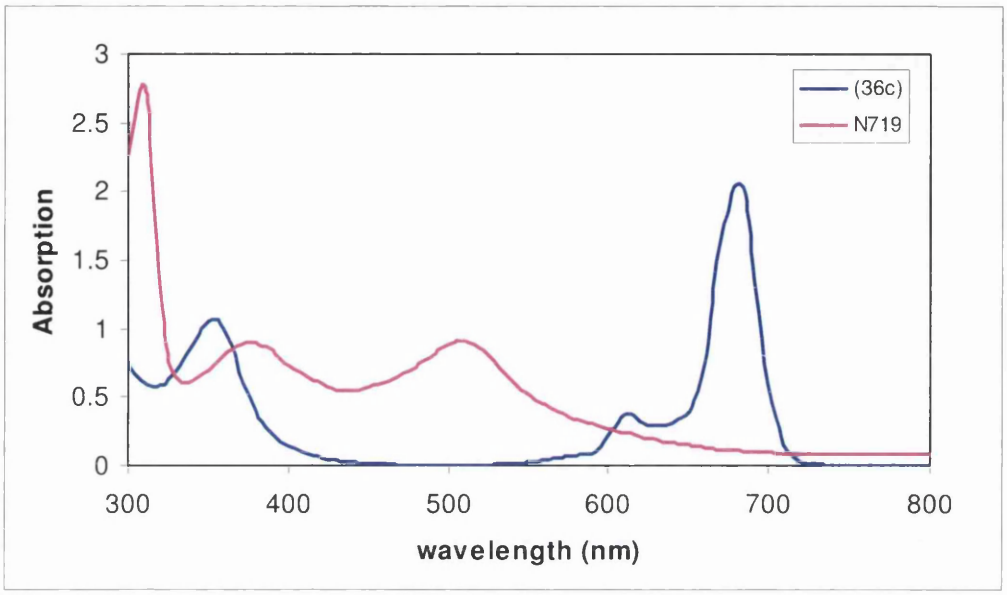

Figure 4.16, UV-Visible spectra of phthalocyanine dye (**36c**) and ruthenium dye N719

All the phthalocyanine dyes tested absorb in the red region of the visible spectrum unlike the N719 dye (Figure 4.16). The azaporphyrine dye **35c** has a maximum IPCE at 660 nm with an IPCE of 9 % compared to an IPCE of 60% at λ_{max} of 535 nm for N719. The phthalocyanine dye **(36c)** has a further shift in the maximum IPCE due to the increased conjugation resulting in a higher efficiency with an IPCE at 690 nm at 10 %. The phthalocyanine dye **(37c)** produced the highest efficiency as seen in the IV curves for this dye as discussed earlier. The IPCE data correlate with the IV data as the highest IPCE was obtained for this dye at 715 nm, 15.3 %.. An overall comparison of the IPCE data is shown below in Figure 4.17.

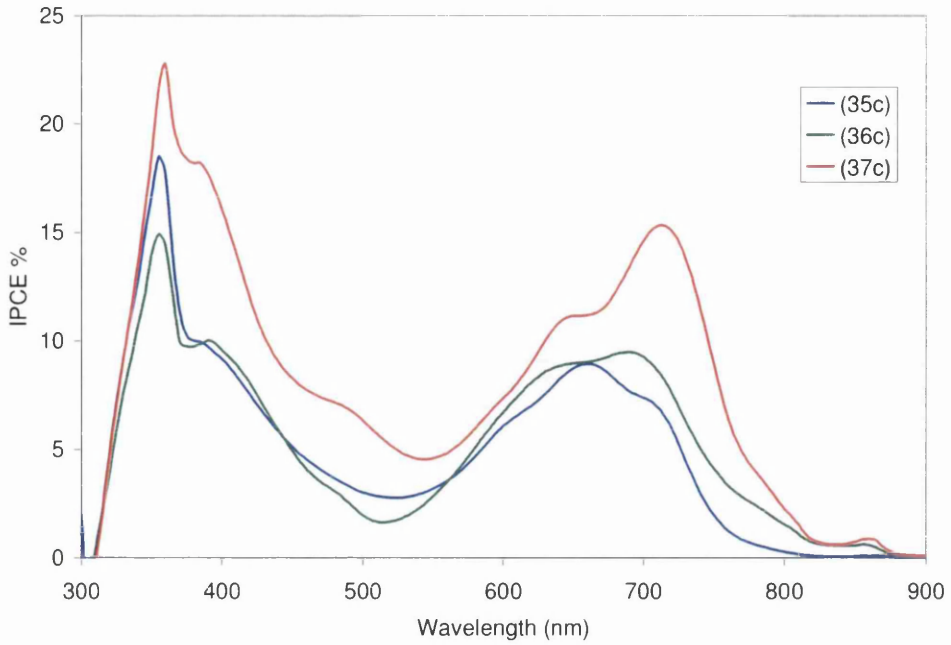

Figure 4.17. Comparison of the IPCE data for DSSC devices sensitised with either **35c**, **36c** or **37c**

4.7 Conclusions

Very low efficiencies were observed for the symmetrical azaporphyrine **34b**, which can be linked to the lack of conjugation in the system and the symmetrical nature of the macrocycle. The unsymmetrical dyes, designed with the aim of providing directionality of electron injection and also to prevent aggregation between the dye macrocycles, all produced higher photovoltaic activity in DSSC devices compared to the symmetrical azaporphyrin. There was also a general trend showing efficiencies increasing with increasing conjugation within the dye macrocycles. Extending the conjugation also resulted in bathochromic shifts in the UV-visible spectra. Solubilising functional groups also had a large effect on the overall efficiency of the cells with long alkoxy chains improving the cell parameters and increasing efficiencies of the devices. One possible reason for this could have been that the alkoxy groups reduced aggregation between the dye molecules, which improved light harvesting. The IPCE data also correlated with this, with phthalocyanine dye (**37c**) producing the highest IPCE recorded at 15 % at 715 nm.

It was apparent from the desorption studies that the impurities detected in the mass spectra could have a limiting factor on the performance of the dyes. It is not known if these by-products possess any photovoltaic activity and instead could just be occupying

space on the TiO_2 semiconductor, reducing the amount of electron injection. The only way to understand this would be to fully separate and purify the individual components from each dye mixture.

This study has also shown that the photovoltaic performance of the DSSC sensitised with the phthalocyanine dye (**36c**) can remarkably depend on the electrolyte components. with preparation of fresh electrolyte solution containing 3-propyl-1-methyl-imidazolium iodide (0.6 M), iodine (0.04 M), lithium iodide (0.025 M), guanidinium thiocyanate (0.05M) and acetonitrile. Tests involving changing the concentrations of the *t*-butylpyridine additive revealed a 100 % increase in cell efficiency to 1.2 % by removing the TBP component within the electrolyte solution without lengthy purification procedures of the dye.

Overall, the unsymmetrical dyes have all shown photovoltaic activity that when fully isolated could further increase device efficiencies and hence these or related dye sensitizers could act as promising alternatives to ruthenium based complexes or be used in combination for tandem cells or cocktail dyeing to fully utilise the whole of the visible spectrum.

Chapter 5

An Investigation Into LDH-Phthalocyanine Interactions And The Application Of These Compounds As Stabilizers In PVC Coatings

5.1 Introduction

As stated previously, phthalocyanines are used extensively as blue pigments in the paint and coatings industry because of their insolubility and high colour intensity. Corus is the market leader in the UK for organic coated steel (OCS) with its plastisol based coatings typically accounting for 1.1M tones per year, a turnover of *ca.* £600M, with much of this output ending up on roofs and walls. As such, the economic importance of this technology is very high. Corus carries out fundamental research into coatings, including all the relevant issues of coating the strip steel (galvanizing, primer and topcoat technology, and the corrosion and coating degradation issues that occur due to weathering). Research into the prevention of degradation of these coatings is required to allow Corus to further enhance their existing guarantee (typically from 25 to 40 years depending on climate), on the corrosion and integrity of the coating. This chapter will discuss the synthesis and testing of clay-phthalocyanine materials as stabilizers in paint systems.

5.1.1 Pre-finished steel

Pre-finished steel (PFS) (Figure 5.1) is an example of a multi-component lamellar material with important engineering applications in packaging, domestic goods and construction. PFS is produced by galvanizing cold-rolled dipped steel and then applying two polymer-based layers, a primer and a top-coat, to improve long-term corrosion resistance[121] In general about 50 % of all metal components rely in part, or in total, on the paint for their corrosion resistance. A paint forms a continuous organic polymeric film, which is adherent and forms an inert impervious coating to a surface to provide both protective and decorative functions.

Figure 5.1. A typical composition of organic coated steel, image courtesy of Corus (© Corus)[121].

Typically for OCS, the top coat of paint consists of three major components, namely the paint vehicle, binder and pigments. In addition, paints usually contain a solvent (or thinner), extenders and additives. Each component is added to the paint for a specific purpose. The binder functions as the film-forming component of the paint, which can be a synthetic resin like polyvinylchloride (PVC)[122]. The solvent gives the paint the correct rheology and is removed by evaporation during curing, while the dispersion of pigment provides colour and/or protection. Plasticizers are then added to modify the paints properties, providing flexibility, while additives for UV protection aid in the prevention of degradation of the film. Chemicals such as ultraviolet absorbers are added as well as scavengers to trap reactive molecules (radicals), which can otherwise degrade the paint films. Fire retardants are also included along with compounds to aid in dispersability of the pigment. For high performance paint systems, a mixture of different additives is used to achieve desired effects and levels of performance for different paint formulations.

5.1.2 Degradation of PVC

TiO_2 is a widely used white pigment for organic coatings in the paint industry because of its high refractive index, low cost and high covering power[123]. Coloured organic paints also contain TiO_2 to act as a base pigment mainly for its covering power. As mentioned in Section 1.2.1, TiO_2 is a semiconducting material and incident radiation of < 388 nm causes promotion of electrons from the valence and into the conduction band of the TiO_2[124]. Electrons will usually recombine with the holes that are formed. If this does not happen, one possibility is that the excited electrons can react with oxygen, reducing it. This can form a highly reactive oxygen radical. The hole left by the electron is then free to oxidise any hydroxyl radicals that are present, returning the TiO_2 to its ground state. The oxygen radical can then further react in the presence of water to form per-hydroxyl radicals[124]. Both the peroxide and hydroxide radicals which can form are highly reactive species, which can cause degradation (mineralisation) of the polymeric coating, producing CO_2 and H_2O[125] (Figure 5.2). The breakdown of the polymer surrounding the TiO_2 leads to a change in the physical properties of the paint. If this occurs, the paint can discolour and become stiff and brittle leading to cracking and increased porosity. If this happens, the coating cannot protect the steel from the external environment leading to undesirable weathering and corrosion effects.

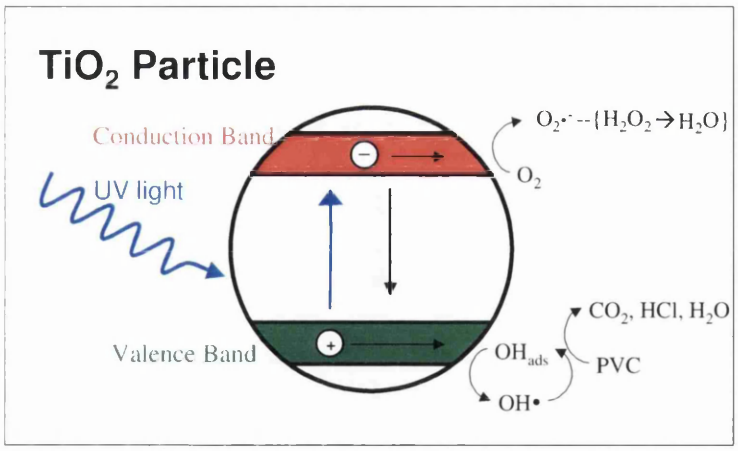

Figure 5.2, Photodegradation catalysed by TiO_2, taken from[126]

The radicals that are produced during photoactivity can also have an impact on the degradation of the pigment itself as well as degrading the polymer. The acid produced during any degradation of PVC can further catalyse the breakdown of the coating in an autocatalytic process and hence stabilisation against HCl production is important. PVC polymer is degraded by an elimination reaction of HCl (dehydrochlorination[127]), which proceeds *via* cleavage of the C-Cl bond to produce radicals on the polymer backbone. Chlorine radicals are also produced which can then induce propagation as the Cl radical reacts with a hydrogen atom from the hydrocarbon chain to produce HCl and a second radical on the polymer back bone. This process causes an unzipping action along the chain forming C=C double bonds resulting in conjugated sequences with time (Figure 5.3).

Initiation:

$$\sim CHCl-CH_2-CHCl-CH_2\sim \longrightarrow \sim CHCl-CH_2-{\bullet}CH-CH_2\sim + Cl{\bullet}$$

Propogation:

$$\sim CHCl-CH_2-CHCl-CH_2\sim + Cl{\bullet} \longrightarrow CHCl-CH_2-CHCl-{\bullet}CH\sim + HCl$$

$$\sim CHCl-CH_2-CHCl-{\bullet}CH- \longrightarrow \sim CHCl-CH_2-CH{=}{=}CH\sim + Cl{\bullet}$$

Termination:

$$2Cl{\bullet} \longrightarrow Cl_2$$

Figure 5.3, The radical dehydrochlorination of PVC,taken from[127]

The degradation of organic coatings is routinely studied to evaluate a paint's performance as a coating. These data are then used to further improve a given paint system. Degradation of the coatings tends to be associated with sunlight (mainly UV exposure), temperature, oxygen, water and other pollutants such as salt and organic residues. The degradation of coatings can be monitored by a variety of techniques such

as electrochemical techniques, gloss loss and delamination testing[128]. The extent of polymer mineralisation can also be evaluated by monitoring the decomposition products, including CO_2, produced when the coating degrades. Carbon dioxide (CO_2) is one of the main volatile gases evolved during the photocatalytic degradation of PVC[125]. In this thesis, a CO_2 flat panel reactor has been used in accelerated testing experiments to quantify the kinetics of photodegradation occurring within a paint system[123]. The FTIR spectrum for CO_2 comprises a peak that occurs between 2300 and 2400 cm^{-1}. By injecting known quantities of CO_2 to calibrate the instrument and then by integration of the CO_2 peak area, the amount of CO_2 evolved can be quantified.

5.1.3 Layered Double Hydroxides (LDHs)

It is known that certain inorganic clays can be formulated to be compatible with the organic coatings that are widely used in industrial steel coatings[129]. Typically such clays are incorporated in the top coat of pre-finished steel. The compatibility of MgAl-LDHs in paint films especially PVC based films has been reported previously[129]. It is thought that LDHs could be used as a cheaper, greener stabilizer in coatings such as PVC[129]. A patent by Kyowa Chemical Industries of Japan has demonstrated that the addition of MgAl-CO_3-LDHs to PVC resin in combination with other additives can enhance the thermal stability of the resin[130].

The term LDH comes from a group of naturally occurring minerals called layered mixed hydroxides. LDHs are essentially magnesium-aluminium hydrocarbonates, which were first discovered in Sweden in around 1842[131], but it wasn't until 1915 that Manasse reported the first exact formula of a natural LDH [$Mg_6Al_2(OH)_{16}CO_3.4H_2O$][132] which also has the mineral name hydrotalcite. The structure of this LDH is based on $M(OH)_2$ brucite-like layers[131] with hydroxyl ions hexagonally close-packed with alternate layers of octahedral sites occupied by divalent cations such as Mg^{2+} and trivalent cations such as Al^{3+}. This results in positively charged layers, compensated for by intercalation of various anions (A^{n-}), usually carbonate, into the interlayer region of the LDH. Both the A^{n-} and the water of crystalisation are found in the interlayers (Figure 5.4).

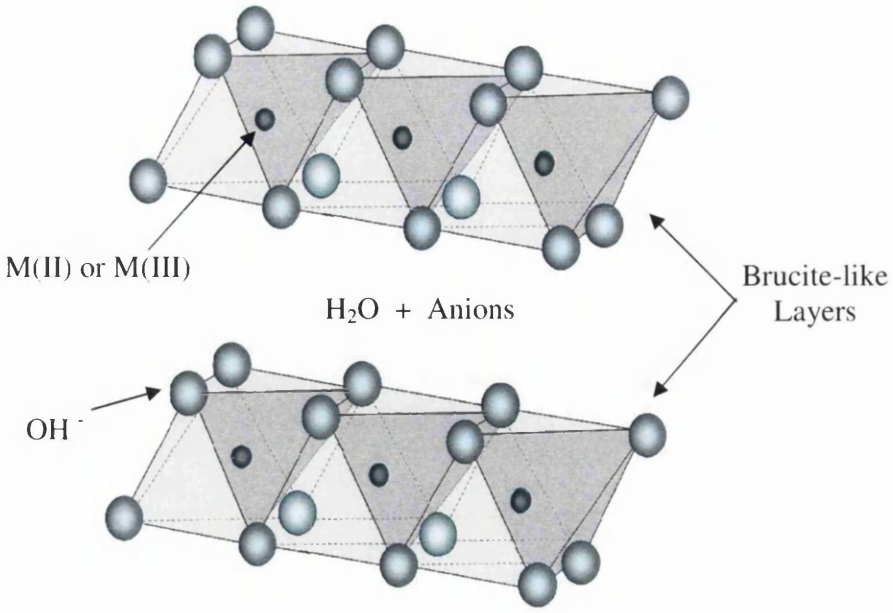

Figure 5.4. A representation of the layered structure of a hydrotalcite. Redrawn from[133]

The LDH structure is believed to be stabilised by the electrostatic interactions between the positively charged metal hydroxide layers and the anions[134]. It is further stabilized by hydrogen bonding between the intercalated water molecules, the anions and the metal hydroxide layers. The hydroxyl groups are bound to the CO_3^{2-} anions, which are situated flat in the inter layer, directly or through hydrogen bonding to water molecules[134]. In some LDHs, both the water and carbonate anions can be reversibly interchanged or eliminated without changing the structure of the host LDH[135]. As such LDHs have found a variety of practical applications from catalysis[136], anion exchange[135] and as absorbents.

There are two types of structure that hydrotalcite-like LDHs can adopt, either a rhombohedral structure, which is found in nature, or the hexagonal symmetry, which is obtained at high temperatures[137]. These structures are due to the OH^- groups in the brucite-like sheets being able to crystallize in either one of two stacking sequences. LDHs synthesized under mild, low temperature conditions tend to adopt the rhombohedral symmetry with the unit cell parameters a = 3.054 Å and c = 3c' where c' is the thickness of one layer consisting of a brucite-like sheet and one interlayer[137].

5.1.4 Layered Double Hydroxide Synthesis

Although the mineral LDH is a naturally occurring mineral, it is rarely found in nature. However, the synthetic equivalent of LDH can be produced in high yields in the laboratory and these have been extensively studied and reported[135,138]. The synthesis Feitknecht adopted in 1942[138] involved reacting dilute amounts of aqueous metal salt solutions with base. This lead to poorly ordered LDHs in which only small quantities could be prepared due to the precipitate being very difficult to filter and wash from any impurities. By comparison, there are now numerous ways to produce LDHs each with their advantages and disadvantages. However, the most practical method of synthesising LDHs commercially is by coprecipitation. This involves the addition of M^{2+} and M^{3+} cations to base *in situ* maintaining a pH of 7, followed by appropriate ageing, filtering and washing. This produces a relatively large yield but generally of low crystalinity[139]. LDHs can then be subjected to hydrothermal treatment under high pressure at 180-200 °C to obtain well-crystallised samples[140]. It should be noted that the direct hydrothermal synthesis from the metal ions and base, of MgAl- LDH and MgCr LDH has also now been reported[141].

Synthetic LDH can also be synthesised from metal ethoxides at pH 12, by a sol gel type method[142]. However, the LDH clays produced by this method are of poor crystallinity, which like LDH prepared by coprecipitation are usually subjected to hydrothermal treatment to produce highly crystalline structures.

Highly crystalline LDHs can be prepared by the urea method[135]. To achieve this, solid urea can be added to aqueous magnesium and aluminium chloride, which can be subsequently heated and stirred for varied periods of time. Urea is a very weak Brønsted base pK_b = 13.8, which means that the urea hydrolysis progresses slowly leading to a low degree of supersaturation during precipitation[143]. The mechanism of hydrolysis consists of the formation of ammonium cyanate, which is the rate determining step, followed by the fast hydrolysis of the cyanate to ammonium carbonate. During the hydrolysis, a pH of 7-9 of NH_3 is reached, which depending on temperature represents the ideal conditions for the precipitation of an LDH. One significant practical advantage of employing this method compared to the coprecipitation method is the ease with which the precipitate can be filtered and washed with water to separate impurities. The use of low metal concentrations, longer ageing times and variable temperature can

control LDH particle size. Low temperatures can produce large crystals while higher temperatures will produce smaller but more uniformly sized crystals. The ability to control the particle size of the LDH particles is important as this can change the optical and adsorbent properties of the material.

It should be noted that synthetic LDH have a general structure, which can be represented as $[M^{2+}_{(1-x)}M^{3+}_{x}(OH)_2]$ for the layer and $[An^{y-}_{x/y}(nH_2O)]$ for the interlayer. This formula indicates that it is possible to synthesise LDHs with different ratios of M^{2+} to M^{3+}, even though in general it is only possible to get single phase LDHs when x is between 0.2 and 0.33[144].

5.1.5 Ion exchange and Adsorption

There has been considerable interest in LDHs to remove negatively charged anions from aqueous solutions by both anion exchange and surface adsorption. Selective removal of anionic pollutants from aqueous systems has been investigated as cheaper, recyclable, more environmentally friendly alternatives to the traditional chemical methods. The high uptake of anionic species by LDHs is attributed to their large surface area and high anion exchange capacities, which is affected by the nature of the initial interlayer anions and the charge density of the brucite-like layers. LDHs are used in the removal of pesticides and synthetic dyes such as naphtol blue black[145], indigo carmine[146] and Evan's blue[146] from industrial effluent[147].

LDHs can remove anions from solutions in three different ways: surface adsorption, anion exchange[148] and reconstitution. Ion exchange involves the exchange of guest anions with the anions present in the interlayer region of the host LDH. Several factors determine the extent of ion exchange such as the affinity of the LDH for the incoming anion. The affinity increases with increased charge and decreasing ionic radius, the exchange medium and the pH of the solution. It is usually accepted that elevated temperatures also favour exchange. For example LDHs have a high affinity for the multivalent carbonate anions (CO_3^{2-}). To assist ion exchange, LDHs are most appropriately synthesised with Cl^- or NO_3^- ions as these are easier to displace than CO_3^{2-}. Reconstitution, or 'the structural memory effect' of a calcined LDHs can also lead to the intercalation of a desired anion into the inner region of the LDH. This property occurs when an LDH is heated to temperatures of 450-570 °C. This eliminates most of

the interlayer water and anions and the hydroxyl groups, producing a mixed metal oxide. At higher calcination temperatures solid state diffusion of the divalent anions occurs to the tetrahedral positions, forming stable spinels, and hence the loss of the memory effect[134]. If the temperature is not too hot, the LDH can then be reconstructed when placed in an aqueous solution of a given anion. Water is readsorbed to form the hydroxyl layers, resuming its original structure, in doing so intercalating a desired anion to maintain electrical neutrality.

5.2 Aims

The aim of this chapter has been to synthesize and investigate LDH-phthalocyanine hybrid materials for their applications as stabilizers for PVC coatings. The preparation of synthetic magnesium-aluminum LDHs has been investigated by both the coprecipitation and urea methods. Phthalocyanines have then been supported and intercalated on to LDHs using the ion exchange and absorption methods described above. These pigments have been incorporated into TiO_2-containing model PVC films and then exposed to UV irradiation while CO_2 evolution has been monitored to test the properties of these pigments as stabilizers for PVC films.

5.3 Synthesis of synthetic Mg-Al LDH

Two methods of producing synthetic magnesium aluminum LDH (MgAl- LDH) have been investigated: the coprecipitation and the urea method, to incorporate into PVC based paint systems. As described earlier these two synthetic procedures are known to produce LDHs with different particle size[139,135].

The coprecipitation method of producing LDH is widely used commercially[139] as this method is easily scaled up and tends to be high yielding. In this work, a ratio of 3:1 Mg:Al was used to prepare the LDH. The precipitation was carried out using two peristaltic pumps, rapidly mixing the $NaHCO_3$ and Mg^{2+} and Al^{3+} ions, while a pH of 7 was maintained by adjusting the flow rate of the basic solution. This formed a white slurry instantaneously which was aged at 70 °C for one hour and then filtered. The LDH was then washed with copious amounts of water to remove any nitrate or carbonate impurities.

The urea synthesis innovated by Costantino *et al*[135] using thermally induced urea hydrolysis produced LDHs with the larger particle sizes. This is due to the slow rate of hydrolysis as discussed in section 5.1.4. The solid urea was added to a ratio of 5:1 Mg:Al metal nitrates and the clear homogeneous solution was then heated at 90 °C for 24 hours. The aging process was much longer than that of the coprecipitate product but it was found in this study that the ageing time of 24-48 h produced large crystalline particles as reported by Oh *et al.*[141].

The MgAl-LDHs were analyzed by X-ray powder diffraction (XRD) with the d-spacing directly correlated to theta using the Bragg equation: $n\lambda = 2d\sin\theta$[134]. On inspection of the diffraction patterns, both the urea and coprecipitate methods produced crystalline LDH. The most intense and characteristic diffractions line (Figure 5.5) of a LDH is the diffraction lines at 11.8 °2θ corresponding to the $d_{(003)}$ spacing at 7.52 Å which is slightly lower than reported in the literature 7.69 Å[148]. This spacing corresponds to the thickness of the interlayer and one of the metal hydroxide layers. Other key data include the diffraction at 23.6 °2θ which can be ascribed to the $d_{(006)}$ spacing 3.77 Å which corresponds to the half-way distance between the metal hydroxide layers and the diffraction with the d-spacing 2.56 Å, (012) at 35.0 °2θ corresponds to a third of the distance and is associated with the interlayer carbonate and water .

On comparison with the coprecipitation product, the 5:1 Mg:Al-LDH synthesized from the urea method produced an LDH with a higher degree of crystalinity than that of the 3:1 Mg:Al-LDH coprecipitate product as shown by the much more intense diffraction observed.

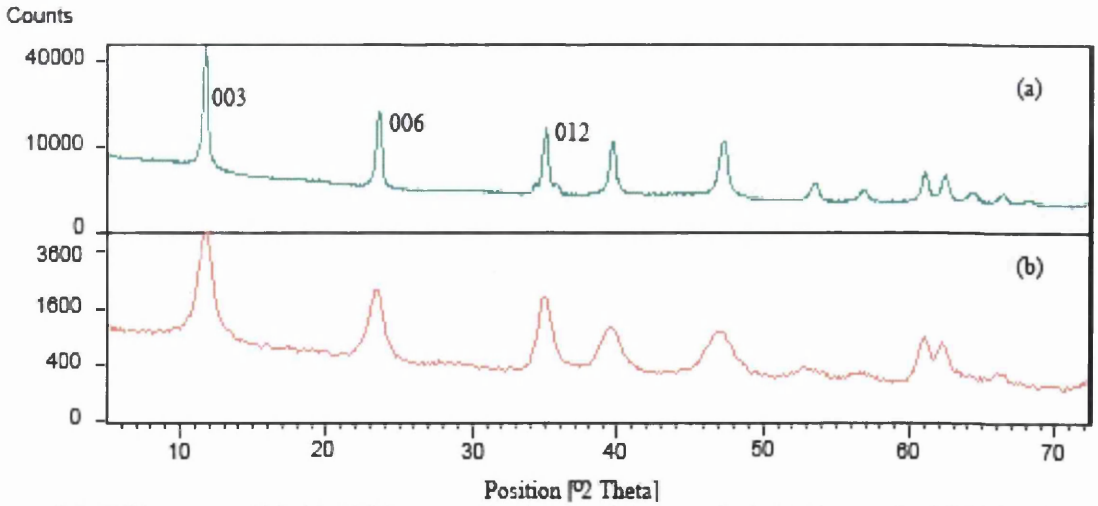

Figure 5.5, XRD pattern of MgAl- LDH, urea method, coprecipitate method, (a) Urea method 5:1 Mg:Al, (b) Coprecipitate method 3:1 Mg:Al

Energy Dispersive X-ray Analysis (EDAX) was carried out on each LDH sample. Although this procedure is not quantitative, it can be used to give a good indication of the ratio of metal ions in each brucite-like layer. Using simple peak height analysis, the MgAl-LDH 3:1 coprecipitation product produced brucite-like layers consisting of a metal ratio of 1.7 : 1, while the urea method, 5:1 Mg:Al ratio of metal ions, produced an LDH with a ratio of 1.3:1.

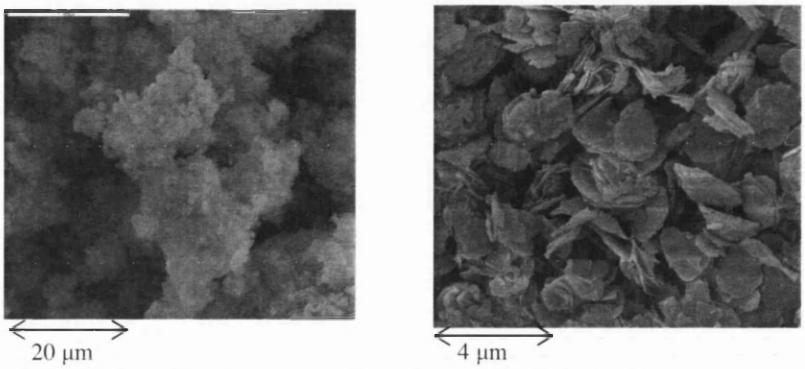

Figure 5.6, SEM image of the (left) coprecipitate product and (right) urea method

SEM analysis of the samples showed that the coprecipitation method produced a very small particle size product, while the Mg:Al 5:1 urea method clearly shows hexagonal platelets of the LDH, with a uniform particle size of *ca.* 2μm horizontally (Figure 5.6).

On inspection of the IR spectral data (Figure 5.7) of the 3:1 coprecipitation product, the absorption around 3450 cm^{-1} with a shoulder at 3000 cm^{-1} can be attributed to the stretching vibrations of the OH group in the brucite-like layers and interlayer water; the broadening of the band being associated with hydrogen bonding. An absorption at *ca.* 1600 cm^{-1} is attributed to the bending mode of hydroxyls and interlayer water. Three bands are observed for the vibrations of the carbonate anion due to its D_3h planar symmetry, the first being at around 1370 cm^{-1}(ν_3), 850 cm^{-1} corresponds to the ν_2 and at 670 cm^{-1} ν_4 mode.

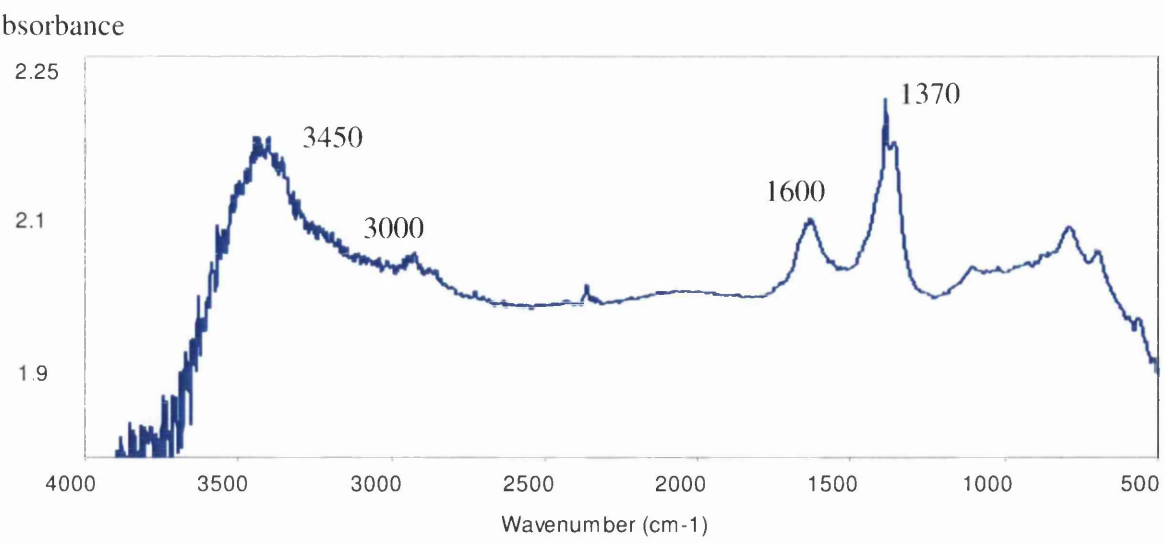

Figure 5.7, IR spectra of LDH prepared from the coprecipitate method, Mg3Al-LDH

Both the coprecipitate and urea methods of synthesizing the LDH were successful and were produced in 48 and 35 % yields, respectively. The coprecipitate, and the urea methods produced clearly defined particles of uniform size and were used in the stabilization experiments.

5.4 Absorption of Copper Phthalocyanine -4,4',4'',4''',Tetrasulfonic Acid, Tetrasodium Salt (CuPc-Ts) on to LDH

In order to intercalate into the clay interlayer or to support phthalocyanines onto the clay particle surfaces, the molecule must first be derivatised to include anionic functional groups that can interact with the charged clay. For this purpose, the blue phthalocyanine pigment derivative chosen was copper phthalocyanine-4,4',4'',4'''tetrasulfonic acid, tetrasodium salt as this is a commercially used phthalocyanine dye[41]. The intercalation of this derivatised phthalocyanine in to an LDH has previously been reported using a rehydration method[149] for photochemical studies and oxidation catalysis[150](Figure 5.8).

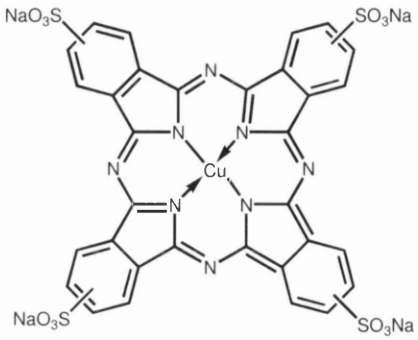

Figure 5.8, Structure of copper phthalocyanine -4',4'',4''',tetrasulfonic acid, tetrasodium salt

The adsorption of CuPc-Ts was carried out using LDH clay samples prepared by both the coprecipitation and urea methods. The clays were placed in solutions containing different concentrations of the phthalocyanine dye. The concentrations of CuPc-Ts used were 0.00008 M, 0.001 M, 0.0125 M. The suspensions were heated at 90 °C for six hours and then filtered. The resulting clays were then analysed using X-ray diffraction. The d-spacing did not change between the hydroxide layers, which would be expected if a large molecule such as a phthalocyanine dye had intercalated perpendicular to the metal hydroxide layers. It was therefore believed that the dye had been adsorbed to the outside of the clay particles and had not been intercalated into the clay. In support of these assertions, the SEM images indicated that there is no change in particle size or aspect ratios from that of the parent LDHs (Figure 5.9).

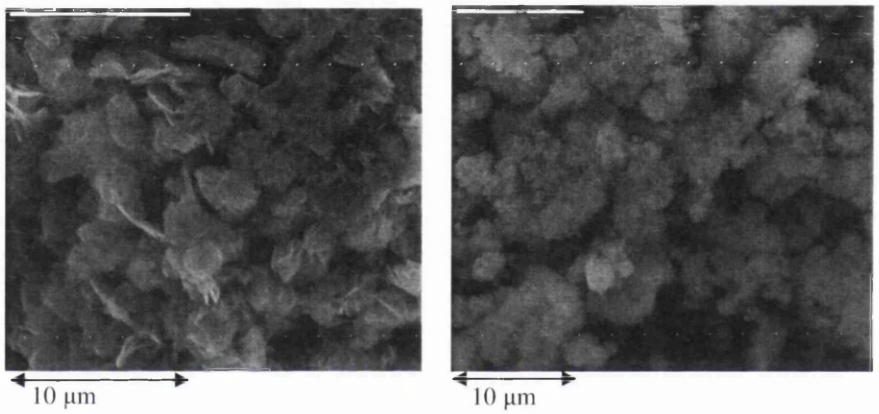

Figure 5.9. SEM images of urea and coprecipitation LDHs after treatment in CuPc-Ts solutions

5.5 Intercalation of CuPc-Ts

Intercalation of the CuPc-Ts dye was explored using three methods: rehydration, self assembly, and ion exchange. For rehydration, the LDH prepared by the urea method was first calcined at 450 °C for 4 hours under a constant stream of air in preparation for rehydration as discussed in Section 5.3. The XRD pattern of the calcined LDH (Figure 5.10) showed that the layered structure of the LDH is no longer present, all the interlayer anions have been eliminated, and a metal oxide, likely to be $Mg_6Al_{1.2}O_{7.8}$, had formed.

Intercalation of the CuPc-Ts was then attempted using the rehydration procedure using the same experimental conditions as reported by Iliev *et al.*[151]. Thus, the LDH was rehydrated in decarbonated water containing CuPc-Ts under a nitrogen atmosphere.

Once filtered, the LDH was dried under inert conditions before X-ray analysis was carried out. The diffraction pattern shows a d-spacing of 7.86 Å indicating that the CuPc-Ts did not form a clay with the dye anion perpendicular to the metal hydroxide layers. Instead the data suggested that either the dye was present horizontal to the clay interlayers or more likely supported on the clay particle outer surfaces.

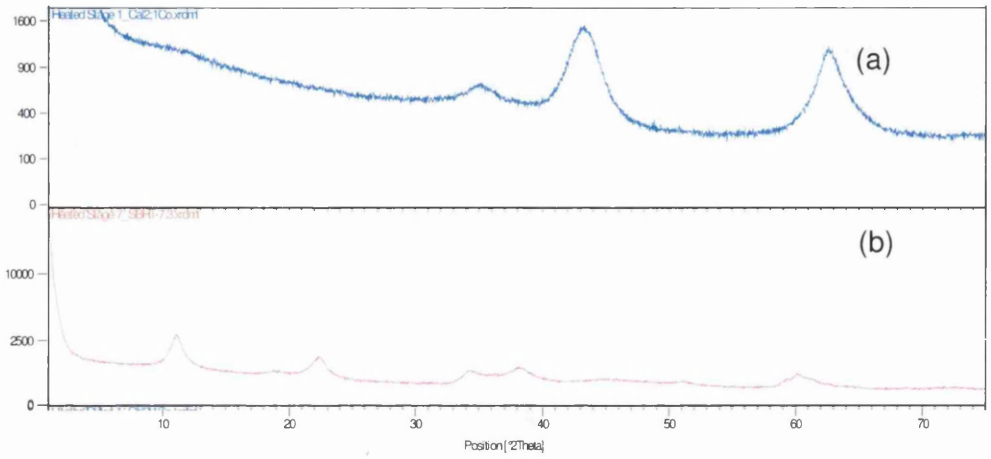

Figure 5.10, XRD pattern of the calcined Mg2Al- LDH coprecipitation product, (a) Calcined LDH, (b) LDH after reconstitution

Another synthetic approach to prepare an LDH intercalated with a phthalocyanine has been reported[151]. The literature states that in this route freshly prepared Mg-Al-LDH was not allowed to dry out after initial synthesis, which is known to enable more efficient interlayer separation for ion exchange, before intercalation with a phthalocyanine. To reproduce this procedure, Mg-Al-LDH was synthesized using the coprecipatate method as discussed in Section 5.3. Excess water was then removed from the suspension to form a thick slurry which was held under inert conditions. The slurry was placed in dye solution and heated at 100 °C for a further 8 hours and then left to stir for a further four days. The product was then analyzed by XRD and on the basis of the basal spacing of 24.3 Å d_{003}, which is comparable to that reported in the literature (23.5 Å), it was evident that the CuPc-Ts anions were arranged in the interlayer region with the molecules perpendicular to the brucite-like layers[152]. This method however proved to be unreliable and reproduction of this compound was difficult to obtain as the LDH has a large affinity for carbonate anions because the brucite-like layers have a large charge density. Exchange between the phthalocyanine molecule and the carbonate ion is therefore not favorable and therefore it is crucial to exclude CO_3^{2-} at all stages of this synthesis.

As this method proved not to be easily reproducible, the intercalation of an 'intermediate guest anion' (anions that are larger than the CO_3^{2-}) into the MgAl-LDH was investigated. It is known that the diffusion of larger anions into the interlayer region of the LDH can be inhibited if the basal spacing of the host LDH is too small[134]. Therefore intercalation of intermediate guest anions using ion exchange or the coprecipitation method is an effective way to enlarge the basal spacing of the host LDH[134]. This makes it more favourable to introduce larger guest anion into the interlayer by ion exchange with the intermediate anion. LDH precursors containing surfactants and terephthalic acid molecules have been synthesized in preparation for the insertion of bulkier anions, producing a diverse range of organo-LDHs.

On this basis, the intercalation of the terephthalate anion (TA) in to LDH was successfully attempted using the coprecipitation method. In this approach, the LDH-TA was firstly prepared by combining two aqueous solutions $Mg(NO_3)_2$ and $Al(NO_3)_3$ with 2M NaOH. The mixed solutions were then added drop wise to a third aqueous solution containing terephthalic acid and a stoichiometric amount of NaOH (0.05 moles), whilst maintaining a pH close to 7.0 by adjusting the flow rate of base.

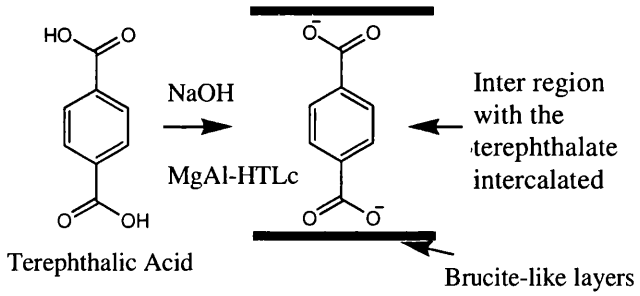

Figure 5.11, Intercalation of terephthalic acid

The product of this reaction was analysed by XRD and a basal spacing of 14 Å is observed in the XRD data, which is significantly larger that that of the parent LDH which correlates with literature data of LDH-TA[148]. Again the interlayer terephthalate anions are believed to be arranged perpendicular to the brucite-like layers (Figure 5.11).

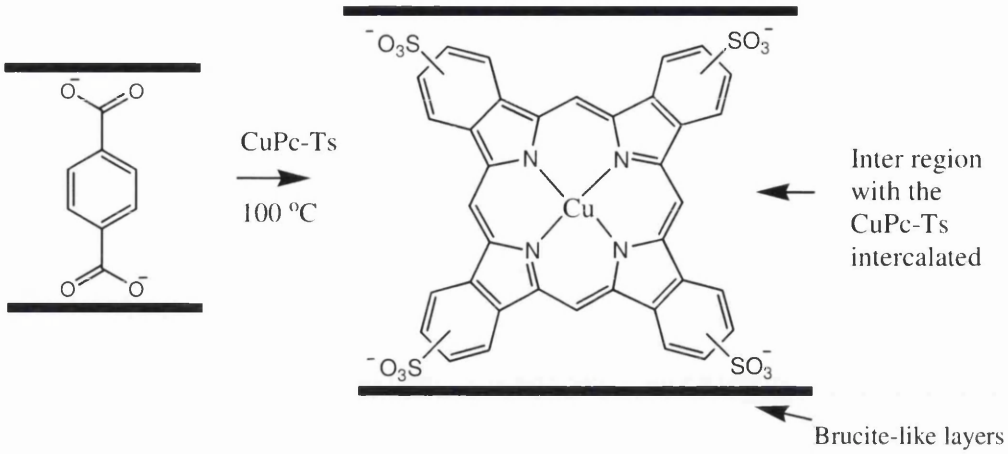

Figure 5.12. Ion exchange between terephthalic acid and copper phthalocyanine-4'-4"-4"-tetrasulfonic acid tetra sodium salt

Direct exchange from the terephthalate intercalated LDH using the CuPc-Ts was then achieved using ion exchange (Figure 5.12). To achieve this, the LDH-TA product was placed in deionised, decarbonated water along with the CuPc-Ts and heated continuously for 20 h under an inert atmosphere.

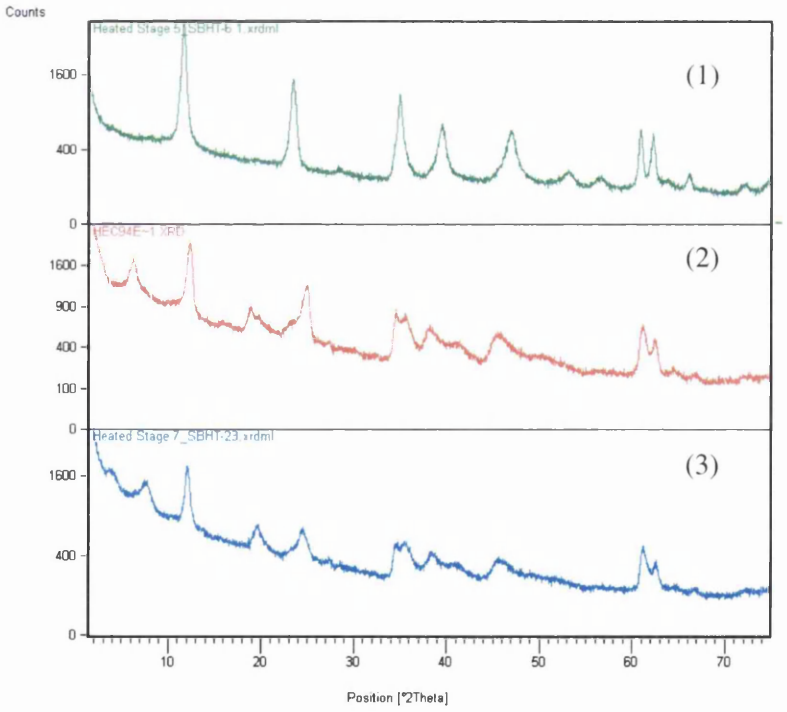

Figure 5.13. XRD data, top-bottom, (1) Coprecipitation product MgAl-LDH, (2) Terephthalic acid product MgAl-TA, (3) phthalocyanine intercalated product MgAl-CuPc-Ts

The XRD data of the MgAl-LDH, LDH-TA and LDH-CuPc-Ts is shown in Figure 5.13. On comparison of the basal spacing's between the LDH-TA and the LDH-CuPc-Ts

product, there is a change in basal spacing from 14.2 to 21.3 Å. It is therefore apparent that ion exchange between the TA anions and the CuPc-Ts anions had occurred. The SEM images (Figure 5.14) show the small particle size consistent with the coprecipitation method.

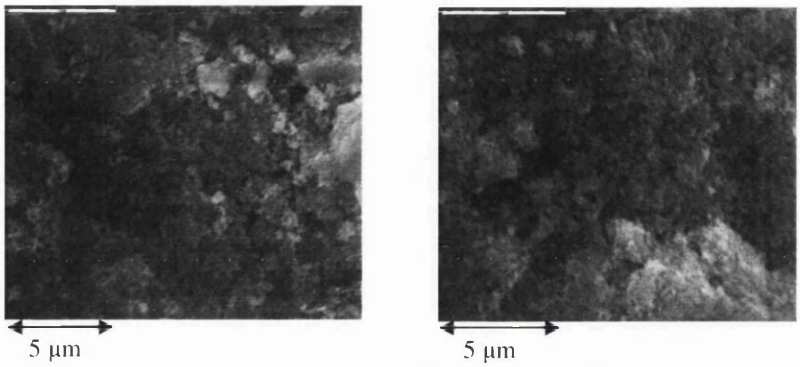

Figure 5.14. SEM images of Mg5Al-TA and Mg5Al-CuPc-Ts

The synthesis MgAl-LDH by the urea and coprecipitation methods with different particle sizes, Large-LDH and Small-LDH respectively were prepared and then were used to produce LDHs supported with the phthalocyanine, Large Pc-LDH and Small Pc-LDH. An LDH intercalated with phthalocyanine, Inter-LDH was also synthesised for further formulation into TiO2 containing PVC based paint systems in order to test the properties of the clays as stabilisers in PVC films.

5.6 Paint Formulation and Experimental Techniques

As mentioned in section 5.1.2, one means of measuring the rate of PVC mineralisation can be to quantify the rate of CO_2 evolution. In this work, both supported and intercalated LDHs have been tested by comparing them to a TiO_2 pigmented model PVC paint system The model paint system consisted of the three basic paint components, a resin, which was poly vinyl chloride (PVC), a solvent (THF) and a pigment (TiO_2).

For the degradation experiments, seven model paint systems were produced based on a 30 % per hundred resin (P.H.R) as a standard level of TiO_2, to test the effects of the intercalated and supported CuPc-Ts and the effect of LDH particle size, shape and preparation method. Details of which are shown for 10 % P.H.R. LDH additions in table 5.1.

Formulations with concentrations of 5 % and 1 % of the LDH loading were prepared by dilution of the 10 % paint systems, outlined in Table 5.1, with the blank control coating. All of the model systems used an unstabilised, highly photoactive grade of TiO_2, (Degussa P25). This grade was chosen to give a fast, reproducible photodegradation rate, whilst allowing the effect of different coating components to be assessed. The paint systems were formulated by dispersing the required amount of TiO_2 and (LDH) pigment in THF. PVC was then added to the vigorously stirring suspension of TiO_2 at a constant rate. The paint was left to stir for a further 24 hours in the dark to ensure complete pigment de-agglomeration and PVC dissolution (to prevent any photodegradation).

Sample Name	LDH information	LDH
Commercial	No LDH, contains just CuPc pigment	0 g
Large LDH	Urea LDH	0.5 g
Small LDH	Coprecipitate LDH	0.5 g
Large Pc-LDH	Supported Urea LDH	0.5 g
Small Pc-LDH	Supported coprecipatate LDH	0.5 g
Inter-LDH	Intercalated LDH	0.5 g
Blank	No LDH	0 g

Table 5.1, Paint formulations with 10 % P.H.R LDH, with the type of LDH and the amount of commercial phthalocyanine (Aldrich Ltd) added to 50 ml THF, 5 g PVC and 1.5 g of Degussa P25 TiO_2

The coatings were cast on to glass panels (70 x 220 mm) for testing in a flat panel CO_2 reactor. The panels consisted of a dried coating of approximately 20 μm thickness which was achieved reproducibly by adding two layers of electrical insulation tape (estimated to be 140 μm in height) down each side of the glass panel. Paint was poured

onto a secondary glass plate and then drawn down the prepared panel in a single smooth movement using a glass bar (Figure 5.15).

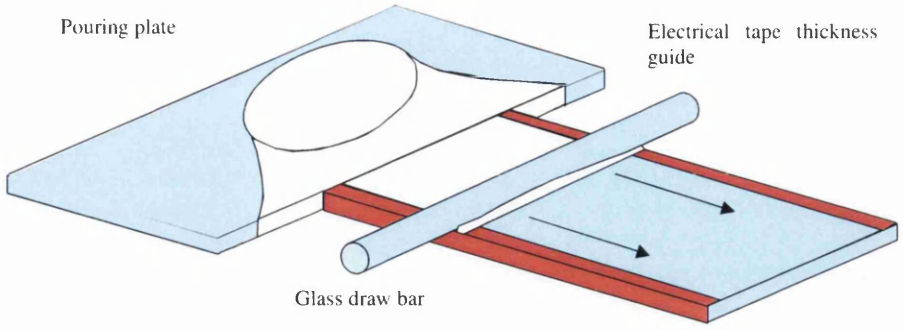

Figure 5.15, Casting process used to draw the paint over the glass panels, taken from[126]

The coated panels were then allowed to dry in a draught free environment to ensure a slow rate of solvent evaporation to reduce the formation of pinholes. The panels were placed in the CO_2 reactor once the tape used in the casting process was removed. This was achieved by placing a glass template to cover an area of 165cm^2 over the film and shaping the coating with a scalpel. The panels were then stored in the dark for a minimum of seven days prior to testing to ensure that all THF had evaporated.

5.6.1 CO_2 Reactor

The panels were then placed in a custom made CO_2 reactor. The reactor was made up of three main components: an irradiation chamber, a pump to circulate the atmosphere within the system, and an FTIR gas detection cell to monitor CO_2 evolution (Figure 5.16).

The FTIR spectrum for CO_2 comprises a peak that occurs between 2300 and 2400 cm^{-1}. By integration of the CO_2 peak area, the amount of CO_2 evolved can be quantified[126]. The atmosphere within the sealed system comprised of *ca.* 78 % nitrogen, 21 % oxygen, 0.9 % Ar, all of which are "invisible" to the IR spectroscopy. An initial background scan taken as a baseline to CO_2 before irradiation was made to correct for residual background CO_2 and water signals.

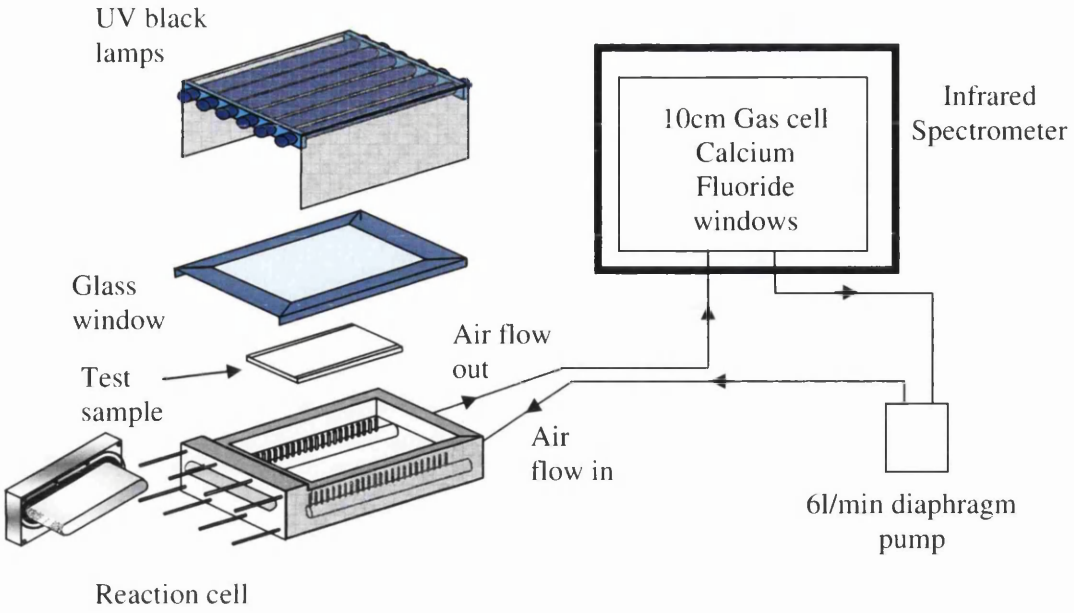

Figure 5.16, Flat Panel UV irradiation FTIR Reactor, taken from[153]

To eliminate gas leaks, the cell was constructed from a single block of aluminium milled to produce a flat sample stage with a narrow opening in the end of the cell to insert the sample. The glass panel is sealed onto the cell using a two-pack epoxy adhesive (Dunlop SAS 520), which is protected from direct irradiation *via* reflective aluminised tape[123].

5.6.2 Calibration

The degradation rate of the model systems was quantified by measuring the amount of CO_2 evolved during UV irradiation. In order to quantify these results, calibration of the apparatus was undertaken. Calibration of the cell was achieved by injecting known volumes of CO_2 into the reactor and recording the response of the FTIR spectrometer.

In the data presented here, the levels of CO_2 evolution from the test panels are presented in the form of (μmol m^{-2}). To calibrate the instrument, injections of 1 ml of CO_2 were introduced into the cell which were then converted directly to a molar value by dividing through by the volume of 1 mole of gas at room temperature (1 mol = 24 dm^{-3}), therefore 1×10^{-3} dm^{-3} CO_2 = 4.167×10^{-8} mol CO_2. Each successive injection of CO_2 has been plotted against the response in absorption units (Figure 5.17). One absorption unit corresponds to 190 microlitres of CO_2. This was then converted to give 7.91 micro moles of CO_2 for one absorption unit. This value was then divided through by the

surface area of samples being irradiated to give moles of CO_2 per unit area. The sample area of the test panels was 0.0154 m^2, giving 64.93 panels per 1 m^2.

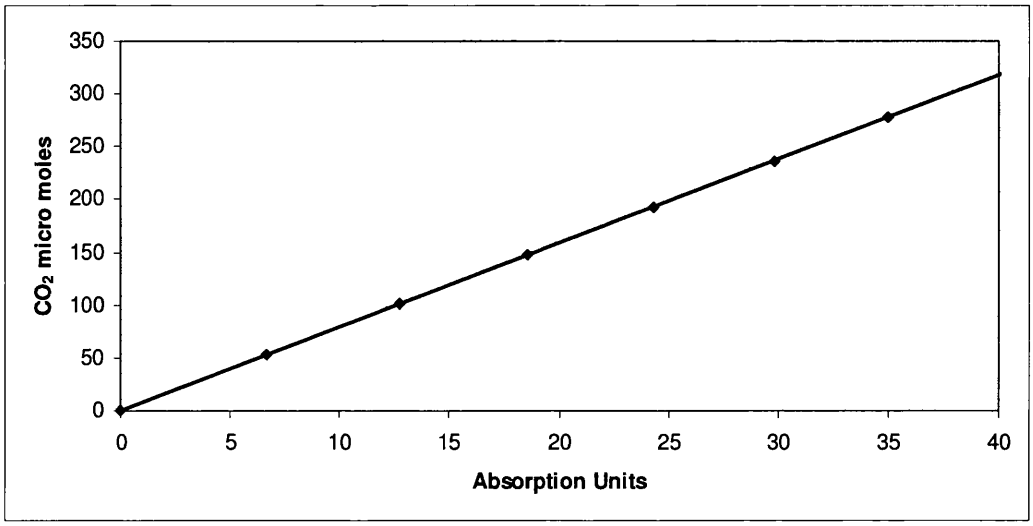

Figure 5.17, Conversion of absorption units to CO_2 μmol

5.6.3 BET analysis

Brunauer, Emmett and Teller (BET) analysis has been used to determine the surface area of the LDH clays. It is known that gas adsorption at low pressures leads to physical adsorption of an adsorbate onto the clean surface of dry powders[154]. With no defined pressure when an exact monolayer is formed, BET analysis can be used to calculate the number of molecules required to form that monolayer.

LDH powders were placed in an oven at 100 °C for 24 hours prior to the analysis. In these analyses, samples were degassed under reduced pressure to purge any unwanted volatile material followed by an controlled dose of an inert gas, in this case nitrogen. The adsorption was carried out at -195.6 °C, the temperature of liquid nitrogen, and then subjected to a range of pressures, which were then used to determine the isotherms. The LDHs were analysed using a multilayer adsorption model given below (Eqn. 1).

$$\frac{P}{n(P_0 - P)} = \frac{1}{cn_m} + \frac{c-1}{cn_m}\frac{P}{P_0} \qquad \textbf{Eqn. 1}^{154}$$

Where P is the adsorbed pressure, P_0 is the saturated vapour pressure, c is a constant, n is the amount adsorbed (moles per gram of adsorbate) at the relative pressure P/P_0, n_m is the monolayer capacity (moles of molecules needed to make a monolayer coverage on

the surface of one gram of adsorbent. The slope and intercept of a plot of $P/n(P_0-P)$ against (P/P_0) was then used to calculate n_m. The surface area S was then derived using Eqn. 2 where N_A is Avogadro's number and σ is the area occupied by one nitrogen molecule, 16.2 $Å^2$.

$$S = N_A n_m \sigma \qquad \textbf{Eqn. 2}^{154}$$

The surface area for the urea and coprecipitate products were found to be 21.3 m^2/g and 71.4 m^2/g respectively with the smaller particle size producing the largest surface area as expected. Once the CuPc-Ts was absorbed on the LDH the surface areas were not largely affected by the absorbed dye with surface areas calculated at 17.4 and 70.0 m^2/g respectively. The surface area for the intercalated LDH was also calculated and found to be 42.9 m^2/g. The BET analysis showed a Type III isotherm, which is typical of weak adsorbate-adsorbate interactions. (Figure 5.18).

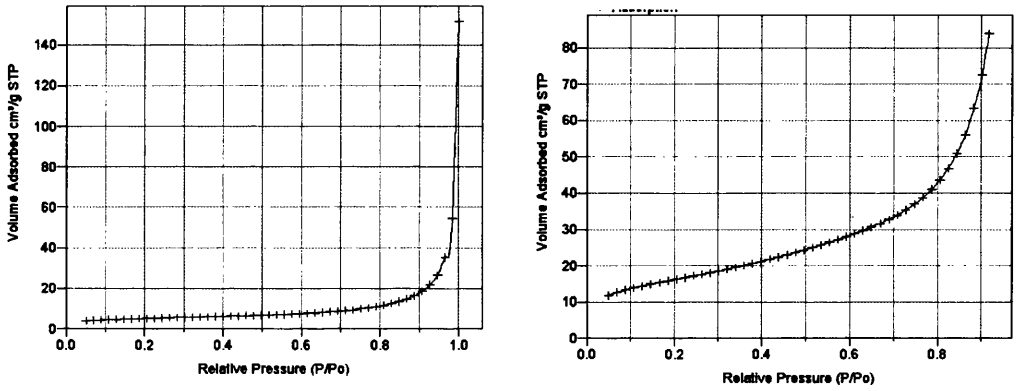

Figure 5.18, Type III isotherms (left) Coprecipitate (right) Urea LDH products

5.7 CO_2 Evolution Studies

Before CO_2 evolution studies were undertaken, it was apparent that the commercial coatings containing the phthalocyanine pigment were a lot darker in color than that of the phthalocyanine-LDH pigments. From initial observations, it was clear that the 1 % commercial phthalocyanine pigment loadings were comparable to the 10 % LDH-phthalocyanine pigment loadings. It was therefore decided to compare the 10 % LDH pigment loadings with the commercial phthalocyanine pigment. Reflectance measurements of the 10 % LDH coatings compared to the 1 % commercial loading are shown below in Figure 5.19 to illustrate this. This decision was taken as pigment loading can have an impact on the rate of degradation as darker colours can absorb more

UV irradiation, shielding the TiO_2, delaying the activation of the TiO_2. The graph (Figure 5.19) shows the reflectance data at 475 nm, which corresponded to the reflectance in the blue region, of the commercial 1 % coating with the 10 % LDH coatings. Reflectance measurements were also carried out on each film to monitor any color changes that occurred during degradation experiments and will be discussed in detail in Section 5.8.

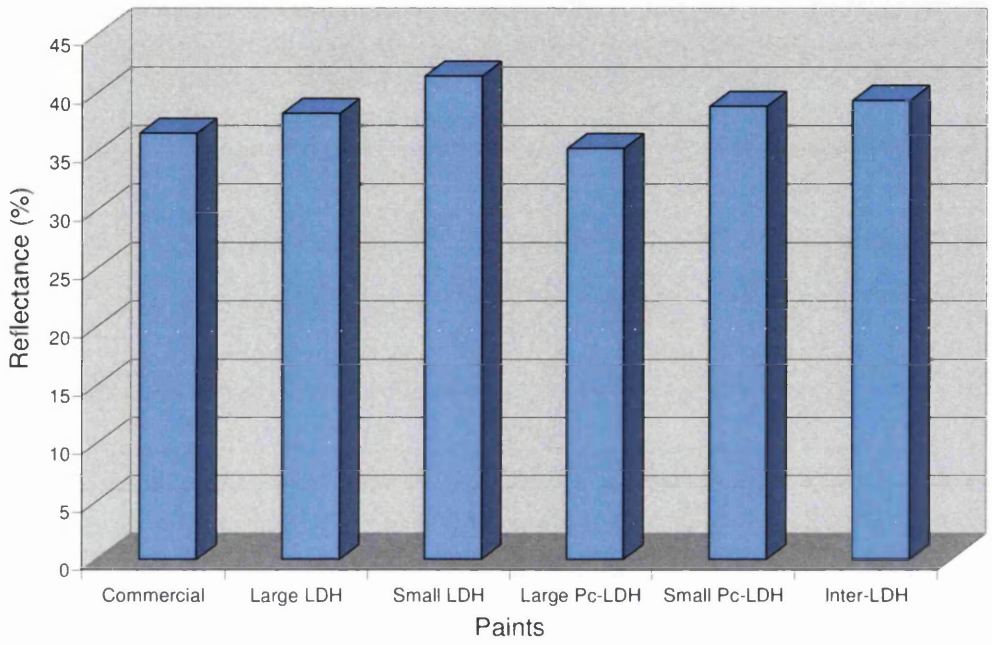

Figure 5.19. Reflectance data at 475 nm for the commercial coating with a pigment loading of 1 % compared to the 10 % LDH loading

The paint films were then irradiated in the CO_2 Flat Panel Reactor for a period of 24 hours and the evolution of CO_2 was recorded at 10 minute intervals. The CO_2 evolution plots obtained from the irradiated panels are shown below. Each plot relates to a sample containing a pigment from Table 5.1.

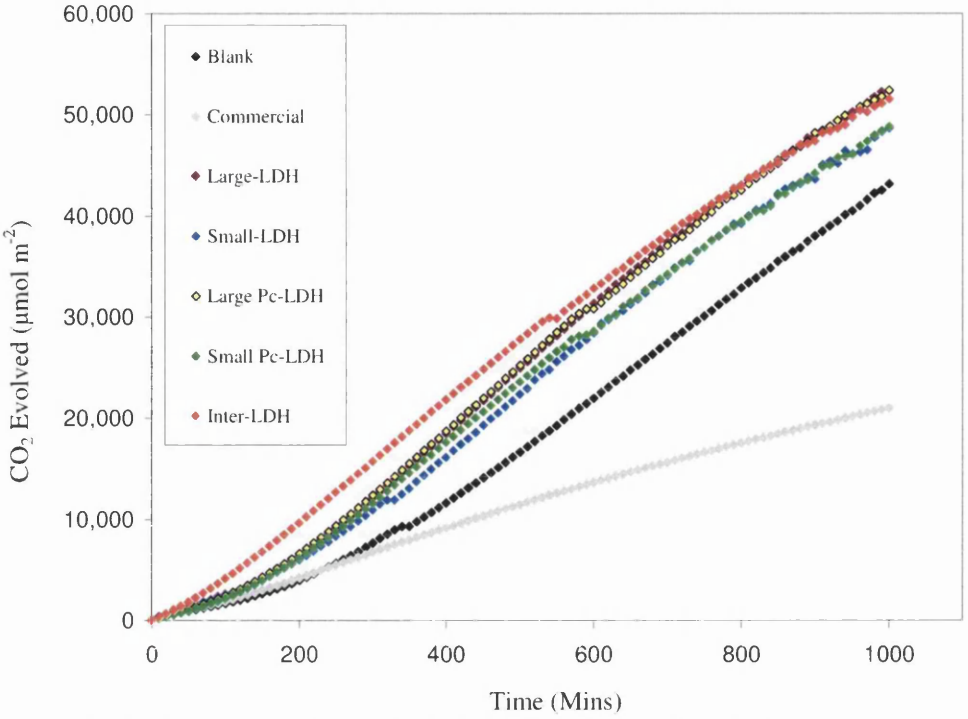

Figure 5.20. CO_2 evolution plots from coatings containing 1 % LDH loadings

The plot (Figure 5.20) shows a typical profile for UPVC coatings containing photoactive TiO_2[153]. An initial rate of CO_2 evolution was observed, followed by a transition to a faster secondary reaction rate. These rates are reported to be related to the formation of HCl, which has been shown to accelerate TiO_2 photocatalysed reactions presumably by an autocatalytic process[153]. Thus, as the PVC is attacked by the TiO_2, HCl is formed. Once a certain level of HCl has been formed, the TiO_2 becomes sensitized and it's degradative attack on the surrounding PVC is dramatically accelerated, resulting in a transition to a faster secondary rate.

In the data presented here, the initial and secondary rates of reaction have been calculated from the gradients of the CO_2 evolution profiles. The initial rate was obtained from the predominant gradient occurring between 100-200 minutes and the secondary rates from the gradient between 800-1000 minutes. This is shown in Figure 5.21 and provides a quantifiable measure of the rate of degradation of each film.

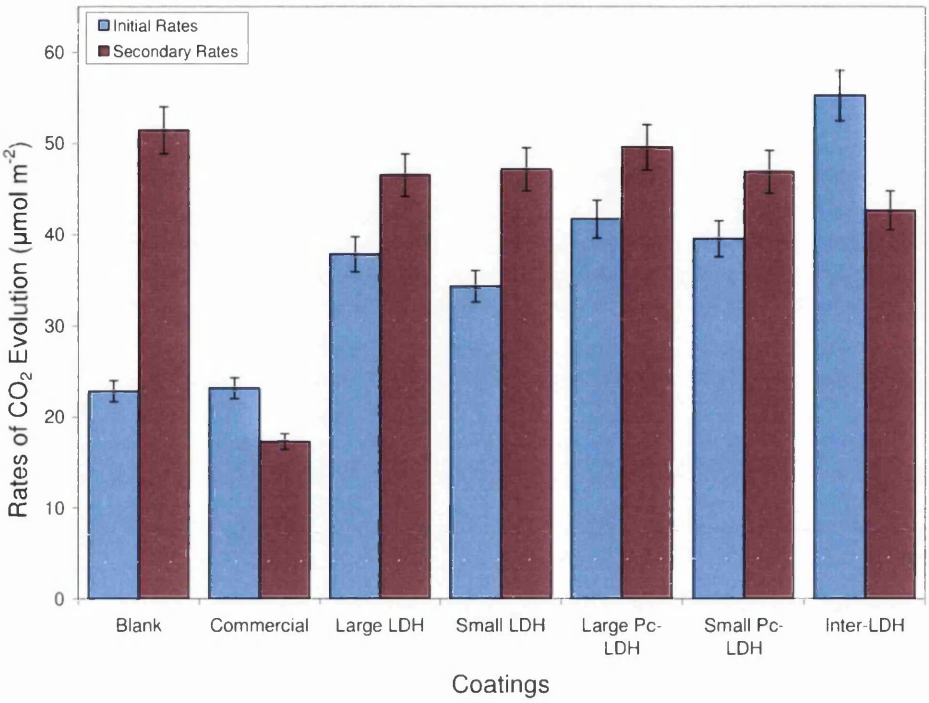

Figure 5.21, Initial and secondary rates of CO_2 evolution with 1 % LDH loadings

At 1 % loading, the films that contained the LDH pigments have no impact on reducing the rate of CO_2 evolved in comparison to the blank sample, which contained no LDH pigment. In fact, an increase in initial CO_2 evolution rate was observed. This is believed to be due to release of CO_2 from the interlayer of the LDH before HCl adsorption takes place. The plot showed that the commercial pigment at 1 % was the most stable coating under these conditions but a much darker colored film was observed compared to the LDH pigments containing the phthalocyanine. It is believed that, for the commercial sample, the pigment absorbed the UV radiation and hence the PVC film was not degraded to the same extent as the lighter LDH pigments.

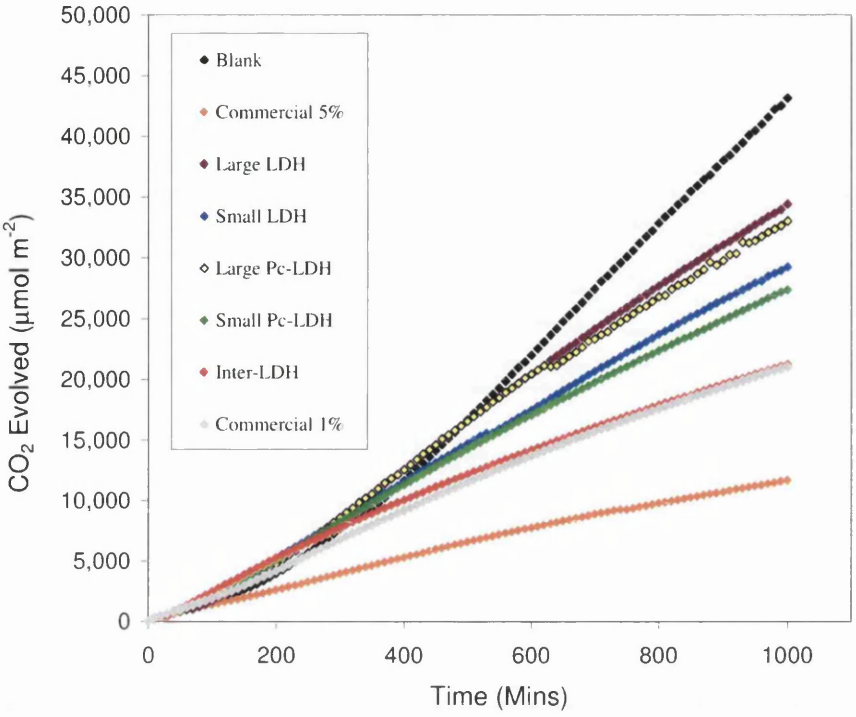

Figure 5.22, CO_2 evolution plots from coatings containing 5 % LDH loadings

Figure 5.22 shows the CO_2 evolution plot for the films that contained LDH or pigment loadings of 5 %. At these loadings, the LDH pigments have started to have an impact on the rates of CO_2 evolution, with all the LDH coatings out performing the blank sample.

The rate of CO_2 evolved for the initial and secondary rates of reaction for the 5 % coatings compared to the commercial sample at 1 % loading is shown below in Figure 5.23. The blank coating, as discussed earlier, contains no pigment or LDH and hence has an initial rate of CO_2 evolution with a transition to a faster secondary rate of CO_2 evolution. The Large LDH shows a drop in CO_2 evolution compared to the blank sample, with the Large Pc-LDH reducing the CO_2 evolution even further, which can be seen in Figure 2.22. The Small LDH pigments follow the same trend with the Small Pc-LDH out performing the non-pigmented Small LDH coating. It is worth noting that with both the Large LDH loadings, the secondary rate of CO_2 evolution is greater than that of initial rates, which follows the same trend as with the blank coating and the 1 % loadings but at reduced rates. This indicates that there is still a transition to an accelerated secondary rate. In comparison with both the Small LDH coatings, the initial rates of CO_2 evolution are greater than the secondary rates. The decrease in secondary

rate of CO_2 evolution can be linked to the LDH removing the HCl generated during the degradation reaction of the film. It is postulated that an ion exchange reaction takes places with LDH interlayer carbonate ions between the brucite-like layers. This can then form carbonic acid and CO_2 as the LDH can also act as a base, which is not as acidic as HCl and hence not sufficient to activate the TiO_2 semiconducting material further. Further activation would allow the more rapid photodegradation, which is seen in the blank coating, pigmented with TiO_2 alone. The LDH coatings that contained the supported phthalocyanine showed reduced CO_2 evolution compared to their non pigmented counterparts. This could be due to the hue of the pigment, with the phthalocyanine absorbing a proportion of the UV irradiation in preference to the TiO_2.

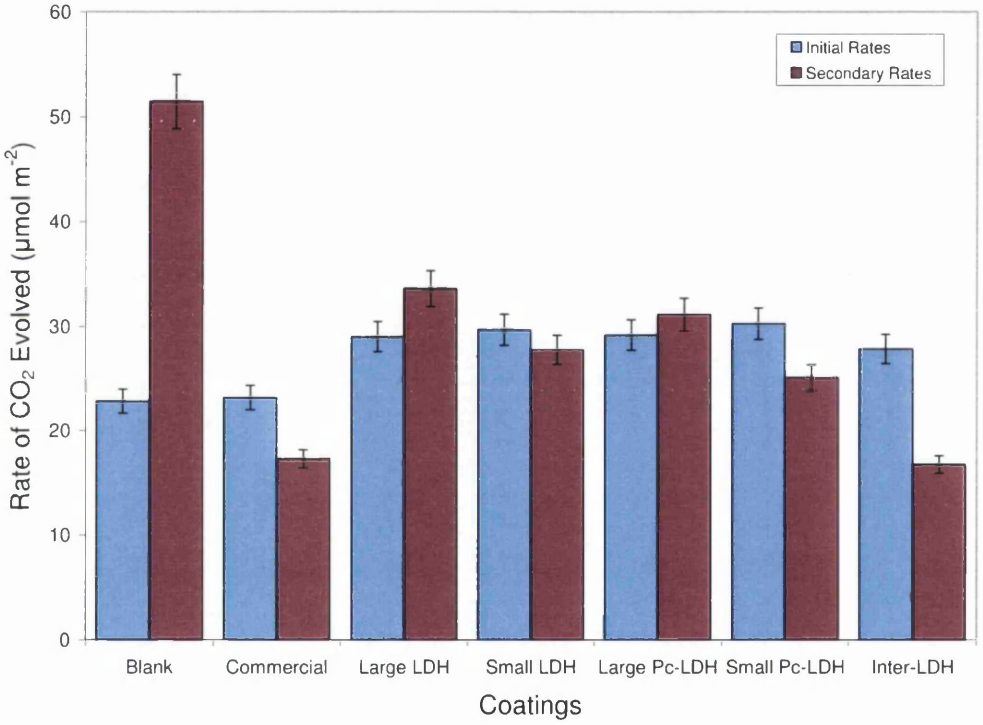

Figure 5.23, Initial and secondary rates of CO_2 evolution with coatings containing 5 % LDH loadings *vs* the commercial 1 % loading

The coating that contained intercalated phthalocyanine dye within the LDH layers (inter-LDH) was the most effective stabilizer at the 5 % loading. This could be due to two possible reasons. Firstly, from the analysis of the BET and SEM data, the inter-LDH consisted of clay particles with a high surface area. This would enable more Cl^- ions to be intercalated and hence reduce the autocatalytic acidity of any HCl produced within the film. However, if this was the only reason for reduced CO_2 evolution, then the coprecipitate products (small LDH and small Pc-LDH) would in theory provide

better stabilization as BET analysis showed an even larger surface area than that of the inter-LDH. Hence, the coating may also be gaining added stability from the intercalation of the phthalocyanine into the brucite-like layers. It could also be possible that when intercalation of the Cl^- anions occurs, there is ion exchange with the CuPc-Ts anion. Hence, exchanging the Cl^- for CuPc-Ts should be more energetically favorable because the LDH gallery region should return to a more favourable 7.62 Å d spacing. In addition, there would be no CO_2 released from the CuPc-Ts clay which would be measured in the CO_2 infrared data and which could also form carbonic acid.

The CO_2 evolution and the initial and secondary rates of CO_2 evolution from films containing 10 % loading of the pigments are shown in Figures 5.24 and 5.25. It is clear to see that the LDH pigments have a considerable effect on the evolution of CO_2 at this loading compared to the blank coating. There is little evidence of a transition from the initial to a secondary rate of CO_2 evolution as observed in the 5 % pigment loadings for the large LDH and large Pc-LDH. At this loading, both the Large LDH and the supported Large Pc-LDH are comparable as there is little evidence that the addition of the supported phthalocyanine has an effect on the rate of CO_2 evolution. This can also been seen to a larger extent with the Small LDH data set which shows a greater reduction in the rate of CO_2 evolution compared to it's supported counterpart, Small Pc-LDH. This could be due to the fact that the supported phthalocyanine is attached to the outside of the clay particles and could have an impact on the rate of HCl intercalation, reducing the efficiency of the system at this loading rate. In general, the rates of CO_2 evolution suggest that the particle size has the largest affect on the CO_2 evolution rates.

As for the 10 % loading data, the inter-LDH coating has proven to be the most efficient pigment to stabilize the coating from UV degradation compared to the commercial pigment at a loading of 1 %. The phthalocyanine is also supported on this LDH but intercalation is also observed. This means that the phthalocyanines supported on the sides of the clay particle are separated by a larger basal spacing than the LDH with the carbonate anions and hence the effect of adsorbed phthalocyanine on the particles may not have an effect on the intercalation of the HCl molecules.

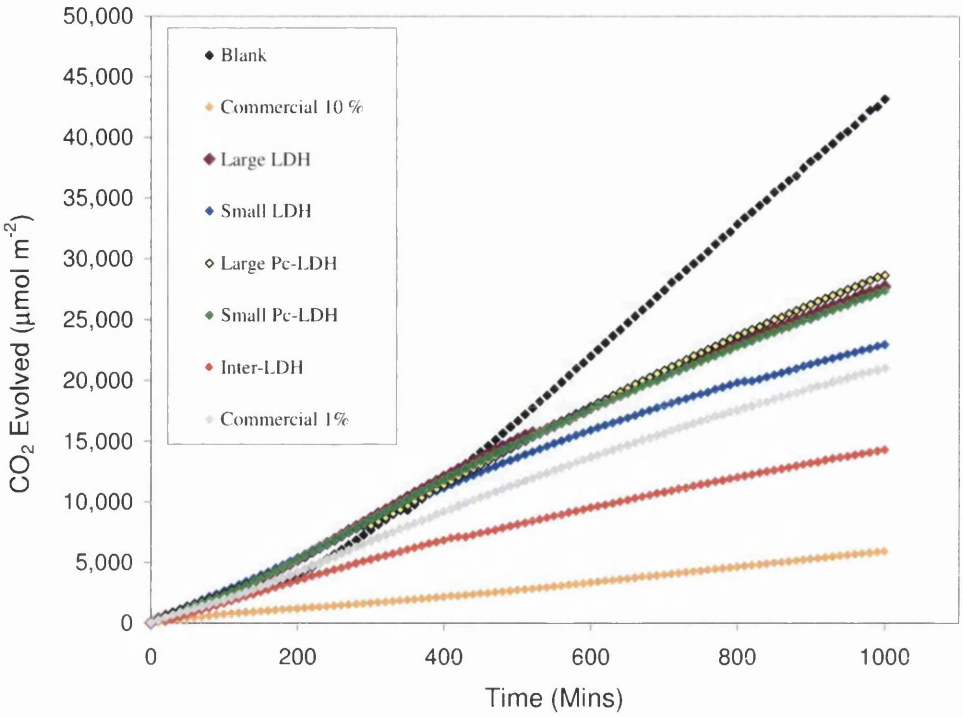

Figure 5.24. CO_2 evolution plots from coatings containing 10 % LDH loadings

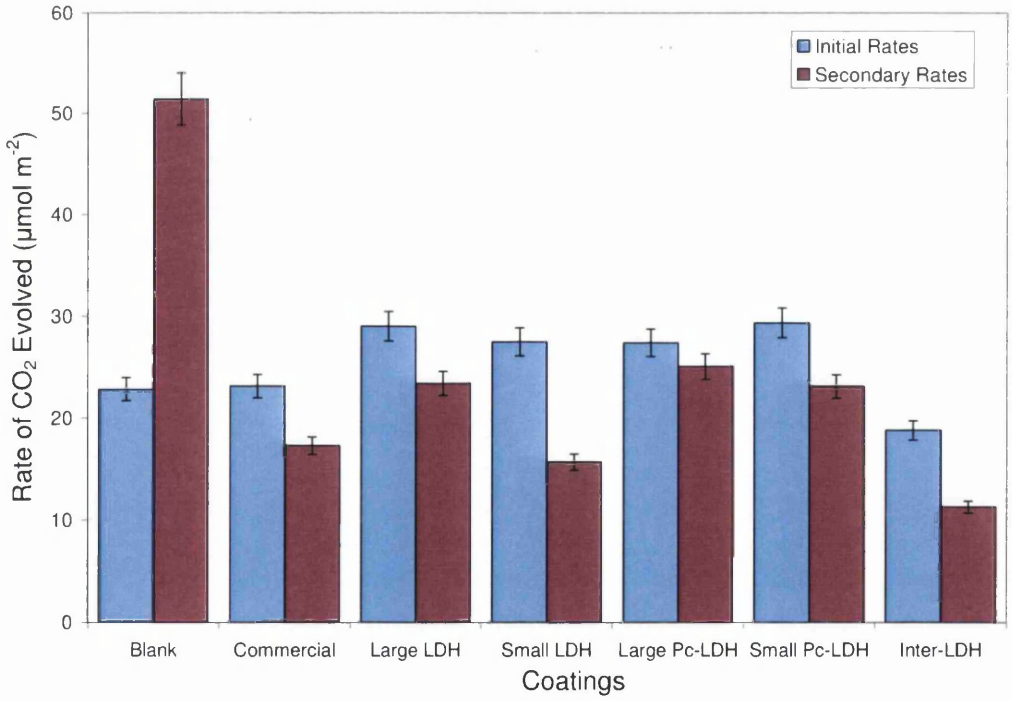

Figure 5.25. Initial and secondary rates of CO_2 evolution form coatings containing 10 % LDH loadings *versus* the commercial 1 % loading

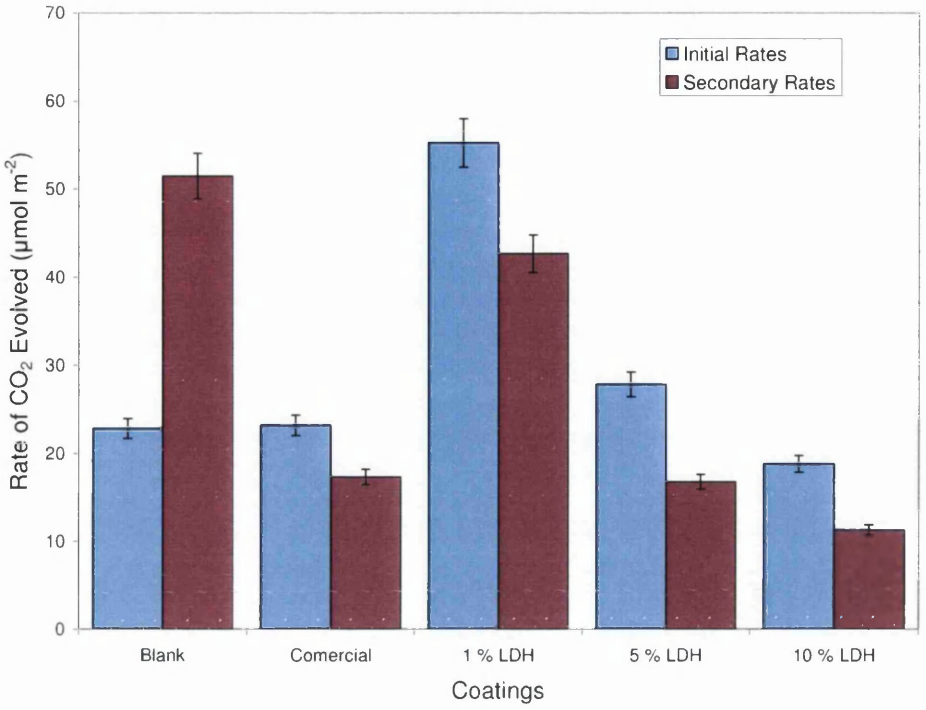

Figure 5.26, Comparison of initial and secondary rates of CO_2 evolution for the 1, 5 and 10 % Inter-LDH loadings

In Figure 5.26, the data show a comparison of the initial and secondary rates of CO_2 evolution between the 1, 5 and 10 % additions of the inter-LDH pigments compared to the 1 % commercial loading. An increased secondary rate is very apparent in the blank coating due to the lack of any stabiliser being present within the film to 'mop up' reactive species such as HCl, whereas in the LDH pigmented coatings no such increased secondary rate is observed. From this data, it is clear that the loading concentration of the LDH has an impact on the degradation process. There is a considerable difference in the rate of CO_2 evolved, with higher CO_2 evolution occurring in loadings of 1 %. A loading of 5 % is required to have an impact on CO_2 evolution but it is worth noting that no formulations with loadings in between 1 and 5 % were tested and so the precise concentration when the LDH has an impact on the rate of evolution is unknown.

5.8 Reflectance Measurements

Reflectance measurements are the ratio of the amount of electromagnetic radiation reflected from a surface to the amount originally striking the surface. There are two main types of reflectance, specular and diffuse reflectance. Specular reflectance occurs

where light from a single direction is reflected by a surface in a single direction where the angle of incidence is equal to the angle of reflection as shown in Figure 5.27. Smooth surfaces and polished metal surfaces mainly give rise to specular reflectance. Rough surfaces, such as matt white objects allow light to enter the surface layer of the object. The light is then scattered multiple times before exiting in random directions; this is diffuse reflectance. Most objects have a mix of both processes.

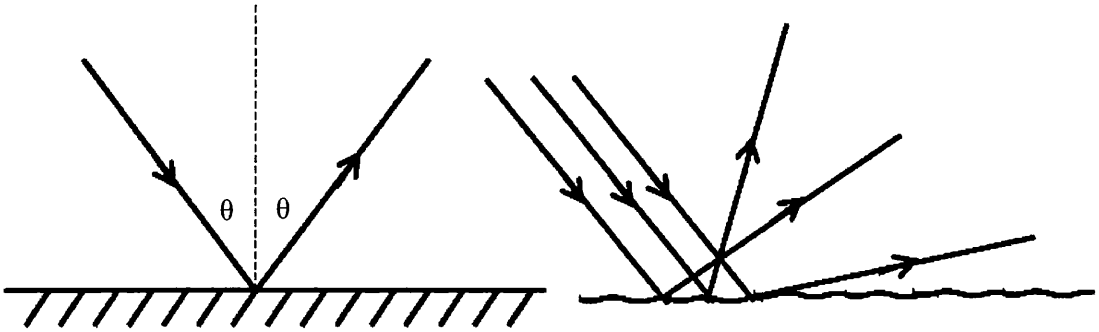

Figure 5.27, Specular (left) and Diffuse (right) reflectance

Reflectance can be used as a measure of how well the coating is performing with time. For instance, changes in reflectance can be caused by a change in the physical properties of a film and hence can be used as a measure of degradation. In the experiments described here, the absorbance at the UV end of the spectra, 200 nm to 388 nm, is the reflectance which gives rise to the photoactivation of the titania particles. The blue phthalocyanine pigments used in these studies have a low reflectance at these wavelengths but reflect at around 450 nm corresponding to the π-π^* transitions of the macrocycle.

Figure 5.28 shows the absorption spectrum of the coating containing the commercial phthalocyanine, along with TiO_2 as formulated in Table 5.1, at time zero before any exposure to UV irradiation. The absorbance peak around 300 nm is due to the anatase form of TiO_2, while the peak 420 nm is due to the small amount of rutile in the Degussa P25 sample. The phthalocycyanine CuPc-Ts is observed at around 600 nm.

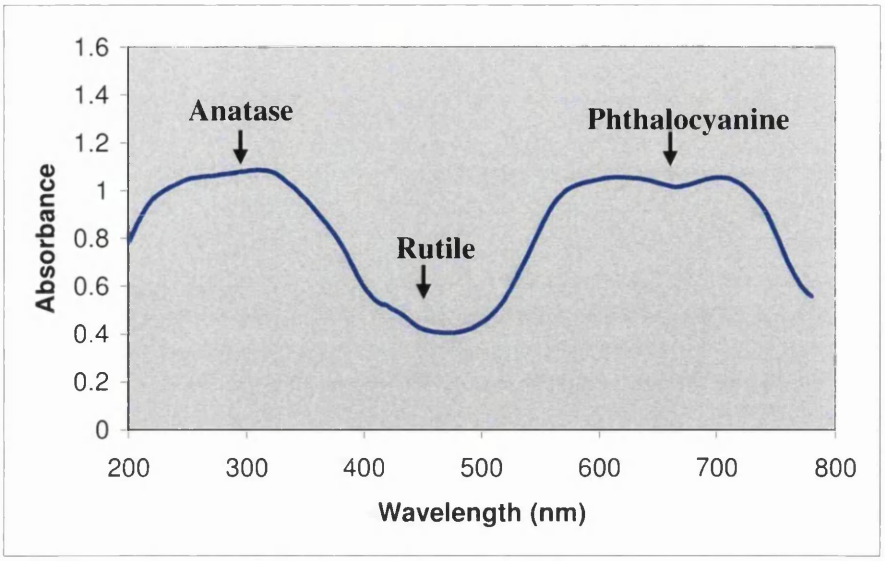

Figure 5.28. Absorption spectrum of coating inter-LDH

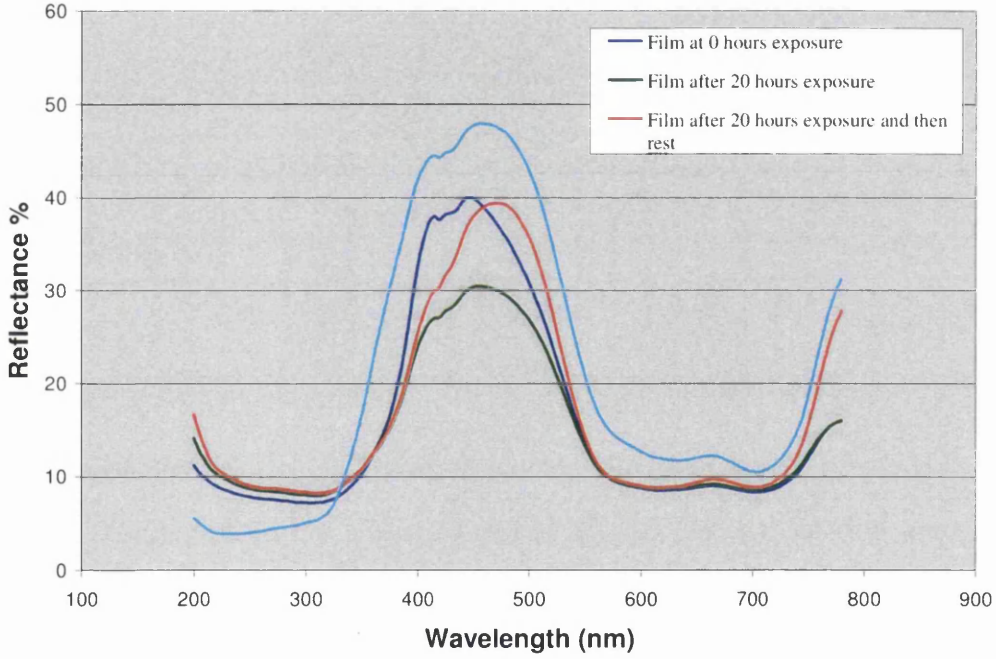

Figure 5.29, Colour reflectance data for the coating containing the commercial pigment at 1 % loading after 0, 20 and 120 hours of UV irradiation

Figure 5.29 shows the similar spectral data (but in reflectance mode) for the commercial phthalocyanine coating at time zero as well as the same film after 20 hours exposure, 20 hours exposure followed by a period of rest (films placed in the dark for a period of 60 days), and after 120 hour of exposure to UV irradiation.

The reflectance data between 200 and 410 nm are believed to correspond to the TiO_2 pigment. The anatase form of the TiO_2 is observed around 200 to 388 nm, while a

shoulder at 410 nm is believed to be due to the rutile form of TiO_2 as shown in the reflectance spectrum at time zero. The blue colour of the phthalocyanine pigment reflects at around 475 nm but absorbs around 600 nm as shown in Figure 5.28. After UV irradiation for 20 hours, the data show very little change associated with the TiO_2 between the initial sample and that after 20 hours of exposure. The films darken between 380nm and 550 nm (where in pristine samples very little light was absorbed) which is evidenced by the decreased intensity of the reflectance peak at 475 nm. This suggests that photo oxidation focuses directly on the PVC matrix and that the oxidation products produced within the PVC film during initial irradiation are responsible for the darkening effect. The films were then placed in the dark after 20 hours of UV irradiation for a period of 60 days. In this time period the films became lighter in colour without any further irradiation. It is also apparent that the reflectance corresponding to the rutile TiO_2 is not so prominent. This could be due to the TiO_2 absorbing more or the pigment absorbing less. It is therefore believed that the TiO_2 is further being exposed even after irradiation ceases due to the remaining HCl produced during the exposure. This exposes some of the TiO_2 at the surface of the coating, causing reflectance from the white TiO_2 particles resulting in a whightening of the film (this phenomenon is known as chalking).

After 120 hours of UV irradiation, there is a decrease in reflectance associated with the TiO_2. This can be explained by the formation of initial decomposition products followed by further PVC degradation, exposing more TiO_2 at the surface of the film and hence the TiO_2 will absorb more light at these wavelengths, reducing the amount of light reflected. As stated above, this effect can appear as chalking in the film. The reflectance at 475 nm increases in intensity, indicating that the film has become lighter in colour, which can be explained by the continuing exposure of the TiO_2 in the PVC matrix, lightening the film and thus, reflecting more around 475 nm. An increase in reflectance is also observed above 600 nm where it is believed that photodegradation is occurring, degrading the phthalocyanine macrocycle, which can also lead to loss of colour, lightening the film.

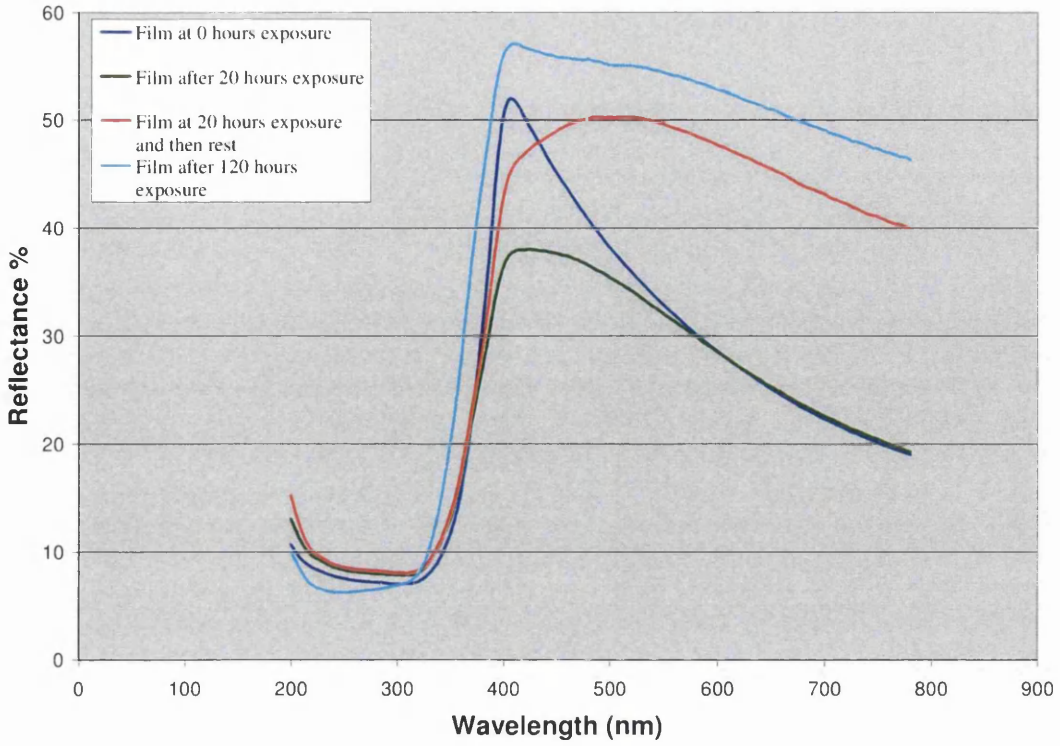

Figure 5.31, Reflectance spectrum for the coating containing Small-LDH at 10 % loading

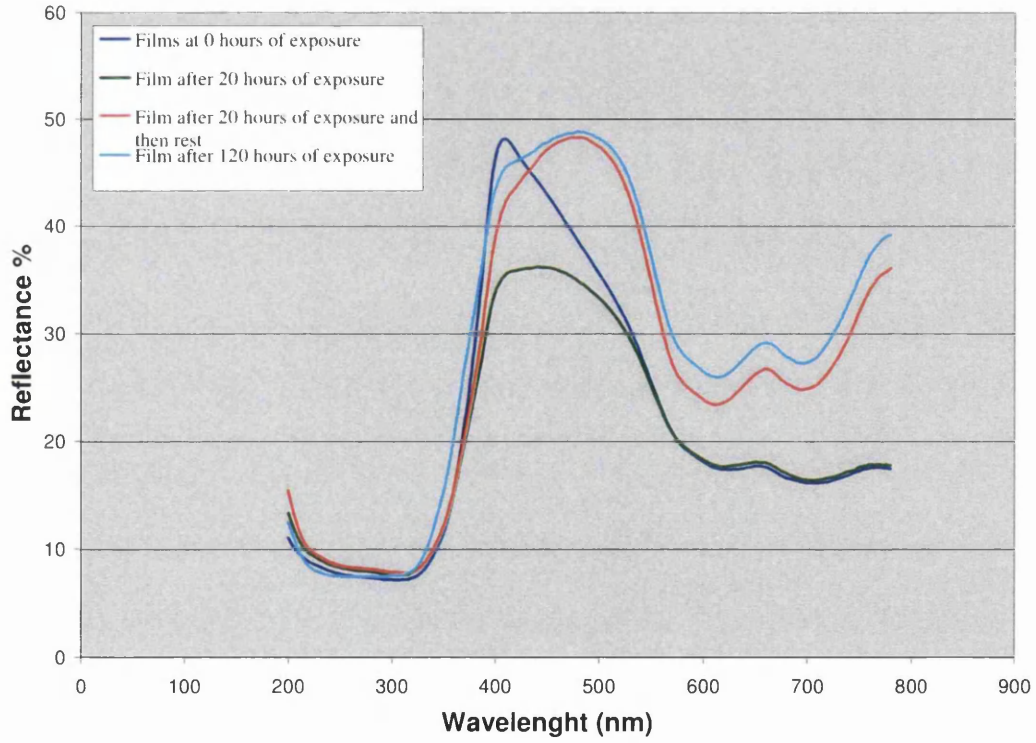

Figure 5.32, Reflectance spectrum for the coating containing inter-LDH at 10 % loading

Figure 5.31 shows the change in reflectance data for the visually white coating containing the Small-LDH pigment. As no blue pigment is present in this coating, the

peak at 410 nm corresponds to the white TiO_2 pigment and the white LDH pigment. This paint again shows the same trend as the commercial pigment with the film darkening in colour upon initial irradiation due to the initial degradation of the PVC, followed by the lightening of the coating as the PVC matrix is degraded, exposing the TiO_2 at the surface.

Figure 5.32 shows the reflectance measurements for the inter-LDH coating at 10 % loading. The data show that, after 20 hours UV exposure, there is no change in the spectral response apart from a decrease in reflectance between 400 and 580 nm ascribed to initial PVC degradation, giving rise to an increase in C-C unsaturation. The data for the sample after 20 hours and rested shows a broadening of the reflectance between 400 and 600 nm which suggests the unsaturated polymeric material has been mineralized. The phthalocyanine related features at 600 to 800 nm show more reflectance after 20 hours and rested then more reflectance again after 120 hours which is ascribed to increasing degradation of the phthalocyanine dye with time and UV exposure.

5.9 Conclusions

The data from a blank PVC film containing only photoactive TiO_2 and PVC show a transition from an initial to a secondary rate of CO_2 evolution which is believed to be related to the formation of HCl, which has previously been shown to accelerate photo-oxidation reactions in PVC films[155]. These workers have shown that photo-oxidation is accelerated once a threshold amount of HCl has been formed from the degradation of the PVC matrix by TiO_2 which is in line with the observations made in this thesis. Therefore, it appears that the transition to a higher degradation rate will not occur until a certain concentration of HCl is formed which can occur at different times but typically in our experiments, seam to occur between 100 and 200 minutes.

In our data, LDH has been used to suppress this acid auto-catalysis of HCl caused by photo oxidation. Our data show that a loading of 5 % or over is required to prevent the transition of CO_2 evolution to the secondary rate. Interestingly, our data show that PVC stabilisation is not simply related to the surface area of the clay additive. Instead, the intercalation of the phthalocyanine dye into the inner region of the LDH clays proved to reduce the secondary rate of CO_2 evolution by a considerable amount compared to the

supported Pc-LDH pigments at 10 % loadings. This has lead to the conclusion that by shielding the phthalocyanine from the UV irradiation, degradation of the pigment has been reduced. It is also possible that when intercalation of the Cl^- anions occurs, there is ion exchange with the CuPc-Ts anion, therefore exchanging the Cl^- for CuPc-Ts. This could be more favourable as there in no CO_2 release forming carbonic acid.

In terms of studying the mechanisms of PVC degradation, our data show photo-oxidation induced by the TiO_2 appears to result in degradation of the PVC matrix, with an initial formation of oxidation products in the form of unsaturated C-C bonds, which cause initial darkening of each film after they are irradiated for 20 hours. Upon continued irradiation the films lighten in colour. It is believed that there are three possible mechanisms for this colour loss, with all of these happening simultaneously. Thus, it appears that the PVC matrix is degraded, leading to TiO_2 being exposed on the surface of the film, causing whitening or chalking. The LDH-pigment can also be exposed at the surface leading to the degradation of the phthalocyanine molecule and hence also leading to colour loss. This is supported by the reduced CO_2 evolution of the intercalated phthalocyanine molecule. Finally, there is complete mineralisation of the unsaturated C=C bond polymer.

LDH is an inert, inexpensive, non-toxic material that is easily handled and therefore it appears to be an ideal material for incorporation within commercial PVC matrices and products that might be subject to high UV environments. The inter-LDH pigment appears to act as both stabiliser and a pigment within the PVC coating, reducing the damaging effects of photo oxidation, which otherwise result in discolouration and degradation of the TiO_2 containing PVC film when exposed to high UV conditions. The dispersion of only one material that acts as both a stabilizer to the pigment and the coating is also advantageous. A uniform film is therefore easier to obtain as only one material is required to be dispersed within the paint during its preparation.

Chapter 6

Conclusion

6.1 Conclusions

The objectives of this project were to synthesise novel tailor made phthalocyanines for applications in DSSC devices and also to study phthalocyanine-LDH interactions for stabilisation experiments in PVC based paint systems. These sub-tasks are related by the absorption of light and it's subsequent effects on a surface coating. Thus, in a DSSC device, the aim is to capture as much solar radiation as possible (in this thesis, through the phthalocyanine dye component of the device) and to convert it into electricity. By comparison, in the second paint-based system, the aim is for the phthalocyanine dye and clay to combine partly to absorb and dissipate light to prevent photochemical degradation but also to chemically absorb HCl, to prevent it accelerating polymer breakdown in the paint.

Early on in this project, it was found that synthesis of halogenated phthalonitriles, precursors to phthalocyanine synthesis, was required in relatively large scales to prepare substituted phthalocyanines for DSSC applications. A novel method of producing 4,5-diiodophthalonitrile (**6**) is described in Chapter 2 of this thesis, which resulted from initial investigations using 30 % fuming sulphuric acid and molecular iodine to iodinate the phthalonitrile. Problematic synthesis of the precursor resulted at all stages of the synthesis, starting with the availability and transport of the 30 % fuming sulphuric acid as well as cost. The acid was then difficult to handle and the resulting product was difficult to purify and affording low yields. Yields were increased using autoclave synthesis but availability and safety concerns using this material were not resolved. This resulted in an investigation to use periodic acid and molecular iodine, which created a more powerful electrophile to iodinate the back of the phthalonitrile, which resolved the safety and availability issues of producing this precursor.

Chapter 2 also discussed various palladium catalysed coupling of desired substituents to the halogenated phthalonitriles, forming the required substituted phthalonitrile in preparation for synthesising tailor made phthalocyanines. Thus, the commercially available *t*-butyl phthalonitrile and the synthesised 4,5-nonoxyphthalonitrile (**24**) were chosen with the aim of providing increased dye solubility and also to try and reduce dye aggregation after cyclisation, as this is known to reduce DSSC device efficiency. In addition, ferrocene substituents were successfully coupled to both mono and dihalogenated phthalonitriles using Negishi coupling using careful control of reagents

and reaction conditions. The aim here was to introduce a redox active centre to the dyes which it was hoped would be a useful property for DSSC devices because they are, in effect, photoelectrochemical cells. It was also hoped that ferrocene would also act as a bulky group again with the aim of enhancing solubility and reducing dye aggregation.

Linking the dyes to a surface is essential for DSSC operation. However, the anchoring group proved difficult to synthesise with failed coupling attempts to the iodinated phthalonitrile with methyliodobenzoate therefore a fumaronitrile group (**19**) was synthesised to anchor the dyes to the titania but this eventually resulted in the loss of conjugation in the resulting core phthalocyanine macrocyclic structure and hence, once cyclised formed azaporphyrines dyes. Acid anchoring group (**20**) was then synthesised by Eu e*t al.*[64] a third of a way through this thesis and hence was prepared to maintain the macrocyclic core structure of the phthalocyanine.

The investigation into the cyclisation of the prepared substituted phthalonitriles was discussed in Chapter 3. Initially, it was first thought that subphthalocyanines were a method of forming the desired unsymmetrical phthalocyanine or derivatives but initial tests revealed that the formation of the subphthalocyanine was very dependant on the substituent attached to the phthalonitrile and the reaction conditions, with *t*-butyl subphthalocyanine proving difficult to synthesis in workable quantities. The formation of a subtriazasubphthalocyanine, designed to incorporate the acid anchoring groups into the structure proved to be unsuccessful. However, halogenated subphthalocyanines were successfully synthesised. Incorporation of the remaining isoindolinone to form phthalocyanines has been reported in the literature by ring expansion with the desired isoindoline. However, this again proved to be troublesome with the desired precursors such as the acid anchoring group, fumaronitrile (**19**) not forming the equivalent isoindoline derivative.

As the subphthalocyanine method of preparation was proving to be difficult, statistical synthesis of azaporphyrines and phthalocyanines were attempted and successfully achieved to gather data on the reaction conditions and products and initially to see if cycilisation with the acid group (**19**) was favourable. This led to a series of novel azaporphyrines and phthalocyanines synthesised, all absorbing in the red region of the spectrum, with each a modification designed to improve efficiency and investigate the effects of substituent exchange. Self cyclotetramisation with (**19**) produced a

symmetrical azaporphyrine (**34b**), which absorbed in the red region of the visible spectrum with a Q-band observed at 644 nm. This was then used to sensitise titiania and this was constructed into a DSSC device. However, very low photovoltaic activity was observed for this dye. Hence, unsymmetrical azaporphyrine (**35c**) was synthesised to provide directionality in the excited state both to try to enhance electron injection in to the titania and also to reduce aggregation between the dye molecules. Azaporphyrine (**35c**) produced a higher photovoltaic efficiency than the symmetrical azaporphyrine (**34b**) as discussed in Chapter 4. It was postulated that this low efficiency was due to the loss of conjugation in the core structure as a low I_{sc} was observed, hence resulting in a low efficiency.

At this time in the project, the anchoring group (**20**) was synthesised, which allowed the full phthalocyanine core structure to be obtained and again further increased efficiency of a DSSC device. The exchange of solubilising groups from *t*-butyl to nonoxyphthalonitrile (**24**) also produced the highest photovoltaic activity with an IPCE reading in the red region of the spectrum of 15 % at 715 nm for dye (**37c**). However, the combination of anchoring and solubilising groups produced all possible by-products and hence made purification more difficult as the *pseudo* statistical by-products were not separated out in column chromatography. This dye therefore had the highest amount of impurities present, which it was believed reduced efficiencies of the DSSC device. It was found that using column chromatography after each synthetic stage helped to reduce the amount of by-products, but this significantly reduced yields to an overall average of 2 %. A pure product was never obtained for any unsymmetrical dye synthesised using the statistical method with azaporphyrine dye (**35c**) the purist dye with the symmetrical *t*-butylphthalocyanine the only impurity in a 1:4 ratio of impurity to dye. The incorporation of ferrocene units onto the phthalocyanine core structure by cyclising the ferrocene substituted phthalonitrile (**16**) unfortunately did not undergo the deprotection process but instead decomposed which was due to the harsh conditions required to deprotect the anchoring groups which caused the molecule to fall apart.

Due to the difficulty in purification of these dyes, it was decided to investigate the effects of adding chenodeoxycholic acid to the dye solution during dye sensitization. It was also decided to carry out an investigation of electrolyte composition as these are known to significantly impact on device efficiency not least by influencing the conduction band of the titania. This latter effect was believed to be important because of

the interaction between the conduction band and the LUMO of the dye affecting electron injection. The addition of chenodeoxycholic acid, which has been reported in the literature[84] to reduce aggregation between phthalocyanine dyes, actually slightly reduced efficiencies of the cells. This could have been due to the competitive adsorption of the acid with the dyes, reducing electron injection as the I_{sc} decreased. This thesis also described that by altering the amount of the *t*-butylpyridine additive in the electrolyte composition, the efficiency of the cell doubled. This suggests that the electrolyte composition could be further optimised for the phthalocyanine based dyes synthesized in this thesis.

It was then found that coupling to the halogenated subphthalocyanines produced ferrocene and acid substituted subphthalocyanines (**40**, **41**) after careful column chromatography but unfortunately, on ring expansion, the compounds degraded. Hence, instead, ring expansion was achieved with the monoiodinated subphthalocyanine (**28**) with *t*-butyl isoindoline (**30**). This successfully produced unsymmetrical phthalocyanine (**30**) without any of the *pseudo* statistical by-products from the statistical cyclisation procedures. However, due to time restraints, palladium catalysed coupling to the 2-*t*-butyl-9,16,23-triiodo-phthalocyanine (**43**) could not be fully investigated. This thesis has therefore demonstrated that subphthalocyanine ring expansions are dependant on substituent and reaction conditions but it is believed that due to the successful synthesis of 2-*t*-butyl-9,16,23-triiodo-phthalocyanine (**43**) without statistical by-products, pure phthalocyanine dyes can now be synthesised by palladium catalysed coupling to the halogenated subphthalocyanines.

In summary, this thesis has reported the synthesis of near infrared absorbing dyes, azaporphyrines and unsymmetrical phthalocyanines, for applications in DSSCs. During this four year project, phthalocyanine synthesis for applications in DSSC has gathered considerable interest in the literature due to the dye's intense absorption in the red region of the spectrum, with only 1.3[80] to 3.5 %[48] efficiencies obtained from devices constructed with unsymmetrical phthalocyanines reported in 2007. Hence, with a full investigation into the isolation of pure phthalocyanine dyes **36c** and **37c,** these phthalocyanines could give much higher efficiencies than that achieved in this thesis when incorporated in DSSC devices. It is also worth noting that the dyes synthesised are stable but their full lifetime efficiencies within DSSC devices has not been evaluated in this project and would need to be assessed. Following this, the next stage of this work

would involve the ring expansion of the dihalogenated subphthalocyanine, chloro[2,3,9,10,16,17-hexachlorosubphthalocyaninato]boron (III) (**27**), with *t*-butyl-1,3-diiminoisoindoline (**30**) to form a pure unsymmetrical phthalocyanine. This phthalocyanine can then be functionalised along with pure unsymmetrical phthalocyanine (**44**) synthesised in this thesis with the acid anchoring groups and the redox ferrocene groups. Palladium cross coupling reactions would be used to form pure dyes with the desired functionality for sensitisation in DSSC devices. The cycilisation of the anchoring group containing one acid functional group, 4-(4-methoxycarbonylphenyl)phthalonitrile (**21**) with the solubilising groups, could also be compared to phthalocyanine dyes (**36c**) and (**37c**) and would be used to investigate what affects one acid anchoring group would have on the cell parameters. It is also worth investigating tandem cells with the N719 and phthalocyanine dyes to utilise the full range of visible spectra with the aim of further increasing DSSC device efficiencies.

The second part of this thesis involved an investigation into the phthalocyanine-LDH interactions for stabilisation experiments in PVC based coatings. Both supported (large and small LDH) and intercalated LDH-Pc were prepared. Phthalocyanine dye supported on LDH was prepared easily from dye solution and the relevant LDH but it was found that intercalation of the phthalocyanine molecule within the clay layers was more problematic and was dependant on the reaction conditions due to the large affinity of CO_3^{2-} with the LDH. It was found that direct exchange was not favourable due to the large size of the phthalocyanine compared to the basal spacing of the LDH and hence an intermediate guest ion was intercalated into the LDH, TA acid which then underwent ion exchange with the phthalocyanine molecule under inert conditions to form the desired inter-LDH.

The paint formulations containing the supported and intercalated LHD are discussed in Chapter 5. These paints were then cast onto glass plates for degradation testing effects using a CO_2 flat panel reactor and reflectance spectroscopy. It was found that LDH additives significantly reduce the transition of CO_2 evolution to a more accelerated secondary rate. It has been postulated that these clay additives appear to suppress the acid auto catalyst of HCl caused by initial photo oxidation. A loading of 5 % or more was needed to have an effect on this process. The intercalated phthalocyanine-LDH produced the lowest rate of CO_2 evolution and it is postulated in this thesis that the LDH is shielding the phthalocyanine from UV irradiation, reducing the degradation of

the pigment as well as the Cl^- ion exchanging with the more favourable CuPc-Ts anion as no carbonic acid will be formed. The next stage in this work would be to formulate the LDH additive in fully formulated paint PVC paint formulations and compare the stabilisation effects against known stabilisers. This would be advantageous as LDH is an inert, non-toxic and inexpensive material that could be incorporated into formulations instead of more expensive and toxic equivalents such as barium zinc stabilisers.

It would be also interesting to evaluate the incorporation of the azaporphyrine (**35c**) and phthalocyanine dyes (**36c** and **37c**), synthesised for DSSC applications, into the LDH systems. This could result in a green pigmented LDH which could then be used for stabilisation testing in PVC paint systems.

Chapter 7

Experimental

7.1 Experimental

This chapter is split into three main sections with the first describing the instrumental methods, the general reagents and conditions of the experiments. The remaining two sections are dedicated to the experimental methods and data for the compounds discussed in Chapters 2 and 3 and the experimental methods and data for the inorganic clay materials discussed in Chapter 5.

7.2 Instrumental Methods

All Reagents were purchased from Aldrich Chemical Company and Alfa Aser and used with out further purification unless otherwise stated. Solvents were purified and dried using methods described in the literature[156] and stored under nitrogen prior to use.

All synthetic reactions were carried out under a dry argon atmosphere using standard Schlenk line techniques, unless otherwise stated. Melting points were recorded with a Gallenkamp MF370 apparatus. ^{1}H NMR spectra were recorded on a Bruker AC 250 MHz spectrometer and/or a Bruker Avance 500 spectrometer at 55 MHz. ^{13}C NMR was also recorded on the Bruker Avance 500 spectrometer at 125 MHz and analysed using WinNMR softwear. Chemical shifts (δ) are given in ppm and are relative to tetramethylsilane. All *J* values are given in Hz while splitting patterns are reported as singlet (s), doublet (d), triplet (t), quartet (q), multiplet (m) or any combination of these. Mass spectra were recorded using electron impact (EI), chemical ionisation (CI) or MALDI at the EPSRC Mass Spectrometry Centre at Swansea. X-Ray crystallography studies were carried out at the EPSRC National Crystallography Centre at the University of Southampton and at the Daresbury Synchrotron. Infra red (IR) spectroscopy was carried out using a Bruker Tensor 27 with all data analysed using OPUS software. UV-Vis spectroscopy was measured on a Unicam UV/Vis spectrometer UV4 and analyzed using the Vision V3.40 software.

The synthesis of all LDHs were carried out under atmospheric conditions using deionised water unless otherwise stated. X-ray diffraction (XRD) data was obtained using the Phillips X'pert diffractometer and the diffraction pattern obtained between the 2 θ values of 2 and 75. The data were then analysed using the X'pert software. Scanning electron microscopy (SEM) images were taken using a Hitachi S-520 instrument using a

voltage of 10 kV. Energy Dispersive X-ray Analysis (EDAX) was obtained using the Oxford Instrument 7497 probe. Thermogravemetric Analysis (TGA) was measured on the TA SDT Q600 with a ramp rate of 10 °C min^{-1} from room temperature to 1000 °C. Surface areas of the LDHs were measured by Brunauer, Emmett and Teller (BET) analysis on a micromeritics Gemini III 2375 surface area analyzer.

CO_2 evolution was measured at Swansea University using a Perkin Elmer Spectrum 100 Fourier Transform Infrared Spectrometer (FTIR) with the data capture automated and analysed using the Spectrum Obey API for Visual Basic 4. Reflectance measurements were also measured at Swansea University using a UV Perkin Elmer Lamda 750S UV-Vis Spectrometer with 60 mm Integrating Sphere

IV curves were measured using a Universal Photovoltaic Testing System (UPTS), purchased from Dyesol Ltd. IPCE measurements were measured at Dyesol UK Ltd. at the Optic centre in St Asaph using an IPCE Measurement Apparatus, using monochromatic light provided by a 75W Xenon lamp and analysed using DSL-SPRO software.

Preparation of 4,5-Dichlorophthalic anhydride (1)[157]

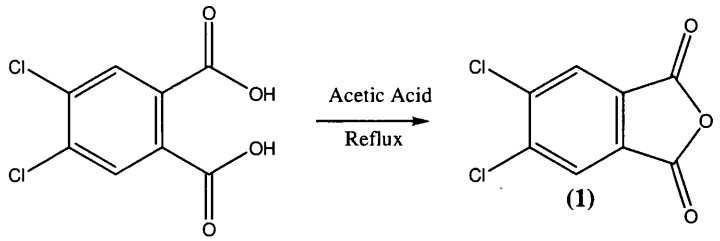

4,5-Dichlorophthalic acid (80 g, 0.34 mol) was added to acetic anhydride (180 ml). The stirring suspension was then heated under reflux for five hours with slow distillation of the acetic acid. The reaction was then allowed to cool to room temperature, filtered and washed with petroleum ether. The pale yellow/green solid was then dried under vacuum to give a yield of 64.12 g, (87 %).

MS EI$^+$ 215.9

Elemental Analysis ($C_8H_2O_3Cl_2$) = Calculated (%) (C) 44.2, (H) 0.9; Found (%) (C) 44.9, (H) 1.1

IR: ν_{max} (KBr) cm^{-1} = 1859, 1781

Mp. 185-186 °C (Lit 183-186 °C[157])

Preparation of 4,5-Dichlorophthalimide (2)[157]

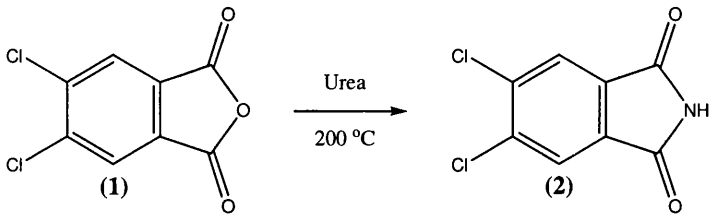

4,5-Dichlorophthalic anhydride **(1)** (0.5 g, 2.3 mmol) was ground to a uniform fine powder with urea (0.21 g, 3.5 mmol). The powder was then placed inside a multi-sample autoclave and heated to 200 °C for 4.5 h. Once cooled to room temperature the white solid produced was placed in 30 ml of distilled water and left to stir for 3.5 hours to remove any excess urea. The white solid was then filtered, washed with 200 ml of water and dried at 60 °C to yield 0.39 g, 73 %.

MS EI$^+$ 215, 217, 219

Elemental Analysis ($C_8H_3NO_2Cl_2$) = Calculated (%) (C) 44.5, (H) 1.4, (N) 6.5; Found (%) (C) 44.9, (H) 1.7, (N) 6.7

IR: ν_{max} (KBr) cm^{-1} = 1778, 1711

Mp. 217-219 °C (Lit 220 °C[157])

Preparation of 4,5-Dichlorophthalamide (3)[157]

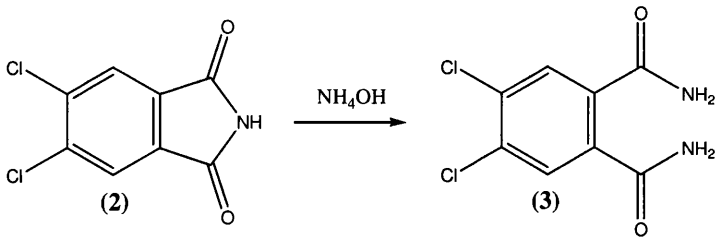

4,5-Dichloropthalimide **(2)** (3.99 g, 18.47 mmol) was added to 32 % ammonia solution (60 ml) and left to stir for 20 hours at room temperature. The white solid was filtered washed with water (600 ml) and dried at 60 °C to yield a white solid 3.91g (90.8 %).

Mp = 240-245 °C, (Lit = 245-247 °C);

Elemental Analysis ($C_8H_6N_2O_2Cl_2$) = Calculated (%) (C) 41.2, (H) 2.6, (N) 12.0; Found (%) (C) 42.1, (H) 2.4, (N) 12.6

IR: ν_{max} (KBr) cm^{-1} = 1689, 1656, 1610, 1579

MS ES$^+$, 232.9 (M^+, 3), 254 (M^+ Na^+, 100)

Preparation of 4,5-Dichlorophthalonitrile (4)[157]

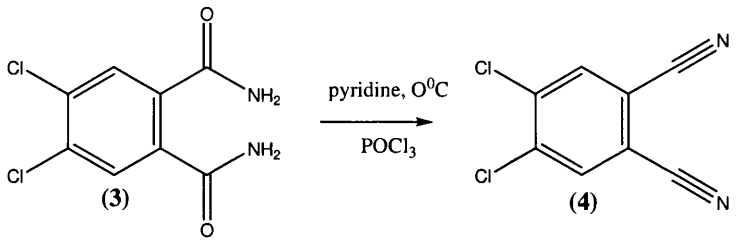

4,5-Dichlorophthalamide **(3)** (1.97g, 8.5 mmol) was added to anhydrous pyridine (20 ml) and cooled to 0°C. To this stirring suspension phosphorus oxychloride (2.4 ml) was added drop wise whilst maintaining the reaction temperature. After the addition was complete, the reaction was allowed to warm to room temperature and left to stir for 20 hours. The purple suspension was poured on to 200 ml of ice water and filtered. The solid was washed with ice cold methanol (90 ml) and dried to yield a purple solid, 1.40 g, (84 %)

^{1}H NMR, $CDCl_3$ δ = 7.92 (s, CH)

^{13}C NMR, $CDCl_3$, δ = 113.60 (C), 115.12, (CN), 134.97 (CH), 139.09 (C-Cl)

Mp 180-181 °C (Lit = 182-184 °C)

Elemental Analysis (%) ($C_8H_2N_2Cl_2$) = Calculated (C) 48.7, (H) 1.0, (N) 14.2; Found (C) 48.1, (H) 1.4, (N) 13.3

IR: ν_{max} (KBr) cm^{-1} = 2236 (CN)

MS EI+ = 218.94 ($M+Na^+$)

Preparation of 4-Iodophthalonitrile (5)[89]

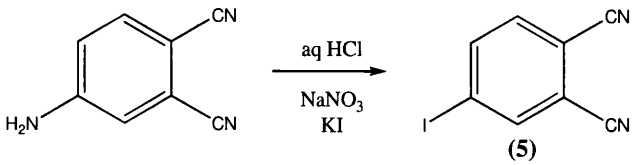

(5)

4-Amino phthalonitrile (2.5 g, 17.5 mmol) was added to a mixture of ice (150 g) and concentrated hydrochloric acid (50 ml). To this solution sodium nitrate (1.93 g, 27.95 mmol) in water (20 ml) was added and left to stir for 5 hours at 0 °C. The solution was then added drop wise to a cold solution of potassium iodide and left to stir for 30 minutes. Benzene (100 ml) was added and the organic layer washed with cold water (30 ml), followed by $NaHCO_3$ (5 %, 30 ml), water (30 ml), saturated $Na_2S_2O_3$ and water (30 ml). The organic layer was then dried over magnesium sulfate and reduced to dryness under vacuum yielding a yellow solid (3.05 g, 76 %).

^{1}H NMR, $CDCl_3$ δ = 7.52 (1H, d, J = 8.2), 8.12 (1H, d, J = 8.2), 8.17 (1H, s)
^{13}C NMR, $CDCl_3$, δ = 99.68 (C-I), 113.83 (C), 114.93 (CN), 115.10 (CN), 117.05 (C), 133.99 (C-H), 142.07 (C-H), 142.46 (C-H)
MS: m/z (%) = 127, (M^+-I, 3), 254.94 (M^+, 100)

Preparation of 4,5-Diiodophthalimide (6)

Method (i), 30 % fuming sulphuric acid[47]

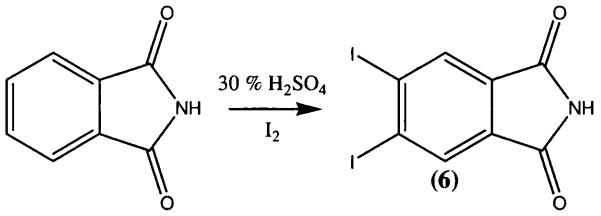

(6)

Phthalimide (14.7 g) was added to 30 % fuming sulphuric acid (60 ml) and heated to 75-80 °C for 24 hours. Iodine (26.7 g) was added over a period of an hour and then heated for a further 24 hours. The mixture was added drop wise to ice (400 g) and the solid was then washed with a solution of K_2CO_3 (10 %), cold water (30 ml), saturated Na_2SO_3 solution and finally water (30 ml). The dried solid was added to 500 ml of acetone and Soxhlet extracted for 48 hours. Acetone (500 ml) was added to the Soxhlet extracted solution and the solid formed in the solvent was then filtered from the acetone. Water (100 ml) was added to the acetone and the solution was concentrated down to 500 ml yielding a yellow precipitate, 5.06 g (12.7) %.

^{1}H NMR, DMSO δ = 8.24 (s, 2 × Ar-H);), 11.43 (bs, 1 × N-H)

Impurities present in ^{1}H NMR - 7.54 (d, J = 7.55) 7.57 (d, J = 7.55), 7.85 (s), 8.13 (s), 8.18 (d, J = 7.85), 8.33 (d, J = 7.55), 8.67 (s), 11.52 (s), 11.65 (s)

^{13}C NMR, DMSO δ = 116.46 (C-I), 132.67 (C), 144.04 (C-H), 167.68 (C=O)

Impurities present in ^{13}C NMR - 104.18 (3,4), 121.09, 123.54, 124.55, 131.34, 132.98, 135.33, 142.84, 166.67, 167.45

IR: ν_{max} (KBr) cm^{-1} = 3178 (NH), 1718 (C=O), 1770 (C=O)

MS EI+ = 398.9 (100, M^+), 524.7 (3, $C_8H_3NO_2I_3$)

Method (ii), Autoclave Preparation

Iodine (25.35 g, 0.099 mol) was added to phthalimide (14.7 g, 0.099 mol) in 30 % fuming sulphuric acid (60 ml). The suspension was then placed inside a PTFE-lined stirring autoclave and heated to 80 °C for 24 hours. The black solution was then poured on to 400 g of ice. The precipitate was then filtered and washed with 10 % $NaHCO_3$ and saturated $NaSO_3$ and water. The dried solid was added to 500 ml of acetone and Soxhlet extracted for 48 hours. Acetone (500 ml) was added to the Soxhlet extracted solution and the solid formed in the solvent was then filtered from the acetone. Water (100 ml)

was added to the acetone and the solution was concentrated down to 500 ml yielding a yellow precipitate, 20.8g, 52 %.

^{1}H NMR, DMSO δ = 8.24 (s, 2 × Ar-H);), 11.43 (bs, 1 × N-H)
Impurities present in ^{1}H NMR - 7.54 (d, J = 7.55) 7.57 (d, j = 7.55), 7.85 (s), 8.13 (s), 8.18 (d, J = 7.85), 8.33 (d, J = 7.55), 8.67 (s), 11.52 (s), 11.65 (s)
^{13}C NMR, DMSO δ = 116.46 (C-I), 132.67 (C), 144.04 (C-H), 167.68 (C=O)
Impurities present in ^{13}C NMR -104.18, 121.09, 123.54, 124.55, 131.34, 132.98, 135.33, 142.84, 166.67, 167.45
MS: EI+, m/z (%) = 398.8 (100, M^+), 524.7 (11, $C_8H_3NO_2I_3$)

Method (iii), Periodic acid preparation

Periodic acid (2.0 g, 8.77 mmol) was dissolved in concentrated sulphuric acid (60 ml) and powdered iodine (6.68 g, 0.026 mol) was added and left to stir at room temperature for one hour. The black solution was then cooled in an ice bath and the phthalimide (2.24 g, 0.015 mol) was added slowly and left to stir for 24 hours and heated to 85 °C for a further 24 hours. Once cooled, the resulting suspension was poured onto ice and filtered. The yellow precipitate was then Soxhlet extracted in acetone (300 ml). Water (50 ml) was added to the acetone and the solvent removed to a third of its volume, the precipitate was filtered to yield 1.15 g (22 %).

^{1}H NMR, DMSO δ = 8.20 (s, 2 × Ar-H);), 11.43 (bs, 1 × N-H)
Impurities present in ^{1}H NMR - 7.56 (d, J = 7.55) 7.58 (d, j = 7.55), 7.85 (s), 8.13 (s), 8.19 (d, J = 7.85), 8.34 (d, J = 7.55), 8.68 (s), 11.52 (s), 11.65 (s)
^{13}C NMR, DMSO δ = 116.46 (C-I), 132.67 (C), 132.98, 144.04 (C-H), 167.68 (C=O)
Impurities present in ^{13}C NMR- 104.18, 121.09, 123.54, 124.55, 131.34, 135.33, 142.84 (3,4), 166.67, 167.45,
MS:EI$^+$ = M^+ 398.9 (100, 524.7 (10, $C_8H_3NO_2I_3$)

Preparation of tetraiodophthalimide (7)

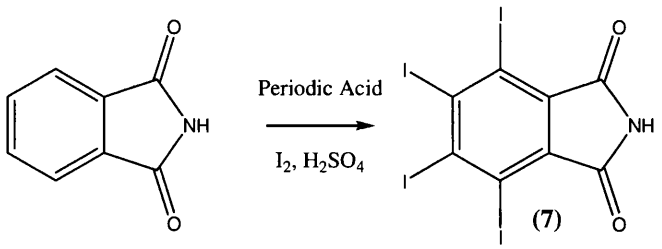

Method (i)

Periodic acid (2.0 g, 8.77 mmol) was dissolved in concentrated sulphuric acid (60 ml), powdered iodine (6.68 g, 0.026 mol) was added and left to stir at room temperature for one hour. The black solution was then cooled in an ice bath and the phthalimide (1.12 g, 7.68 mmol) was added slowly and left to stir for 24 hours and heated to 85 °C for a further 24 hours. Once cooled, the resulting suspension was poured onto ice and filtered. The bright yellow precipitate was then washed with methanol until all the excess iodine was removed. The yellow solid was then recrystalised from THF to yield 1.89 g, 38 %.

^{1}H NMR, DMSO δ = No signal

^{13}C NMR, DMSO, δ = 103.89 (C-I), 134.88 (C), 135.50 (C-I), 165.16 (C=O)

MS EI = 650.6 (M^+)

HRMS EI = Calculated = 650.6181, Found = 650.6175

Elemental Analysis ($C_8H_1NO_2I_4$) = Calculated (C) 14.74, (N) 2.15: Found (C) 14.70 (N) 2.18,

IR: ν_{max} (KBr) cm^{-1} = 3455, 3276, 1781, 1718, 1641

Method (ii) Autoclave

Periodic acid (2.0 g, 8.77 mmol) was dissolved in concentrated sulphuric acid (60 ml), to which, powdered iodine (6.68 g, 0.026 mol) was added and left to stir at room temperature for one hour. The black solution was then transferred to a PFTE lined autoclave and phthalimide (1.12 g, 7.68 mmol) was added slowly and heated to 85 °C for 24 hours. Once cooled, the resulting suspension was poured onto ice and filtered. The bright yellow precipitate was then washed with methanol until all the excess iodine was removed. The yellow solid was then recystalized from THF to yield 3.75 g, 74 %.

^{1}H NMR, DMSO δ = no signal

^{13}C NMR, DMSO, δ = 103.90 (C-I), 134.84 (C), 135.52 (C-I), 165.14 (C=O)

MS EI: 650.6 (M^+)

HRMS EI: Calculated = 650.6181, Found = 650.6175

Preparation of tertaiodophthalic anhydride (8)

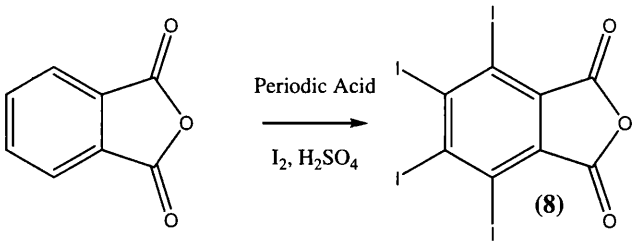

Periodic acid (2.0 g, 8.77 mmol) was dissolved in concentrated sulphuric acid (60 ml). To this clear solution, powdered iodine (6.68 g, 0.026 mol) was added and left to stir at room temperature for one hour. The black solution was then cooled in an ice bath and phthalic anhydride (1.14 g, 7.68 mmol) was added slowly and left to stir for 24 hours and heated to 105 °C for a further 48 hours. Once cooled, the resulting suspension was poured onto ice and filtered. The bright yellow precipitate was then washed with methanol until all the excess iodine was removed. The yellow solid was then recrystalised from THF and further impurities removed by sublimation yielding 2.38 g, 47 %.

^{1}H NMR, DMSO δ = No signal

^{13}C NMR, DMSO, δ = 106.65 (C-I), 134.40 (C-I), 137.31 (C), 159.49 (C=O)

MS: EI$^+$ 651.6 (M^+)

HRMS (EI): Calculated = 651.6021, found = 651.6022

Elemental Analysis ($C_{24}H_{16}N_2O_4$) = Calculated (%) (C) 14.72, (N) 0.0, (H) 0.0 found (C) 15.00, (N) 0.0, (H) 0.0

Preparation of 4,5-Diiodophthalamide (9)[47]

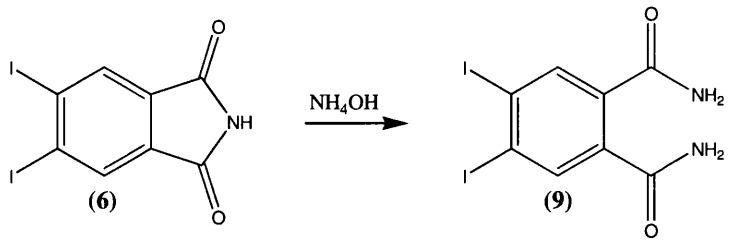

4,5-Diiodophthalimide **(6)** (5 g, 0.03 mol) was added to concentrated ammonia (55 ml) and bought to reflux for 3 hours. The solution was filtered and the solid washed with ice cold water (40 ml) and methanol (3 x 20 ml). The solid was then dried to yield a white powder, 2.75 g (53 %).

^{1}H NMR, DMSO δ = 7.42 (s, N-H), 7.85 (s, N-H), 7.92 (2H, s, C-H)

^{13}C NMR, DMSO δ = 109.83 (C-I), 137.01 (C), 137.60 (C-H), 167.84 (C=O)

IR: ν_{max} **(KBr) cm^{-1}** = 3428, 3297, 3166 , 1693, 1653, 1605, 1561

MS EI+: 416.9

HRMS, Calculated Mass = 416.8591, Found = 416.8593

Preparation of 4,5-Diiodopthalonitrile (10)[47]

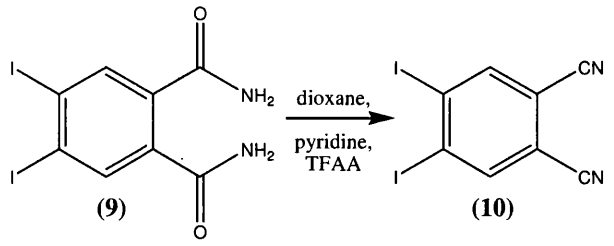

4,5-Diiodophthalamide **(9)** (5 g, 12.0 mmol) was added to anhydrous dioxane (27 ml) and cooled to 0 °C. To this solution, anhydrous pyridine (7 ml) was added followed by trifluoroacetic anhydride (7ml). The mixture was allowed to warm to room temperature and left to stir for 16 hours. The stirring solution was then poured in to ice and extracted with ethyl acetate (3 x 30 ml). The combined organic layers were washed with water (30 ml), 1M HCl (20 ml), Na_2CO_3 (10 %, 30 ml) and cold water (30 ml). The organic layer was then dried with magnesium sulfate and reduced to dryness under vacuum and recrystalised from methanol. 1.44 g, 31.5 %.

^{1}H NMR, $CDCl_3$ δ = 8.3 (s, C-H)

^{13}C NMR, $CDCl_3$, δ = 113.59 (C-I), 115.09 (C), 115.42 (CN), 142.70 (C-H)

MS EI+: 379.9 (M^+)

IR: ν_{max} (KBr) cm^{-1} = 2234 (CN)

Preparation of Ferrocene Aldehyde (11)[95]

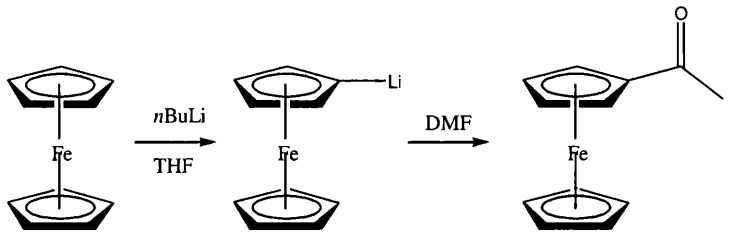

(11)

Ferrocene (10.0 g, 0.054 mol) was dissolved in anhydrous THF (200 ml) under inert conditions. *n*BuLi (32 ml, 0.081 mol) was added and left to stir for 16 hours. Anhydrous DMF (5 ml, 0.065 mol) was added to the stirring solution and left to stir for one hour. The solution was then quenched with water (90 ml) and 1 M HCl (10 ml) and extracted with dichloromethane (3 x 50 ml). The combined organic extracts were dried over magnesium sulfate and the organic layer was then reduced to dryness under reduced pressure. The red solid was then placed onto silica gel, the product eluted with ether (9.68 g, 84 %).

^{1}H NMR, ($CDCl_3$), δ_{ppm} = 4.20 (5H, s, Cp), 4.56 (2H, s, C-H), 4.78 (2H, s, C-H), 9.93 (1H, s, COH),

^{13}C NMR: ($CDCl_3$), δ_{ppm} = 69.66 (Cp), 70.90 (C-H), 73.19 (C-H), 74.20 (C), 192.85 (C=O)

MS (EI) m/z: 55.9 (Fe, 87), 120.9 (100), 186.0 ($C_{10}H_{10}Fe$, 68), 214.0 (M^+, 82)

Preparation of 2-Chloro-l-Ferrocenylethene (12)[95]

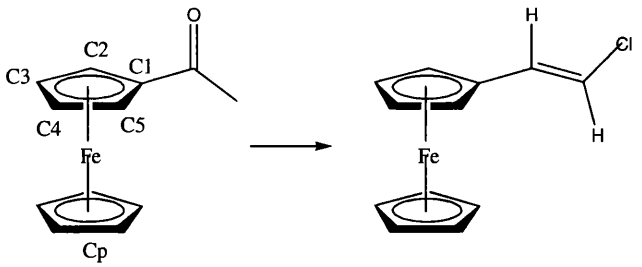

(11) **(12)**

Chloromethyltriphenylphosphonium chloride (1.63 g, 4.9 mmol) in anhydrous THF (10 ml) was cooled to 0 °C and potassium *t*-butoxide (0.6 g, 4.9 mmol) was added and the yellow suspension was left to stir for 15 mins. Ferrocene carboxaldehyde **(11)** (1.05 g, 4.9 mmol) in anhydrous THF (10 ml) was added dropwise to the stirring suspension and stirred for a further fifteen hours at room temperature. The solvent was removed and the crude product was placed onto silica with the product eluting in a petroleum spirit and diethyl ether mix 95:5. (2.06 g, 52 %)

^{1}H NMR; ($CDCl_3$) δ_{ppm} = 4.11 (5H, s, Cp), 4.23 (2H, s, CH), 4.28 (1H, s, CH), 4.72 (1H, s, CH), 6.07 (1H, d, *J*=7.9, z), 6.20 (1H, d, *J*=13.6, e), 6.39 (1H, d, *J*=7.9, z), 6.57 (1H, d, *J*=13.6, e)

^{13}C NMR; ($CDCl_3$) δ_{ppm} = 66.55 (C2, C5, *E*), 69.03 (C3, C4), 69.30 (Cp), 69.45 (C2, C5, *Z*), 69.92 (C1, *Z*), 80.61 (C1, *E*), 114.00 (=CH-Cp, *E*), 114.46 (=CH-Cp, *Z*), 127.99 (=CHCl, *Z*), 130.95 (=CHCl, *Z*)

MS EI, 246.1

HRMS (EI^+) calculated 245.9896, found 245.9919

Preparation of Ethynylferrocene (13)[95]

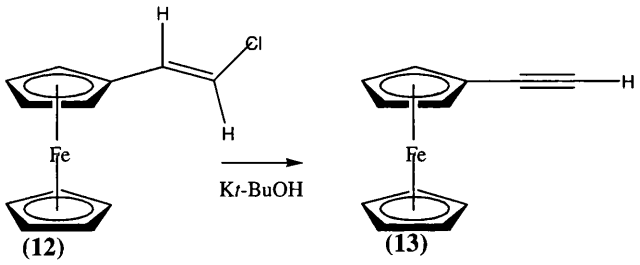

2-Chloro-l-ferrocenylethene **(12)**, (1.5 g, 6.01 mmol) was dissolved in anhydrous THF (20 ml). Potassium *t*-butoxide (1.32 g, 12.20 mmol) was added and the solution was refluxed for three hours under inert conditions. Water (10 ml) was added and the organic layer was extracted with dichloromethane (3 x 20 ml). The combined organic washings were dried over magnesium sulphate and reduced to dryness under reduced pressure. The crude product was placed onto silica and the product eluted in petroleum spirit and diethyl ether 95:5, which was then reduced to dryness under reduced pressure (0.49 g, 53 %)

^{1}H NMR; ($CDCl_3$) δ_{ppm} = 2.74 (1H, s, =CH), 4.22 (2H, s, CH), 4.25 (5H, s, Cp), 4.49 (2H, s, CH)

^{13}C NMR; ($CDCl_3$) δ_{ppm} = 63.87(C1), 68.72 (C2, C5), 70.05 (Cp), 71.76 (C3, C5), 73.50 (=CH), 82.61 (Cp-C=)

MS EI, 210.05

HRMS (EI^+) calculated 210.0132, found 210.0136

Preparation of 1,1'-Dibromoferrocene (14)[158].

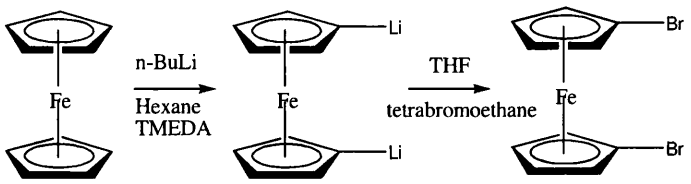

(14)

Dibromoferrocene was prepared using a modified literature procedure[98]. Ferrocene (20.05 g, 0.11 mol) was dissolved in hexane (200 ml). To this stirring suspension, *n*-butyl lithium (94.8 ml, 0.24 mol) and TMEDA (16.2 ml, 0.11 mol) was added and left to stir for 16 hours. Anhydrous THF (300 ml) was then added to the suspension and cooled to -78 °C (dry ice/acetone) bath and 1,1,2,2-tetrabromoethane (81.77 g, 0.237 mol) was added drop wise to the stirring suspension. The reaction was then warmed to room temperature and stirred for 16 hours. The solution was then hydrolyzed with water (150 ml) and extracted with diethyl ether (3 x 100 ml). The combined organic layers was filtered and dried over magnesium sulfate and reduced to dryness under high vacuum yielding brown crystals (28.37 g, 76.5 %)

^{1}H NMR: ($CDCl_3$) δ_{ppm} = 4.12 (4H, s, C-H), 4.38 (4H, s, C-H)

^{13}C NMR, ($CDCl_3$), δ_{ppm} = 69.94 (β-C), 72.68 (α –C), 78.26 (C-Br),

MS (EI) m/z: 184 (13), 263 (20), 265 (20), 342 M^+ (48), 344 M^+ (100), 346 M^+ (49)

Reaction between 1,1'-Dibromoferrocene (14) and 4,5-dichloro - phthalonitrile (4), resulting in 4-ferrocenyl-5-chlorophthalonitrile (15) and 4-(1-bromoferrocene)-5-chlorophthalonitrile (16)

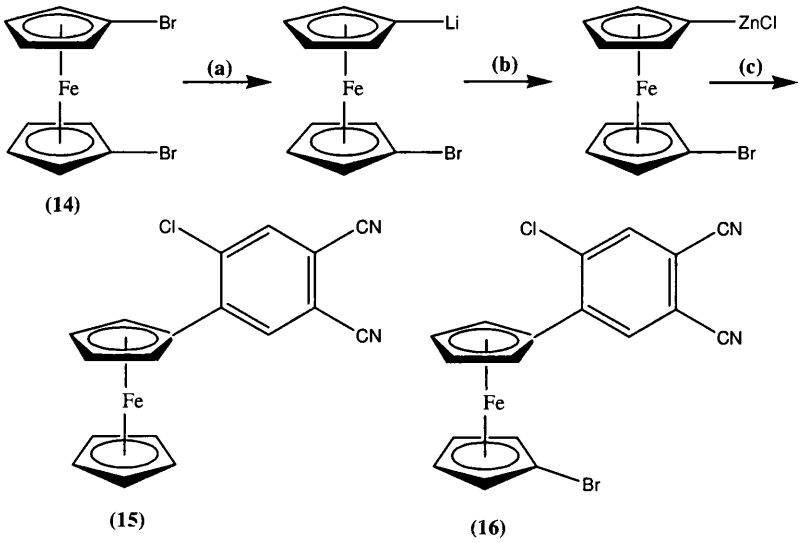

1,1'-Dibromoferrocene **(14)** (1.84 g, 5.3 mmol) was dissolved in anhydrous THF (30 ml) and cooled to -78 °C (dry ice/acetone). To this solution *n*-butyl lithium (2.4 ml, 6.12 mmol) was added under inert conditions and left to stir for 1 hour, while cold, zinc chloride (2.56 ml) was added followed by tetrakis(triphenylphosphine)palladium (0) (50 mg) and 4,5-dichlorophthalonitrile (0.5 g, 1.97 mmol). The reaction was then allowed to warm to room temperature and left to stir for 2 hours before heating to 90 °C for 12 hours. Water (20 ml) was added to the solution and extracted with dichloromethane (3 x 20 ml). The combined organic layers were then dried over magnesium sulfate and reduced to dryness under reduced pressure. The crude product was combined with alumina and the product was eluted with diethyl ether ; petroleum spirit (55:45) to yield red crystals.

4-ferrocenyl-5-chlorophthalonitrile (15)

Yield = 0.21 g, 18 %

^{1}H NMR; ($CDCl_3$) δ_{ppm} = 4.11 (5H, s, Cp). 4.49 (2H, s, CH), 4.80 (2H, s, CH), 7.67 (1H, s, CH), 7.90 (1H, s, CH)

^{13}C NMR; ($CDCl_3$) δ_{ppm} = 70.22 (Cp ring), 70.40 (β-C), 70.96 (α-C), 112.31 (C-CN), 113.62 (C-CN), 114.68 (CN), 114.94 (CN), 135.15 (C-H), 135.44 (C-H), 136.68 (C-Cl), 145.81 (C)

MS; (EI), m/z (%) = 120.9 (C_5H_5Fe, 52), 163.9 ($C_8H_2ClN_2$, 39), 225 ($C_{13}H_6ClN_2$, 6)

HRMS Calculated 345.9955, Found 345.9957

4-(1-bromoferrocene)-5-chlorophthalonitrile (16)

Yield = 0.42 g, 61 %

^{1}H NMR; ($CDCl_3$) δ_{ppm} = 4.14 (2H, s, CH), 4.39 (2H, s, CH), 4.61, (2H, s, CH) 4.91 (2H, s,CH), 7.79 (1H, s, CH), 8.04 (1H, s, CH)

^{13}C NMR; ($CDCl_3$) δ_{ppm} = 69.20 (β'-C), 70.26 (β-C), 72.20 (α'-C), 73.31 (α-C), 78.45 (C-Br), 81.25 (C), 112.73 (C-CN), 113.76 (C-CN), 114.61 (CN), 114.88 (CN), 135.36 (C-H), 135.57 (C-H), 136.92 (C-Cl), 144.10 (C)

MS; (EI), m/z (%) = 63.2 (100), 91.0 (22), 137.0 (24), 199.0 (18), 253.3 (20), 426.1 (10)

HRMS Calculated 423.9060, Measured 423.9058

Reaction between 1,1'-Dibromoferrocene (14) and 4—iodo-phthalonitrile (5), resulting in 4-(1-bromoferrocene)phthalonitrile (17) and 4-ferrocenyl phthalonitrile (18)

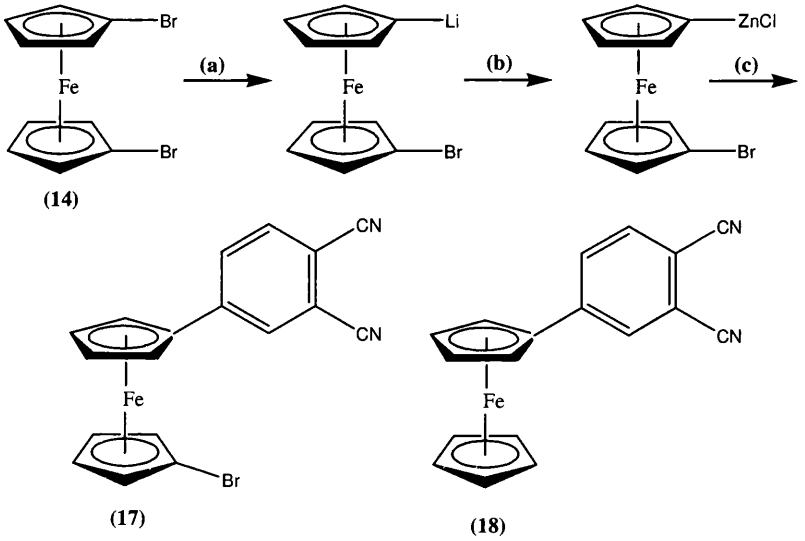

1,1'-Dibromoferrocene **(14)** (0.67 g, 1.97 mmol) was dissolved in anhydrous THF (30 ml) and cooled to -78 °C (dry ice/acetone). To this solution, *n*-butyl lithium (0.94 ml, 2.36 mmol) was added under inert conditions and left to stir for 1 hour, while cold, zinc chloride (2.16 ml, 2.16 mmol) was added followed by tetrakis(triphenylphosphine)palladium0 (50 mg) and 4-iodophthalonitrile (0.5 g, 1.97 mmol). The reaction was then allowed to warm to room temperature and left to stir for 16 hours. Water (20 ml) was added to the solution and extracted with dichloromethane (3 x 20 ml). The combined organic layers were then dried over magnesium sulfate and reduced to dryness under reduced pressure. The crude product was combined with alumina and the product was eluted with diethyl ether ; petroleum spirit (55:45) to yield red crystals.

4-(1-Bromoferrocene)phthalonitrile (17)

Yield = 0.58 g, 75 %

^{1}H NMR; ($CDCl_3$) δ_{ppm} = 3.99 (2H, t, J = 1.9, CH), 4.19 (2H, t, J = 1.9, CH), 4.52 (2H, t, J = 1.9, CH), 4.66 (2H, t, J = 1.9, CH), 7.69 (1H, d, J = 8.2, C-H), 7.74 (1H, d, 8.2, C-H), 7.82 (1H, s, CH)

^{13}C NMR; ($CDCl_3$) δ_{ppm} = 68.96 (β'-C), 69.36 (β-C), 72.23 (α'-C), 73.26 (α-C), 78.58 (C-Br), 81.86 (C), 111.94 (C-CN), 115.88 (CN), 115.90 (C-CN) 116.11 (CN), 129.87 (C-H), 130.52 (C-H), 133.53 (C-H), 145.58 (C)

MS; (EI), m/z = 390.1 (M+ 79Br), 392 (M+, 81Br)

HRMS ($+NH_4$); found - 407.9797**, calculated** 407.9793

4-Ferrocenyl Phthalonitrile (18)

Yield = 0.11 g, 18 %

^{1}H NMR; ($CDCl_3$) δ_{ppm} = 4.02 (2H, s, 2H), 4.49 (2H, s, 2H), 4.68 (5H, s, Cp), 7.66 (1H, d, J = 8.1, C-H), 7.71 (1H, d, J = 8.1, C-H), 7.78 (1H, s, C-H)

^{13}C NMR; ($CDCl_3$) δ_{ppm} = 60.40 (Cp), 67.13 (β-C), 70.21 (α-C), 79.90 (C), 111.41 (C-CN), 115.64 (C-CN), 115.95 (CN), 116.06 (CN), 129.46 (C-H), 130.14 (C-H), 133.47 (C-H), 147.62 (C)

MS; (EI), m/z = 312.1

Preparation of Di-(4-methylbenzoate)-fumaronitrile (19)

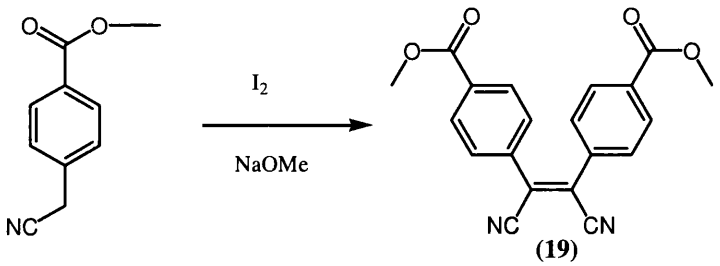

(19)

Methyl 4-(cyanomethyl)-benzoate (5 g, 0.029 mol) and iodine (7.3 g, 0.029 mol) were dissolved in anhydrous diethyl ether and cooled to -78 °C. Sodium methoxide (3.2 g, 0.06 mol) in anhydrous methanol (18 ml) was added drop wise into the reaction solution under inert conditions. The stirring black solution was then allowed to warm to 0-5 °C and kept at this temperature for 4 hours. The reaction was quenched with 3-6 % hydrochloric acid at less than 10 °C and then filtered to isolate the solid. The precipitate was then washed with a cold methanol-water solution to wash away ionic substances and dried over P_2O_5 to yield an off white solid (3.87 g, 78 %).

^{1}H NMR; ($CDCl_3$) δ_{ppm} = 3.99 (s, 6H), 7.92 (d, J = 8.55, 4H), 8.21 (d, J = 8.55, 4H)

^{13}C NMR; ($CDCl_3$) δ_{ppm} = 52.69 (CH_3), 115.95 (CN), 125.97 (C-CN), 128.89 (C-H), 130.53 (C-H), 133.22 (C), 135.43 (C-CO), 165.76 (CO)

MS; (ES), = 346.3 (M^+)

HRMS Calculated = 347.1026, Found 347.1029 $[M + H]^+$

IR: ν_{max} (KBr) cm^{-1} = 3427 (C-H aromatic), 2962 (CH_3), 2222 (CN), 1727 (C=O), 1608 (C=C)

Elemental Analysis ($C_{20}H_{14}N_2O_4$) = Calculated % (C) 69.35, (H) 4.05, (N) 8.09, Found (C) 68.91, (H) 4.04, (N) 8.11

Preparation of 4,5-bis(4-methoxycarbonylphenyl)phthalonitrile (20)[64]

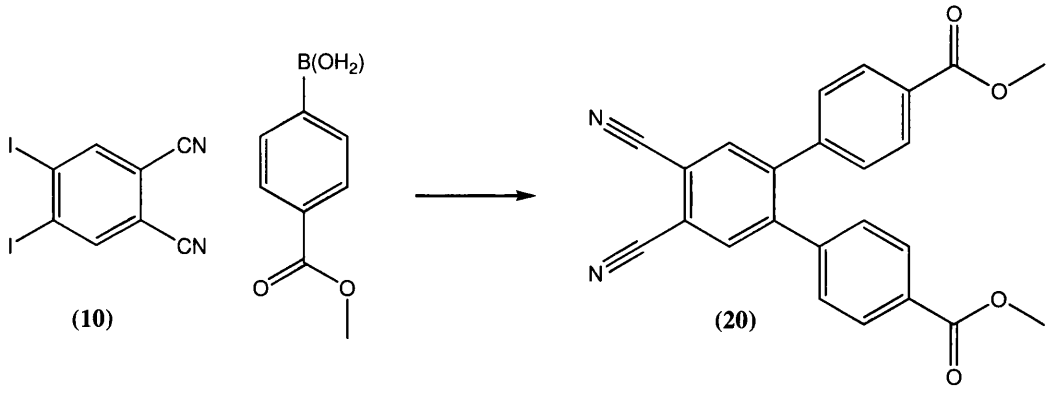

(10) (20)

A flask was charged with 4,5-diiodophthalonitrile **(10)** (0.18 g, 0.9 mmol), 4-(methoxycarbonylphenyl)boronic acid (0.5 g, 2.8 mmol), anhydrous toluene (10 ml), palladium (II) acetate (20 mg), 2-(2',6'-dimethoxybiphenyl)dicyclohexylphosphine (20 mg) and potassium phosphate (0.8 g, 3.8 mmol) under an argon atmosphere. The orange suspension was heated to 90 °C for 24 hours. Once cooled to room temperature the solution was washed with water (2 x 25 ml) and the combined organic layers were dried over magnesium sulphate and reduced to dryness. The residue was then recrystalised from ethyl acetate to form off white crystals 0.311 g, 85 %.

^{1}H NMR; ($CDCl_3$) δ_{ppm} = 3.94 (6H, s, C$\underline{H}_3$), 7.20 (4H, d, J = 8.15, C$\underline{H}$), 7.91 (2H, s, C$\underline{H}$), 7.99 (4H, d, J = 8.2, C$\underline{H}$)

^{13}C NMR; ($CDCl_3$) δ_{ppm} = 52.38 (C$\underline{H}_3$) 114.96 (C-CN), 115.29 (C$\underline{N}$), 129.38 (C$\underline{H}$), 129.99 (C$\underline{H}$), 130. 21 (C-CO), 135.37 (C$\underline{H}$), 141.56 (C-Ar), 144.84 (C-Ar), 166.19 (C$\underline{O}$)

MS; (ES), m/z (%) = 414.1 ($M^+ + NH_4^+$)

HNES Calculated = 414.1453 Found = 414.1451

Elemental Analysis ($C_{24}H_{16}N_2O_4$) = Calculated %: C 72.72, H 4.06, N 7.07; found %: C 72.14, H 4.19, N 7.29

IR: ν_{max} (KBr) cm^{-1} = 3037, 3004, 2958, 2849, 2237, 1729, 1609

Preparation of 4-(4-methoxycarbonylphenyl)phthalonitrile (21)

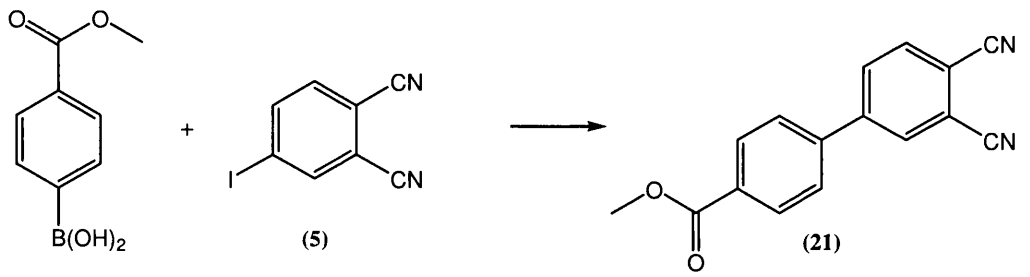

A flask was charged with 4-iodophthalonitrile **(5)** (1 g, 3.9 mmol), 4-(methoxycarbonylphenyl)boronic acid (0.92 g, 5.1 mmol), anhydrous toluene (10 ml), paladium (II) acetate (20 mg), 2-(2',6'-dimethoxybiphenyl)dicyclohexylphosphine (20 mg) and potassium phosphate (1.46 g, 6.9 mmol) under an argon atmosphere. The reaction was heated to 90 °C for 24 hours. The organic solution was then washed with water (2 x 25 ml) and the combined organic layers were dried over magnesium sulphate and reduced to dryness. The residue was placed on alumina and eluted with ethyl acetate and petroleum spirit to yield an off white solid (0.23g, 22.5 %).

^{1}H NMR; ($CDCl_3$) δ_{ppm} = 3.90 (3H, s, C<u>H</u>$_3$), 7.60 (2H, d, J = 8.5, C<u>H</u>), 7.83 (1H, d, J = 8.2, C<u>H</u>), 7.90 (1H, d, J = 8.2), 7.91 (1H, s, C<u>H</u>), 8.13 (2H, d, J = 8.5, C<u>H</u>)

^{13}C NMR; ($CDCl_3$) δ_{ppm} = 52.48 (<u>C</u>H$_3$), 114.88 (C), 115.24 (<u>C</u>N), 116.76 (<u>C</u>N), 127.29 (<u>C</u>H), 130.71 (C), 131.31 (<u>C</u>H), 131.64 (C), 132.07 (<u>C</u>H), 132.18 (<u>C</u>H), 134.11 (<u>C</u>H), 141.06 (C), 145.31 (C), 166.26 (CO)

MS; (CI), m/z (%) = 280.2 $[M + NH_3]^+$

HRMS Calculated = 280.1081, found = 280.1079

IR: ν_{max} (KBr) cm^{-1} = 3112, 2969, 2930, 2234, 1717, 1612

Preparation of 1,2-dinonoxybenzene (22)[48]

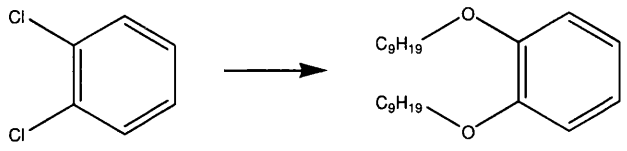

(22)

Catechol (5.0 g, 0.045 mol) was added to a solution of 1-bromononane (22.5 g, 0.109 mol) in toluene (50 ml). Sodium hydroxide solution (4 g) and tetrabutylammonium bromide (0.8 g, 2.5 mmol) were then added to the reaction and heated to reflux for 6 hours. The reaction mixture was cooled to room temperature and the organic phase extracted and reduced to dryness under reduced pressure to afford a solid in 9.44 g, 58 % yield.

^{1}H NMR; ($CDCl_3$) δ_{ppm} = 0.90 (6H, t, *J* = 7.0, CH_3), 1.37 (20H, m, CH_2), 1.58 (2H, s, CH_2), 1.82, (4H, quintet, *J* = 7.0, CH_2), 3.43 (2H, t, J = 6.6, CH_2), 4.01 (4H, t, J = 6.6, CH_2-O), 6.91 (4H, s, Ar)

^{13}C NMR; ($CDCl_3$) δ_{ppm} = 14.11 ($\underline{C}H_3$), 22.66 ($\underline{C}H_2$), 29.30 ($\underline{C}H_2$), 29.37 ($\underline{C}H_2$), 29.46 ($\underline{C}H_2$), 29.52 (CH_2), 29.61 ($\underline{C}H_2$), 31.92 ($\underline{C}H_2$), 69.30 ($\underline{C}H_2$-O), 114.17 ($\underline{C}H$), 121.01 ($\underline{C}H$), 149.28 ($\underline{C}$)

HNES Calculated = 380.3528, Found = 380.3523

IR: ν_{max} (KBr) cm^{-1} = 3064, 2925, 2855, 1592, 1504

Preparation of 1,2-dibromo-4,5-dinonoxybenzene (23)[48]

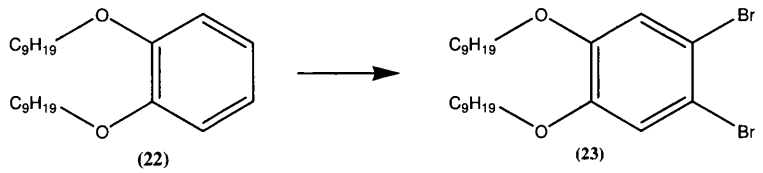

Bromine (4.6 g, 0.028 mol) was dissolved in dichloromethane (100 ml) at 0 °C and added dropwise to a stirring solution of the catechol ether **(22)** (4.73 g, 0.013 mol) in dichloromethane (100 ml). The solution was stirred at room temperature for one hour and then poured on to ice (150 g). The organic phase was extracted and washed with $NaHCO_3$ (5 %) and then water (50 ml). The organic solvent was reduced to dryness under reduced pressure to afford the product in 5.93 g, 88 % yield.

^{1}H NMR; ($CDCl_3$) δ_{ppm} = 0.89 (6H, t, *J* = 7.0, CH_3), 1.37 (20H, m, CH_2), 1.55 (2H, s, CH_2), 1.80, (4H, quintet, *J* = 7.0, CH_2), 3.42 (2H, t, J = 6.7, CH_2), 3.94 (4H, t, J = 6.7, CH_2-O), 7.06 (2H, s, Ar)

^{13}C NMR; ($CDCl_3$) δ_{ppm} = 14.11 (CH_3), 22.68 (CH_2), 25.93 (CH_2), 29.06 (CH_2), 29.26 (CH_2), 29.35 (CH_2), 29.54 (CH_2) 31.89 (CH_2), 69.64 (CH_2-O), 114.68 (C-H), 118.07 (C-Br), 149.07 (C-O)

HNES M^+ NH_4, (Calculated = 538.1895 Found = 538.1705

IR: ν_{max} (KBr) cm^{-1} = 3430, 2924, 2851

Preparation of 4,5-dinonoxyphthalonitrile (24)[48]

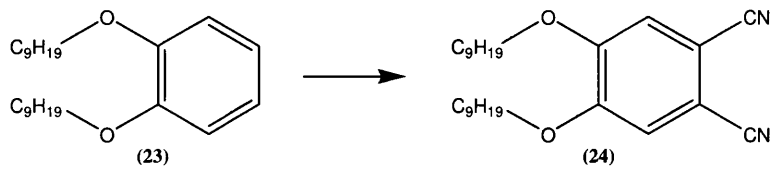

Copper cyanide (1.98 g, 0.024 mol) was added to a solution of 1,2-dibromo-4,5-dinonoxybenzene **(23)** (5.77 g, 0.011 mol) in dimethylformamide (60 ml) and was heated to reflux for 8 hours. Once cooled to room temperature, the reaction mixture was poured into concentrated ammonium hydroxide solution (200 ml). The brown precipitate was collected by filtration, washed with water and dried. The solid was then dispersed in CH_2Cl_2 (200 ml) and filtered through a celite pad. The filtrate was then washed with water (200 ml) until the washings were colourless. The organic solution was then reduced to dryness under reduced pressure and then redissolved in hot heptane (30 ml) treated with activated charcoal and stirred for 30 mins before filtering. The filtrate was then cooled to 6 °C and the precipitate isolated to yield a white solid in 1.10 g, 25 % yield.

^{1}H NMR; ($CDCl_3$) δ_{ppm} = 0.89 (6H, t, J = 6.7. CH_3), 1.37 (20H, m, CH_2), 1.56 (2H, s, CH_2), 1.86, (4H, quintet, J = 6.70, CH_2), 4.05 (6H, t, J = 6.7, CH_2-O), 7.12 (2H, s, Ar)

^{13}C NMR; ($CDCl_3$) δ_{ppm} = 14.10 (CH_3), 22.67 (CH_2), 25.83 (CH_2), 28.72 (CH_2), 29.22 (CH_2), 29.26 (CH_2), 29.49 (CH_2), 31.87 (CH_2), 69.75 (CH_2-O), 108.42 (C-CN), 115.82 (CH), 115.96 (CN), 152.49 (C-O)

HNES Calculated = 430.3433 Found = 430.3426

IR: ν_{max} (KBr) cm^{-1} = 3060, 2923, 2853, 2229

Chloro[subphthalocyaninato]-boron (III)[61] (25)

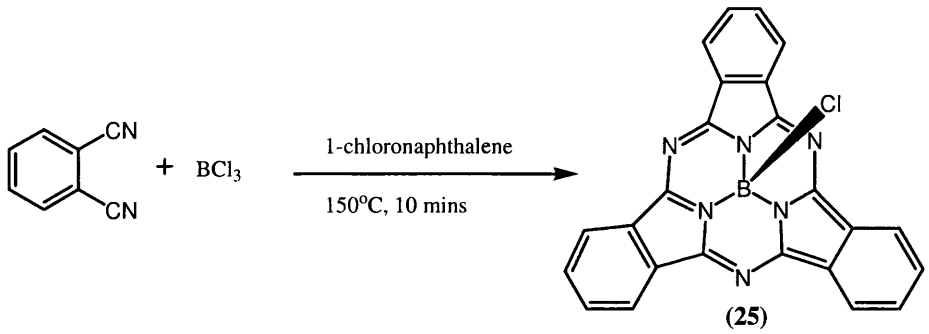

(25)

To a three-necked round bottomed flask, anhydrous phthalonitrile (5.04 g, 0.039 mol) and freshly distilled 1-chloronaphthalene (6 ml) were added under an argon atmosphere. Boron trichloride in CH_2Cl_2 (19.95 ml, 0.020 mol) was then added *via* a syringe. The reaction was stirred at room temperature and an exothermic reaction took place with the formation of a brown precipitate. The mixture was then heated to 160 °C, distilling the dichloromethane off, for 15 minutes. Once the reaction had cooled to room temperature, the mixture was diluted with methanol and filtered. The bronze solid was then placed in a Soxhlet extractor and washed with methanol for 48 hours to yield a bronze solid; yield 2.34 g (14 %).

^{1}H NMR, $CDCl_3$ δ = 7.97 (m, A_2B_2, 6H) 8.92 (m, A_2B_2, 6H)

UV/Vis (CH_2Cl_2)**: λ (rel. intens.),** 232 (0.51), 268s (0.39), 304 (0.54), 530 (sh, 0.35), 564 (1.00)

IR: ν_{max} (KBr) cm^{-1} = 3445, 1631

MS; (CI), m/z (%) = 430 (100), 464 (12), 500 (3)

Preparation of Chloro[tri *t*-butylsubphthalocyaninato]boron (III) (26)[61]

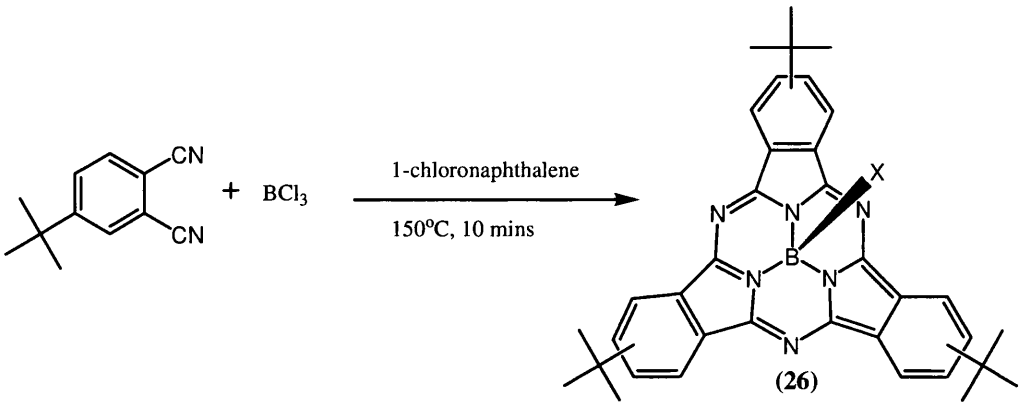

(26)

A three-necked round bottomed flask was charged with anhydrous *t*-butylphthalonitrile (0.5 g, 2.7 mmol) under an argon atmosphere. Boron trichloride in xylene (2.36 ml, 2.36 mmol) was then added *via* a syringe. The mixture was then heated to 240 °C for 2 hours. Once the reaction had cooled to room temperature, the mixture was washed with hexane. The purple solid was then placed in a Soxhlet extractor and extracted with diethyl ether to yield a purple solid, 0.04 g, 2.4 %.

UV/Vis (CH_2Cl_2)**:** λ **(rel. intens.),** = 284 (1.0), 528 (sh, 0.18), 568 (0.48)
MS; (EI), = 598.3 (13)

Preparation of Chloro[2,3,9,10,16,17-hexachlorosubphthalocyaninato]boron (III)[61] (27)

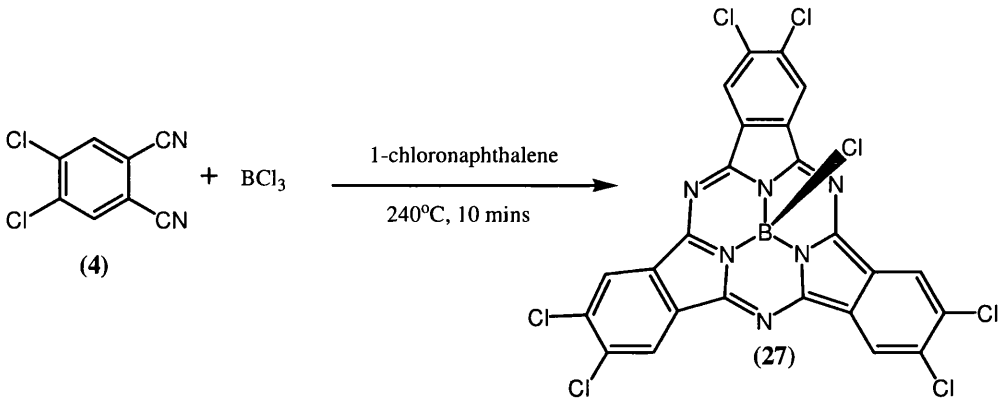

To a three-necked round bottomed flask, anhydrous 4,5-dichlorophthalonitrile **(4)** (1.0 g, 5.1 mmol) and freshly distilled 1-chloronaphthalene (1 ml) was added under an argon atmosphere. Boron trichloride in CH_2Cl_2 (0.83 ml, 0.8 mmol) was then added *via* a syringe. The reaction was stirred at room temperature and an exothermic reaction took place with the formation of a purple precipitate. The mixture was then heated to 240 °C, distilling the dichloromethane off, for 30 minutes. Once the reaction had cooled to room temperature, the mixture was washed with hexane and filtered. The solid was then Soxhlet extracted in CH_2Cl_2 to yield 1.43 g, 44 %.

UV/Vis (CH_2Cl_2)**:** λ **(rel. intens.),** = 240 (0.75), 276 (0.59), 312 (0.58), 520 (sh, 0.33), 572 (1.00)

IR: ν_{max} **(KBr)** cm^{-1} = 2923, 2828, 1721, 1610

MS; (ES), = 633.9

HRMS Calculated = 632.8598, Found = 632.8602

Preparation of Chloro[triiodosubphthalocyaninato]-boron (III)[61] (28)

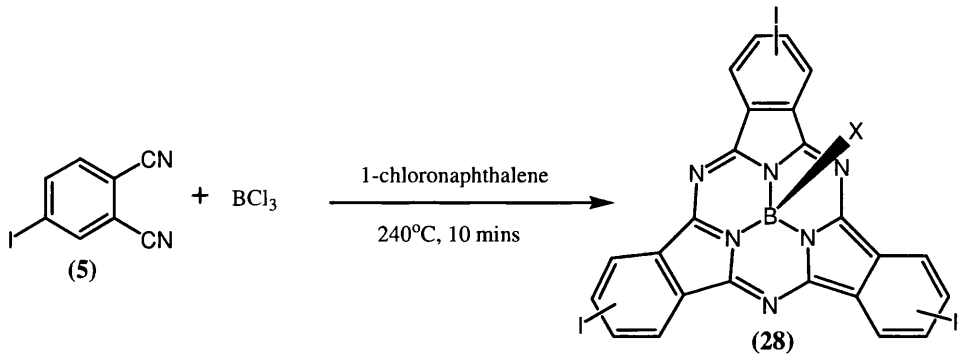

To a three-necked round bottomed flask, anhydrous 4-iodophthalonitrile **(5)** (1.05 g, 4.1 mmol) and freshly distilled 1-chloronaphthalene (1 ml) was added under an argon atmosphere. Boron trichloride in CH_2Cl_2 (2 ml, 2.07 mmol) was then added *via* a syringe. The reaction was stirred at room temperature and an exothermic reaction took place with the formation of a red precipitate. The mixture was then heated to 240 °C for 30 minutes. Once the reaction had cooled to room temperature, the solvent was removed by washing with hexane. The purple solid was then placed in a Soxhlet extractor and extracted with CH_2Cl_2 for 8 hours. The solvent was evaporated to yield a purple powder; yield: 0.52 g, 16 %.

MS; (EI), = 807.8

HRMS Calculated = 807.7799, Found = 807.7805

UV/Vis (CH_2Cl_2)**:** λ **(rel. intens.),** = 232 (0.93), 276 (0.73), 312 (0.50), 520 (sh, 0.30), 572 (1.00)

IR: ν_{max} **(KBr)** cm^{-1} = 3425, 1718, 1631

Preparation of 1,3-Diiminoisoindoline [111] (29)

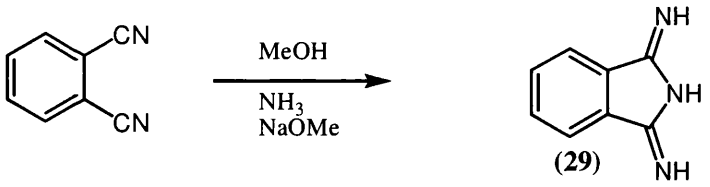

(29)

Phthalonitrile (0.97 g, 7.6 mmol) was added to a three-necked round bottomed flask equipped with condenser and bubbler. Anhydrous methanol (60ml) was added followed by sodium methoxide (0.043 g, 0.8 mmol). Ammonia gas was bubbled through the reaction at a steady rate at room temperature for 1 hour and then heated to reflux for 6 hours. Once cooled to room temperature the solvent was removed under reduced pressure and the green solid was washed with saturated NH_4Cl to yield 1.05 g, 96 %.

^{1}H NMR, DMSO δ = 7.63 (2H, m, ArH), 7.96 (2H, m, ArH) 9.31 (2H bs, NH)

IR: ν_{max} (KBr) cm^{-1} = 3332, 2923, 2853, 1640, 1544

MS; (EI), m/z (%) = 42.2 (67), 50.2 (51), 76.6 (83), 103.3 (39), 129.1 (75), 145.2 (100)

Preparation of *t*-Butyl-1,3-Diiminoisoindoline (30)[111]

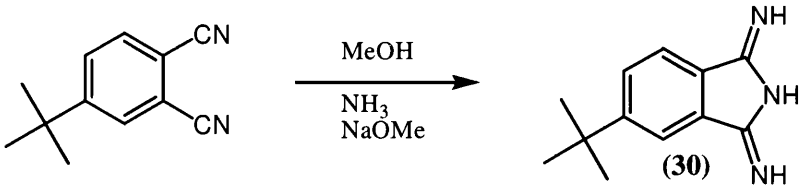

t-Butylphthalonitrile (1.010 g, 5.4 mmol) was reacted with sodium methoxide (0.029 g, 0.5 mmol) in anhydrous methanol (60ml). Ammonia gas was bubbled through the reaction at a steady rate at room temperature for 1 hour and then heated to reflux for 6 hours. Once cooled to room temperature the solvent was removed under reduced pressure and the residual solid washed with saturated NH_4Cl to yield a green solid 0.90 g, 82 %.

^{1}H NMR, DMSO, δ = 1.34 (9H, s, CH_3), 7.59 (2H, d, J = 7.9, C-H), 7.72 (2H, d, J = 7.9, C-H), 7.90 (1H, s, C-H), 8.47 (bs, NH)

^{13}C NMR, DMSO, δ = 31.26 (CH_3), 35.16 (C-CH_3), 118.11 (C), 120.78 (C-H), 127.62 (C-H), 134.12 (C-H), 136.76 (C-*t*-butyl), 153.98 (C=NH)

MS (EI) m/z (%) = 43.3 (64), 115.0 (46), 141.0 (35), 144.2 (42), 169.2 (46), 186.2 (100), 201.3 (M^+ 47)

Preparation of Dichloro-1,3-Diiminoisoindoline (31)[39,111]

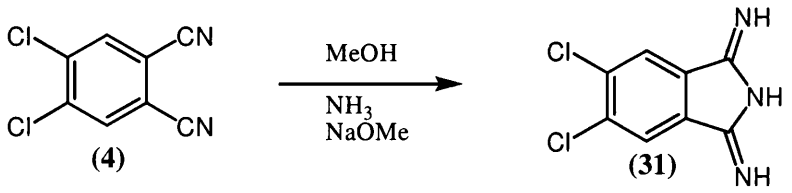

4,5-Dichlorophthalonitrile **(4)** (1.058 g, 5.4 mmol) was reacted with sodium methoxide (0.029 g, 0.5 mmol) in anhydrous methanol (60ml). Ammonia gas was bubbled through the reaction at a steady rate at room temperature for 1 hour and then heated to reflux for 6 hours. Once cooled to room temperature, the solvent was removed under reduced pressure and the green solid was washed with saturated NH_4Cl to yield a solid 0.73 g, 64 %.

^{1}H NMR, DMSO δ = 8.09 (2H, s, ArH), 8.71 (bs, NH)

^{13}C NMR, DMSO, δ = 113.54 (C), 123.06 (CH), 133.31 (C-Cl), 167.84 (C=NH)

IR: ν_{max} (KBr) cm^{-1} = 3270, 2919, 1726, 1632, 1550

MS; (EI), m/z (%) = 42.3 (100), 52.3 (32), 74.2(31), 100.2 (21), 136.1(16), 197.2 (21), 213.2 (M^+, 31)

Elemental Analysis: Calculated C = 44.88, H = 2.35, N = 19.63, Found C = 44.54, H = 2.41, N = 19.30

Preparation of Diiodo-1,3-Diiminoisoindoline (32)[111]

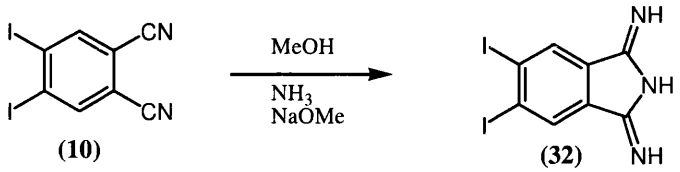

(10) (32)

4,5-Diiodophthalonitrile **(10)** (0.515 g, 1.3 mmol) was reacted with sodium methoxide (0.007 g, 0.1 mmol) in anhydrous methanol (60ml). Ammonia gas was bubbled through the reaction at a steady rate at room temperature for 1 hour and then heated to reflux for 6 hours. Once cooled to room temperature, the solvent was removed under reduced pressure and the green solid was washed with saturated NH_4Cl to yield a solid 0.33 g, 61 %.

^{1}H NMR, DMSO δ = 8.43 (2H, s, ArH), 8.98 (bs, NH)

IR: ν_{max} (KBr) cm^{-1} = 3390, 2925, 1637, 1541

MS; (ES), = m/z (%) EI+, 43.3 (68), 74.2 (65), 100.2 (59), 127.1 (100), 253.9 (21), 270.1 (21), 397.0 (M^+,37)

Elemental Analysis: Calculated C = 24.20 H = 1.26, N= 10.58 Found C = 24.33, H = 1.50 N = 9.97,

Preparation of Phthalocyanine (33)[118]

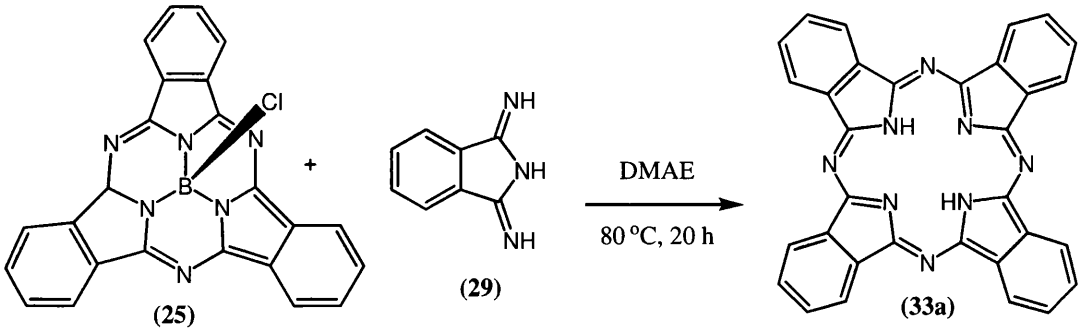

(25) (29) (33a)

Chloro[subphthalocyaninato]-boron (III) **(25)** (0.130 g, 0.3 mmol) was added to a stirring suspension of 1,3-diiminoisoindoline (0.129 g, 0.9 mmol) and dimethylaminoethanol (20 ml). The purple solution was heated to 80 °C for 20 hours before being cooled to room temperature. The reaction mixture was diluted with methanol and filtered. The solid was washed with methanol and CH_2Cl_2 and dried to yield a blue solid, 0.2 g, 43 %.

MS; (EI), m/z (%) = 514 (100, M^+)

HRMS (EI) = Found = 514.1645, calculated = 514.1649

IR: ν_{max} (KBr) cm^{-1} = 3264, 1720, 1639

Preparation of 2,3,7,8,12,13,17,18- Octa(4-pentoxybenzoate)-5,10,15,20-tetrazaporphyrin zinc (34a)

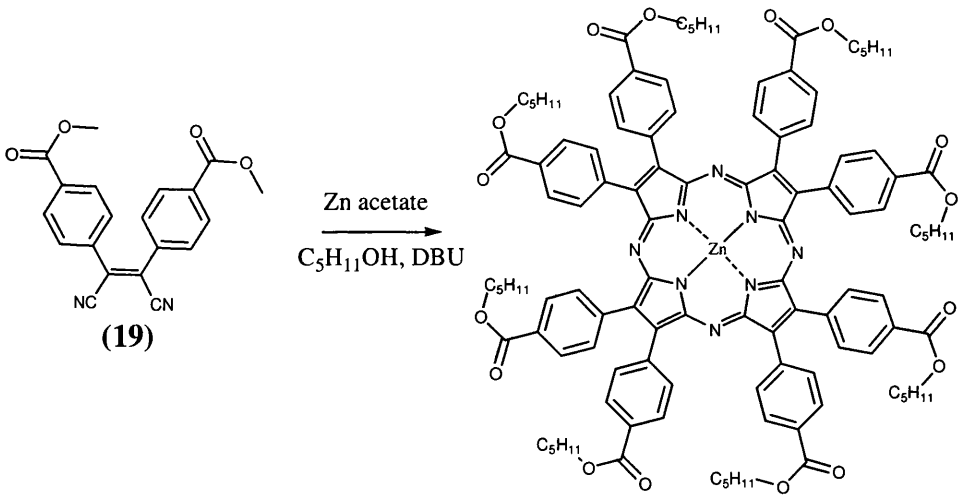

(19) **(34a)**

Di-(4-methylbenzoate)-fumaronitrile **(19)** (0.64 g, 1.85 mmol) was reacted with zinc acetate (0.16g, 0.92 mmol) in pentanol (10 ml) in the presence of DBU (0.1 ml 0.7 mmol) at 140 °C for 20 hours. After one hour, a green solution was formed. The solvent was then removed by distillation and the green residue was subjected to flash column chromatography on alumina. The product was eluted in ethyl acetate to yield 0.72 g, 21 %.

^{1}H NMR, THF δ = 0.91 (24H, t, J =7.25, $C\underline{H}_3$), 1.44 (32H, m, $C\underline{H}_2$), 1.81 (16H, quintet, J = 6.90, $C\underline{H}_2$) 4.33 (16H, t, J = 6.95, O-$C\underline{H}_2$), 8.05 (32H, m, Ar)

^{13}C NMR, THF, δ = 13.46 (CH_3), 22.42 (CH_2), 28.30 (CH_2), 28.54 (CH_3), 64.74 (O-CH_2), 129.11 (CH), 130.16 (CH), 132.44 ($\underline{C}$-CO), 137.66 (C-Ar), 142.26 (C=C), 156.88 (C-N), 165.45 (CO)

MS EI+ = 1898 (100)

IR: ν_{max} (KBr) cm^{-1} = 3419, 2957, 2871, 1718, 1608, 1468

UV/Vis (THF): λ (rel. intensity) = 380 (0.76), 588 (s, 0.16), 640 (1.0)

Preparation of 2,3,7,8,12,13,17,18-Octa(benzoate)-5,10,15,20-tetrazaporphyrin zinc (34b)

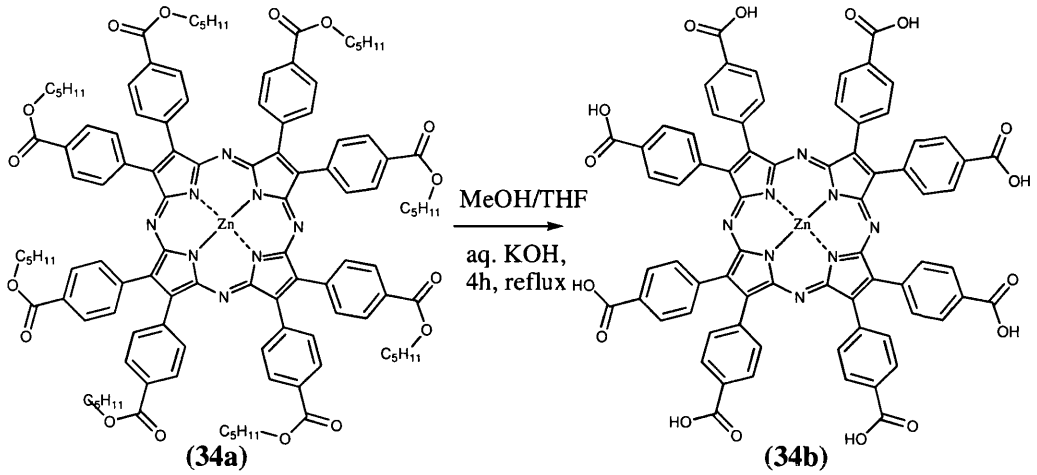

(34a) (34b)

2,3,7,8,12,13,17,18- octa(4-pentoxybenzoate)-5,10,15,20-tetraazaporphyrin zinc (**34a**) (0.059g, 0.03 mmol) was dissolved in THF (10 ml). To the green solution, methanol (5 ml) was added along with KOH (15 ml, 2 M). The reaction mixture was then brought to reflux for 4 hours before being cooled to room temperature. The organic solvent was then removed and the remaining aqueous layer acidified with HCl. The precipitate was filtered to yield a dark green solid (0.0256 g, 64 %).

^{1}H NMR, THF δ = 8.07 (m, Ar)

MS (EI) = 1337.3 (100)

IR: ν_{max} (KBr) cm^{-1} = 3419, 2958, 2865, 1718, 1609

UV/Vis (THF): λ (rel. intensity) = 380 (1.0), 604 (s, 0.56), 644 (0.93)

Mp = decompose above 300 °C

Preparation of 2,3-(4-Pentoxybenzoate)-7^2,12^2,17^2-tri-*tert*-butyl-tribenzo-5,10,15,20-tetraazaporphyrin (35a)

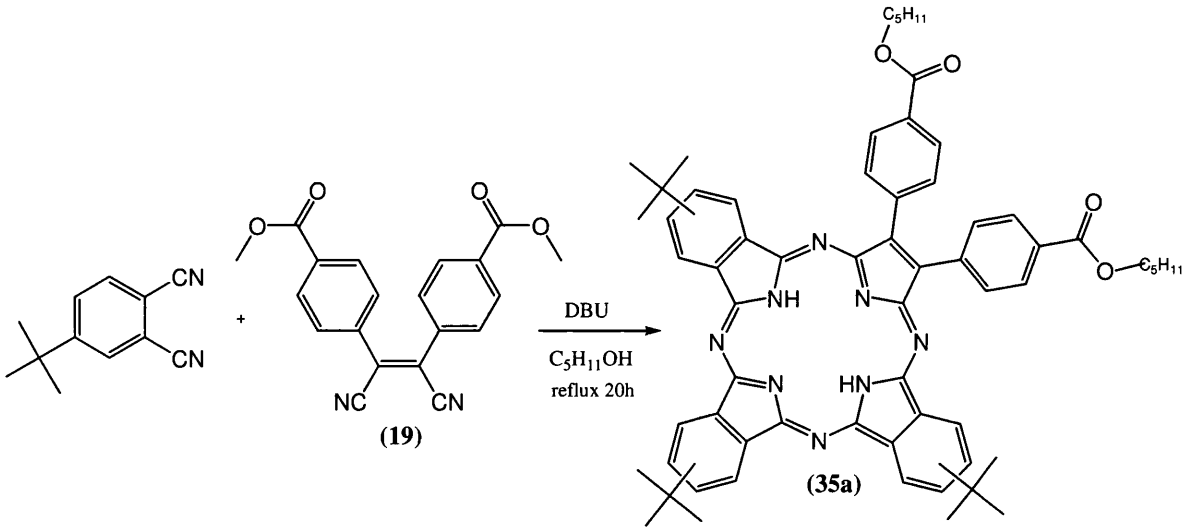

A three-necked round bottomed flask was charged with *t*-butylphthalonitrile (0.5 g, 2.7 mmol), di-(4-methylbenzoate)-fumaronitrile **(19)** (0.31 g, 0.9 mmol), anhydrous pentan-1-ol (10 ml) and DBU (0.07 g, 0.5 mmol) under an argon atmosphere. The solution was then heated to reflux for 20 hours. The solvent was removed under vacuum and the blue/green residue was placed on to alumina and the product eluted with petroleum spirit and ethyl acetate 85 : 1 mix to yield a dark blue solid (244 mg, 7.35%).

^{1}H NMR; ($CDCl_3$) δ_{ppm} = 0.96 (m CH_3), 1.05 (m, t-butyl), 1.28 (s, t-butyl) 1.42 (m, CH_2), 1.72 (m, CH_2), 1.96 (m, CH_2), 4.33 (m, O-CH_2), 4.51 (m, O-CH_2), 7.93-8.50 (m, phenyl), 8.90-9.28 (m, phenyl)

MS; (MA), = 738.3 (100), 881.3 (3), 1012.3 (16), 1286.4 (3)

IR: ν_{max} (KBr) cm^{-1} = 3297, 2958, 2871, 1719, 1609

UV/Vis (THF): λ (rel. intens.), 292 (0.61), 348 (0.89), 600 (0.46), 636 (0.44), 660 (0.79), 696 (1.00)

Preparation of 2,3-(4-Pentoxybenzoate)-7^2,12^2,17^2-tri-*tert*-butyl-tribenzo-5,10,15,20-tetraazaporphyrin zinc (35b)

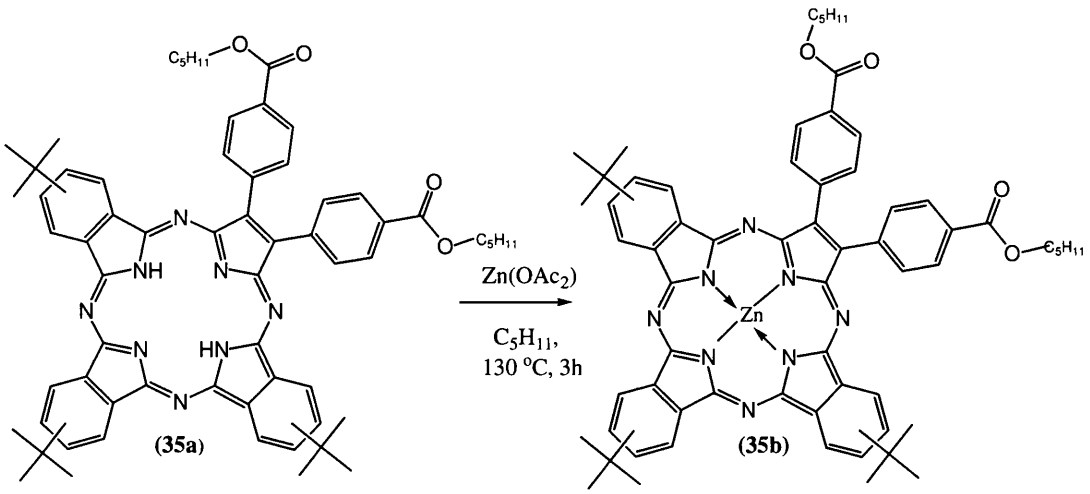

2,3-(4-Pentoxybenzoate)-7^2,12^2,17^2-tri-*tert*-butyl-tribenzo-5,10,15,20-tetraazaporphyrin **(35a)** (158 mg, 0.17 mmol) was dissolved in freshly distilled pentan-1-ol under an argon atmosphere. Anhydrous zinc acetate (0.08 g, 0.44 mmol) was added to the blue/green solution and then heated to 130 °C for 3 hours. The solvent was then removed under reduced pressure and the residue placed onto alumina. The product was eluted with petroleum spirit : ethyl acetate (1:1) mix to yield 0.068 g. (4.1 %).

^{1}H NMR; ($CDCl_3$) δ_{ppm} = Crude product - 0.91 (t, J = 6.95, CH_3), 1.18 (s, t-butyl), 1.27 (s, t-butyl), 1.37 (m, CH_2), 1.79 (m, CH_2). 4.32 (t, J = 6.95, CH_2-O), 8.10-8.48 (m, phenyl), 9.01-9.46 (m, phenyl)

MS; (EI), m/z (%) = 800 (100), 1076 (8), 1350 (3)

IR: ν_{max} (KBr) cm^{-1} = 3245, 2958, 2869, 1717, 1608

UV/Vis (THF): λ (rel. intens.), 284 (0.44), 356 (0.72), 620 (0.47), 644 (0.54), 672 (1.00), 692 (0.59, s)

Preparation of 2,3-(4-Benzoate)-7^2,12^2,17^2-tri-*tert*-butyl-tribenzo-5,10,15,20-tetraazaporphyrin zinc (35c)

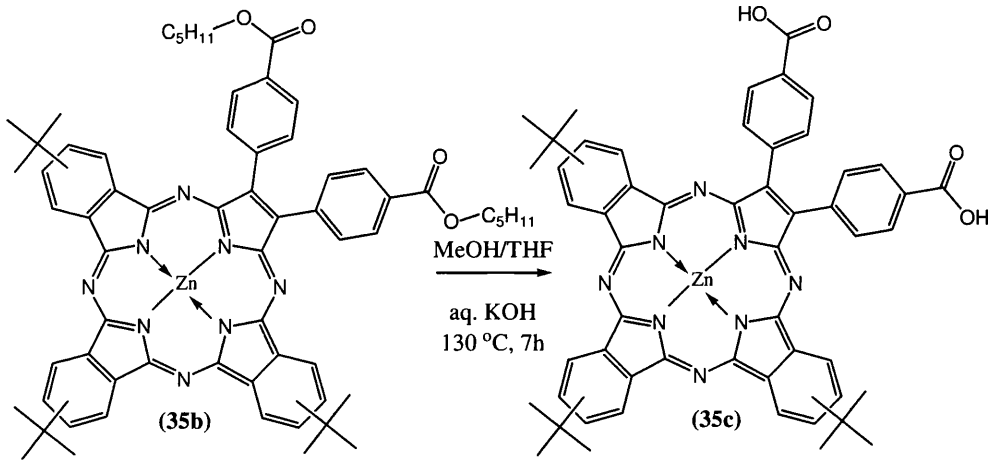

2,3-(4-pentoxybenzoate)-7^2,12^2,17^2-tri-*tert*-butyl-tribenzo-5,10,15,20-tetraazaporphyrin zinc **(35b)** (0.048 g, 0.07 mmol) was dissolved in THF (10 ml), methanol (5 ml) and 30% potassium hydroxide (15 ml). The solution was then heated to reflux for 7 hours and left to stir at room temperature for a further 16 hours. The organic residue was then removed. The aqueous layer was then acidified to pH 2 by the addition of HCl and then filtered. The precipitate was then washed with water and dried. The remaining solid was suspended in dichloromethane (30 ml) and stirred at reflux for 1 hour. The suspension was the filtered and the solid dried to afford a dark green solid (0.03 g, 64.5 %) .

^{1}H NMR; (THF) δ_{ppm} = Crude product - 1.18 (s, *t*-butyl), 1.27 (s, *t*-butyl), 8.34 (3H, m, carboxyphenyl), 8.48 (3H, m, carboxylphenyl), 8.52 (3H, m carboxylphenyl), 9.12 (1H, t, phenyl), 9.31 (5H, m, phenyl), 9.50 (2H, m, phenyl), 10.69 (2H, s, COOH), 10.83 (s, COOH)

MS; (MA), m/z (%) = 934.2 (100)

HRMS (EI): Found = 971.2600 (M+ Cl), calculated = 971.2613

IR: ν_{max} (KBr) cm^{-1} = 3439, 2963, 2871, 1716, 1608

UV vis = 364 (1.0), 584 (s, 0.29) 628 (0.75), 648 (0.79), 696 (0.99)

Mp = decompose above 300 °C

Preparation of 2,9,16–Tetra-*tert*-butyl-23,24-bis(4-pentoxycarboxyphenyl) phthalocyanine (36a)

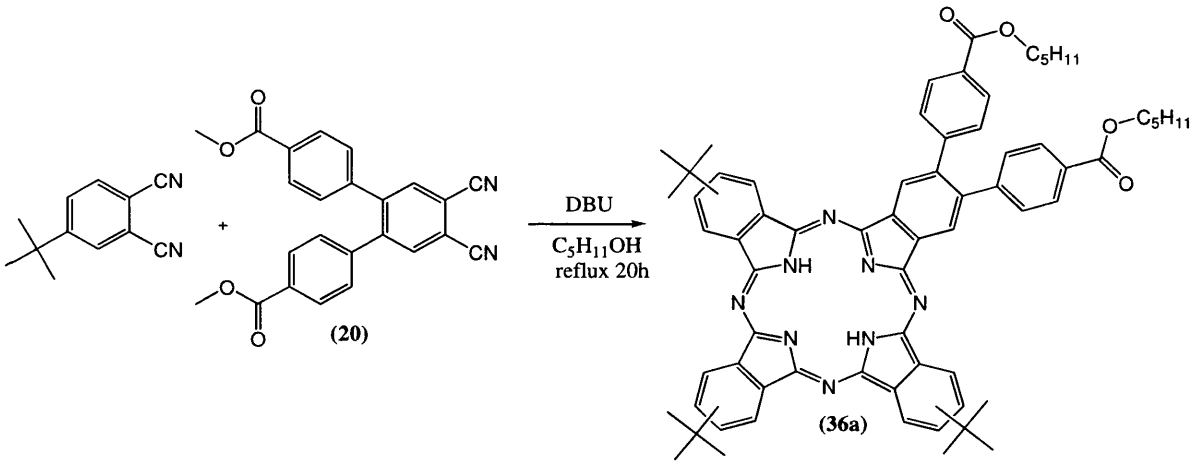

A three necked round bottomed flask was charged with *t*-butylphthalonitrile (0.5 g, 2.7 mmol), 4,5-bis(4-methoxycarbonylphenyl)phthalonitrile **(20)** (0.35 g, 0.9 mmol), anhydrous pentan-1-ol (10 ml) and DBU (0.07 g, 0.5 mmol) under an argon atmosphere. The solution was then heated to reflux for 20 hours. The solvent was removed under vacuum and the blue/green residue was placed on to alumina and the product eluted with petroleum spirit and ethyl acetate 3 : 1 mix to yield a dark blue solid (240 mg, 9.4 %).

^{1}H NMR; (THF) δ_{ppm} = Crude product - 0.96 (t, J = 6.90, CH_3), 1.32 (m, t-butyl), 1.39 (m, CH_2), 1.48 (s, t-butyl), 1.71 (m, CH_2), 4.26 (O-CH_2), 4.46 (m O-CH_2) 8.10-8.48 (m, phenyl), 9.01-9.46 (m, phenyl)

MS; (EI), m/z (%) = 738 (100), 1063 (60), 1387 (24), 1711 (8)

IR: ν_{max} (KBr) cm^{-1} = 3431, 2956, 2852, 2221, 1716, 1608

UV/Vis (THF): λ (rel. intens.), 292 (0.59), 348 (0.68), 612 (0.23, s), 644 (0.38, s), 668 (0.77), 698 (1.00)

Mp: Decomposes above 300 °C

Preparation of 2,9,16–Tetra-*tert*-butyl-23,24-bis(4-pentoxycarboxyphenyl) phthalocyanine Zinc (36b)

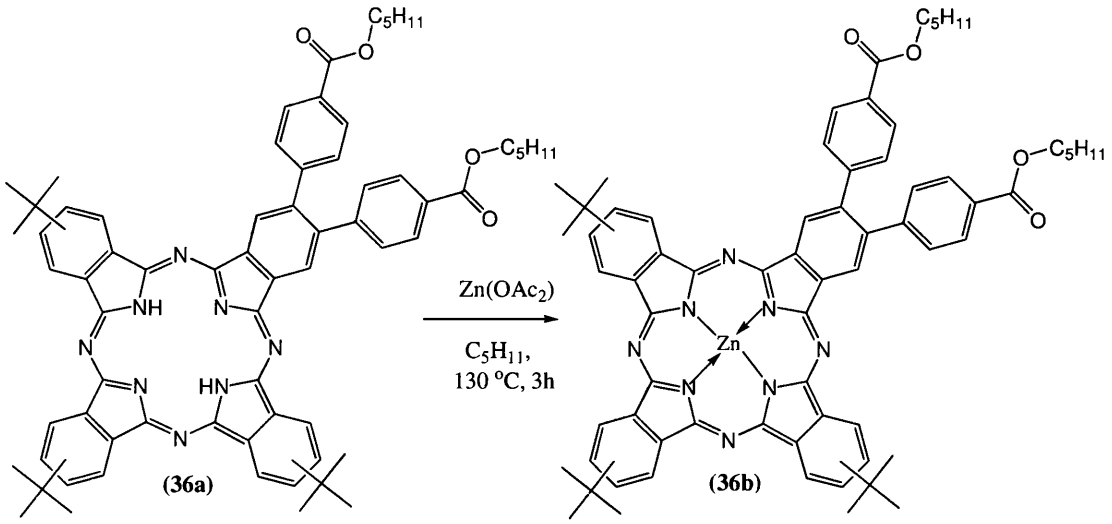

2,9,16–tetra-*tert*-butyl-23,24-bis(4-pentoxycarboxyphenyl)phthalocyanine **(36a)** (220 mg, 0.23 mmol) was dissolved in freshly distilled pentan-1-ol under an argon atmosphere. Anhydrous zinc acetate (0.10 g, 0.58 mmol) was added to the blue/green solution and then heated to 130 °C for 3 hours. The solvent was then removed under reduced pressure and the residue placed onto alumina. The product was eluted with petroleum spirit : ethyl acetate (1:1) mix to yield g. (0.177 g, 68 %).

^{1}H NMR; (THF) δ_{ppm} = Crude product - 0.97 (m, CH_3), 1.33 (s, t-butyl), 1.41 (s, t-butyl), 1.45 (m, CH_2), 1.71 (m, CH_2), 1.81 (m, CH_2), 4.22 (m, O-CH_2) 4.34 (m, O-CH_2), 7.81-8.12 (m, Phenyl),

MS; (EI), m/z (%) = 800 (37), 1124 (100), 1448, (54) 1773 (23)

IR: ν_{max} (KBr) cm^{-1} = 3440, 2929, 2856, 1720, 1606

UV/Vis (THF): λ (rel. intens.), 292 (0.30), 352 (0.48), 612 (0.18), 640 (0.17, s), 672 (1.00)

Preparation of 2,9,16-*tert*-Butyl-23,24-(4-carboxyphenyl)-phthalocyanine Zinc (36c)

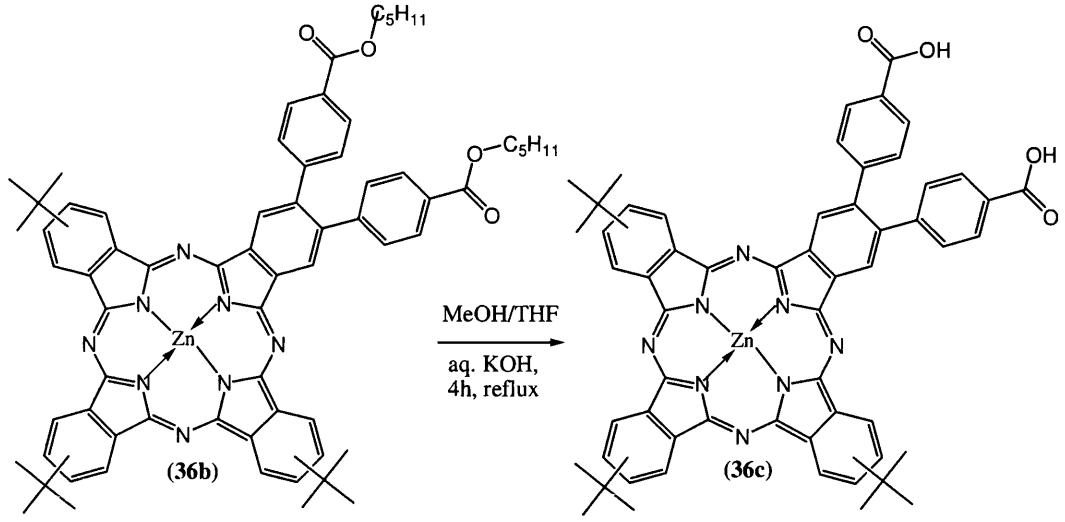

2,9,16–Tetra-*tert*-butyl-23,24-bis(4-pentoxycarboxyphenyl) phthalocyanine zinc **(36b)** (0.177 g, 0.12 mmol) was dissolved in THF (10 ml), methanol (5 ml) and 30 % potassium hydroxide (15 ml). The solution was then heated to reflux for 5 hours. The organic solvent was then removed and the aqueous layer acidified to pH 2 by the addition of HCl and then filtered. The precipitate was then washed with water and dried. The remaining solid was suspended in dichloromethane (30 ml) and stirred at reflux for 1 hour. The suspension was the filtered and the solid dried to afford a dark green solid (0.08 g, 68 %).

^{1}H NMR; (THF) δ_{ppm} = Crude product - 1.18 (s, *t*-butyl), 1.23 (s, *t*-butyl), 1.27 (s, *t*-butyl), 7.17 (m, phenyl), 7.61 (d, J = 7.6, phenyl), 7.78 (m, phenyl), 8.03 (bs, phenyl)
MS; (EI), m/z (%) = 800 (100), 984 (M+, 28)
IR: ν_{max} (KBr) cm^{-1} = 3443, 3138, 2971, 1715, 1600
UV/Vis (THF): λ (rel. intens.), 292 (0.44), 352 (0.51), 612 (0.18), 680 (1.00)
Mp = decomposes above 300 °C

Preparation of 2,3,9,10,16,17 – Nonoxy – 23,24- bis(4-pentoxycarboxyphenyl) phthalocyanine (37a)

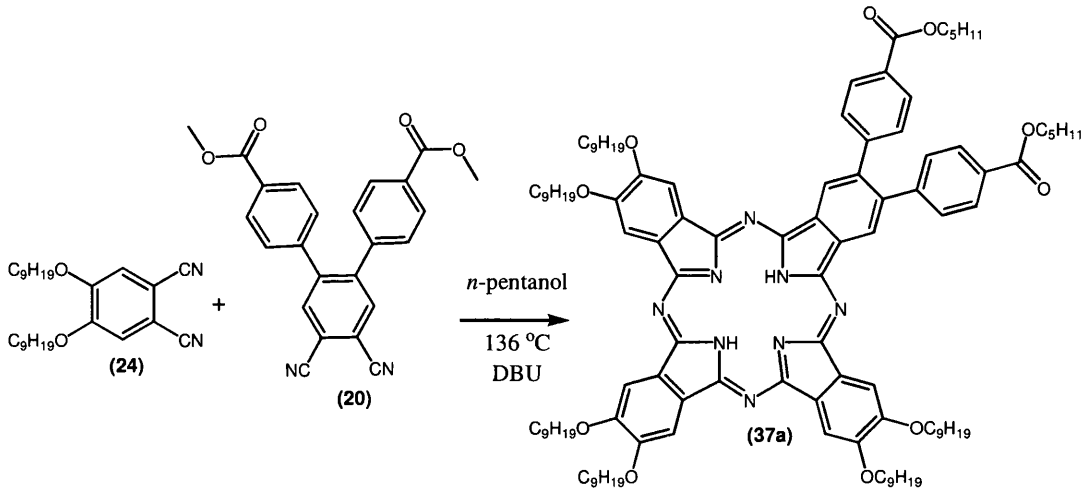

A three-necked round bottomed flask was charged with 4,5-dinonoxyphthalonitrile **(24)** (0.5 g, 1.2 mmol), 4,5-bis(4-methoxycarbonylphenyl)phthalonitrile **(20)** (0.16 g, 0.4 mmol), anhydrous pentan-1-ol (10 ml) and DBU (0.07 g, 0.5 mmol) under an argon atmosphere. The solution was then heated to reflux for 20 hours. The solvent was removed under vacuum and the blue/green residue was placed on to alumina and the product eluted with petroleum spirit and ethyl acetate 1 : 1 mix to yield a dark blue solid (0.168 g, 8.0 %).

^{1}H NMR; (THF) δ_{ppm} = Crude product - 0.83 (m, CH_3), 1.21 (m, CH_2), 1.30 (m, CH_2), 1.71 (CH_2), 4.01 (m, O-CH_2), 4.31 (m, O-CH_2), 7.33 (m, (CH), 7.5 (m, C-CH), 7.79 (m, CH), 8.03 (m, CH)

MS; (ES), = 1652 (77), 1748 (100), 1844 (62), 1939 (27), 2035 (6)

IR: ν_{max} **(KBr) cm^{-1}** = 3435, 2929, 2856, 2221, 1721, 1608

UV/Vis (THF): λ **(rel. intensity)** = 264 (1.0), 352 (0.69), 616 (s, 0.15), 684 (0.57), 696 (0.57)

Preparation of 2,3,9,10,16,17 – Nonoxy – 23,24- bis(4-pentoxycarboxyphenyl) phthalocyaninato zinc (37b)

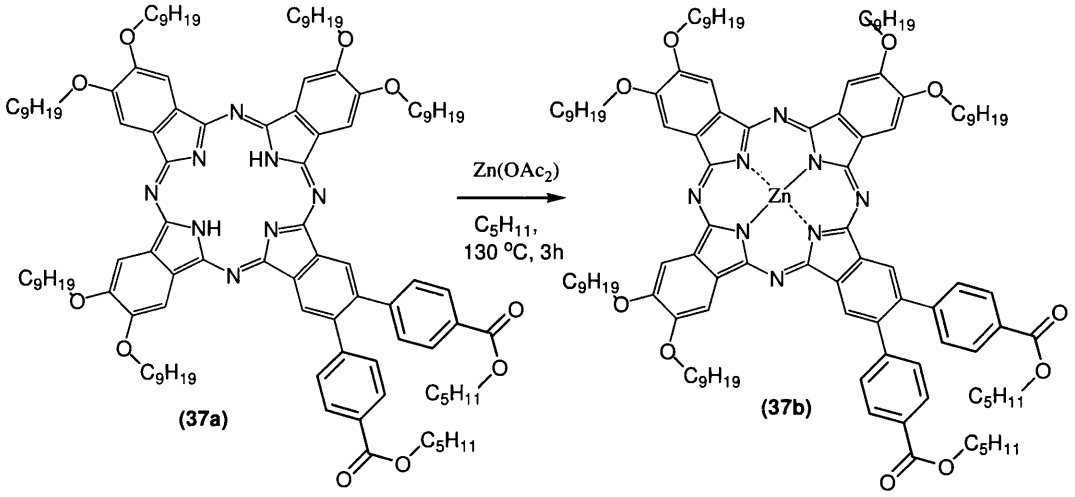

2,3,9,10,16,17-Nonoxy-23,24-(4-pentoxycarboxyphenyl)-phthalocyanine **(37a)** (0.161 g, 0.09 mmol) was dissolved in freshly distilled pentan-1-ol under an argon atmosphere. Anhydrous zinc acetate (0.08 g, mmol) was added to the blue/green solution and then heated to 130 °C for 3 hours. The solvent was then removed under reduced pressure and the residue placed onto alumina. The product was eluted with petrolium spirit : ethyl acetate (1:1) mix to yield g. (0.061 g ,37 %).

^{1}H NMR; (THF) δ_{ppm} = Crude product - 0.85 (m, CH_3), 1.26 (m, CH_2), 1.32 (m, CH_2), 1.75 (CH_2), 4.03 (t, O-CH_2), 4.26 (m, O-CH_2), 4.42 (m, O-CH_2), 7.31 (m, (CH), 7.5 (m, C-CH), 7.61 (m, CH2), 7.79 (m, CH), 8.03 (m, CH)

MS; (ES), = 1652 (38), 1714 (94), 1809 (100), 1907 (45), 2002 (9)

IR: ν_{max} (KBr) cm^{-1} = 3440, 2929, 2858, 1721, 1608

UV/Vis (THF): λ (rel. intensity) = 264 (0.88), 360 (0.73), 620 (s, 0.18), 688 (0.90)

Preparation of 2,3,9,10,16,17 – Nonoxy – 23,24- bis(4-carboxyphenyl) phthalocyanine zinc (37c)

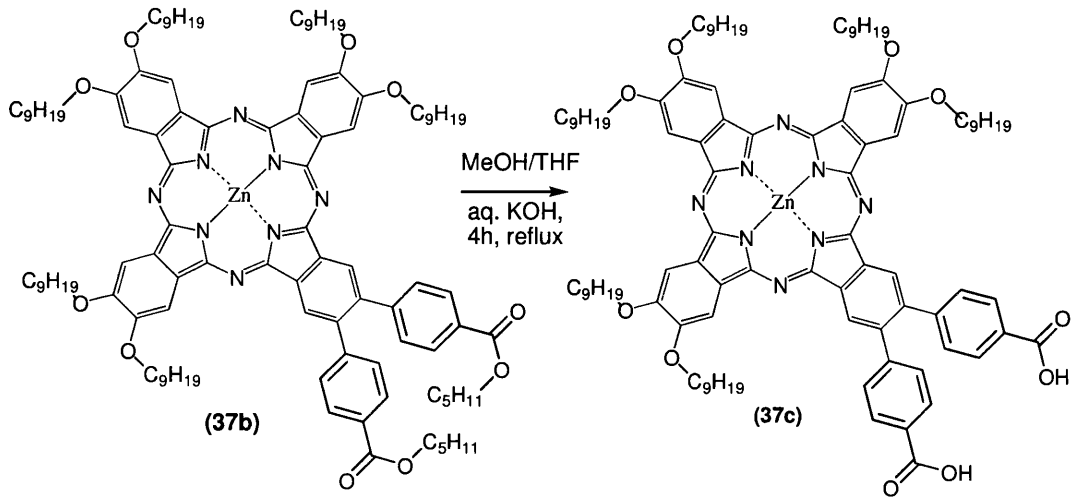

2,3,9,10,16,17-Nonoxy-23,24-(4-pentoxycarboxyphenyl)-phthalocyanine zinc (**37b**) (0.058 g, 0.03 mmol) was dissolved in pyridine (10 ml), KOH (2 ml, 5 M) and heated to reflux for 2 hours. After cooling to room temperature, the reaction mixture was acidified to pH 2 by the addition of HCl and then filtered. The precipitate was then washed with water and acetone and dried. The remaining solid was suspended in dichloromethane (30 ml) and stirred at reflux for 1 hour. The suspension was the filtered and the solid dried to afford a dark green solid (0.04 g, 78 %).

^{1}H NMR; (THF) δ_{ppm} = Crude product - 0.93 (m, CH_3), 1.37 (m, CH_2), 1.46 (m, CH_2), 1.89 (m, CH_2), 4.33 (m, O-CH_2), 7.43 (d, J = 6.3, CH), 7.71 (m, CH), 8.00 (d, J = 8.2, CH), 8.13 (m, CH)

MS; (ES), = 1626 (18), 1655 (14), 1669 (62), 1714 (100)

IR: ν_{max} (KBr) cm^{-1} = 3420, 2925, 2846, 1719, 1609, 1510

UV/Vis (THF): λ (rel. intensity) = 264 (0.76), 360 (0.73), 620 (s, 0.18), 688 (0.90)

Mp = decomposes over 300 °C

Preparation of 2,9,16,23-(Tetra-1-bromoferrocene)-3,10,17,24-chlorophthalocyaninezinc(II) (38)

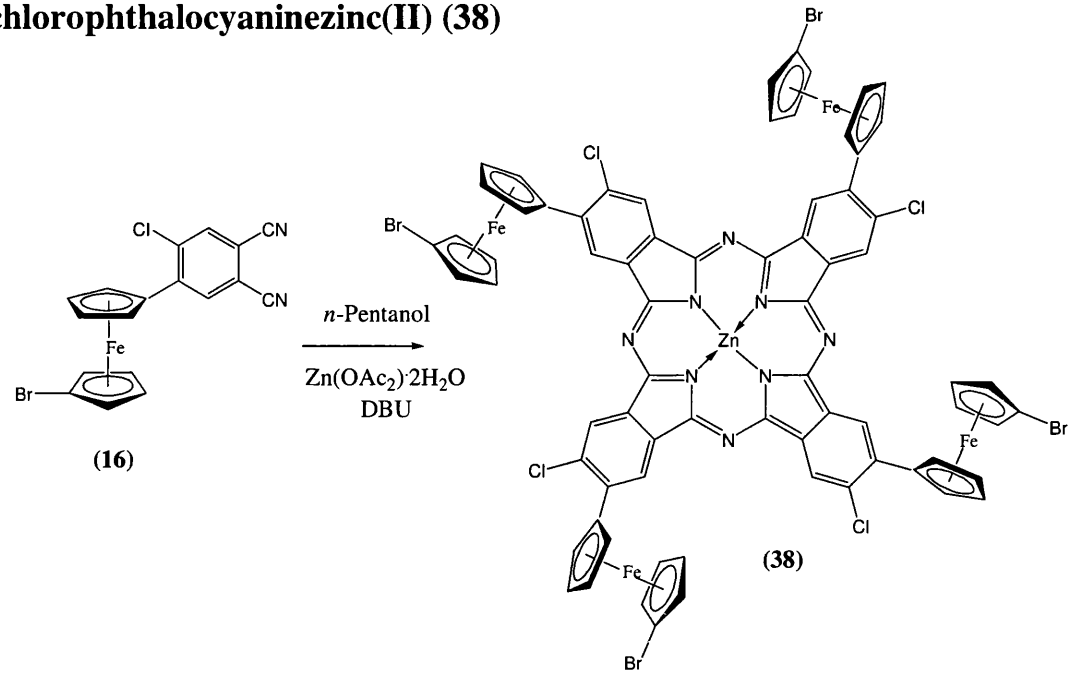

4-(1-Bromoferrocene)-5-chlorophthalonitrile **(16)** (0.101 g, 0.2 mmol) was added to *n*-pentanol (10 ml), freshly distilled, under an argon atmosphere. To this zinc acetate dehydrate (0.026 g, 0.1 mmol) and DBU was added. The red solution was heated to 130 °C for three hours after which the solvent was removed under reduced pressure. The resulting green residue was the purified by flash chromatography using chloroform as the eluting solvent.

^{1}H NMR; (THF) δ_{ppm} = Crude product - 4.20 (s, CH), 4.29 (m, CH), 4.33 (s, CH), 4.47 (s, CH), 4.58 (m, CH), 4.65 (s, CH), 8.78-9.01 (m, phenyl)

MS; (ES), = 1609 (24), 1687 (- bromine, 85), 1767 (100)

IR: ν_{max} **(KBr)** cm^{-1} = 3436, 2925, 2853, 1723, 1629

UV/Vis (THF): λ **(rel. intensity)** = 364 (0.62), 640 (32), 708 (1.0)

Preparation of 2,9,16-(Tetra-1-bromoferrocene)-3,10,17-chloro-23,24-bis(4-methoxycarboxyphenyl) phthalocyaninezinc(II) (39)

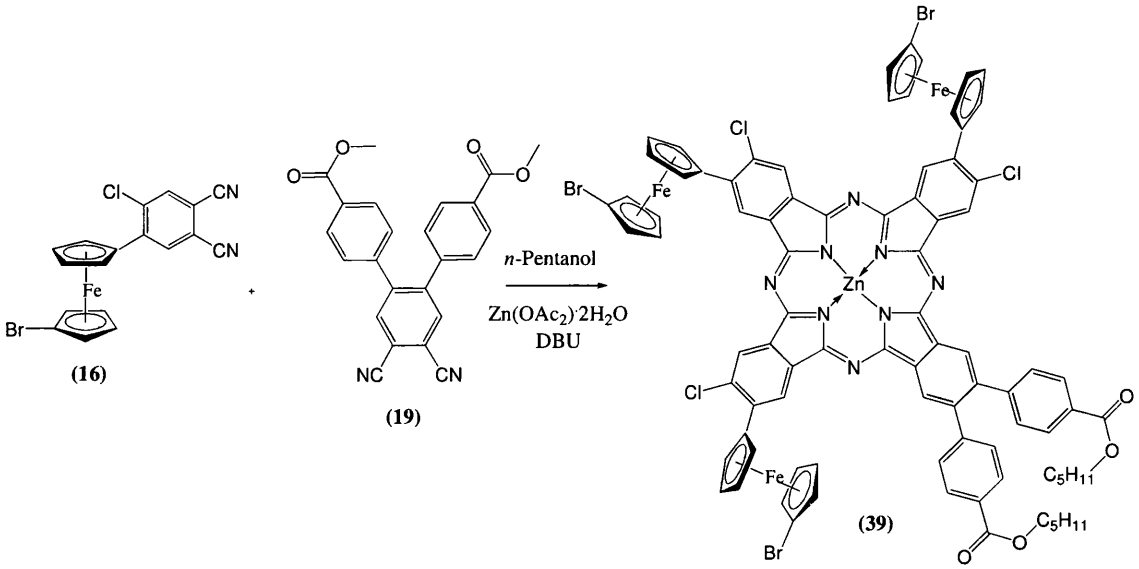

4-(1-Bromoferrocene)-5-chlorophthalonitrile **(16)** (0.103 g, 0.24 mmol) and 4,5-bis(4-methoxycarbonylphenyl)phthalonitrile **(19)** (0.031 g, 0.008 mmol) were added to *n*-pentanol (10 ml), under an argon atmosphere. To this zinc acetate dihydrate (50 mg) and DBU (0.1 ml) was added. The red solution was heated to 136 °C for 16 hours after which the solvent was removed under reduced pressure. The resulting green residue was the purified by flash chromatography using ethyl acetate as the eluting solvent.

^{1}H NMR; (THF) δ_{ppm} = Crude product - 0.89 (m, CH_3), 1.48 (m, CH_2), 1.71 (CH_2), 4.01 (s, CH), 4.14 (s, CH), 4.26 (s, CH), 4.32 (m, O-CH_2), 4.53 (s, CH), 7.14-8.00 (m, Ar)

MS; (MALDI), =1772 (27), 1850 (M^+, 42), 1903 (100)

IR: ν_{max} **(KBr)** cm^{-1} = 3228, 3113, 2948, 1716, 1648

Preparation of Chloro[2,9,16,(ferrocenylethynyl)subphthalocyanine] boron (III) (40)

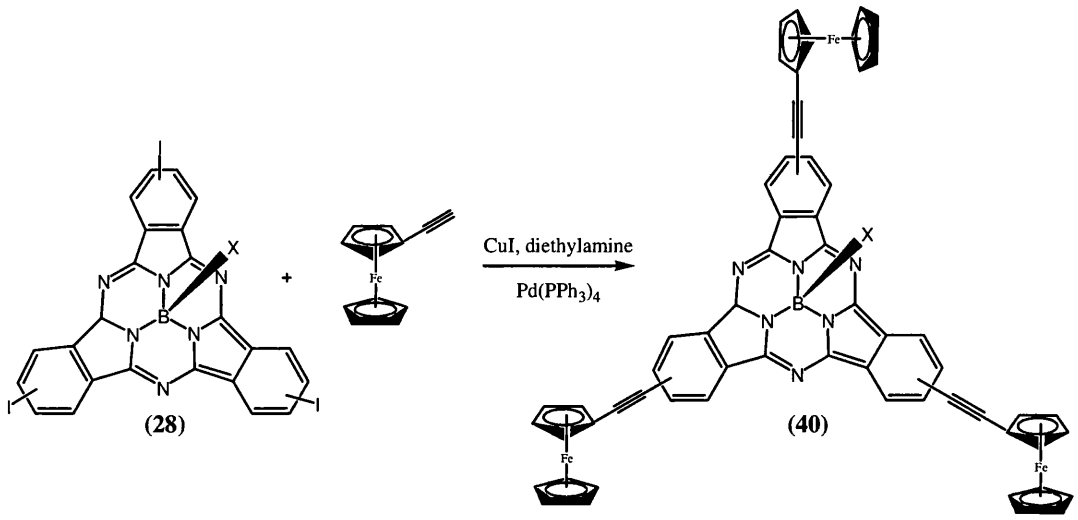

Copper iodide (50 mg) was added to a flask containing diethylamine (10 ml) and tetrakis(triphenylphosphine)palladium (20 mg). Chloro[triiodosubphthalocyaninato]-boron (III) **(28)** (0.706 g, 0.87 mmol) was added followed by ferrocene acetylene (0.55 g, 6.63 mmol). The reaction mixture was then heated to efflux for six hours. On cooling to room temperature, the reaction was quenched with water (20 ml) and extracted with CH_2Cl_2 (3 x 20 ml). The combined organic layers were then dried and reduced to dryness under reduced pressure. The solid residue was then subjected to column chromatography with the product eluting with petroleum spirit, ethyl acetate mix (1:1) to yield a purple solid, 0.42 g, 46 %.

^{1}H NMR; ($CDCl_3$) δ_{ppm} = 4.28 (2H, s, βH), 4.33 (5H, s, Cp), 4.63 (2H, s, αH), 7.76 (1H, s,), 8.01 (1H, d, J=8.52), 8.80 (1H, d, J = 8.82) 9.01 (1H, s, CH)

MS; (ES), = 1054 (100)

IR: ν_{max} (KBr) cm^{-1} = 3435, 2971, 2860, 2204, 1716, 1632

UV/Vis (THF): λ **(rel. intens** 292 (0.90), 360 (s, 0.56), 544 (s, 0.49), 600 (1.0)

Preparation of Chloro[2,9,16,(4-methoxycarboxyphenyl) subphthalocyanine] boron (III) (41)

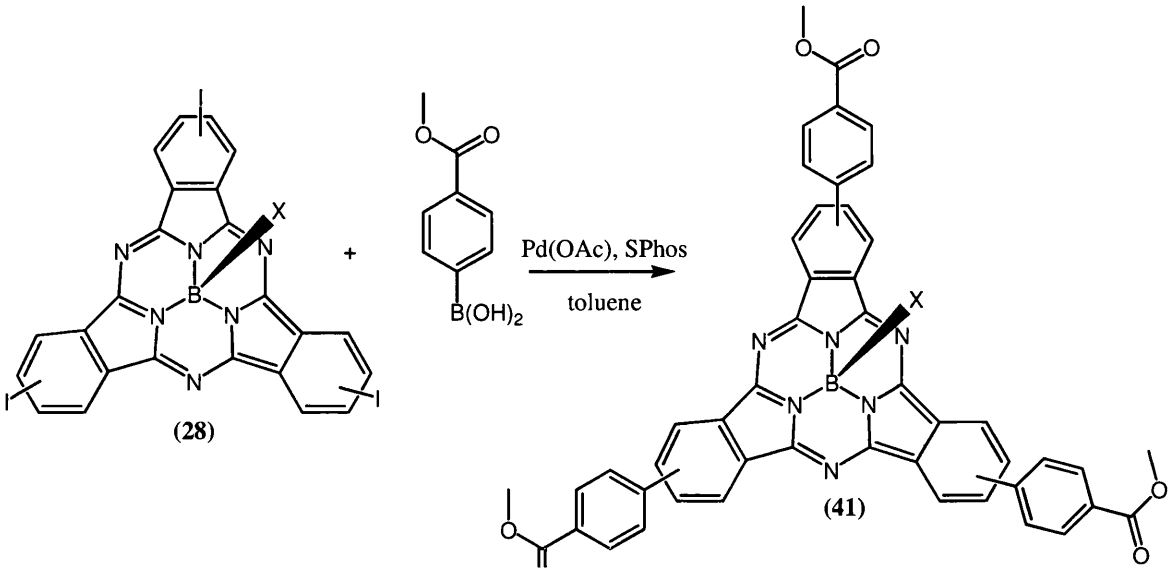

A flask was charged with chloro[triiodosubphthalocyaninato]-boron (III) **(28)** (0.5 g, 0.6 mmol), 4-(methoxycarbonylphenyl)boronic acid (0.44 g, 2.5 mmol), anhydrous toluene (10 ml), palladium (II) acetate (20 mg), 2-(2',6'-dimethoxybiphenyl)dicyclohexylphosphine (20 mg) and potassium phosphate (0.8 g, 3.8 mmol) under an argon atmosphere. The reaction mixture was heated to 90 °C for 24 hours. The organic layer was then washed with water (2 x 25 ml) and the combined organic layers were dried over magnesium sulphate and reduced to dryness. The residue was then purified by column chromatography from ethyl acetate 10 % and petroleum spirit mix to yield a purple solid (0.13g, 26%).

^{1}H NMR; ($CDCl_3$) δ_{ppm} = 3.92 (9H, s, C<u>H</u>$_3$), 7.88 (6H, m, Ar), 8.16 (6H, m, Ar) , 8.90 (6H, m, Ar), 9.10 (3, m, Ar)

MS; (ES), = 832

HRMS Calculated 833.2089, Found = 833.2065

IR: ν_{max} (KBr) cm^{-1} = 3112, 2969, 2930, 1717, 1608

UV/Vis (THF): λ (rel. intensity) 284 (1.0), 340 (s, 0.46), 528 (s, 0.3), 580 (0.8)

Preparation of Butyl-(2-hydroxyethyl)-dimethylammonium Bromide[119] (42)

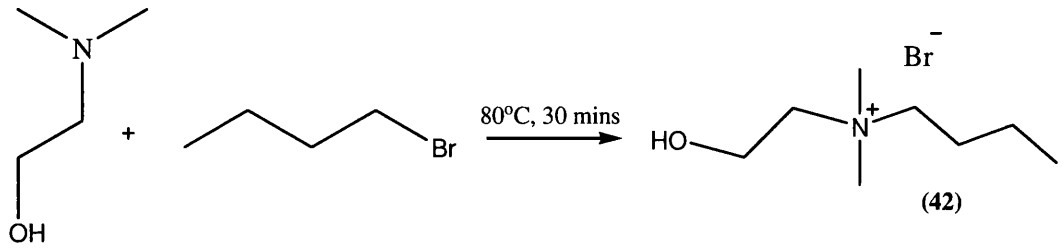

(42)

N,*N*-dimethylethanolamine (10 g, 0.11 mol) was added to a flask containing bromo butane (16.9 g, 0.12 mol) and heated to 80 °C for 30 minutes. The reaction mixture was then cooled to room temperature and the solid obtained was dissolved in 1-propanol and methanol in a ration of 1:3. The solution was then heated to reflux for 30 minutes before cooling to room temperature. The solvent removed under vacuum and the resulting solid was recrystalised by dissolving in THF and methanol (1:3) followed by an addition of petroleum spirit to yield (12.04 g, 48 %).

^{1}H NMR; ($CDCl_3$) δ_{ppm} = 1.04 (3H, t, J = 7.25, CH_3-CH_2), 1.45 (2H, sextet, J = 7.25, $CH_3CH_2CH_2$), 1.80 (2H, quintet, J = 7.20, $C_3H_5CH_2$), 3.19 (6H, s, N-CH_3), 3.44 (2H, m, CH_2-N), 3.50 (2H, m, N-CH_2), 4.01 (2H, m, CH_2-OH)

^{13}C NMR; ($CDCl_3$) δ_{ppm} = 13.52 (CH_3), 20.72 ($CH_3\underline{C}H_2$), 25.62 ($C_3H_5\underline{C}H_2$), 52.29 (N-CH_3), 56.92 (CH_2-OH), 66.58 (N-CH_2)

HRMS Calculated =, found = 146.1541 (Calculated 146.1539

IR: ν_{max} (KBr) cm^{-1} = 3385, 2965, 2880, 1489

Preparation of Phthalocyanine zinc (43)[118]

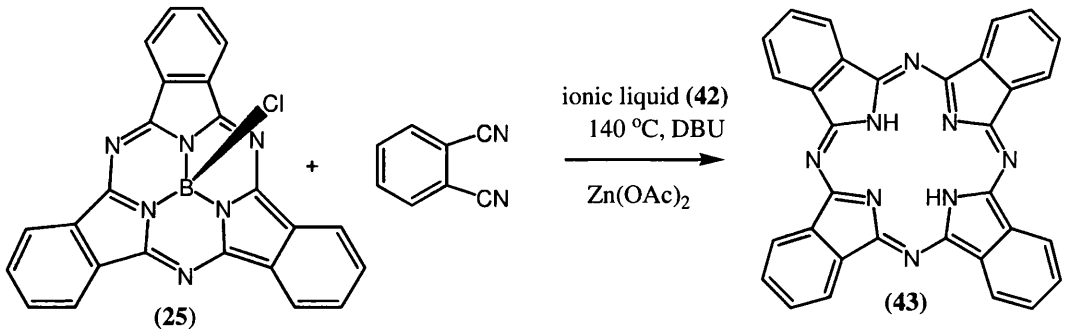

(25) (43)

Subphthalocyanine boron (III) (0.86, 2mmol) and the ionic liquid butyl-(2-hydroxyethyl)-dimethylammonium bromide **(42)** (4.5g, 19.9 mmol) was heated to 140 °C under an argon atmosphere for 5 minutes. Phthalonitrile (0.26, 2 mmol), DBU (0.30, 2 mmol) and anhydrous zinc acetate (0.37, 2 mmol) was added to the reaction mixture and heated for 5 hours. Once cooled to room temperature, the solution was washed with water (50 ml) and methanol (100 ml) and then placed in a Soxhlet extractor for 24 hours. The blue solid in the Soxhlet extractor bulb was then dried to yield zinc phthalocyanine (**33b**) 0.72 g, 62 %

MS; (EI), m/z (%) = 577 (100, M^+)
UV/Vis (THF): λ **(rel. intensity)** = 340 (0.37), 604 (0.23), 640 (sh, 0.21), 668 (1.0)
IR: ν_{max} **(KBr)** cm^{-1} = 3271, 1728, 1650

Preparation of 2-*t*-Butyl-9,16,23-triiodo-phthalocyanine (44)

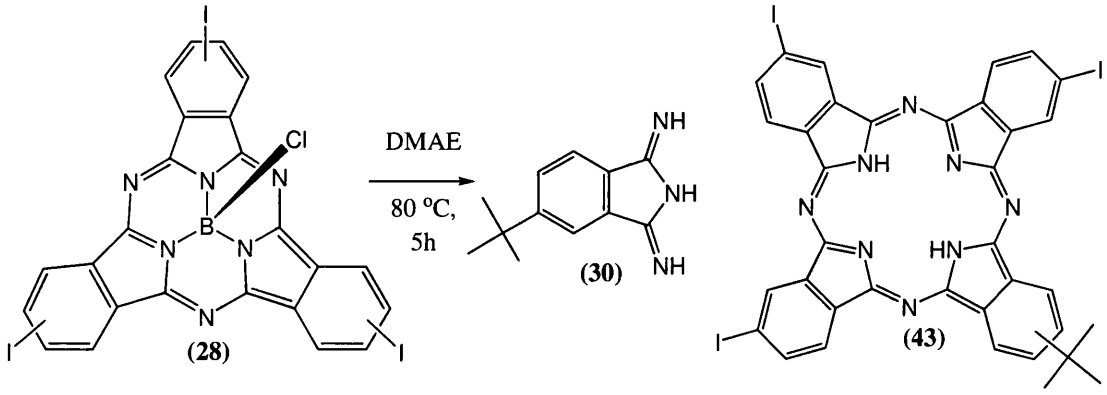

t-Butyl-1,3-diiminoisoindoline **(30)** (0.16 g, 0.80 mmol) was added to a stiring solution chloro[triiodosubphthalocyaninato]-boron (III) **(28)** (0.13 g, 0.16 mmol) in DMAE (20 ml). The reaction mixture was heated to 80 °C for 5 hours before being cooled to room temperature. Petroleum spirit was added and the suspension was filtered. The residue was then washed with petrol, methanol and ethyl acetate to yield a blue solid 0.42 g, 55 %.

^{1}H NMR; ($CDCl_3$) δ_{ppm} = 1.55 (m, *t*-butyl), 6.50-7.96 (m, Ar)
MS; (EI), m/z (%) = 947 (M^+, 100)
HRMS; (EI) = Found = 947.9176 calculated = 947.9177
IR: ν_{max} (KBr) cm^{-1} = 3443, 3281, 2844, 1750, 1596
UV/Vis (THF): λ (rel. intensity) = 292 (0.42), 344 (0.80), 608 (s, 0.44), 632 (0.62), 664 (1.0), 692 (0.93)

Layered Double Hydroxide Synthesis

Coprecipitation Method – (Small-LDH)

A solution containing magnesium nitrate hexahydrate (46.16 g, 0.18 mol) and aluminium nitrate nonahydrate (22.5 g, 0.06 mol) in deionised water (360 ml) was heated to 70 °C. A separate solution of 2M $NaHCO_3$ was also heated to 70 °C. Using two peristaltic pumps the two solutions were combined dropping in to a third solution containing deionised water heated to 70 °C. The pH of the solution was maintained to pH 7 by adjusting the flow rate of the basic solution. The solution was then aged for a further 1.5 hours at 70 °C and then allowed to cool to room temperature. The solution was then filtered and washed with copious amounts of distilled water and dried at 70 °C for 16 hours to yield a white powder in 48 % yield.

IR: ν_{max} (KBr) cm^{-1} = 3412, 2912, 1620, 1382, 1350, 1089, 775

XRD data are shown below in Table 6.1

Urea Method – MgAl-HT (Large-LDH)

To a stirring solution containing magnesium nitrate hexahydrate (76.9g, 0.3 mol) and aluminium nitrate nonahydrate (22.5g, 0.06 mol) in deionised water (200 ml), solid urea (48.6g, 0.81 mol) was added. The clear homogenous solution was then left to stir at 90 °C until a white precipitate appeared. This was then filtered, washed and dried at 70 °C for 16 h to yield a white powder in 35 % yield

IR: ν_{max} (KBr) cm^{-1} = 3402, 2894, 1629, 1361, 1053, 775

Small-LDH Coprecipitate Method		Large-LDH Urea Method		Reference Pattern – 014-0191		
d-spacing	Relative Intensity	d-spacing	Relative Intensity	d-spacing	Relative Intensity	h,k,l
7.52	100	7.5	100	7.69	100	003
3.77	45	3.74	55	3.88	70	006
2.56	42	2.56	100	2.58	20	012
2.27	29	2.26	73	2.3	20	
1.94	18	1.92	72	1.96	20	
				1.85	10	
		1.71	13	1.75	10	
1.63	4	1.61	9	1.65	10	
1.52	18	1.52	50	1.53	20	
1.49	14	1.49	33	1.5	20	
1.31	1	1.45	5	1.28	10	

Table 6.1, XRD data for the Coprecipitate (Small-LDH) and Urea method (Large-LDH) and reference pattern 014-0191, Space group R3m

Adsorption of copper phthalocyanine 3,4',4'',4'''-tetrasulfonic acid tetra sodium salt. (Small Pc-LDH, Large Pc-LDH)

The MgAl-LDH clays (0.5 g) synthesised by the coprecipitation method and urea methods were each suspended in 100 ml of deionised water containing 0.0125 M of copper phthalocyanine 3,4',4'',4'''-tetrasulfonic acid tetra sodium salt (CuPc-Ts). The products were then heated to 90 °C for 6 hours and left to stir for 24 hours at room temperature. In each case, the blue slurry was then filtered and washed until the filtrate ran clear. In each case, the blue products were then dried at 70 °C for 16 hours.

Small Pc-LDH - IR: ν_{max} (KBr) cm^{-1} = 3433, 302, 1612, 1346, 1170, 1126, 1178, 1024, 775, 675

Large Pc-LDH - IR: ν_{max} (KBr) cm^{-1} = 3421, 2948, 1629, 1350, 1118, 777, 675

XRD shown below in Table 6.2

Small Pc-LDH		Large Pc-LDH				
Coprecipitate Method		Urea Method		Reference Pattern -		014-0191
d-spacing	Relative Intensity	d-spacing	Relative Intensity	d-spacing	Relative Intensity	h,k,l
7.7	100	7.69	100	7.69	100	003
3.76	70	3.82	49	3.88	70	006
		3.54	6			
2.54	92	2.61	23	2.58	20	012
2.24	78	2.35	9	2.3	20	
1.91	89	1.95	8	1.96	20	
				1.85	10	
				1.75	10	
1.67	17	1.52	19	1.65	10	
1.5	18	1.5	18	1.53	20	
1.47	25	1.41	4	1.5	20	
		1.3	1	1.28	10	

Table 6.2, XRD data for the copper phthalocyanine tetrasulphonic acid tetra sodium saltderivatized Small-LDH, Large-LDH products and the LDH reference pattern 014-0191

Intercalation of copper phthalocyanine 3,4',4'',4'''-tetrsulfonic acid tetra sodium salt

Rehydration Method

The MgAl-LDH sysnthesised by the urea method was calcined at 450 °C in a Carbolite MTF tube furnace under flowing air for 4 hours with an initial ramp rate of 10 °C per minute. The calcined clay (0.5 g) was then added to a solution of CuPc-Ts (0.0125 M) in decarbonated, deionised water (100 ml) and heated to 90 °C for 24 hours under an inert atmosphere. The solution was then filtered, washed until the filtrate ran clear and dried at 70 °C for 16 hours.

Rehydration Method, IR: ν_{max} (KBr) cm^{-1} = 3417, 2987, 1622, 1352, 1118, 777, 675
1126, 1168, 1020, 777, 675

XRD shown below in Table 6.3

Direct Exchange Method

A solution containing magnesium nitrate hexahydrate (46.16 g, 0.18 mol) and aluminium nitrate nonahydrate (22.5 g, 0.06 mol) in deionised water (360 ml) was heated to 70 °C. A separate solution of 2M $NaHCO_3$ was also heated to 70 °C. Using two peristaltic pumps the two solutions were combined dropping in to a third solution containing deionised water heated to 70 °C. The pH of the solution was maintained to pH 7 by adjusting the flow rate of the basic solution. The solution was then aged for a further 1.5 hours at 70 °C and then allowed to cool to room temperature. Excess water was then filtered from the white slurry, which was then transferred under an inert atmosphere to a sealed vessel. To this white slurry, copper phthalocyanine 3,4',4'',4'''-tetrasulfonic acid tetra sodium salt (CuPc-Ts) (0.0125 M) in decarbonated, deionised water was added. The clay was then heated for 8 hours at 100 °C and then left to stir for 96 hours at room temperature. The blue slurry was then filtered and washed with deionised water until the filtrate ran clear. The blue product was then dried at 70 °C for 16 hours.

Direct Exchange, IR: ν_{max} (KBr) cm^{-1} = 3415, 3002, 1620, 1558, 1382, 774, 675

XRD shown below in Table 6.3

Synthesis of MgAl-TA Layered Double Hydroxide

A solution containing magnesium nitrate hexahydrate (38.4 g, 0.15 mol) and aluminium nitrate nonahydrate (18.8g, 0.05 mol) in deionised water (70 ml) was heated to 70 °C. The separate solution contained aqueous NaOH (70 ml, 2.00 M) were combined together through a Pyrex glass T-piece, then dropping into a third aqueous solution also heated to 70 °C containing terephthalic acid (8.3 g, 0.05 moles) and NaOH (0.05 moles). The pH of the solution was then maintained at pH7 by adjusting the flow rate of the basic solution. The solution was heated for a further 4 hours and the filtered, washed and dried at 70 °C for 16 hours.

LDH-TA, IR: ν_{max} (KBr) cm^{-1} = 3419, 3024, 1614, 1560, 1384, 829, 663, 551

XRD shown below in Table 6.3

Exchange of terephthalic acid with copper phthalocyanine tetrasulfonic acid, tetra sodium salt, (Inter-LDH)

The MgAl-TA (0.5 g) was suspended in 50 ml of deionised, degassed water containing copper phthalocyanine tetrasulfonic acid, tetra sodium salt (200 mg/L) under inert conditions. The clay was then heated for 20 hours at 90 °C and then left to stir at room temperature for a further 24 hours. The clay was then filtered, washed with deionised water and dried at 70 °C for 16 hours.

Inter-LDH, IR: ν_{max} (KBr) cm^{-1} = 3402, 3039, 1622, 1562, 1392, 754, 671

XRD shown below in Table 6.3

XRD Tables

Rehydration Method		Direct Exchange		LDH-TA		Inter-LDH	
d-spacing	Relative Intensity	d-spacing	Relative Intensity	d-spacing	Relative Intensity	d-spacing	Relative Intensity
7.62	100	24.31985	41.69	14.68	100	21.18662	7.3
3.83	40	20.25578	32.74	7.25	69.09	13.52127	21.99
3.55	5	12.66343	22.96	4.79	38.68	12.21251	27.43
2.57	40	7.4974	48.66	3.61	42.68	7.33246	100
2.3	19	6.22931	39.4	2.64	22.32	5.46402	5.49
2.09	4	5.4517	42.22	2.56	23.45	4.56389	10.45
1.95	15	3.95923	94.91	2.4	15.7	3.64487	26.7
		3.28564	23.78	2.2	4.4	2.6212	14.3
1.52	22	2.56476	17.93	2	16.7	2.5517	10.45
1.5	19	2.27129	4.47	1.53	25.83	2.37164	4.87
1.42	2	1.92836	4.3	1.49	9.97	2.00859	5.65
1.31	2	1.51896	8.77	1.46	2.5	1.5232	15.37
				1.4	0.79	1.49111	8.86

Table 6.3, XRD data for the rehydration method, direct exchange, LDH-TA and Inter-LDH

References

(1) Energy Information Admisistration *International Energy Outlook 2008* http://www.eia.doe.gov/oiaf/ieo/index.html **(16/01/09)**.

(2) Gonçalves, L.; Bermudez, V.; Ribeiro, H.; Mendes, A. *Energy Environ. Sci.* **2008**, *1*, 655-667.

(3) *Handbook of Photovoltaic Science and Engineering*; Luque, A.; Hegedus, S., Eds.; Wiley, 2002.

(4) Hoffmann, W. *Sol. Energy Mater. Sol. Cells,* **2006**, *90*, 3285-3311.

(5) Pizzini. S; Acciarri. M; Binett. S *phys. stat. sol. (a),* **2005**, *202*, 2928-2942.

(6) O'Regan, B.; Grätzel, M. *Nature* **1991**, *353*, 737-740.

(7) Holliman, P. *Bangor University.*

(8) Sayama, K.; Sugihara, H.; Arakawa, H. *Chemistry of Materials* **1998**, *10*, 3825-3832.

(9) Kalyanasundaram, K.; Grätzel, M. *Coord. Chem. Rev.,* **1998**, *177*, 347-414.

(10) Kay, A.; Grätzel, M. *Sol. Energ. Mater. Sol. Cell,* **1996**, *44*, 99-117.

(11) Mor, G.; Shankar, K.; Paulose, M.; Varghese, O.; Grimes, C. *Nano Letters* **2006**, *6*, 215-218.

(12) Adachi, M.; Murata, Y.; Takao, J.; Jiu, J.; Sakamoto, M.; Wang, F. *J. Am. Chem. Soc.,* **2004**, *126*, 14943-14949.

(13) Jiu, J.; Isoda, S.; Wang, F.; Adachi, M. *J. Phys. Chem. B,* **2006**, *110*, 2087-2092.

(14) Wang, Z.; Sayama, K.; Sugihara, H. *J. Phys. Chem. B,* **2005**, *109*, 22449-22455.

(15) Oskam, G.; Bergeron, B.; Meyer, G.; Searson, P. *J. Phys. Chem. B,* **2001**, *105*, 6867-6873.

(16) Liu, Y.; Hagfeldt, A.; Xiao, X.; Lindquist, S. *Sol. Energy Mater. Sol. Cells,* **1998** *55*, 267-281.

(17) Nazeeruddin, M.; Kay, A.; Rodicio, I.; Humphry-Baker, R.; Mueller, E.; Liska, P.; Vlachopoulos, N.; Grätzel, M. *J. Am. Chem. Soc.,* **1993**, *115*, 6382-6390.

(18) Robertson, N. *Angew Chem. Int. Ed* **2006**, *45*, 2338-2345.

(19) Grätzel, M. *J. Photochem. Photobiol. C Photochem. Rev.,* **2003**, *4*, 145-153.

(20) Fang, J.; Mao, H.; Wu, J.; Zhang, X.; Lu, Z. *Appl. Surf. Sci.,* **1997**, *119*, 237- 41.

(21) Ghanem, R. *Spectrochim. Acta. Mol. Biomol. Spectros.,* **2009**, *72*, 455-459.

(22) Lee, W.; Lee, J.; Min, S.; Park, T.; Yi, W.; Han, S. *Mater. Sci. Eng. B,* **2009**, *156*, 48-51.

(23) Nazeeruddin, M.; P, P. c.; M, G. *Chem. Comm.,* **1997**, 1705 - 1706.

(24) Nazeeruddin, M.; De Angelis, F.; Fantacci, S.; Selloni, A.; Viscardi, G.; Liska, P.; Ito, S.; Takeru, B.; Grätzel, M. *J. Am. Chem. Soc.,* **2005**, *127*, 16835-16847.

(25) Cao, Y.; Bai, Y.; Yu, Q.; Cheng, Y.; Liu, S.; Shi, D.; Gao, F.; Wang, P. *J. Phys. Chem. C,* **2009**, *113*, 6290-6297.

(26) Dyesol; https://secure.dyesol.com/index.php?template=category-page&catid=4&currency=GBP: 20.01, 29/01/10.

(27) Gao, F.; Wang, Y.; Zhang, J.; Shi, D.; Wang, M.; Humphry-Baker, R.; Wang, P.; Zakeeruddin, S.; Grätzel, M. *Chem. Comm.,* **2008**, 2635-2637.

(28) Gao, F.; Wang, Y.; Shi, D.; Zhang, J.; Wang, M.; Jing, X.; Humphry-Baker, R.; Wang, P.; Zakeeruddin, S.; Grätzel, M. *J. Am. Chem. Soc.,* **2008**, *130*, 10720-10728.

(29) Wang, P.; Klein, C.; Moser, J.; Humphrey-Baker, R.; Cevey-Ha, N.; Charvet, R.; Comte, P.; Zakeeruddin, S.; Grätzel, M. *J. Phys. Chem. B.* **2004,**, *108*, 7553.

(30) Ito, S.; Zakeeruddin, M.; Humphry-Baker, R.; Liska, P.; Charvet, R.; Comte, P.; Nazeeruddin, M. K.; Péchy, P.; Takata, M.; Miura, H.; Uchida, S.; Grätzel, M. *Advanced Materials* **2006**, *18*, 1202-1205.

(31) Choi, H.; Lee, J.; Song, K.; Kang, S.; Ko, J. *Tetrahedron* **2007**, *63*, 3115-3121.
(32) Jung, I.; Lee, J.; Song, K.; Song, K.; Kang, S.; Ko, J. *J. Org. Chem.,* **2007**, *72*, 3652-3658.
(33) Qin, H.; Wenger, S.; Xu, M.; Gao, F.; Jing, X.; Wang, P.; Zakeeruddin, S.; Grätzel, M. *J. Am. Chem. Soc.,* **2008**, *130*, 9202-9203.
(34) Hara, K.; Kurashige, M.; Dan-oh, Y.; Kasada, C.; Shinpo, A.; Suga, S.; Sayama, K.; Arakawa, H. *New J. Chem* **2003**, *27*, 783–785.
(35) Hara, K.; Kurashige, M.; Ito, S.; Shinpo, A.; Suga, S.; Sayama, K.; Arakawa, H. *Chem. Comm.,* **2003**, 252 - 253.
(36) Ma, X.; Hua, J.; Wu, W.; Jin, Y.; Meng, F.; Zhan, W.; Tian, H. *Tetrahedron* **2008**, *64*, 345-350.
(37) Linsted, R. *J.Chem. Soc,* **1934,,** *Phthalocyanines. Part I.*
(38) Robertson, J. *J. Chem. Soc,* **1936**, 1195.
(39) *Industrial Inorganic Pigments,*; Herbst, W.; Hunge, K., Eds.; VCH-Wiley, ; Vol. third edition.
(40) Mckeown, N.; Phthalocyanine Materials: Synthesis, Structure and Function, Cambridge University Press: 1988.
(41) *Phthalocyanines: Properties and Applications,* ; Leznoff, C.; Lever, A., Eds.; VCH, Weinheim,, 1993,Vol. 4,.
(42) Leznoff, C.; Black, S.; Hiebert, A.; Causey, P.; Christendat, D.; Lever, A. *Inorganica Chimica Acta,* **2006**, *359*, 2690,2699.
(43) Claessens, C.; Hahn, U.; Torres, T. *The Chemical Record,* **2008**, *8*, 75-97.
(44) Kobayashi, N.; Nakajima, S.; Ogata, H.; Fukuda, T. *Chem. Eur. J.* **2004**, *10*, 6294 - 6312.
(45) Sessler, L.; Seidel, D. *Angew Chem. Int. Ed.* **2003**, *42*, 5134-5175.
(46) Dini, D.; Barthel, M.; Schneider, T.; Ottmar, M.; Verma, S.; Hanack, M. *Solid State Ionics* **2003**, *165*, 289-303.
(47) Terekhov, D.; Nolan, K.; McArthur, C.; Leznoff, C. *J. Org. Chem.,* **1996**, *61*, 3034-3040.
(48) Yanagisawa, M.; Korodi, F.; Bergqusit, J.; Holmberg, A.; Hagfeld, A.; Akermark, B.; Sun, L. *J. Porphyrins Phthalocyanines,* **2004**, *8*, 1228-1235.
(49) Hideg, K.; Sar, C.; Hankovszky, O.; Tamas, T.; Jerkovich, G. *Synth,* **1992**, 390-393.
(50) Poon, K.; Liu, W.; Chan, P.; Yang, Q.; Chan, T.; Mak, T.; Ng, D. *J. Org. Chem.,* **2001**, *66*, 1553-1559.
(51) Leznoff, C.; Li, Z.; Isago, H.; D'ascanio, A.; Terkhov, D. *J. Porphyrins Phthalocyanines,* **1999**, *3*, 406-416.
(52) Sugimori, T.; Okamoto, S.; Kotoh, N.; Handa, M.; Kasuga, K. *Chemistry Letters* **2000**, 1200-1201.
(53) Turchi, S.; Nesi, R.; Giomi, D. *Tetrahedron,* **1998**, *54*, 1809-1816.
(54) Balakireva, O.; Maizlish, V.; Shaposhnikov, G. *Russ. J. Gen. Chem.,* **2003**, *73*, 292 - 296.
(55) Christe, R. *Colour Chemistry entire, RSC paperbacks* **2001**.
(56) Kasuga, K.; Idehara, T.; Handa, M. *Inorg. Chim. Acta,* **1992**, *196*, 127-128.
(57) Diaz-Garcia, M.; Agull6-L6pez, F.; Sastre, A.; Torres, T.; Torruellas, W.; Stegeman, G. *J. Phys. Chem.,* **1995,** , *99*, 14988-14991.
(58) Kobayashi, N.; Ishizaki, T.; Ishii, K.; Konami, H. *J. Am. Chem. Soc.,* **1999**, *121*, 9096-9110.
(59) Meller, A.; Ossko, A. *Monursh. Chem.,* **1972**, *103*, 150-155.
(60) del Rey, B.; Keller, U.; Torres, T.; Rojo, G.; Agulló-López, F.; Nonell, S.; Martí, C.; Brasselet, S.; Ledoux, I.; Zyss, J. *J. Am. Chem. Soc.,* **1998**, *120*, 12808-12817.

(61) Geyer; Plenzig, F.; Rauschnabel, J.; Hanack, M.; del Rey, B.; Sastre, A.; Torres, T. *Synthesis* **1996**, 1139-1151.
(62) Ali, H.; Sim, S.; van Lier, J. *J. Chem. Research,* **1999**, 496-497.
(63) Rey, B.; Torres, T. *Tetrahedron Lett.,* **1997**, *38*, 5351-5354.
(64) Eu, S.; Katoh, T.; Umeyama, T.; Matano, Y.; Imahori, H. *Dalton Trans.* **2008**, 5476-5483.
(65) Sharman, W.; van Lier, J. *Bioconjgate Chem* **2005**, *16*, 1166-1175.
(66) Pfeiffer, M.; Leo, K.; Karl, N. *Journal of Applied Physics* **1996**, *80*, 6880-6883.
(67) Rostalski, J.; Meissner, D. *Sol. Energ. Mater. Sol. Cell,* **2000**, *63*, 37-47.
(68) Vivo, P.; Ojala, M.; Chukharev, V.; Efimov, A.; Lemmetyinen, H. *Journal of Photochemistry and Photobiology A: Chemistry* **2009**, *203*, 125-130.
(69) Reddy, P.; Giribabu, L.; Lyness, C.; Snaith, H.; Vijaykumar, C.; Chandrasekharam, M.; Lakshmikantam, M.; Yum, J.; Kalyanasundaram, K.; Grätzel, M.; Nazeeruddin, M. *Angew. Chem. Int. Ed.* **2007**, *46* 373 -376.
(70) Nazeeruddin, M.; De Angelis, F.; Fantacci, S.; Selloni, A.; Viscardi, G.; Liska, P.; Ito, S.; Bessho, T.; Grätzel, M. *J. Am. Chem.Soc.* **2005**, *127.*, 835.
(71) Giribabu, L.; Kumar, C.; Gopal Reddy, V.; Reddy, P.; Srinivasa Rao, C.; Jang, S.; Yum, J.; Nazeeruddin, M. K.; Grätzel, M. *Sol. Energ. Mater. Sol. Cell,* **2007**, *91*, 1611-1617.
(72) Palomares, E.; Martinez-Diaz, M.; Haque, S.; Torres, T.; Durrant, J. *Chem. Comm.,* **2004**, 2112-2113.
(73) Nazeeruddin, M.; Humphry-Baker, R.; Grätzel, M.; Wohrle, D.; Schnurpfeil, G.; Schneider, G.; Hirth, A.; Trombach, N. *J. Porphyrins Phthalocyanines,* **1999**, *3*, 230-237.
(74) Nazeeruddin, M.; Humphry-Baker, R.; Grätzel, M.; Murrerb, B. *chem. commun.,* **1998**, 719-720.
(75) He, J.; Hagfeldt, A.; Lindquist, S. *Langmuir,* **2001,**, *17*, 2743-2747.
(76) Wang, P.; Zakeeruddin, S.; Moser, J.; Nazeeruddin, M.; Sekiguchi, T.; Grätzel, M. *Nat. Mater,* **2003**, *2*, 402.
(77) Hanack, M.; Haisch, P.; Lehmann, H.; Subramanian, L. *Synth,* **1993**, 387-390.
(78) Wróbel, D.; C, R. *Chimie,* **2003**, *6*, 417-429.
(79) He, J.; Benk, G.; Korodi, F.; Polvka, T.; Lomoth, R.; Kermark, B.; Sun, L.; Hagfeldt, A.; Sundstrm, V. *J. Am. Chem. Soc.,* **2002**, *124*, 4922-4932.
(80) Reddy, P.; Giribabu, L.; Lyness, C.; Snaith, H.; Vijaykumar, C.; Chandrasekharam, M.; Lakshmikantam, M.; Yum, J.; Kalyanasundaram, K.; Grätzel, M.; Nazeeruddin, M. K. *Angew. Chem. Int. Ed.* **2007**, *119*, 377 –380
(81) Giribabu, L.; Vijay Kumar, C.; Raghavender, M.; Somaiah, K.; Ready, P.; Venlateswara Rao, P. *J. Nano Research* **2008**, *2*, 39-48.
(82) Giribabu, L.; Kumar, C.; Ready, P.; Yum, J.; Grätzel, M.; Nazeeruddin, M. K. *J. Chem. Sci.,* **2009**, *121*, 75-82.
(83) Cid, J.; Yum, J.-H.; Jang, S.; Nazeeruddin, M. K.; Martinez-Ferrero, E.; Palomares, E.; Ko, J.; Grätzel, M.; Torres, T. *Angew. Chemie Int. Ed.,* **2007**, *46*, 8358.
(84) Yum, J.; Jang, S.; Humphry-Baker, R.; Grätzel, M.; Cid, J.; Torres, T.; Nazeeruddin, M. K. *Langmuir,* **2008**, *24*, 5636-5640.
(85) Kay, A.; Grätzel, M. *Solar Energy Materials and Solar Cells,* **1996**, *44*, 99-117.
(86) Hanke, Z. *Phys. Chem* **1999**, *212*, 1-9.
(87) Hanack, M.; Metz, J.; Pawlowski, J. *Chem. Ber.* **1982**, *115*, 2836.
(88) Kuo, C.; Zhu, J.; Wu, J.; Chu, C.; Yao, C.; Shia, K. *Chem. Comm* **2007**, 301–303
(89) Marcuccio, S.; Svirskaya, P.; Greenberg, S.; Lever, A.; Leznoff, C. *Can. J. Chem* **1985**, *63,* 3057-3069

(90) Mattern, D. *J. Org. Chem.* **1984**, *49*, 3051-3053.
(91) Suzuki H, G. R. *Bulletin of the Chemical Society of Japan* **1963**, *36*, 389-391.
(92) Yagupol'skii, L.; Popov, V.; Kondratenko, N. *J. Org. Chem. USSR* **1976**, *12*, 923-924
(93) Wang, Z.; Tian, H.; Chen, K. *Dyes. Pigments,* **2001**, *51*, 161-165.
(94) Delaire, J.; Delouis, J.; Zakrzewski, J. *J. Photochem. Photobiol. Chem.,* **2001**, *141*, 169-173.
(95) Rodriguez, J.; Oñate, A.; Martin-Villamil, R.; Fonseca, I. *J. Organomet. Chem.,* **1996**, *513*, 71-76.
(96) Lai, L.; Dong, T. *J. Chem. Soc. Chem. Comm,* **1994**, 2347-2348.
(97) Lai, L.; Dong, T. *Synthesis* **1995**, 1213-1232.
(98) Dong, T.; Lai, L. *J. Organomet. Chem.,* **1996**, *509*, 131-134.
(99) Butler, I.; Cullen, W.; Ni, J.; Rettig, S. *Organometallics* **1985**, *4*, 2196-2201.
(100) Jin, Z.; Nolan, K.; McArthur, C.; Lever, A.; Leznoff, C. *J. Organomet. Chem.,* **1994**, *468*, 205-212.
(101) Negishi, E.; King, A.; Okukado, N. *J. Org. Chem.,* **1977**, *42*, 1821-1823.
(102) Bach, T.; Heuser, S. *J. Org. Chem.* **2002**, *67*, 5789- 5795.
(103) Negishi, E.; Owczarczyk, Z. *Tetrahedron Lett.,* **1991**, *32*, 6683-6686.
(104) Casares, J.; Espinet, P.; Fuentes, B.; Salas, G. *J. Am. Chem. Soc.,* **2007**, *129*, 3508-3509.
(105) Kurppa, M.; Imperato, G.; König, B. *Tetrahedron* **2006**, *62*, 1360-1364.
(106) Yeh, H.; Wu, W.; Wen, Y.; Dai, D.; Wang, J.; Chen, C. *J. Org. Chem.* **2004**, *69*, 6455-6462.
(107) Barder, T.; Walker, S.; Martinelli, J.; Buchwald, S. *J. Am. Chem. Soc.* **2005**, *127*, 4685-4696.
(108) Haisch, P.; Winter, G.; Hanack, M.; Luer, L.; Egelhaaf, H.; Oelkrug, D. *Adv. Mater* **1997**, *9*, 316-321.
(109) Sastre, A.; Rey, B.; Torres, T. *J. Org. Chem.* **1996**, *61*, 8591-8597.
(110) Rauschnabel, J.; Hanack, M. *Tetra.Lett,* **1995**, *36*, 1629-1632.
(111) Schneider, G.; Heckmann, H.; Barthel, M.; Hanack, M. *Eur. J. Org. Chem,* **2001**, 3055-3065.
(112) Chauhan, S.; Agarwal, S.; Kumari, P. *Synth. Commun.* **2007**, *37*, 2917-2925.
(113) Matlaba, P.; Nyokong, T. *Polyhedron* **2002**, *21*, 2463-2472.
(114) Chauhan, S.; Kumari, P.; Agarwal, S. *Synth,* **2007**, *23*, 3713-3721.
(115) Schmidt, E.; Calderwood, T.; Bruice, T. *Inorg. Chem.,* **1986**, *25*, 3718-3720.
(116) Sonogashira, K.; Tohda, Y.; Hagihara, N. *Tetrahedron Lett.,* **1975**, 4467-4470.
(117) Chinchilla, R.; Najera, C. *Chemical Reviews* **2007**, *107*, 874-922.
(118) Chauhan, S.; Kumari, P. *Tetrahedron* **2009**, *65*, 2518-2524.
(119) Domanska, U.; Bogel-Lukasik, R. *J. Phys. Chem. B,* **2005**, *109*, 12124-12132.
(120) Haraa, K.; Nishikawab, T.; Kurashigea, M.; Kawauchic, H.; Kashimac, T.; Sayamaa, K.; Aikab, K.; Arakawa, H. *Sol. Energ. Mater. Sol. Cell,* **2005**, *85*, 21-30.
(121) P.Jones *Corus Colours, Personal Communications* **2006**.
(122) N. McMurray *Coated Steels, 1st year EngD notes, Swansea University* **2005**.
(123) A. Robinson, J. S., D. Worsley, *Mater. Sci. Tech.,* **2004**, *20*, 1041-1048.
(124) Marganski, R.; Diebold, M. *Photocatalytic Properties of Titanium Dioxide, Modern Paint and Coatings,* **1999**, 30.
(125) P. Christensen, A. D., T. Edgerton, J. Temperley *J. Mater. Sci* **1999**, *34*, 5689-5700.
(126) Robinson, A. *The Development of Organic Coatings for Strip Steels with Improved Resistance to Photo Degradation* **2003**, Swansea University.

(127) N. Allen, M. E. In *Fundementals of Polymer Degradation and Stabilisation*; Elsivier Applied Sciences: London, 1992.
(128) *Coatings technology: fundamentals, testing and processing techniques*; Tracton, A., Ed.; CRC Press, 2006.
(129) van der Ven, L.; van Gemert, M.; Batenburg, L.; Keern, J.; Gielgens, L.; Koster, T.; Fischer, H. *Appl. Clay Sci.,* **2000,** *17*, 25-34.
(130) Miyata, S.; Kuroda, M. *US Patent 4,299,759* **1981**.
(131) Cavani, F.; Trifiro, F.; Vaccari, A. *Catal. Today,* **1991**, *11*, 173-301.
(132) E. Mannasse *Atti Soc. Toscanna Sc. Nat.,Proc. Verb,* **1915**, *24*, 92.
(133) Pérez-Ramírez, J.; Abelló, S.; van der Pers, N. *Chem. Eur. J.* **2007**, *13*, 870-878.
(134) *Layered Double Hydroxides (Structure and Bonding)*; Duan, X.; Evans, D., Eds.; Springer, 2006.
(135) Costantino, U.; Marmottini, F.; Nocchetti, M.; Vivani, R. *Eur. J. Org. Chem,* **1998**, 1439-1446
(136) Anastas, P.; Bartlett, L.; Kirchhoff, M.; Williamson, T. *Catal. Today,* **2000**, *55*, 11-22.
(137) Kavanda, F.; Koloušek, D.; Cilova, Z.; Hulinsky, V. *Appl. Clay Sci.,* **2005**, *28*, 101-109.
(138) Feitknecht, W. *Helv. Chim. Acta,* **1942**, *25*, 131-137.
(139) Reichle, W. *Solid State Ionics,* **1986**, *22*, 135-141.
(140) Kovanda, F.; Kolousek, D.; Cilova, Z.; Hulinsky, V. *Appl. Clay Sci.,* **2005**, *28*, 101-109
(141) Oh, J.; Hwang, S.; Choy, J. *Solid State Ionics,* **2002**, *151*, 285-291.
(142) López, T.; Bosch, P.; Asomoza, M.; Gómez, R.; Ramos, E. *Mat, Lett,* **1997**, *31*, 311-316.
(143) Rao, M.; Reddy, B.; Jayalakshmi, M.; Jaya, V.; Sridhar, B. *Mater. Res. Bull.,* **2005**, *40*, 347-359.
(144) Miyata, S. *Clay Miner.,* **1980**, *28*, 50-56.
(145) Hussein, M.; Zainal, Z.; Yahaya, A.; Aziz, A. *Mater Sci. Eng. B,***2002**, *88*, 98-102.
(146) Park, I.; Kuroda, K.; Kato, C. *J. Chem. Soc. Dalton Trans.* **1990**, *2*, 3071-3074.
(147) Orthman, J.; Zhu, H.; Lu, G. *Separ. Purif. Tech.,* **2003**, *31*, 53-59.
(148) Crepaldi, E.; Tronto, J.; Cardoso, L.; Valim, J. *Colloid. Surface. Physicochem. Eng. Aspect,* **2002**, *211,* , 102-114.
(149) Tagaya, H.; Ogata, A.; Kuwahara, T.; Ogata, S.; Karasu, M.; Kadokawa, J.; Chiba, K. *Microporous Mater.,* **1996**, *7*, 151-158.
(150) E. Prrez-Bernal, R. R.-C., T. Pinnavaia, *Catal Lett.,* **1991**, *11*, 55-62,.
(151) Iliev, V.; Ileva, A.; Dimitrov, L. *Applied Catalysis A: General* , **1995**, *126*, 333-340.
(152) Carrado, K.; Forman, J.; Botto, R.; Winans, R. *Chem. Mater.* **1993**, *5*, 472-478.
(153) Martin, G.; Robinson, A.; Worsley, D. *Mater. Sci. Tech.,* **2006**, *22*, 375-378.
(154) *Partition and adsorption of organic contaminants in environmental systems*; Chiou, C., Ed.; John Wiley and Sons, 2002.
(155) Robinson, A.; Searle, J.; Worsley, D. *Mater. Sci. Tech.,* **2004**, *20*, 1041-1048.
(156) Leonard, J.; Lygo, B.; Procter, G. *Advanced Practical Organic Chemistry* **2001**, *Nelson Thornes Ltd.*
(157) M. Hanack, J. M., J. Pawlowski *Chem. Ber.* **1982**, *115*, 2836.
(158) L. Lai, T. D. *J. Chem. Soc. Chem. Comm,* **1994**, 2347-2348.